University of Sussex

Air-fuel Homogeneity Effects on Direct Injection Diesel Engine Performance and Emission

Pavlos Dimitriou

Submitted for the degree of Doctor of Philosophy

University of Sussex

May 2015

UNIVERSITY OF SUSSEX

Pavlos Dimitriou, Doctor of Philosophy

Air-fuel Homogeneity Effects on Direct Injection Diesel Engine Performance and Emission

Summary

The temporal and spatial distribution of fuel in cylinders is a key factor affecting the combustion characteristics and emission generation of a DI diesel engine. The air-fuel mixing quality is critical for controlling ignition timing and combustion duration. Avoiding fuel-rich areas within the cylinder can significantly reduce soot formation as well as high local temperatures resulting in low NO_x formation. The present investigation is focused on the effects of advanced fuel injections and air path strategies as well as the effects of piston geometry and fuel spray angle on air-fuel homogeneity, combustion process and their impacts on the performance and emission of the engine.

A Ricardo Hydra single-cylinder engine in combination with AVL Fire CFD software was used in this investigation. An experimental analysis was conducted to assess the combustion characteristics and emissions formation of the engine under various injection strategies such as different injection timing, quantity, ratio, dwell angles between injections with various exhaust valve opening times and exhaust back pressures. A quan-

titative factor named Homogeneity Factor (HF) was employed in the CFD code in order to quantify the air-fuel mixing and understand how the air-fuel homogeneity within the cylinder can influence the combustion and emissions of the engine.

The investigation concludes that multiple injection strategies have the potential to reduce diesel emissions while maintaining meaningful fuel economy. Split injection can be used to improve the air-fuel mixture locally and control temperature generation during the start of combustion. Increased air-fuel homogeneity results in fewer fuel-rich areas within the cylinder and contributes to the reduction of soot emission. Extending the pre-mixed combustion phase has a direct effect on the reduction of soot formation while NO_x generation is highly dependent on the scale of the primary fuel injection event.

Acknowledgments

This thesis would certainly not have been possible without the help and support provided by several people. First and foremost, I would like to thank my main supervisor for the first two years of my studies, Dr Zhijun Peng, for giving me the chance to be involved in the Smart COntrol and Diagnostics for Economic and Clean Engines (SCODECE) research project and for the many enthusiastic discussions we had.

I want to thank my main supervisor after Dr Peng's move, Dr William Wang, for his support and for being available for discussions and comments on the work at all times. I would also like to thank my co-supervisor and internal examiner Dr Julian Dunne and my annual reviewer Dr Zhiyin Yang for the guidance and valuable comments on my work. Prof Marouan Nazha is also thanked for acting as my external examiner and his time spent reading this thesis. The help and support of Prof Abdel Aitouche and Mr David Lemon into this work was also appreciated very much.

Many thanks go to the technicians, Mr Ian Wallis and Mr Barry Jackson. The development and maintenance of the experimental test rig would not be possible without their skills and commitment.

A special thank goes to Ms Sharon Turner and Kistler company for borrowing me an in-cylinder pressure transducer, free of charge for a month, in order to complete my experimental research work after the original sensor's damage. The help from AVL support team and especially Mr Zoran Pavlovic as well as Mr Guillaume Faber from Delphi and the technical support team of Skynam Company is really appreciated.

Thanks also go to Mr Ioannis Michalakoudis for passing to me some of his mechanical knowledge on internal combustion engines and Mr Li Cheng for being a great colleague.

Everyone else, who in one or another way has contributed to the completion of this work, is really acknowledged.

Finally I would like to express my gratitude to my dear father, Christos, mother, Alexandra, and brother for their support and patience.

Publications

1. **Dimitriou, P.**, Peng, Z., "Diesel Engine PCCI combustion control", 8th International Conference, 16-18 October 2011, Beihang University, China.

2. **Dimitriou, P.**, Peng, Z., Lemon, D., Gao, B. and Soumelidis, M., "Diesel Engine Combustion Optimization for Bio-diesel Blends Using Taguchi and ANOVA Statistical Methods", SAE Paper 2013-24-0011, 2013.

3. **Dimitriou, P.**, Wang, W., Cheng, L., Peng, Z., Wellers, M. and Gao, B., "Analysis of Diesel Engine In-Cylinder Air-Fuel Mixing with Homogeneity Factor: Combined Effects of Pilot Injection Strategies and Air Motion", SAE International Journal of Engines, 7(4):2045-2060, 2014.

4. **Dimitriou, P.**, Peng, Z., Wang, W., Gao, B. and Wellers, M., "Effects of Advanced Injection Strategies on the In-cylinder Air-fuel Homogeneity of Diesel Engines", Proceedings of the Institution of Mechanical Engineers, Part D: Journal of Automobile Engineering, 229(3):330-341, 2015.

5. **Dimitriou, P.**, Wang, W., Peng, Z., "A Piston Geometry and Nozzle Spray Angle Investigation into a DI Diesel Engine by Quantifying the Air-fuel Mixing", International Journal of Spray and Combustion Dynamics, 7(1):1-24, 2015.

Contents

List of Tables

List of Figures

Nomenclature

Abbreviations

ABDC	After Bottom Dead Centre
ANOVA	Analysis of Variance
ATDC	After Top Dead Centre
BBDC	Before Bottom Dead Centre
BMEP	Brake Mean Effective Pressure
BSFC	Brake Specific Fuel Consumption
BSFC	Brake Specific Fuel Consumption
BTDC	Before Top Dead Centre
BTHE	Brake Thermal Efficiency
CA	Crank Angle
CFD	Computational Fluid Dynamics
CI	Compression Ignition
CO	Carbon Monoxide
CO2	Carbon Dioxide

CR	Common Rail
CR	Compression Ratio
DEF	Diesel Exhaust Fluid
DI	Direct Injection
DICI	Direct Injection Compression Ignition
DISI	Direct Injection Spark Ignition
DOC	Diesel Oxidation Catalysts
DOH	Degree of Heterogeneity
DPF	Diesel Particulate Filter
EBP	Exhaust Back Pressure
ECFM-3Z	Extended Coherent Flame Model 3 Zones
ECU	Electronic Control Unit
EGR	Exhaust Gas Recirculation
EPA	Environmental Protection Agency
ER	Equivalence Eatio
ETAB	Enhanced Taylor Analogy Break-up
EVC	Exaust Valve Closure
EVO	Exhaust Valve Opening
FIPA	Fractionnement Induit Par Acceleratio
HC	Hydrocarbons
HCCI	Homogeneous Charge Compression Ignition

HeterF	Heterogeneity Factor
HF	Homogeneity Factor
HSDI	High-Speed Direct Injection
HTM	Hybrid Turbulence Model
i-VTEC	intelligent Variable Valve Timing and Lift Electronic Control
IDI	In-direct Injection
IMEP	Indicated Mean Effective Pressure
IMV	Inlet Metering Valve
IVC	Inlet Valve Closure
IVO	Inlet Valve Opening
KH-RT	Kelvin Helmholtz-Rayleigh Taylor
LIF	Laser Induced Fluorescence
LP	Long Pressure
LR	Long Route
LTC	Low Temperature Combustion
N-VCT	Nissan Variable Cam Timing
NLEV	National Low Emission Vehicle
NO	Nitric Oxide
NO2	Nitrogen Dioxide
NOx	Nitrogen Oxides
NVO	Negative Valve Overlap

O	Oxygen
PCCI	Premixed Charge Compression Ignition
PID	Proportional-Integral-Derivative
PIV	Particle Image Velocimetry
PM	Particulate Matter
ppm	parts per million
rpm	revolutions per minute
RSM	Reynolds Stress Model
S/N	Signal-to-Noise
SCR	Selective Catalytic Reduction
SO4	Sulfate
SOC	Start of Combustion
SOF	Soluble Organic Fraction
SOI	Start of Injection
TAB	Taylor Analogy Break-up
TDC	Top Dead Centre
TDCI	Turbo Diesel Common rail Injection
TKE	Turbulence Kinetic Energy
UHC	Unburned Hydrocarbons
VCR	Variable Compression Ratio
VGT	Variable Geometry Turbocharger

VVA	Variable Valve Actuation
VVL	Variable Valve Lift and Timing
VVT	Variable Valve Timing
VVT-i	Variable Valve Timing with intelligence

Greek Symbols

Φ	Fuel-Air Equivalence Ratio
Λ	Wavelength
Ω	Frequency

Chapter 1

Introduction

1.1 Introduction

The invention of the first Compression Ignition (CI) engine dates back to 1892, when Rudolph Diesel designed the first engine that ran on pure peanut oil [1]. Between 1893 and 1897, the first diesel engine was manufactured and tested by Rudolph Diesel and Maschinenfabrik Augsburg-Nürnberg (MAN), a German engineering company. In 1903, the first two diesel-powered ships were launched by Russia [2] while a year later, the French navy built the first diesel-powered submarine, the Z [3]. Almost three decades later, automobiles started to incorporate diesel engines. Citroën was the world's first automobile manufacturer by launching the "Rosalie" diesel-powered car in 1935. A few years earlier, Clessie Cummins, the founder of Cummins Engine Co. (now Cummins, Inc.), was the first to install a diesel engine into his "Diesel Special" race car, hitting 101 mph at Daytona and 86 mph at the Indianapolis 500 race. In 1936, Mercedes-Benz and Hanomag launched their first diesel-powered passenger cars, the Mercedes-Benz 260 D and the Hanomag Rekord [4].

Although the production of diesel cars started in the early 1930s, diesel cars did not become popular modes of passenger travel until the 1960s. In 1967, the world's first compact high-speed diesel car was introduced by Peugeot. The Peugeot 204BD was fitted with a 1.3 L XL4D engine capable of producing 46 PS (34kW) at 5,000 rpm. The

Golf model was the first diesel car introduced to the market by Volkswagen in May, 1974. The car ran on a naturally aspirated indirect injection 1.5 L engine. In 1978, the first turbo-diesel car was produced by Mercedes-Benz. The Mercedes-Benz 300SD, which was launched only in the United States, used a Garrett AiResearch turbocharger for boosting the amount of air supplied to the engine [4]. In early 1979, Peugeot 604 was the first turbo-diesel car launched in Europe. Since then, turbo-diesel cars have been produced in huge numbers and sold all over the world [5].

Diesel cars were steadily and successfully introduced into the automobile market as they benefit from high torque, improved fuel efficiency and increased life span compared to other reciprocating engines. In 1973, diesels comprised 2.5% of the European market. Two years later, following the 1973 oil crisis, the share increased to 4.1%. By 1980, the diesel share in the European market doubled to 8.6%, and in 1983 almost 11% of new car sales in Europe were diesel-powered [6]. The increase of the diesel share in the European market was rapid in the following years. By 2000, more than 31% of new car sales in Europe were diesel-powered. Since 2000, the increase of the diesel share in the European market was steady until 2007 when the European diesel share peaked at 51.78% [7]. By 2009, Luxembourg and Belgium were the two European countries with the highest percentage of diesels, with more than 60% of vehicles there being diesels, in the automobile market [8]. In the UK, the sale of diesel cars outstripped petrol cars for first time in 2011 [9].

The growth of the diesel share in the automobile market is due to the robustness, reliability and capability of the engine to produce outstanding torque at low speeds. However, concerns over the emissions of diesel cars have led to the introduction of legislated emission standards. The first emissions legislation was promulgated by the State of California in 1966, and two years later the standards were adopted by United States Environmental Protection Agency (EPA) for the whole country [10]. The legislation standards were progressively tightened over the following years. The European Union has launched "Euro" emission standards since 1993. The Euro 1 legislation for diesel cars limits the NO_x formation of cars to 2 g/kWh and Particulate Matters (PM) to 0.36

g/kWh. The most recent legislation, Euro 6, set in 2014, has dramatically reduced the maximum allowed standards to 0.46 g/kWh for NO_x emission and 0.01 g/kWh for PM emission [11].

The demanded emissions drop set by the European and American legislation has been impressive over the last 20 years. In order to meet the constantly changing emission standards, manufacturers of diesel engines and cars have invested heavily in new technologies that could help reduce the amount of pollution coming from diesel cars. The reduction of emissions output from diesel cars can be achieved initially by controlling the combustion process using various techniques such as Exhaust Gas Recirculation (EGR), advanced injection strategies, alternative fuels and modes of combustion. In addition, the formed emissions could be further reduced by implementing after-treatment systems such as catalysts and particulate filters.

The combustion process and pollution of a diesel engine are directly influenced by the spatial and temporal distribution of fuel within the cylinders. The development and use of common rail direct fuel injection technology in the mid-1990s has improved the flexibility of the fuel injection strategy in the cylinder. Modern DI diesel engines with common rail technology can reach fuel pressures up to 2,500 bar and up to nine injections per cycle [12]. Extended research has been carried out aimed at investigating the effects of fuel pressure, injection timing and advanced injection strategies (such as number of injections and injection ratio) on the performance and pollution of diesel engines. Multiple injection strategies have been used in the past for reducing the noise and pollutants of diesel engines. At the same time, high-pressure fuel injections have enhanced fuel vapourization within the cylinder and improved air-fuel mixing quality.

Improving air-fuel mixing quality within the combustion chambers of diesel engines has been a crucial objective for diesel engine manufacturers. Homogeneous Charge Compression Ignition (HCCI) and Premixed Charge Compression Ignition (PCCI) modes of combustion are frequently used partially in diesel engines for improving the homogeneity of the air-fuel mixture within the cylinder for low-temperature combustion and reduced NO_x and soot formation. The two combustion modes facilitate an early fuel injection

within the cylinder, creating a well-mixed air-fuel charge at the start of combustion.

With the increased freedom of injection control, multiple injections and alternative combustion modes can be simultaneously used for improving the diesel engine's performance, reducing fuel consumption, noise and pollutant emissions.

1.2 Aims and Objectives

The aim of this study is to quantify important parameters affecting the combustion process of diesel engines and that play a key role in performance and harmful emission characteristics. The main driving force behind this research work was the need for low-emission engines that comply with the stringent emission regulations for diesel vehicles.

The study investigates the effects of advanced air and fuel injection strategies, as well as piston geometry and spray angle on air-fuel homogeneity and the combustion process of the engine. The main objectives of this investigation are as follows:

- Gain sufficient understanding about the effects of multiple injections, injection pressure and ratio and dwell angles on combustion characteristics and emission mechanisms of diesel engine combustion.
- Investigate the effects of split injection strategies and highlight the benefits of reducing harmful emissions.
- Study the effects of early pilot injection on the combustion process.
- Measure air-fuel homogeneity in the combustion chamber of the engine using various injection strategies and analyse the effects of air-fuel mixing quality on the engine's performance and emissions.
- Investigate the effects of piston geometry and fuel spray angle on air-fuel mixing quality.
- Quantitatively define the premixed combustion ratio in PCCI mode and its effects on performance and engine emissions.
- Study the effects of injection ratio for multiple injection strategies with variable exhaust back pressure and exhaust valve opening times on combustion characteristics

and emissions formation.

1.3 Outline of Thesis

This thesis is divided into nine chapters, including this one, which provides background information and objectives of this research. In Chapter 2, a literature review of diesel engine combustion, including conventional and Low Temperature Combustion (LTC) engines, is presented. The chapter includes a detailed analysis of the harmful diesel engine emissions and the most advanced after-treatment systems used in the automotive industry. The effects of advanced air and fuel injection strategies on the performance and emission characteristics of diesel engines are outlined. The effects of combustion chamber geometry on the air and fuel flow phenomena and mixing quality are also discussed.

Chapter 3 gives a description of the combustion analysis tools used in this study. Two new parameters called Homogeneity Factor (HF) and Pre-mixed Charge Compression Ignition Strength (PCCI strength) are introduced and proposed as a measure of the air-fuel mixing quality and combustion characteristics, respectively. Statistical methods for reducing the number of experiments to a practical set are also analysed in this chapter.

Chapter 4 focuses on the Computational Fluid Dynamic (CFD) code and the mathematical models adapted in this research work. A detailed analysis of the sub-models used is presented, followed by a grid independence analysis and a model validation using experimental results conducted in a single-cylinder research engine.

Chapter 5 details the experimental test facility and gives a step-by-step guide to the assembly of the single-cylinder research engine. A detailed description of the instrumentation and measurement equipment is also provided.

Chapter 6 outlines the effects of split and multiple injections on the performance and emission characteristics of diesel engines. The chapter includes CFD simulation studies under single, split and multiple fuel injection strategies, and the results are analysed with the aid of the Homogeneity Factor.

In Chapter 7, an experimental analysis is performed for studying the effect of the

pre-mixed combustion phase on a diesel engine's combustion characteristics. In addition, the effects of exhaust back pressure with multiple injections strategies are investigated with the aid of statistical methods.

Chapter 8 presents a study on piston geometry and nozzle spray angle. Nine different piston geometries and three different injection angles have been simulated using variable fuel injection timings, quantities and pressures for understanding the air-fuel mixing phenomena and for measuring air-fuel homogeneity.

Chapter 9 details the major conclusions drawn, and possible areas for future investigation in line with this research work are recommended.

Chapter 2

Literature Review

The technology in internal combustion engines has developed rapidly in recent decades. Although the evolution of engine technology has been impressive, the need for further improvement in terms of low-emissions engines is challenging for engineers and vehicle manufacturers. Future diesel engines should incorporate greener, more economic and high-power capabilities into their designs in order to stay competitive and respond to environmental and sustainability issues. Combustion control is a key characteristic of economic, clean and powerful Direct Injection (DI) diesel engines. The combustion process can be controlled directly by modifying air-fuel mixing quality within the combustion chamber. In addition, alternative combustion modes can be partially used at the moment or fully used in the near future for emission minimization. After-treatment technology has also evolved over the years, proving that emissions could be reduced without sacrificing durability or fuel economy or without increasing maintenance costs.

In this chapter, a literature review is presented on diesel engine emissions characteristics. Next, current after-treatment technology is discussed. Finally, a thorough review of the conventional and alternative modes of diesel combustion as well as the air-fuel path effects on the emissions and performance characteristics of engines is conducted.

2.1 Diesel Engine Emissions

The introduction of emission legislation for automobiles began in the late 1960s after a series of studies into the numerous sources of air pollution in the United States. The studies attributed a significant portion of the air pollution to automobiles and concluded that air pollution should be bounded. Initial emission legislation was promulgated by the State of California, and two years later the standards were adopted by United States Environmental Protection Agency (EPA) for the whole country [10]. The standards were reviewed every couple of years.

In 1987, Tier 0 was the new emission standard adopted by federal US legislation, followed by Tier 1 standards for light-duty vehicles in 1994[13]. Before the introduction of Tier 2 standards in 2004, the National Low Emission Vehicle (NLEV) program for passenger vehicles and light-duty tracks certified the low emission levels of vehicles [14]. Tier 2 standards use eight certification "bins" to allow averaging across a greater level of emission diversification. Tier 3 standards were finalized in March, 2014 and are expected to be phased in from 2017 and fully adopted by 2025 [15].

The first emission legislation adopted in Europe was directive 70/220/EEC in March of 1970. In July of 1992, the Euro 1 standards were introduced, followed by Euro 2 in 1996 and Euro 3 in January of 2000. The Euro 3 standards were the first European legislation setting a limit of 0.5 g/km on NO_x emission caused by passenger diesel cars. The limit was reduced to half in 2004 by Euro 4 standards and was further tightened to 0.18 g/km by Euro 5 standards in September, 2009 [16]. The most recent European regulation, Euro 6, was adopted in September of 2014. Many countries now adhere to stricter emission standards. Tier and Euro emission standards are the governing legislative standards for automobiles in the world. Figure 2.1 presents the NO_x and particulate matter Euro and Tier limits for light-duty diesel vehicles.

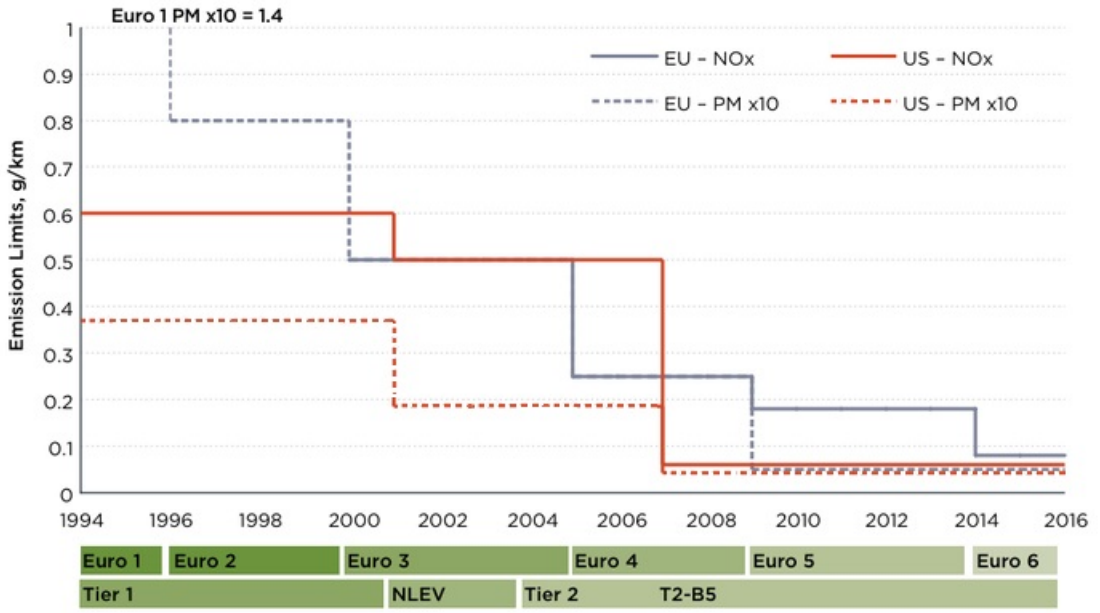

Figure 2.1: European and American NO_x and PM emissions standards of light-duty diesel vehicles [17].

2.1.1 Particulate Matter

Particulate matter is a complex aggregate of solid, liquid materials and chemical constituents. It contains both primary components, which are emitted directly into the atmosphere, and secondary components, which are formed within the atmosphere as a result of chemical reactions [18]. Diesel engines are one of the major sources of particulate emissions. It is estimated that approximately 0.2-0.5% of fuel mass is emitted as small (~0.1 μm diameter) particulates [1]. The amount of particulate matter emitted by a diesel engine is extremely dependent on equivalence ratio. The soot fraction is mainly formed in fuel-rich areas where fuel pyrolysis, the process of hydrocarbon chain decomposition at a certain temperature and in the presence of oxygen, is likely to take place [19]. Although most of the soot formed in the cylinder is oxidized during the expansion process where the gases have cooled considerably, particulate matter remains a significant contaminant produced by diesel engines.

The PM is generally divided into three basic fractions [20].

1. Solids - Dry carbon particles, commonly known as soot.
2. Soluble organic fraction (SOF) - Heavy hydrocarbons absorbed and condensed on the carbon particles.
3. SO4 - Sulphate fraction, hydrated sulphuric acid.

The composition of particulate matter is dependent on the engine and driving conditions. Wet particulates are rich in hydrocarbon, while dry particulates mostly consist of carbon particles. The particles are also divided into two main categories according to their size. Coarse particles (PM_{10}) are between 2.5 and 10 μm, and fine particles ($PM_{2.5}$) are smaller than 2.5μm. Figure 2.2 compares the size of PM_{10} and $PM_{2.5}$ with a human hair and a fine grain of beach sand.

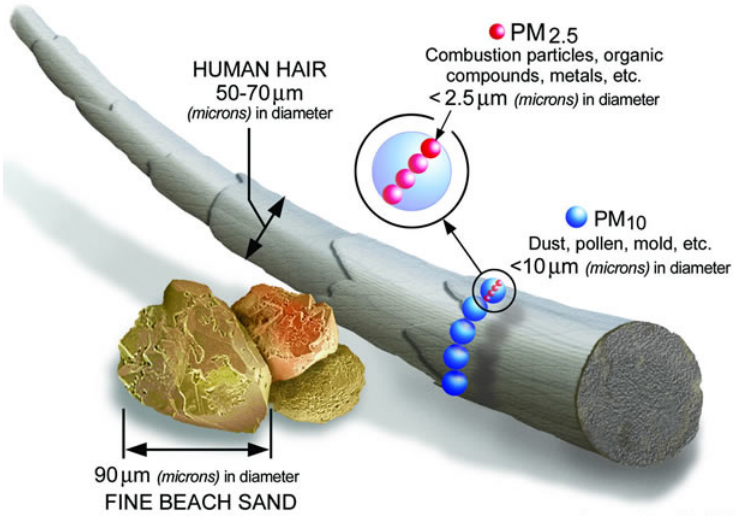

Figure 2.2: Size of airborne particles [21].

2.1.1.1 Particulate Matter Effects

The $PM_{2.5}$ can cause serious health effects compared to PM_{10}, as they are highly respirable. Larger particles pose little health risk, and although they can be inhaled, they

cannot penetrate beyond the mouth and nose. Particulate pollution can have serious effects on the human body. Figure 2.3 shows the effects of different sizes of PM on the human body. Recent studies [22, 23] have indicated that PM can cause inflammation of lung tissue and lung irritation, which can lead to lung tissue permeability and immune susceptibility. In addition, particulate matter can contribute to environmental damage by depleting forests and farm crops, as well as causing sulfuric acid rain, which, in turn, damages nutrients in the soil and makes lakes and streams acidic. Aesthetic damage can also occur by staining culturally important statues and monuments.

Particulate matter, when combined with ground-level ozone, can cause smog, a combination of smoke and fog. Smog is extensively formed near coastal cities with high levels of pollution and humidity. It can reduce natural visibility, aggravate asthma and irritate the eyes and respiratory tract [24].

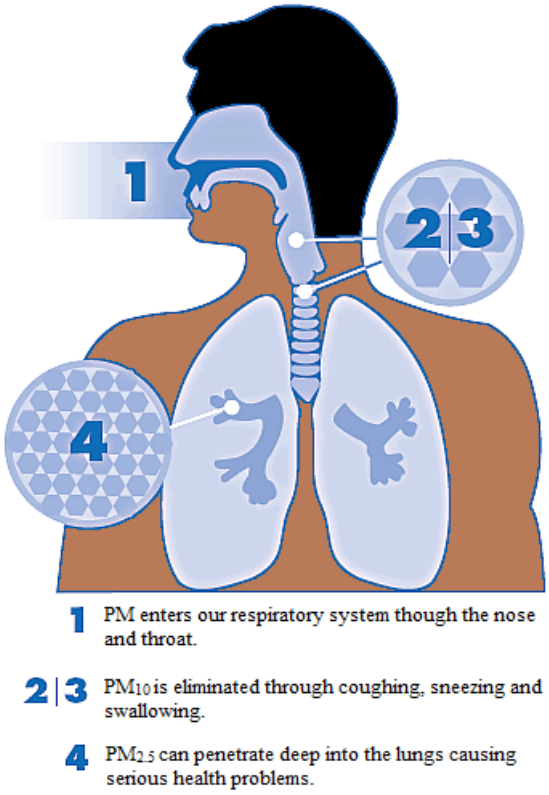

Figure 2.3: How particulate matter enters our body.

2.1.2 NO_x Emission

Nitrogen oxide is another major pollutant formed during diesel engine combustion. The mixture of nitric oxide (NO) and nitrogen dioxide (NO_2) is referred to as NO_x. Nitrogen oxides are produced by the reaction of nitrogen and oxygen in the air at temperatures exceeding 1640K [25]. Concentrations of NO_x in diesel exhaust are typically between 50 and 1000 ppm depending on the engine and its load and speed conditions [26]. Approximately 70-90% of nitrogen oxides consist of NO, while only 10-30% is actual NO_2. The NO composition is higher (approximately 95%) in old naturally aspirated diesel engines compared to turbocharged diesel engines (without after-treatment) in which the NO_2 composition can reach 15%. According to British data, the fraction of NO_2 in vehicle NO_x emissions (all fuels) increased from around 5-7% in 1996 to 15-16% in 2009 [27].

2.1.2.1 NO_x Formation

The process of NO_x formation is described below by the highly temperature-sensitive extended Zeldovich mechanism.

$$O + N_2 \longleftrightarrow NO + N \tag{2.1}$$

$$N + O_2 \longleftrightarrow NO + O \tag{2.2}$$

$$N + OH \longleftrightarrow NO + H \tag{2.3}$$

Equations 2.1 and 2.2 were developed by Zeldovich [28], while equation 2.3 was identified by spectroscopic means and added later by Lavoie *et al.* [29]. As stated earlier, NO formation is only significant in high-temperature regions as a result of excess oxygen exposure to nitrogen molecules. In the presence of excess oxygen, NO_2 is formed as a result of NO and O_2 reaction. The reaction time is relatively slow and depends on the NO concentration in the air [30].

NO_x formation in DI diesel engines is significant due to the air-fuel heterogeneity in the cylinder, leading to fuel-rich regions and high local combustion temperatures. The temperatures within the cylinder are often higher than 1700K, leading to excess NO_x

formation. Figure 2.4 illustrates the NO_x and soot formation areas for a diesel engine running at 1,600rpm. As stated in chapter 2.1.2.1, soot formation mainly occurs in the presence of fuel-rich mixtures, while NO_x formation takes place in higher-temperature regions.

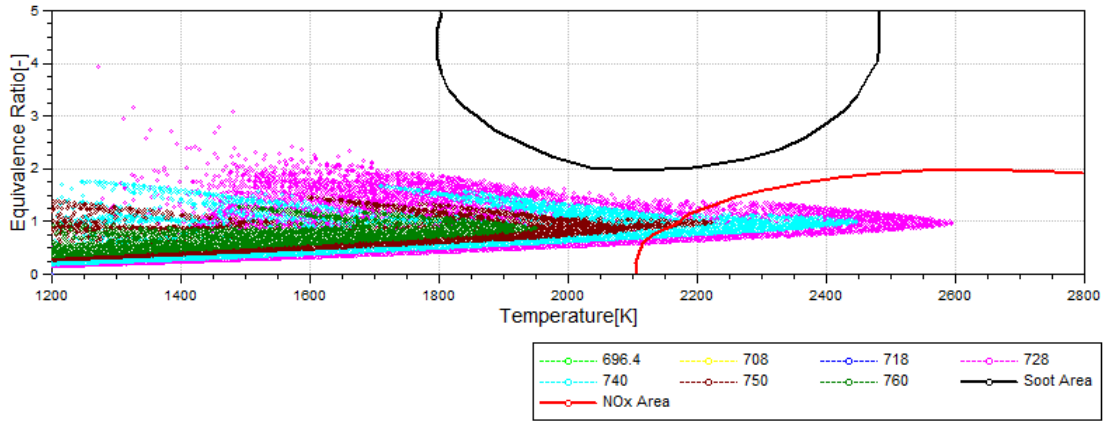

Figure 2.4: Fuel-air equivalence ratio (Φ) - T diagram.

Achieving a homogeneous air-fuel mixture at lean operating conditions by facilitating premixed combustion can significantly reduce the near-stoichiometric regions and, therefore, reduce the temperature within the combustion chamber of a diesel engine. Premixed combustion can be partially achieved in modern diesel engines by implementing early advanced injection strategies or by adopting alternative combustion modes such as HCCI and PCCI. The drawback of premixed combustion is that most of the time it leads to an increase of PM. The reduction in excess oxygen caused by resending inert gases back to the combustion chamber is an effective method that has been used in the automotive industry for controlling NO_x formation. In addition, more techniques such as alternative fuels, water injection and emulsified fuel with water are under investigation as prospective solutions to further reduce NO_x formation [31, 32, 33, 34, 35, 36, 37]. Although the use of such techniques can significantly reduce NO_x formation, they may result in an increase in fuel consumption.

2.1.2.2 NO_x Emission Effects

Nitrogen oxides are poisonous to humans and are serious health hazards. It has been proven that exposure to small levels of NO_x can cause nausea, eye and nose irritation and shortness of breath. High levels of NO_x can have serious effects on the respiratory system and lead to lung irritation and/or death [38]. In addition, when NO_x is reacted with volatile organic compounds in the presence of heat and sunlight, ground-level ozone is formed. Ozone can have serious human health hazards, as well as damage plants, crops and textiles and other materials. NO_2 reacted with water in the form of rain results in the formation of nitric acid, known as acid rain. Acid rain is harmful to the environment, as it can damage plants, trees and cars and structures like buildings and historical monuments. In addition, NO_2 contributes to the formation of smog.

2.1.3 Unburned Hydrocarbons

Hydrocarbon emission generally refers to unburned fuel [39]. Unburned Hydrocarbons (UHC) consist mainly of major and minor species of fuel composition, as well as species from incomplete chemical reactions within the cylinder. UHC in diesel engines are generated due to the following reasons.

1. Flame-quenching layer caused within the cylinder as a result of the flame extinguishing near the cold boundaries [40].

2. Unburned fuel trapped within the piston crevices.

3. Fuel dribbling from injector nozzle sac after completion of injection [41].

Under extreme operating conditions such as cold starting or long idling, UHC could also be formed as a result of wall wetting and cyclic misfire[42].

Hydrocarbon emissions are higher in rich air-fuel mixtures. However, a very lean air-fuel mixture will also increase the UHC emissions due to reduced flammability in the combustion chamber. HC formation in regards to the engine parameters has been investigated by many research groups. Ikegami *et al.* [43] and Xiao *et al.* [44] investigated

the effects of ignition delay on UHC formation and found that a long delay could have a negative impact on hydrocarbon emissions. Nakayama *et al.* [45] studied the effects of valve timing on the formation of UHC, and Tsunemoto *et al.* [46] investigated the effects of combustion and injection systems on HC and PM emissions. A trade-off between simultaneous reduction of NO_x and soot formation and an increase in UHC emissions has been observed for alternative combustion strategies [47, 48].

2.1.3.1 Unburned Hydrocarbons Effects

Hydrocarbons as well as NO_x are hazardous in the presence of sunlight due to the formation of photochemical smog and ground-level ozone. The negative effects of smog and ozone have been analysed in section 2.1.1.1 and 2.1.2.2. Hydrocarbons are harmful and extended exposure can cause drowsiness and eye irritation. In more severe cases, hydrocarbons can be carcinogenic, damage lung tissue and cause pneumonia or death [49].

2.2 Aftertreatment

The reduction of emissions from diesel engines can be achieved initially by optimizing the choice of operating parameters and controlling the combustion process. In the second stage, emissions can be further reduced with the implementation of after-treatment systems. However, the increased cost and weight, as well as the servicing cost of such systems, make them reliable secondary measures in reducing exhaust emissions and not a replacement of combustion controlling techniques [50].

2.2.1 Diesel Particulate Filter

When the Euro 5 legislation came into force, new diesel cars were required to have a Diesel Particulate Filter (DPF) in their exhausts. A DPF is designed for the removal of diesel particulate matter or soot from the exhaust tailpipes of diesel cars. A DPF can usually remove a large amount of the soot that can sometimes reach nearly 100% under

certain conditions [51]. A DPF has a honeycomb shape made of ceramic or metal fibre, which restricts the flow of the exhaust gas. As a result of the restricted flow within the DPF, exhaust gas is forced through the walls of the DPF where the PM is trapped by the pores of DPF.

The major challenge in the design of a DPF is to clean the trap from collected particulate matter in a reliable and cost-effective matter [20]. Regeneration is the process of emptying the filter of particulates in order to maintain performance. Regeneration can be achieved either passively when the exhaust temperature is high or by using active techniques. Due to low diesel exhaust temperatures, active regeneration is often applied in modern DPF systems. Active regeneration can be achieved by facilitating late post-combustion fuel injection to increase the exhaust temperature [52, 53]. Post-injection is usually triggered when the filter reaches a soot level of about 45%. Low-pressure fuel injection in the exhaust manifold to increase temperature is also another more rarely used method of active regeneration. The use of an oxidizing liquid catalyst additive in the fuel for lowering the regeneration temperature of the soot is also applied by some DPF models. By lowering the regeneration temperature is more like the passive regeneration to be successful. In addition, the use of a catalytic coating for achieving continuous catalytic regeneration is available in some DPF models.

2.2.2 NO_x Absorber

The reduction of NO_x emissions formed during CI engine combustion can be reduced by destroying the NO_x molecule. This destruction can be achieved by removing the oxygen (O) molecule, leading to formation of gaseous N_2 when nitrogen molecules combine. However, this is inherently difficult to facilitate in the exhaust emissions of a diesel engine where a large amount of the exhaust gas consists of oxygen. The NO_x absorber, also known as an NO_x trap, is a device designed to absorb nitrogen oxides from the exhaust of diesel engines. This technology has made significant progress in recent years and is now being applied to gasoline- and diesel-powered vehicles. The reduction in NO_x emissions can be as high as 90% or even exceed this figure for light-duty diesel-powered

vehicles [54, 55].

The NO_x conversion to nitrogen gas and water takes place in two sequential steps. Initially, the NO is catalytically oxidized to NO_2 by employing precious metal on the surface of the absorber. In lean-burn conditions, the NO_2 is adsorbed by an adjacent alkaline earth oxide site where it chemically reacts and is stored as a nitrate [54]. The second stage of the process, which involves the regeneration of the trapped emission, takes place before the absorber reaches its full capacity. In rich-burn conditions, large amounts of emitted unburned hydrocarbons and carbon monoxide (CO) contribute to the conversion of trapped NO_x to carbon dioxide and nitrogen gas. The regeneration process is critical to the performance of the absorber and must be accurately managed in order to ensure that nitrogen oxides will not escape the trap and be released into the environment.

2.2.3 Selective Catalytic Reduction

Selective Catalytic Reduction (SCR) is another method of converting nitrogen oxides to N_2 and water. The conversion takes place by injecting a liquid reductant agent, usually ammonia or urea, through a special catalyst in the exhaust system of the vehicle. The liquid reductant agent, also known as Diesel Exhaust Fluid (DEF), catalytically reacts with NO_x, forming nitrogen gas, water vapour and tiny amounts of CO_2.

SCR is a promising technology that can reduce NO_x levels up to 90% under certain conditions [56], and it does not affect engine performance and fuel consumption, as the engine design and combustion parameters are not altered. This technology has been widely adopted by most heavy-duty vehicle manufacturers since the beginning of the decade. However, the need to store DEF and other disadvantages like the need for DEF refilling and ammonia leakage make this system less desirable for light-duty diesel-powered vehicles where issues of size and weight are of great concern.

2.2.4 Diesel Oxidation Catalyst

Diesel Oxidation Catalysts (DOC) are used on all diesel-powered engines for the oxidation of carbon monoxide, unburned hydrocarbons and soluble organic fraction of particulate matter. DOC benefit from a honeycomb structure with many small parallel channels coated with an active catalyst substance such as platinum or palladium. The large number of parallel channels increases the contact area and promotes the conversion of exhaust pollutants into CO_2 and water.

DOC is a cost-effective and robust method that can convert more than 90% of CO and UHC and more than 50% of SOF of the exhaust gas under certain conditions [57]. In addition, a DOC can promote the passive regeneration of particulates in a DPF system. The released fuel energy from oxidation reactions increases the exhaust gas temperature before it reaches the DPF system and, therefore, passive regeneration is more likely [58].

2.3 Diesel Combustion

A diesel engine is an internal combustion engine that uses the heat generated by the compression of air to ignite and burn the fuel that has been previously injected into the combustion chamber. Diesel engines can be divided into two main categories based on the number of strokes the engine cycle completes.

1. Two-stroke diesel engine.

2. Four-stroke diesel engine.

In addition, diesel engines are categorized as direct (DI) and indirect (IDI) injection engines based on fuel injection system. Indirect injection engines utilize a pre-combustion chamber where the fuel is injected at lower fuel pressure (usually between 100 to 350 bar) and rapidly mixes with the air before it enters the combustion chamber. In DI engines, the fuel is injected under high pressure directly into the combustion chamber. DI engines are the most popular and used exclusively in vehicles today.

2.3.1 Conventional Diesel Combustion

A two-stroke engine is mechanically simpler than a four-stroke engine. However, the thermodynamic and aerodynamic processes involved are much more complicated due to the fact that more than one function occurs during each stroke of the engine. A two-stroke engine lacks an inlet valve, which allows air to enter the cylinder through ports. The air entering into the cylinder forces out any combustion gases from the previous cycle. As the air is compressed within the cylinder by the rising piston, fuel injection takes place near the top dead centre (TDC) (in DI engines), resulting in the combustion of the mixture due to extremely high pressure and temperature within the cylinder. The combustion force moves the piston downwards where the exhaust gases are being expelled from the exhaust port out of the cylinder with the help of the fresh air inlet charge. Figure 2.5 illustrates the cycle of a two-stroke diesel engine.

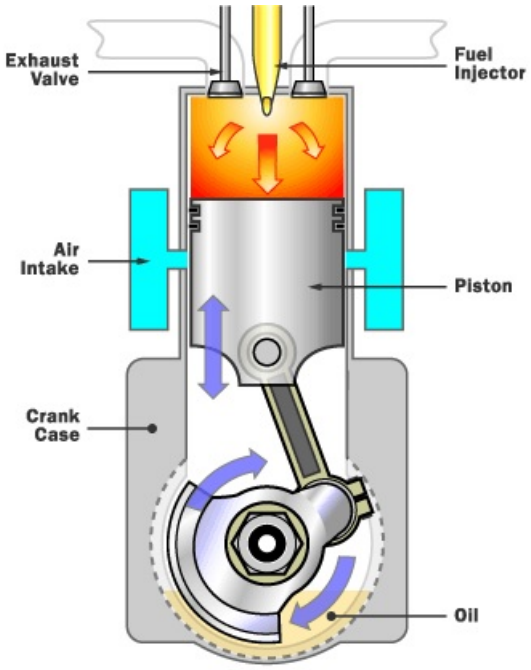

Figure 2.5: Two-stroke DI diesel engine [59].

Two-stroke diesel engines can produce twice the power of four-stroke engines in the

same time. They are commonly used for on- and off-road trucks, as well as in marine, railway and stationary applications. However, there are some basic disadvantages that limit their use in light-duty vehicles. Two-stroke engines are noisy, more polluting and require extensive cooling and lubrication.

On the other hand, in a four-stroke diesel engine, the cycle is completed after four separate strokes. The first stroke involves the opening of the intake valve for air introduction into the cylinder. The air is then compressed by the piston moving upwards, and fuel injection occurs once the piston approaches TDC (in DI engines). The power stroke follows, and the piston is forced downwards after combustion within the cylinder. The final stroke is the exhaust where the upward-moving piston forces the exhaust gases out of the cylinder through the exhaust port. Figure 2.6 shows the cycle of a four-stroke diesel engine.

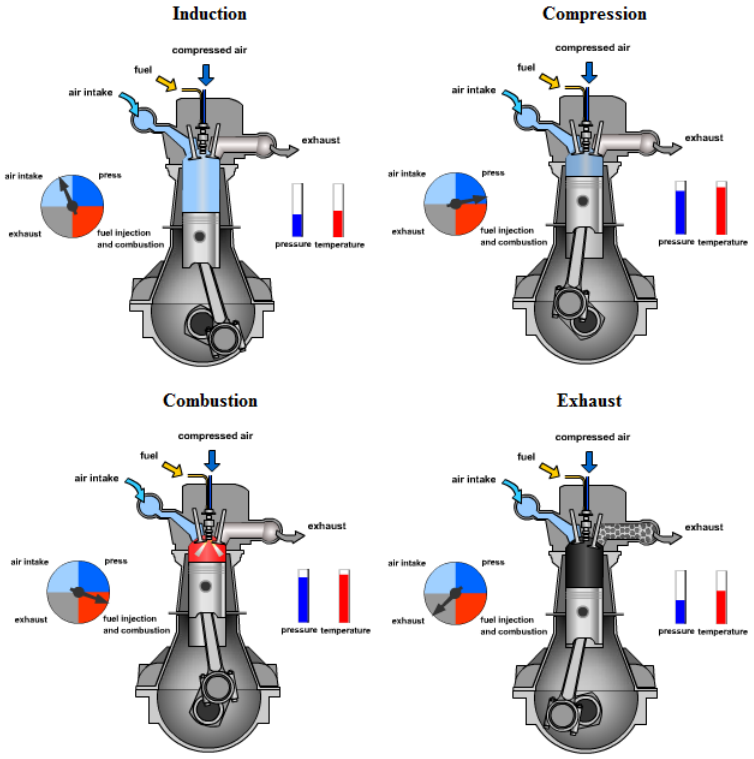

Figure 2.6: Four-stroke DI diesel engine cycle [60].

Four-stroke engines have a more complex design, are heavier, cost more and produce less power than two-stroke engines. However, they are highly preferred in the automotive industry due to the fact that they produce significantly fewer emissions, have a longer life expectancy and are less noisy.

The combustion process of a four-stroke diesel engine based on the heat generated during the engine cycle is illustrated in Figure 2.7. The combustion process consists of several interdependent phases.

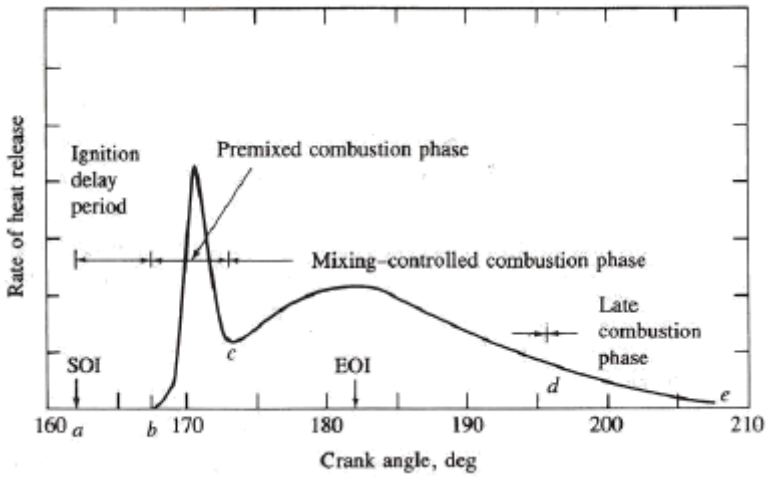

Figure 2.7: Diesel combustion heat release rate [1].

The ignition delay is the period between the Start of Injection (SOI) and the Start of Combustion (SOC). The duration of the ignition delay can have a significant effect on the combustion process that follows. A long ignition delay can result in a rapid in-cylinder pressure increase at the SOC, which will contribute to increased NO_x formation. The air-fuel combustion process can be divided into three stages. The first stage is the premixed combustion where the evaporated fuel and air mixture created during the ignition delay period auto-ignites. The air-fuel mixing at that point is slightly rich, nearly stoichiometric, which results in a rapid and intense in-cylinder pressure and temperature increase. The premixed combustion phase is mainly responsible for NO_x formation due to high in-cylinder temperatures. Once the premixed fuel is ignited,

diffusion of the flame to the remnant or newly introduced fuel occurs during mixing in the controlled combustion phase. The lack of oxygen during this phase, as it was mostly burnt during the premixed phase, leads to a slower combustion rich in soot production. The last stage of the combustion involves the partial oxidization of the remaining fuel. The temperature during this phase of combustion is relatively low, which leads to the termination of combustion.

2.3.2 Low Temperature Combustion

Advanced combustion concepts such as Homogenous Charge Compression Ignition (HCCI) and Premixed Charge Compression Ignition (PCCI) are promising solutions for reducing the emissions of DI diesel engines and meet the very strict standards set in recent years. The recently developed combustion concepts aim at reducing exhaust pollutants, while maintaining respectable fuel economy and combustion efficiency. The term Low Temperature Combustion (LTC) can be used to describe a combustion process where the in-cylinder combustion temperature is kept low in order to reduce NO_x generation within the engine. LTC is used as a general term including advanced combustion concepts like HCCI and PCCI discussed below. Alternative combustion methods (HCCI, PCCI) can be implemented by altering the fuel injection timing in order to achieve a more homogeneous air-fuel mixing, which results in low-temperature combustion. With modern advanced injection systems fitted in direct injection compression ignition engines (DICI), alternative combustion modes can be easily adopted by early fuel injection(s) within the cylinder. Injection timing plays a vital role in the combustion characteristics of the engine and in emissions formation. In addition, LTC can be achieved by introducing significantly cooled EGR rates back into the inlet manifold or by in-cylinder water spraying without necessarily altering the fuel injection characteristics.

2.3.2.1 Homogenous Charge Compression Ignition

In 1979, Onishi *et al.* [61] and Noguchi *et al.* [62] investigated auto-ignition phenomena in two-stroke engines to achieve lean combustion at part-throttle. They referred to this

combustion method as Active Thermo-Atmosphere Combustion (ATAC) and Toyota-Soken (TS) respectively. A few years later, Najt and Foster [63] were the first to use this combustion method, named as Compression-Ignited Homogenous Ignition (CIHI) combustion by them, in a four-stroke diesel engine. The term Homogenous Charge Compression Ignition (HCCI) was first used by Thring [64] in 1989 when he investigated the stability of HCCI operating conditions of a four-stroke engine.

The principle of the HCCI combustion method is to achieve a homogeneous mixture before the start of combustion. A homogeneous air-fuel mixture can reduce combustion temperatures and, hence, NO_x formation, while the lack of fuel-rich regions can significantly reduce soot generation. In order to achieve low-temperature combustion, well-mixed air and fuel enter the combustion chamber and are compressed to the point of auto-ignition. Figure 2.8 illustrates the principle of NO_x and soot reduction for the HCCI, PCCI and LTC (described below) combustion modes compared to conventional diesel engine. In HCCI strategy, the air-fuel mixture ignites without the help of any direct combustion initiator; therefore, the auto-ignition timing is solely dependent on the chemical-kinetic reactions of the mixture [65]. The auto-ignition timing in HCCI engines occurs over a wide range of operating conditions, i.e. low load and cold start, has been a challenging issue, with many researchers using alternative methods such as EGR, air induction heating, Variable Valve Timing (VVT) and Variable Compression Ratio (VCR) for controlling SOC timing [66, 67, 68, 69].

In 1996, Ryan *et al.* [70] modified a single-cylinder DI diesel engine to operate in HCCI mode. Their investigation proved that HCCI ignition timing can be determined by looking further into the compression ratio (CR), EGR and air-fuel ratio of the engine which are the practical controlling factors in achieving satisfactory operation. Olsson *et al.* [71] and Law *et al.* [72] studied the effects of VCR on ignition timing control. They investigated the effects of VCR by ranging the compression ratio from 10:1 to 28:1 and showed that NO_x and smoke emissions were not affected by CR. However, there was an increase in UHC and a decrease in combustion efficiency at high compression ratios. Law *et al.* [73] reported the need for high CR to maintain correct maximum

brake torque in engine modes with low inlet temperatures and lambdas, and concluded that VCR can be used instead of inlet heating to achieve HCCI combustion. The effects of EGR on HCCI combustion and emission performance have been investigated by many researchers. Shi *et al.* [74] analysed the effects of internal and cooled EGR ratios on HCCI engine performance. They found that cooled external EGR can delay the start of combustion effectively, which is very useful for high cetane fuels like diesel, which tend to self-ignite more easily compared to other fuels. Shi et al. also showed that formation of a homogeneous mixture and further reduction in smoke emissions, though lowering the high load limits of HCCI, is an internal EGR benefit. Peng *et al.* [75] experimentally investigated the effects of air-fuel ratios and EGR rates on HCCI combustion rates. They found that auto-ignition timings of diesel HCCI combustion are very sensitive to EGR rates, but combustion durations primarily depend on the air-fuel ratios. Low-temperature combustion helps to keep NO_x emissions near zero. However, HC and CO emissions were high due to incomplete combustion caused by misfire.

Variable valve timing (VVT) technology has also been used for changing the effective compression ratio and/or the amount of hot exhaust gases trapped in the cylinder in order to control ignition timing in HCCI engines. VVT technology is particularly attractive due to the rapid response time, which could easily handle rapid transients (i.e. accelerations/decelerations) [76]. Peng and Jia [66] carried out an investigation into the effects of variable valve timing (VVT) and variable valve actuation (VVA) on gas exchange and fuel-air mixing processes in a diesel HCCI engine with early fuel injection. They found that reducing valve lifts alone is not an efficient way to retain the residual gas, but the function of reduced valve lifts will become obvious by combining it with an increase in negative valve overlap (NVO). Longer NVO will increase in-cylinder temperature because of the higher residual gases trapped in the cylinder, but will also improve the in-cylinder temperature homogeneity. Peng and Jia showed that VVT and VVA technology could be used for controlling HCCI ignition timing in transient conditions. HCCI technology can be achieved either with port fuel injection or DI engines. DI engines have the ability to maintain advanced injection strategies, which can improve

air-fuel mixing, balance the temperature and also work as an ignition trigger.

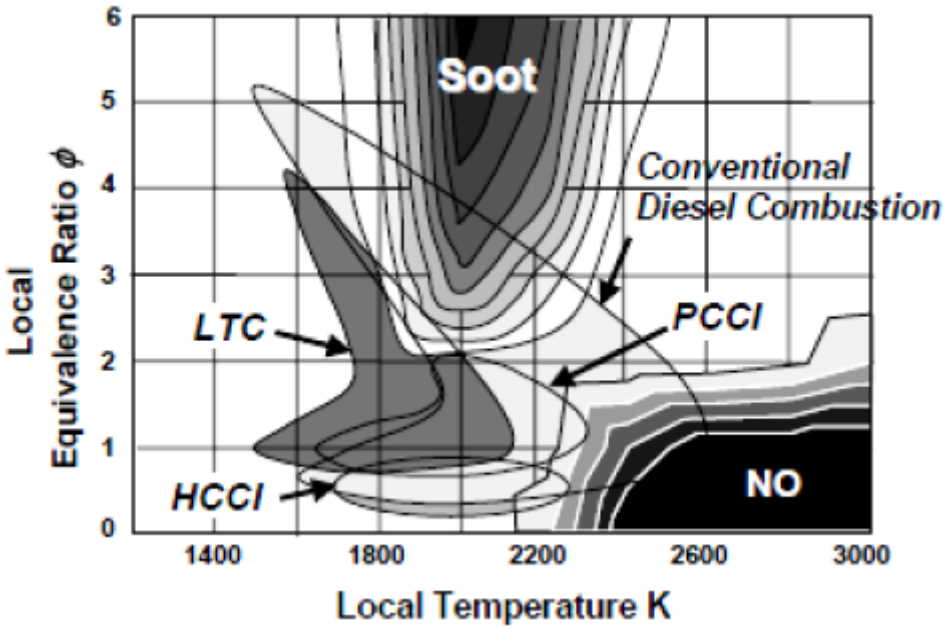

Figure 2.8: Φ-T diagram of conventional, HCCI and PCCI strategies [77].

Although HCCI is a promising technology in the reduction of NO_x and soot emissions, it suffers from relatively high UHC and CO emissions. Low-combustion temperatures of HCCI engines reduce the oxidization rate of any hidden fuel near the walls and in the crevice volumes of the cylinder. This incomplete combustion becomes evident near the low-load limit of HCCI engines, reducing combustion efficiency and, thus, indicated efficiency [65]. In addition, the fuel injection process is important for optimization of the air-fuel mixture and the avoidance of any fuel spray colliding with the cylinder walls causing wall-wetting. Increasing the fuel temperature, changing the fuel pressure, decreasing the injector hole diameters and applying multiple injections are some of the measures that can help to eliminate the wall-wetting effect of HCCI strategy and mitigate UHC and CO emissions [78].

2.3.2.2 Premixed Charge Compression Ignition

In 1996, Aoyama *et al.* [79] used the term Premixed Charge Compression Ignition (PCCI) for the first time in their experimental study on a converted single-cylinder engine with port gasoline injection. Later, the term was used by many researchers to define an alternative combustion strategy that uses one or more direct injection pulses for achieving a homogeneous air-fuel mixture. PCCI nowadays is a promising strategy that incorporates early fuel injection directly into the cylinder during the early-to-mid compression stroke in order to prepare a well-agitated ignitable mixture. The mixture can be either ignited by compression without the help of any combustion initiation, or a second (or more) fuel injection can follow near TDC, which works as an ignition trigger of the mixture.

Keeler and Shayler [80] defined PCCI combustion as an increased fraction of fuel burned at the premixed combustion stage compared to conventional diesel engines. In 1996, Takeda *et al.* [81] performed experimental analysis by implementing a very advanced injection timing to allow thorough mixing and avoid fuel-rich regions before the initiation of combustion. The authors concluded that early injection timing can reduce NO_x formation; however, UHC and CO increased due to mixture over-leaning. The high level of premixed charge in PCCI strategy leads to fast and rapid combustion with increased noise. In addition, PCCI benefits from reduced wall-wetting of the cylinder due to the moderately early injection timing [82]. However, the relatively advanced fuel injection timing and short combustion duration results in the combustion phase taking place far from TDC, which is not conducive to work conversion [83].

In order to avoid an early SOC within the cylinder, large amounts of cooled EGR are incorporated in PCCI combustion in order to reduce the in-cylinder temperature and delay the initiation of combustion [84]. The reduced temperature can contribute to the reduction in NO_x as well as prolong the mixing time, which results in fewer fuel-rich regions and lower soot generation. However, the extended use of high EGR rates for cooling the in-cylinder temperature negatively affects the evaporation period of the fuel, which can result in wall impinging, increase of UHC, fuel consumption and a reduction

in soot oxidation.

Kiplimo *et al.* [85] investigated the effect of EGR on the combustion characteristics of PCCI strategy. They observed that high EGR rates can reduce NO_x and soot emissions, though UHC and CO emissions were further increased. Hardy and Reitz [86] analysed the effect of EGR on a heavy-duty diesel engine for PCCI combustion. The authors applied an early injection at 60°BTDC and EGR rates up to 75%. High levels of EGR reduced NO_x formation, while soot emission was reduced by lowering the equivalence ratio through the use of intake air boosting. On the other hand, UHC and CO increased. Moreover, high EGR rates reduced combustion noise and decreased Brake Specific Fuel Consumption (BSFC) due to the decreased thermodynamic efficiency when the combustion phase retarded further after TDC. They also reported that the use of EGR reduced the in-cylinder peak pressure responsible for knocking due to instantaneous combustion after early fuel injection and, therefore, increased the range of operation. Zala [87] conducted experimental analysis with diesel fuel in a naturally aspirated four-stroke DI engine under constant speed and different EGR rates varying from 10% to 40%. He found that NO_x emissions could be reduced by up to 80% when using high rates of EGR. Figure 2.9 presents the emission trends at various EGR rates and injection pressures.

PCCI combustion seems to offer solutions for the reduction of NO_x and soot formation without significant impingement on fuel consumption. However, the increased UHC and CO emissions, as well as the limited operating range, hinder the application of this technology in modern diesel engines. The improvement of mixing by adopting alternative air induction, fuel injection and combustion techniques can potentially improve the performance of PCCI strategy.

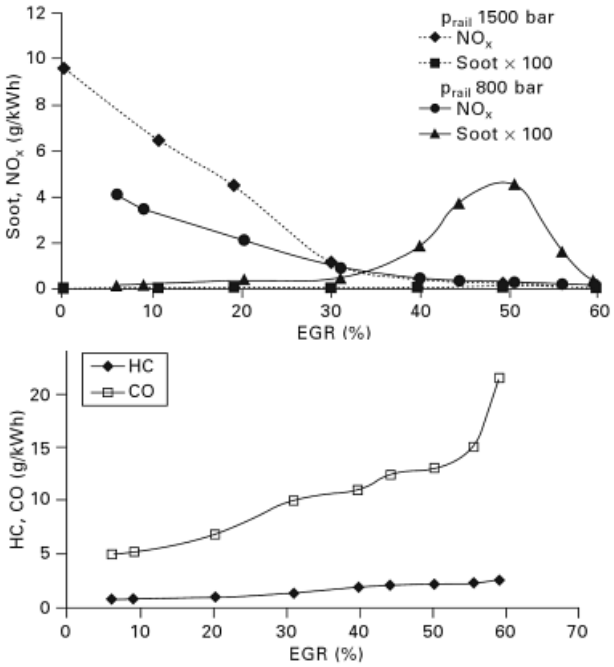

Figure 2.9: NO_x, Soot, HC and CO emissions trends at various EGR rates and fuel injection pressures [88].

Kimura *et al.* [89] developed the concept of Modulated Kinetics (MK) combustion by applying a late injection timing close to TDC in order to extend the ignition delay and promote mixing. The authors used high EGR rates, low CR and an optimized combustion chamber to control the ignition delay. They found that significant reduction in PM, NO_x and UHC can be achieved due to improved mixing and combustion chamber geometry. Park and Bae [90] explored the optimal injection timing for PCCI combustion by performing an experimental analysis on a single-cylinder engine. They found that ignition delay was longer in cases where the injection timing was increased to more than 20°BTDC. They also concluded that an injection timing between 20°and 30°BTDC provides sufficient timing for an enhanced air-fuel homogeneous mixture. The authors also investigated the effects of pilot injection with split ratios of 10% to 30% at 35°BTDC. The results indicated that pilot injection can contribute to the reduction of emissions and an increase in Indicated Mean Effective Pressure (IMEP) of PCCI engines. Horibe

et al. [91] and Kokjohn *et al.* [92] performed experimental analysis on the effect of split injection on PCCI combustion. The authors suggested different splitting strategies combined with boost pressure and EGR rates for low NO_x and soot formation with relatively minimal impingement by UHC and CO emissions. Mosbach *et al.* [93] and Su *et al.* [94] investigated the effects of direct injection timing on PCCI combustion and the use of a second late injection as an ignition trigger of the mixture. They found that two-stage injection is capable of triggering the charge ignition as a result of the local rich fuel parcels formed by the second injection. This can consequently extend the PCCI operating range. However, the second fuel injection led to local fuel-rich areas, higher combustion temperatures and, therefore, increased NO_x emission.

The effect of spray angles on the exhaust emissions of a PCCI engine was studied by Lee and Reitz. The authors, by using different spray angles ranging from 50°to 154°, found that soot and CO emissions are highly influenced by the spray angle, while NO_x emissions were not affected. Murata *et al.* [95] used a VVT system to study the effects of valve timing and Variable Valve Actuation (VVA) on a PCCI engine. The authors expanded the operating range of the engine to an IMEP of 1.30 MPa, while they simultaneously reduced NO_x and soot formation. Kook *et al.* [96] investigated the effects of swirl ratio on the air-fuel mixing behaviour of a PCCI engine. Their results showed that the influence of swirl ratio on the combustion mixing was lower than the influence of advanced injection timing. They also concluded that an optimal swirl ratio with certain injection timing can reduce CO emission and fuel consumption.

2.4 Air Path

The operation of diesel engines is based on the principle of air and fuel combustion with the aid of heat generated by the compression of the air trapped in the cylinder. The quality of the mixture as well as the air and fuel characteristics are principal factors in the quality and efficiency of combustion. Air is a mixture of oxygen and nitrogen molecules plus a small amount of other gases as shown in Table 2.1.

Table 2.1: Primary components of air.

Component	**% by Volume**	**% by Mass**
Nitrogen	78	75.5
Oxygen	21	23.1
Argon	0.9	1.3
Carbon dioxide	0.03	0.05

Oxygen is the only requisite component of air in the reaction with fuel to release energy, while the presence of nitrogen is responsible for NO_x formation at high combustion temperatures. Altering the quantity of the oxygen trapped within the combustion chamber can have a significant effect on the performance and emission characteristics of the engine. Boosting the air volume can ensure that there is sufficient oxygen for complete combustion, while the dilution of air with inert gases can control combustion temperatures. In addition, an optimized air swirl motion in the cylinder can contribute to enhanced air-fuel mixing.

2.4.1 In-cylinder Air Motion

In-cylinder flow patterns including swirl, squish and tumble motion are well-known to strongly influence both engine performance and pollutant emissions, by playing a major role in mixture formation, early ignition development stages, mixing-controlled combustion and late-combustion fuel consumption [97].

Swirl motion is the ordered rotation of air about the cylinder axis, and the swirl ratio, given by Equation 2.4, is altered by the design of the inlet passage. The swirl speed of an engine varies during the induction and compression stroke; therefore, the average value is used for calculating the swirl ratio.

$$swirl\ ratio = \frac{swirl\ speed\ (rpm)}{engine\ speed\ (rpm)} \tag{2.4}$$

Squish flow is the radially inward gas motion occurs in a diesel engine during the compression stroke as a result of the bowl-in piston shape. The squish flow is increasingly

generated when the piston is approaching the TDC by air squished into the piston bowl. Both the squish and the swirl flows have a significant effect on the air-fuel mixing procedure and, therefore, on the quality of the ignited mixture. Tumble flow is defined as a swirling motion of cylinder air around the transverse axis of the cylinder in the direction of the crankshaft axis [98].

It has been proven that swirl flow has the capability of enhancing air-fuel mixing and reducing soot emissions and fuel consumption of diesel engines. Karuppa and Manimaran [99] using Computational Fluid Dynamics (CFD) simulations showed that by varying the swirl ratio from 1.4 to 4.1 in a constant speed DI diesel engine, the peak pressure, peak temperature and peak heat release rate increased by 7%, 8.6% and 31% respectively. In addition, soot level reduced by 30 % but peak NO_x emissions increased by 54 %. Shundoh *et al.* [100] showed that a low swirl ratio reduced NO_x formation in a DI diesel engine by restricting air utilization as a result of limiting local mixture leaning. Ogawa *et al.* [101] used KIVA code to analyse the effect of swirl ratio on DICI engines. They concluded that by increasing the swirl ratio, soot emission decreased, but NO_x increased. However, very high swirl ratios led to an increase in soot emissions due to the increased fuel vapour concentration at the centre of the combustion chamber.

Gunasekaran *et al.* [102] investigated the effects of tumble motion with regards to fuel injection timing. They found that a high tumble flow with late injection provides a better mixture distribution and combustion characteristics compared to other flow structures. Jie *et al.* [103] investigated the effects of different tumble ratios on a single-cylinder engine. They revealed that in case of high tumble ratios, the BSFC and UHC decreased and NO_x increased at part-load. The Brake Mean Effective Pressure (BMEP) and combustion peak pressure increased at full load.

In contrast to swirl and tumble flows, squish turbulence is generated during the compression stroke of the engine cycle. The magnitude of the squish flow increases as the piston approached TDC and is mainly dependent on combustion chamber geometry. The level of squish and swirl flow interaction within the cylinder can have significant effects on air-fuel mixing quality, fuel economy and emissions generation.

2.4.2 Air Boosting

Downsizing of IC engines has been of great interest in recent years. Engine downsizing is the most important indirect fuel-economy measure [104]. By decreasing the cylinder's displacement volume and/or the number of cylinders of an engine, the friction, moving mass and thermal loss can be reduced, contributing to better fuel economy. Downsizing can be achieved by increasing the air pressure and, hence, density of the air before entering the engine cylinder. The air pressure can be altered by using a boosting device such as a supercharger or turbocharger.

Superchargers are seldom used in diesel engines, as they operate by absorbing power from the engine, thus reducing the efficiency. On the other hand, turbochargers are driven by the exhaust gas expelled from the cylinders. The exhaust gases from the cylinders spin the turbine, which transfers the motion to the compressor through a shaft that connects the two parts of the turbocharger as shown in Figure 2.10.

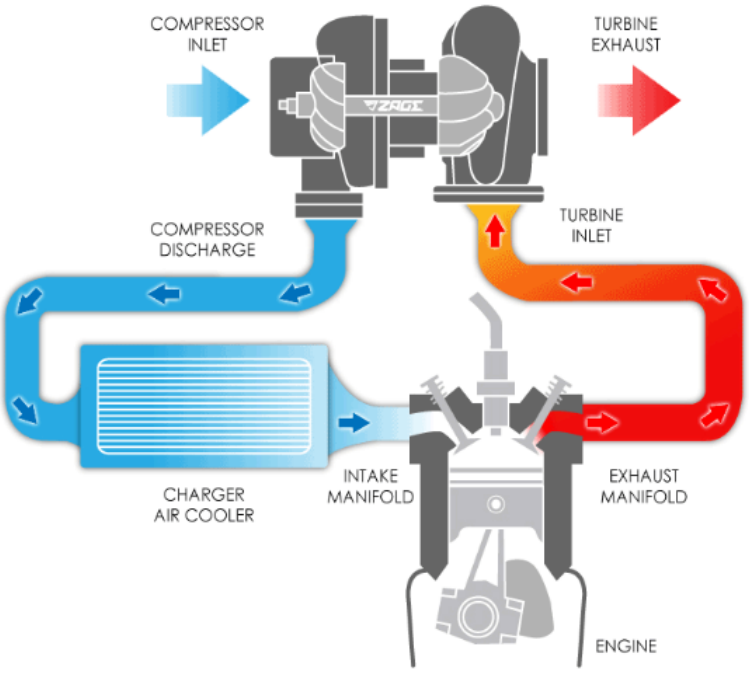

Figure 2.10: How a turbocharger works [105].

One of the main concerns of air boosting is using the right size of turbocharger for obtaining good performance at all operating speeds of the engine. Turbo lag in IC engines refers to throttle lag occurring due to insufficient exhaust gases driving the turbine at low engine speeds. This phenomenon can be reduced by implementing a smaller turbocharger, though this will result in lower performance at higher speeds.

Variable Geometry Turbochargers (VGT) , also known as Variable Nozzle Turbines (VNT), benefit from a ring of vanes that can be adjusted in order to alter the gas swirl angle and, therefore, the speed of air spinning the turbine of a turbocharger. The vanes of VGT, which are controlled electronically, remain closed at low engine speeds for higher exhaust gas acceleration and turbine speeds. At higher engine speeds, the desired boost is achieved by changing the opening range of the vanes. However, one of the main drawbacks of VGT is the increased pumping loss associated with vane closure, leading to poorer fuel economy [88].

The effects of air boosting on IC engine performance and emission characteristics have been investigated by many research groups in recent years. Uchida *et al.* [106] investigated the effects of air boosting on CI engines. They concluded that supercharging can reduce the ignition delay and enhance the diffusion combustion of an engine. This resulted in optimized fuel economy and lower emissions. However, NO_x emissions increased due to retarded injection timing. Tanin *et al.* [107] studied the effects of boost pressure by performing experimental analysis on a single-cylinder engine. They found that high intake pressures can contribute to the reduction of soot emissions due to the increased availability of air for soot oxidation at elevated intake pressures. Brake-specific NO_x emission remained constant. Zhang *et al.* [108] studied the effects of supercharging by conducting experimental analysis on an optically accessible DI diesel engine. They observed that in the diffusion combustion stage, the high boost pressure weakened the turbulence effect of the fuel injection and resulted in a smaller and less active flame movement. Consequently, at higher boost pressures, this might reduce the advantage of increased air availability. However, the authors observed increased soot oxidation at the surface of the flames as a result of the large amount of air available in the cylinder.

2.4.3 Exhaust Gas Recirculation

Exhaust Gas Recirculation (EGR) is a widely adopted method in diesel engines for reducing NO_x emissions. Burnt exhaust gases are recirculated back to the inlet manifold where they are reintroduced into the combustion chambers of the engine. The amount of EGR is dependent on the engine load and speed. The introduction of burnt gases into the cylinders lowers the in-cylinder charge temperature due to their higher specific heat capacity than air and reduces the amount of oxygen available during the combustion process. This results in a longer ignition delay with reduction in combustion rate and peak temperature. The low combustion temperatures lead to significant reduction of NO_x emissions. However, increased CO, UHC or even fuel penalty is observed. In addition, issues of increased engine wear and lower combustion efficiency are associated with the use of EGR.

The use of burnt gases in diesel engine combustion can be achieved by implementing an EGR valve (external EGR), which controls the amount of exhaust gas admitted to the intake manifold. Moreover, the internal EGR technique can be used in diesel engines without an EGR valve. Internal EGR can be achieved by valve timing arrangement in order to achieve some back-flow of the exhaust gas into the combustion chamber.

2.4.3.1 External EGR

External EGR is applied by adopting an EGR valve fitted at the exhaust manifold of an engine, which regulates the amount of burnt gas admitted to the intake manifold. The early EGR valves were operated using a vacuum diaphragm to allow and cut off the exhaust flow. Some of the early EGR valves were also fitted with a temperature-controlled shut-off valve in order to keep the valve closed in low-temperature conditions and ensure smooth engine operation. However, vacuum-operated valves lacked the control of EGR flow at idle and low speed, both conditions under which the use of EGR can cause rough engine operation. Later, EGR valves used a positive back pressure system, where the exhaust gas pressure pushes against a spring-loaded stem valve in order to allow the flow of EGR into the inlet manifold. At low engine speeds and idle, the exhaust

back pressure is not sufficient enough to open the passage and, therefore, there are no burnt gases flowing into the inlet manifold. Modern EGR valves are controlled by the Electronic Control Unit (ECU) of the engine. The ECU opens and closes the valves in response to input from engine sensors such as temperature sensor, VGT sensor, etc.

The external EGR concept benefits from the fact that burnt gas is expelled from the cylinder and is then reintroduced back to the inlet manifold. This makes it possible for the gas to be diverted through a heat exchanger, or EGR cooler, where it will be cooled down prior to its reintroduction into the engine. EGR cooling can contribute to further reduction of combustion chamber temperatures and NO_x emission.

Ladommatos *et al.* [109] investigated the effects of EGR on diesel engine emissions by performing experimental analysis on a 2.5L DI engine. The authors attributed the reduction of NO_x emission and the increase in PM to the dilution function of residual gas and to inlet charge oxygen. Ladommatos *et al.* [110] also observed that EGR caused a delay in the ignition of the air-fuel mixture, which moved the combustion process further towards the expansion stroke. This resulted in the combustion gases spending shorter periods at high temperature and, therefore, lower NO_x formation and reduced soot oxidation.

Matarelli *et al.* [111] studied the effects of cooled and uncooled EGR in a 2.5L turbocharged diesel engine. The authors found that cooled EGR was preferred for improving NO_x emissions, particularly at high load. They also recommended that the application of EGR should be combined with other optimization strategies such as fuel injection for improved results. Hountalas *et al.* [112] studied the effect of EGR temperature on diesel engine performance and emissions. They concluded that the decrease in EGR gas temperature resulted in reduced BSFC and soot emission, while there was only a small positive effect on NO. As revealed, the effect of low EGR temperature is more pronounced at high EGR rates. Ladommatos *et al.* [113] found that at a given engine speed and load, cooling the EGR increased the density of the inlet charge and the volumetric efficiency of the engine in comparison to cases with hot EGR. They showed that a substantial improvement in the trade-off between exhaust NO_x and soot emission could

be achieved by cooling the EGR. Arcoumanis *et al.* [114] found that cold EGR results in lower NO_x emission when the amount of EGR reintroduced to the inlet manifold is less than 30%. For EGR rates higher than 30%, uncooled EGR was preferred for NO_x reduction.

Peng *et al.* [115] conducted an experimental analysis on the effects of EGR on the combustion and emissions during cold starts of a DI diesel engine. The authors found that at maximum EGR, the lowest average opacity was achieved during several initial firing cycles of cold starts. However, at a later stage, high EGR rates led to excessive white smoke emission. NO_x formation was gradually reduced when combustion stabilized. Dürnholz *et al.* [116] found that EGR not only helps to reduce NO_x, but it also leads to lower HC emissions when hot EGR was used.

2.4.3.2 Internal EGR

The use of EGR is nowadays mandatory for controlling the NO_x emissions of diesel engines in order to comply with stringent emission regulations. However, electronically controlled EGR valves are still an expensive technology often unsuitable for small diesel engines or off-road vehicle applications. Internal EGR is a method that can be used instead of an EGR valve in order to reduce oxygen concentration within the cylinder and, therefore, regulate NO_x formation.

Internal EGR can be achieved by the configuration of the opening and closing of valves. By closing the exhaust valve earlier before TDC, or by reopening the exhaust valve during the intake process, exhaust gas can get trapped in the combustion chamber and be used as a diluent for the forthcoming cycle's combustion process. Using the first method, the burned gases are trapped inside the cylinder and compressed by the movement of the piston to the TDC [117]. The intake valve is opened later after the TDC in order to make sure that there is no repression of the gases into the intake manifold due to the higher pressure from the cylinder. The amount of exhaust gas trapped within the cylinder is solely dependent on the timing of the valves opening and closing. The variation in the amount of gas trapped can be achieved by implementing Variable Valve

Timing (VVT) systems described in section 2.4.4. Although internal EGR is a low-cost method for reducing NO_x emissions, it is much less effective due to the non-cooling of the burnt gas, such as that which occurs in external EGR.

Millo *et al.* [118] performed an analysis of different internal EGR solutions for small diesel engines. Using 1D simulations, they picked five operating points for valves' lift profiles that could vary the amount of the exhaust gas trapped in the cylinder. Then, the lift profiles selected were experimentally tested. The authors highlighted a potential reduction in NO_x emissions by up to 13% without remarkably detrimental effects on fuel consumption. Li *et al.* [119] studied the effects of internal EGR on a turbo-diesel engine. The research focused on the influence of internal EGR on the power, economy and emission of the engine through the engine test rig. The results show that internal EGR can effectively decrease NO_x emission. However, exhaust smoke was observed.

2.4.4 Variable Valve Timing / Actuation

Valve actuation of a CI engine is designed to work mechanically based on the rotation of the crankshaft, which transfers motion to the camshaft and valves. The opening and closing times are dependent on the position of the crankshaft and the profile of the camshaft. This means that valve timing is the same for all operating conditions, and the opening duration time is only dependent on the speed.

Variable Valve Timing (VVT) is a technology that allows alteration of the timing and/or the valve lift of an engine. It is often used to improve performance, fuel economy and emissions of modern engines. The change in inlet valve opening timing can have a significant effect on the air flow within the cylinder and, as a result, affect the air-fuel mixture. In addition, VVT technology is also used for implementing internal EGR in the combustion strategy of an engine by trapping residual gases in the combustion chamber, as described in section 2.4.3.2, for controlling combustion timing and duration.

The VVT can be achieved in many ways, including electro-hydraulic, mechanical and camless systems. This technology has already been used by many vehicle manufactures such as Toyota (VVT-i) [120], Honda (i-VTEC)[121], Nissan (N-VCT and VVL) [122],

etc. It is a promising technology for controlling SOC in HCCI/PCCI engines, and it is expected to be widely used in future vehicles.

2.4.5 Exhaust Back Pressure

Exhaust back pressure (EBP) is defined as the pressure at the outlet of the exhaust manifold or the exhaust turbine in naturally aspirated engines and turbocharged engines, respectively. The EBP can be presented due to the application of complex after-treatment systems such as diesel particulate filters and emission catalysts, which minimise exhaust gases. In some cases where Long Route (LR) or Low Pressure (LP) EGR is implemented, the EBP is deliberately increased using EBP valves in order to facilitate EGR flow towards the inlet manifold [123, 124, 125, 126].

Increased EBP can have many significant negative effects on the combustion process and performance of a diesel engine such as the following:

- Additional pumping work for compressing the exhaust gases, which means increased mechanical work and less combustion efficiency.
- Cylinder scavenging and combustion effects.
- Affects the performance of the turbocharger and reduces intake manifold boost pressure.
- Increase the exhaust temperature, which, in return, can overheat the exhaust valves and potentially increase NO_x formation.

The effect of exhaust back pressure on a 1971 Ford 351-W, V8 engine was investigated by Bolt *et al.* [127] in 1973. The authors varied the EBP from 0.5 to 1.5 bar within a wide range of engine speeds and loads. They found that increased EBP leads to lower NO_x emission due to the increased exhaust gas remaining in the cylinder. In addition, HC emission also decreased due to the fact that exhaust gases with higher HC concentration leave the cylinder last.

Cong *et al.* [128] investigated the effects of EBP on engine combustion and emissions in conventional and low-temperature diesel combustion modes on a naturally aspirated single-cylinder diesel engine. They found that increased EBP resulted in more pumping work in both combustion modes. They also concluded that EBP did not significantly influence the performance of conventional diesel engines, while for the LTC mode the effects were more obvious. Under low-load conditions, high EBP increased the charge temperature and advanced the SOC; under intermediate-load conditions, the reduction in oxygen concentration delayed the SOC and significantly reduced soot formation.

2.5 Fuel Path

In DI diesel engines, the fuel is sprayed directly into the combustion chamber in order to achieve optimum fuel atomization as a result of high injection pressure and, therefore, better combustion efficiency. The injection strategy followed in a diesel engine plays a vital role in the combustion and emission characteristics of the engine. Parameters such as injection pressure, timing, multiple injections and different injection rates can significantly change the performance and heat release rate of the engine.

2.5.1 Common Rail Technology

The latest and by far most significant change to Rudolf Diesel's engine is the development of the Common Rail (CR) fuel system. The first successful application in a production vehicle came in 1995 by DENSO Corporation, which launched a newly developed CR system mounted on the Hino Rising Ranger truck [129]. The modern common rail injection systems, which benefit from high injection pressures, over 1,000 bar, are governed by the ECU of the engine, which electronically controls the solenoid valves of the injectors for fueling of the cylinders. The third-generation common rail system recently developed by DENSO Cooperation features piezoelectric injectors and benefits from injection pressures up to 3,000 bar [12].

The use of advanced common rail fuel injection systems allows the adoption of dif-

ferent injection strategies and fuel pressures over different engine loads and speeds. CR injection systems can facilitate multiple injections per cycle within the cylinder at high injection pressures with flexible injection timing and volumes. These systems can provide a continuously high injection pressure that improves the fuel atomization from the beginning to the end of the injection. The relatively new fuel injection technology has been primarily used to reduce the noise level and exhaust emissions of diesel engines [130, 131, 132, 133].

2.5.2 Injection Pressure

Modern common rail injection systems exhibit high fuel pressure injections within the combustion chamber and benefit from better fuel atomization and higher momentum of the fuel jet which leads to a faster and more complete combustion with less soot pollutants [78, 134]. Badami *et al.* [135] studied the effect of fuel injection pressure on the soot formation. They achieved to get a reduction of particulate emissions up to 27% by increasing the injection pressure from 1300 to 1500 bars in a High-Speed Direct Injection (HSDI) diesel engine at 4000 rev/min. Badami *et al.* proved that particulate emissions can be reduced via enhanced spray penetration caused by the injection pressure increase. Agarwal *et al.* [136] and Gumus *et al.* [137] have also proved with their experiments that increasing the fuel injection pressure is effective for reducing the number concentration of particulates along with mass of particulates at all loads.

In spite of the low particulate matter achieved, NO_x emission and Brake Specific Fuel Consumption (BSFC) are negatively affected by the injection pressure increase. Gumus et al. showed that the increased injection pressure causes a decrease in smoke opacity, UHC, and CO, while it causes an increase in the emissions of CO_2, O_2 and NO_x. İçıngür and Altiparmak [138] studied the effects of fuel pressure and fuel cetane number on the performance and emission characteristics of a DI diesel engine. They observed that NO_x emission is increased and smoke is decreased when the injection pressure is adjusted from 100 to 250 bars. Hountalas *et al.* [139] conducted extensive research on the injection pressure effects in a heavy-duty DI diesel engine. They revealed that the increase of

injection pressure resulted to fast combustion and a serious reduction of soot especially at part load and low engine speeds but at the same time to a considerable increase of NO_x emissions. The authors stated that the increase in NO_x formation can be possibly controlled using after-treatment technologies or EGR and thus benefits of soot reduction can be partially maintained. In addition, the increase of injection pressure resulted to a penalty in BSFC at low injection timings but as injection timing was advanced a slight improvement was observed.

Jindal *et al.* [140] investigated the effects of injection pressure and CR in a DI diesel engine running on Jatropha methyl ester. The authors performed an analysis on the effects of different injection pressures, varying from 150 to 250 bar, and different CR, varying from 16 to 18, on the BSFC, Brake Thermal Efficiency (BTHE) and emissions of CO, CO_2, HC, NO_x and smoke. They found that the highest performance is delivered by the engine at 250 bar injection pressure and compression ratio of 18 at which BSFC improves by 10% and BTHE improves by 8.9%. High injection pressure kept the emissions of HC, NO_x and smoke at a lower level while CO emission and temperature of exhaust were increased.

DENSO cooperation compared their 2,500 bar injection system with an older version of up to 2,000 bar. They summarized that the higher injection pressure common rail system can increase fuel efficiency by up to 3% while also reducing particulate matter by up to 50% and NO_x by up to 8%. These changes allowed the fuel to atomize into finer droplets, which improved fuel ignition and combustion efficiency, resulting in increased fuel economy and cleaner exhaust emissions [141].

2.5.3 Injection Timing

The start of injection within the combustion chamber of the engine significantly affects the ignition delay of the mixture, which has an impact on the pre-mixed combustion as well as diffusion and late combustion phases. The injection timing strategy varies depending on the engine load and speed conditions. Typically, direct fuel injections in diesel engines take place close to TDC. Injections occurring before or after TDC are

referred to as being advanced or retarded, respectively.

Advancing the injection timing leads to a longer ignition delay since the in-cylinder conditions are not adequate for auto-ignition of the fuel. The longer combustion delay can contribute to better air-fuel mixing and lower soot emission since there is more time available for this process. However, the longer combustion delay will result in an increased premixed combustion phase with high in-cylinder temperatures, which, at one point, further contribute to soot oxidation, but generate high amounts of NO_x emissions. In addition, in the case of a very early injection at a point where in-cylinder pressure and temperature are relatively low, the evaporation rate of the fuel droplets is low, which can result in wall wetting, lower power rate and high UHC emission. Moreover, in case of fuel auto-ignition before the TDC, the pressure rise opposes the rising piston and, thus, negative work is performed.

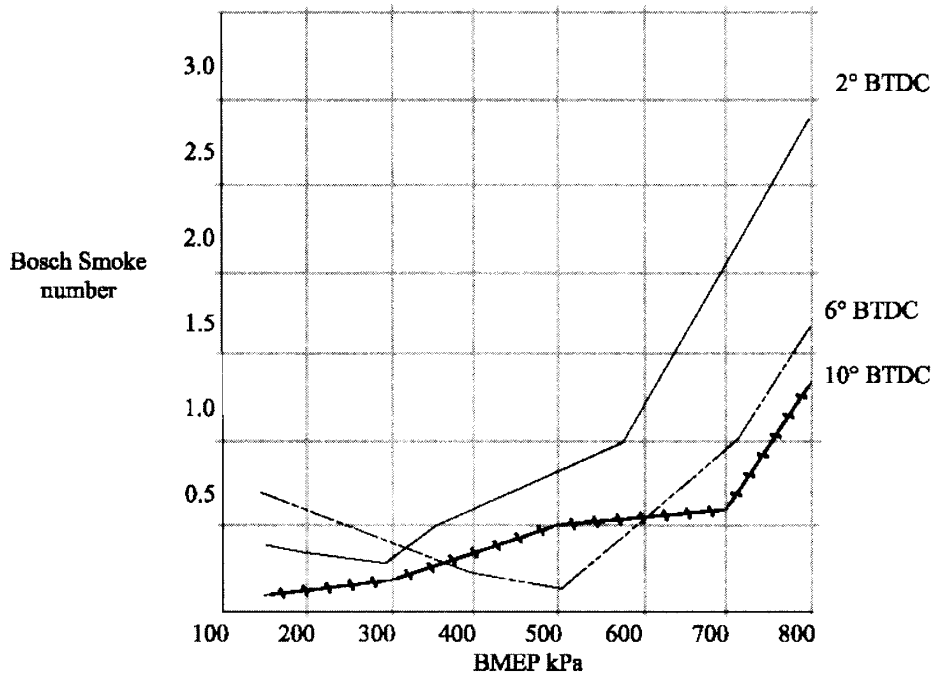

Figure 2.11: Effect of injection timing on smoke (in Bosch Smoke number scale) [20].

On the other hand, a retarded injection can result in a short ignition delay and a

shorter pre-mixed combustion phase, which leads to low NO_x formation and reduced combustion noise. However, the diffusion combustion phase will be enhanced, which will subsequently increase soot formation. However, combustion that is postponed significantly might lead to incomplete combustion and losses in expansion work and, thus, efficiency. Figure 2.11 shows the effect of injection timing on the smoke levels under various BMEP ratings.

2.5.4 Injection Strategy

Adopting optimum injection strategies for different engine operating conditions is a challenging task for modern diesel engines. Achieving high performance with the lowest possible fuel consumption and emissions is very challenging. Multiple injection strategies have the potential to improve the air-fuel mixture while keeping emissions formation low. Applying an optimum injection strategy involves decision making on many aspects such as the number of injections, the injection ratio and the time between the end of one injection and the start of the next, which is known as the dwell angle.

2.5.4.1 Multiple Injections

The primary investigations carried out on the effects of pilot injection on combustion can be traced back to 1995 with work from Pierpont *et al.* [142] and Minami *et al.* [143]. They demonstrated that, by having a pilot injection in the combustion process, the ignition delay could be reduced and this led to a lower heat release rate (HRR), with lower NO_x emissions and lower combustion noise. Montgomery and Reitz [144] studied the effect of combining multiple-fuel-injection strategies and EGR for reducing the NO_x emissions. They showed that, by combining EGR and multiple injections, NO_x emissions could be further reduced by lowering the peak in-cylinder temperature. However, soot emissions were raised because some regions with increased temperature were created as a result of the oxygen reduction within the cylinder.

Yamaki *et al.* [145] performed experiments on a turbocharged heavy duty DI diesel engine to address the effects of pilot injection on exhaust emissions. The authors found

that pilot injection was effective for the reduction of smoke at high load, particularly in low speed ranges. They also concluded that pilot injection was useful for reduction of NO_x and HC at low load and also for reduction of noise in all engine operating ranges. Uchida *et al.* [146] conducted an experimental analysis on a turbocharged and after-cooled prototype heavy duty diesel engine for optimizing combustion and emission formation by means of common rail injection system. They found that pilot injection can improve the NO_x-fuel consumption trade-off. However, the combination of pilot injection and EGR had little advantages in further improving NO_x-PM trade-off since smoke increases especially in low load conditions.

Mikulic *et al.* [147] performed an engine exhaust-emission optimization by combining high EGR rates and pilot injection. Their results revealed that EGR is a much more effective method for NO_x reduction. However, the lower NO_x emission could be only reached by combining high EGR rates and pilot injection. In contrast, they found that pilot injection resulted in an increase of soot emission at high EGR rates. Moreover, they observed that pilot injection in combination with EGR effects no deterioration of fuel consumption and HC emission.

Park *et al.* [148] investigated the effects of multiple injections in a HSDI diesel engine equipped with CR injection system. They found that pilot injection reduces the ignition delay for the main injection and enhances the power output by controlling the intensity of premixed combustion. They also noted the importance of the post-injection in completing the oxidation process and reducing the particulate emissions even when small fuel quantities were injected. According to their results, multiple injection strategies could reduce particulate emissions by more than 40% in some cases. In addition, the effect of post injection on reduction of soot emission has been examined by Han *et al.* [149] and Farrell *et al.* [150]. Their results showed that the high combustion temperature during mixing controlled combustion phase caused by post injection improved soot oxidation and reduced soot emission.

Mendez *et al.* [151] proved that combustion noise and instantaneous fuel burning rate could be decreased by splitting the heat release process as a result of multiple fuel

injections per cycle. They also demonstrated that multiple injection strategies could be used for better control of the spatial fuel distribution and enhancing the air use in the combustion chamber. As a result, this could lead to a reduction in particulate emissions at intermediate engine loads.

Shayler *et al.* [131] studied the effect of split injection on a heavy duty diesel engine. They used three different split injection strategies with two injections per cycle weighting 50:50, 55:45, and 70:30 respectively with EGR levels varying between 10 to 25%. They found that the use of split injection combined with EGR can simultaneously reduce NO_x and soot emissions. This was achieved due to the lower in-cylinder oxygen concentration as a result of the EGR and the better air-fuel mixing caused by the split injection which as return increased the in-cylinder temperatures during diffusion combustion, maximizing soot oxidation.

Montgomery and Reitz [144] investigated the effects of two-stage combustion on the exhaust emission of a diesel engine. They used a split injection strategy accompanied with a pilot injection for improved fuel evaporation process. They found that strategies with higher fuel quantity during first injection compared to the second injection benefit from less particulate matter without affecting NO_x emission. They also reported that a two-stage combustion, consisting of an early stage pilot injection and a late stage main injection can lead to simultaneous reduction of exhaust emissions with no penalty.

2.5.4.2 Dwell Angle

Multiple injections can be used for the simultaneous reduction of NO_x and soot emission. However, for optimum results, the angle between the end of the pilot or first main injection and the start of the subsequent injection needs to be adjusted. Tow *et al.* [152] showed the importance of the dwell angle between injections in order to control soot formation and suggested that there would be an optimal dwell angle under a particular operating condition. Mobasheri *et al.* [153] studied the effect of the dwell angle between two injections and proved that, for the testing operating conditions used, the optimum dwell angle between the injection pulses was around 20°CA.

Ricaud *et al.* [154] investigated the effect of advanced pilot injections combined with one main or one split injection strategy in an HSDI diesel engine. Their results showed that there is practically no advantage in long pre-injection dwell times, unless completely homogeneous combustion is desired. They also concluded that dwell angles between pulses must be carefully determined to achieve optimized performance. Diez [155], using a 30:70 split injection, investigated the effect of dwell angle on the emission formation of a single-cylinder optical diesel engine with the help of a sensitive shaft encoder providing 1800 pulses per revolution. He found that a small dwell angle (11.8°CA) led to poor air-fuel mixing and high UHC and soot emissions.

2.6 Combustion Chamber Geometry

The phenomena in DI internal combustion engines are very complicated with many chemical and physical processes occurring and interacting on each other. The complex geometries of modern IC piston geometries aggravate the analysis of these processes. In direct injection diesel engines, piston geometry is usually characterized by a re-entrant bowl piston with a protuberance in the middle to improve air-fuel mixing. The air-fuel mixing quality is of great importance for the combustion process which as a result affects the engine's performance and emissions formation.

Extensive research has been conducted into the effects of piston geometry characteristics to the air-fuel mixing and combustion process. Jaichandar and Annamalai [156] investigated the effect of injection timing and bowl geometry on the combustion and performance characteristics of a bio-diesel fueled diesel engine. The authors introduced three different bowl geometry configurations, namely Hemispherical Combustion Chamber (HCC), Toroidal Combustion Chamber (TCC) and Shallow depth Combustion Chamber (SCC). They found that there was a higher brake thermal efficiency and a significant decrease of CO, UHC and PM emissions for the TCC piston geometry compared to the HCC and SCC, although a slight increase in the NO_x formation was observed. Li *et al.* [157] using a similar piston configuration simulated the effects of piston bowl

geometry on combustion and emissions of a diesel engine under medium load conditions. They observed that a narrow entrance of the re-entrant combustion bowl could generate a strong squish, hence enhance the air-fuel mixing. They concluded that the performance of the pistons varies with the engine speed and none of the piston geometries had the optimum performance for all the engine speed loads tested. The authors used velocity vector fields and temperature contours to present the effects of piston geometry on the combustion process.

Harshavardhan *et al.* [158] used STAR-CD Es-ice code to carry out a CFD analysis on the in-cylinder fluid flow and air-fuel interaction in a Direct Injection Spark Ignition (DISI) engine with three different piston geometries compared to a flat piston. They found that air-fuel mixture is distributed all over the combustion space in all the piston configurations. The equivalence ratio was slightly rich at the centre of the geometries. The authors presented their results using velocity, turbulence kinetic energy (TKE) and equivalence ratio contours. However, the effect of piston geometry variation on the equivalence ratio and hence the air-fuel mixing, could not be clearly observed by the equivalence ratio contours. Payri *et al.* [159] performed a CFD analysis to investigate the flow characteristics inside a diesel engine's cylinder equipped with three different piston configurations. The results showed that the piston geometry had little influence on the in-cylinder flow during the intake stroke and the first part of the compression stroke. However, the flow varies within the cylinder for the three piston configurations near TDC and in the early stage of the expansion stroke. They concluded that pistons with larger bowl diameter generate a significantly smaller swirl around TDC. On the other hand, the highest swirl occurred in the piston with the smallest entry radius.

More than a decade earlier, Heywood [1] concluded that for a fixed compression ratio, the swirl at TDC is enhanced when the bowl diameter of the piston is reduced. He found that the higher levels of swirl lead to less smoke but higher NO_x and HC emissions. Tsao and Dong [160] used KIVA-II code to analyse the influence of the piston's bowl depth to the in-cylinder air flow. They found that the fuel velocity in the centre of the chamber of pistons with increased bowl depth is higher due to the higher inertia. In addition,

the higher clearance improved the squish motion and hence, the fuel distribution within the cylinder. In 1995 Zhang *et al.* [161] noted the importance of adopting a re-entrant chamber in diesel engines. They found that within a piston with a re-entrant chamber, the combustion is enhanced during the expansion stroke, preventing the diffusion of the flame in the squish region and giving lower soot levels. They also stressed that the mean combustion velocity increases with the combustion chamber radius and is lower in the case of flat-bottom bowls.

In recent years, several engine modeling research groups [162, 163, 164, 165, 166] have applied genetic algorithms to optimize the complex engine design parameters. By coupling genetic algorithms to CFD codes, it can be simultaneously optimized a large number of engine operating parameters at a relatively low computational cost. De Risi *et al.* [162] mentioned in their discussion the importance of including several modes in the piston's geometry optimization process since the performance of each chamber is strongly affected by the operating conditions. They found that NO_x reduction can be achieved by adopting a narrow and deep combustion chamber with a shallow re-entrance and a low protuberance on the cylinder axis. Additionally, they focused on the importance of the fuel spray to be oriented towards the bowl entrance for optimized air-fuel mixing.

Genzale *et al.* [163] by using genetic algorithms detected a general trend in bowl shapes where a deep, small diameter bowl was preferred for NO_x reduction and a shallow, wider bowl was preferred for reduced fuel consumption. They also found that by increasing the air swirl ratio entering into the cylinder resulted in increased NO_x and decreased soot and fuel consumption. Song *et al.* [167] performed three-dimensional flow calculations of the in-cylinder flow for a DI diesel engine with different combustion chambers. Their investigation showed that swirl becomes more homogenous as cylinder moves upwards during early phase of compression stroke. The piston geometry had negligible effect during the intake stroke and the early phase of compression stroke.

Siewert [168] explored the effects of varying nozzle spray angle and rail pressure on emissions and thermal efficiency of a diesel engine. He found that increased rail pressure improves atomization and vapourization of the spray as evidenced by significant reduc-

tions in smoke. However, he concluded that for conditions where the spray misses the bowl due to a wide spray angle (158°), increased rail pressure exacerbates the deterioration in emissions and thermal efficiency due to increased spray penetration outside of the bowl. Mobasheri and Peng [153] performed a computational investigation into the effects of included spray angle on a heavy-duty diesel engine. They concluded that 105°spray cone angle along with an optimized split injection strategy could significantly reduce NO_x and soot emissions without much penalty of the fuel consumption, as compared to wider spray angles.

The results in literature confirm that is difficult to adopt optimum piston geometry suitable for all operating conditions. The effect of the piston chamber's geometry on the engine performance is very complex due to its dependence on the engine's specifications, flow field and the air-spray interaction. The piston bowl geometry has a close relationship with the combustion and emission formation processes of a of DI diesel engine as it can strongly affect the air-fuel mixing quality before the start and during the combustion.

2.7 In-cylinder Air-fuel Flow

The air-fuel distribution within the combustion chamber is crucial for understanding the behaviour of diesel combustion and to control the combustion phases for optimized results with minimum harmful emissions. Many techniques such as Particle Image Velocimetry (PIV), Laser Induced Fluorescence (LIF), droplet sizing techniques (Phase Doppler and/or planar techniques) and high-speed imaging have been used by investigators in order to address the effects of different air and fuel injection strategies on the air-fuel flow phenomena within the cylinder and their impact on combustion characteristics.

Particle Image Velocimetry has been used by many researches [169, 170, 171, 172] to visualize the in-cylinder air-fuel flow in DI diesel engine combustion. The system uses a special charge-coupled camera that captures two successive images of laser pulses. The images are then divided into small subsections, and each subsection of the first image

is cross-correlated with the corresponding subsection of the following image in order to identify the common particle displacement. Figure 2.12 shows the apparatus used for the PIV technique on a DI optical diesel engine.

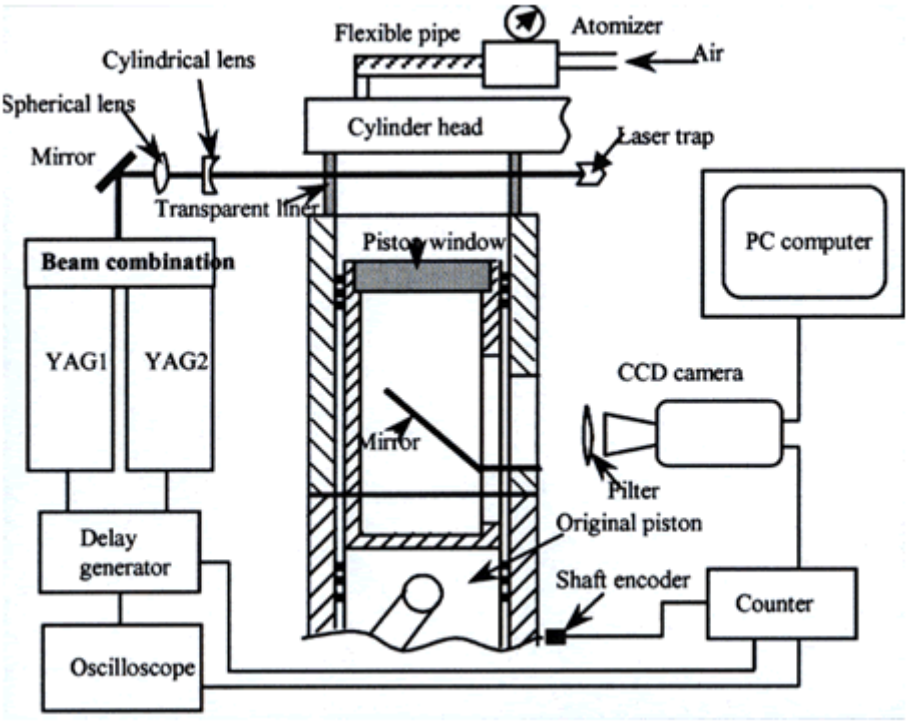

Figure 2.12: Particle Image Velocimetry technique apparatus on a DI optical diesel engine [173].

Laser Induced Fluorescence is another technique used for visualizing the air-fuel flow within the cylinder [174, 175, 176, 177]. This technique uses a laser beam to excite the species (atom or molecule) of interest. When the specie is excited, it spontaneously emits light known as fluorescence. The intensity of the light corresponds to the species concentration. Phase droplet techniques and high-speed imaging have also been used by many researchers [178, 179, 180] to investigate air-fuel mixing behaviour within the combustion chamber of optical diesel engines.

While many research studies have been conducted to investigate the effects of various

injection strategies on air-fuel mixing, the combustion process and emissions formation, there is very limited work that directly takes into account specific information on the fuel distribution in the chamber and particularly quantitative analysis of the air-fuel mixture. In 2002, Nandha and Abraham [181] defined a mathematical parameter called the Degree of Heterogeneity (DOH) for scaling the fuel distribution in the cylinder. They tested the definition using computational simulations to study the effects on the heterogeneity of the mixture under different operating conditions, including multiple injection strategies and spray orientation. To achieve a more directly quantitative parameter to classify air-fuel mixing quality, Peng *et al.* [182] developed a factor to measure air-fuel mixing in the diesel engine. The authors implemented this factor in CFD KIVA-3V code to examine the influences of various operating parameters on in-cylinder mixing quality, and this showed that the advance of injection timing does not always result in an increase in air-fuel mixing homogeneity.

2.8 Summary

This chapter has provided details about the most important aspects of diesel engines: harmful emissions and recent emission legislation. The most recent after-treatment technology and advanced combustion strategies for reduced emissions were analysed, and the benefits and drawbacks of each emission-reduction solution were highlighted. The chapter also included a literature review of the effects of air and fuel paths as well as the effects of combustion chamber geometry on the combustion and emission characteristics of diesel engines.

Chapter 3

Advanced Combustion Analysis

This chapter presents two newly introduced factors used in the study for measuring the air-fuel homogeneity and combustion process of diesel engines. The first section of this chapter introduces the Homogeneity Factor (HF) for measuring air-fuel mixing quality within the combustion chamber at any point of the engine's cycle. The second section defines the PCCI strength factor, which provides a measurement of the strength of the premixed combustion phase compared to the total combustion phase. Finally, the last section describes the statistical methods used in this study for reducing the number of experimental tests and finding the optimum parameters for reduced emissions.

3.1 Homogeneity Factor

The air-fuel mixing quality in diesel engines is very critical for controlling the engine's performance and emission characteristics. Extensive research has been carried out by many research groups to investigate the effect of air-fuel mixing on the behaviour characteristics of the engine by using different air-fuel mixing visualization methods as described in Section 2.7. However, so far there is not a measure for quantitatively describing air-fuel mixing quality. The quantitative description of air-fuel mixing can be used for assessing the mixing quality and for studying its influence on ignition, combustion and emission. It could be also used for acquiring a more accurate control to the mixing and

combustion, in particular for PCCI combustion for which a measure of charge mixing quality will be very helpful as a control medium used for the prediction of the start of combustion timing.

Nandha and Abraham's were the first research group tried to quantify the Degree of Heterogeneity (DOH) [181] of air-fuel mixing in DI engines. The DOH actually represents the standard deviation of the equivalence ratio normalized by the overall equivalence ratio. In our new definition, the Heterogeneity Factor (HeterF) is the standard deviation of fuel amount normalized by the overall fuel amount. This will be a more reasonable measure to the non-uniformity in the mixture. The mixing quality parameter used in this research work is the Homogeneity Factor (HF), originally developed by Peng *et al.* [182], which is the vice versa of the HeterF. The parameter was modified for more accurate air–fuel mixing results within the cylinder. The role of this parameter is to define the air-fuel homogeneity within the combustion chamber at the start and during the combustion cycle based on the air and fuel strategies followed as shown in Figure 3.1.

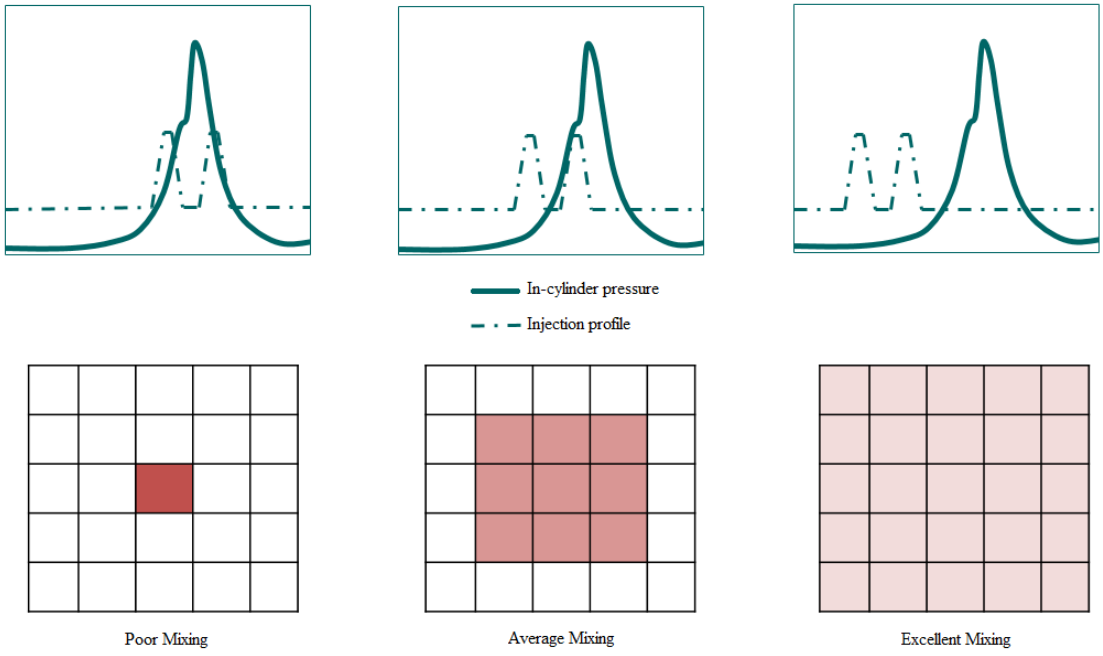

Figure 3.1: Air-fuel homogeneity at the SOC with different injection timing strategies.

In the definition, we first need to find the fuel difference in a calculated cell (e.g. cell i), compared to the average equivalence ratio:

$$\frac{\Phi_i}{AFR_{st}+\Phi_i}\delta m_i - \frac{\Phi_0}{AFR_{st}+\Phi_0}\delta m_i = \frac{(\Phi_i-\Phi_0)AFR_{st}}{(AFR_{st}+\Phi_i)(AFR_{st}+\Phi_0)}\delta m_i \tag{3.1}$$

Where

AFR_{st}	is the stoichiometric air-fuel ratio
Φ_i	is the equivalence ratio in cell i
Φ_0	is the average equivalence ratio
δm_i	is the mass of the mixture in the computational cell i

The Total fuel amount in the cylinder is given by:

$$\frac{\Phi_0}{AFR_{st}+\Phi_0}M \tag{3.2}$$

Where M is the total mass of mixture

Then, a parameter named Heterogeneity Factor (HeterF) can be expressed as:

$$HeterF(\theta) = \sum_{i=1}^{Ncells} \frac{\sqrt{(\Phi_i-\Phi_0)^2}\delta m_i}{2\Phi_0 M\left(1+\frac{\Phi_i}{AFR_{st}}\right)} \tag{3.3}$$

As the increased fuel amount in a cell actually comes from the decrease of fuel amount in other cells, the half of the standard deviation is used in the definition to reflect the non-uniformity more accurately.

Based on HeterF, the homogeneity factor (HF) can be derived for having a quantitative demonstration to the charge mixing quality.

$$HF(\theta) = (1 - HeterF(\theta))\% \tag{3.4}$$

Compared to Nandha and Abraham's [181] definition for Degree of Heterogeneity (DOH) which actually represents the standard deviation of the equivalence ratio normalized by the overall equivalence ratio, the HeterF is the standard deviation of fuel

amount normalized by the overall fuel amount. This will be a more reasonable measure to the non-uniformity in the mixture.

The programming language for the HF implemented on AVL Fire software is disclosed in the Appendix A.

3.2 PCCI Strength

The combustion process in diesel engines is a key factor in the performance and emission-formation characteristics of the engine. As shown earlier in Figure 2.7 of Chapter 2.3.1, the combustion process of a four-stroke diesel engine can be divided into four phases based on the heat generated during the engine cycle. The first phase, ignition delay, has a significant effect on the combustion process that follows, while the second phase, premixed combustion, plays a key role in NO_x formation due to high in-cylinder temperatures experienced within the combustion chamber.

Research on the role of the premixed combustion phase ratio in the performance and emission formation of diesel engines is limited. Many studies have been conducted and have validated the importance of premixed combustion in understanding NO_x emission behaviour, though little effort has been made to quantify the ratio of premixed combustion and describe how this is affected by various air-fuel strategies.

Maiboom *et al.* [183] mentioned the importance of the premixed combustion by proving that the increase of inlet air temperature at constant EGR does not always lead to higher NO_x formation as traditionally observed. This is due to the low concentration of oxygen in the hot EGR rates, which could lead to a different premixed combustion ratio and, therefore, lower NO_x emissions.

The premixed combustion phase is sometimes difficult to identify in the PCCI combustion mode. For this purpose, the derivative of the HRR rate graph is used in this study for spotting the change in the combustion mode as shown in Figure 3.2.

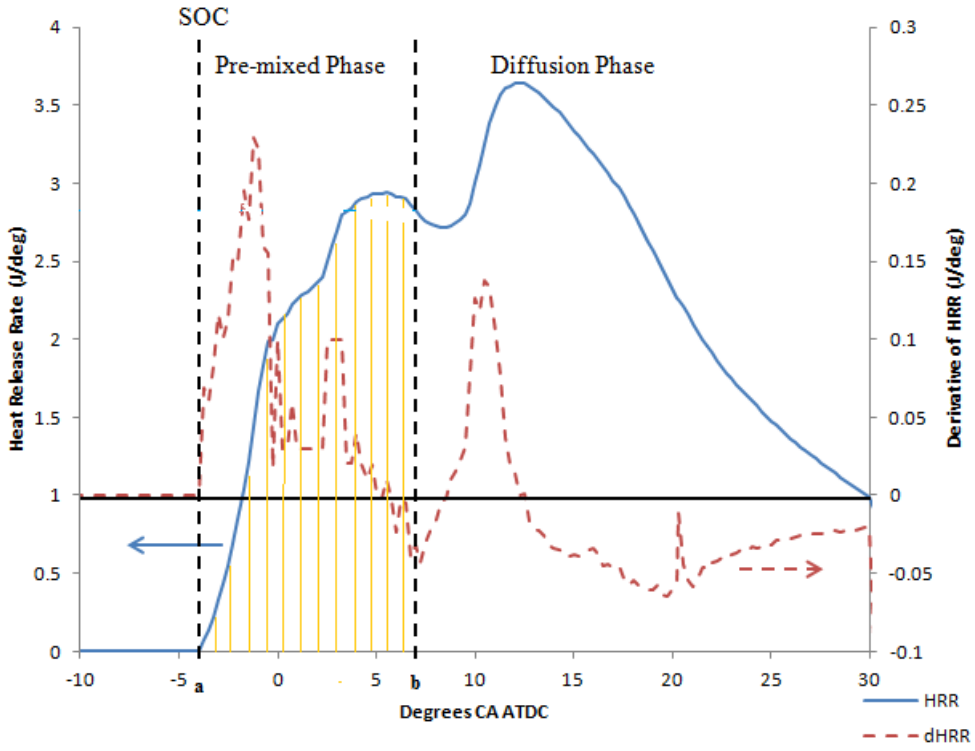

Figure 3.2: Derivative of HRR for spotting the start of diffusion combustion phase.

Then, using integration, the amount of HRR for the premixed combustion phase and the whole combustion process is calculated by estimating the area under the curve. The area under the curve for the pre-mixed combustion phase is estimated using the trapezoidal rule according to the following equation:

$$A_{(pre-mixed\,phase)} = f(x)dx \simeq \frac{h}{2}\sum_{k=1}^{N}(f(x_{k+1}) + f(x_k)) =$$

$$\frac{b-a}{2N}(f(x_1) + 2f(x_2) + 2f(x_3) + ... + 2f(x_N) + 2f(x_{N+1})) \tag{3.5}$$

$$\text{Where} \quad \begin{matrix} a = x_1 < x_2 < .... < x_{N+1} \\ h = (b-a)/N \end{matrix}$$

The final factor, named PCCI strength, which defines the strength of premixed combustion during the whole combustion process, is given by dividing the area under the

pre-mixed phase of the heat release rate curve over the whole area of the curve.

$$PCCI\ Strength = \frac{A_{(pre-mixed\ phase)}}{A_{(full\ combustion)}} \tag{3.6}$$

3.3 Statistical Methods

Statistical methods have been used in the past by many researchers to reduce the number of experiments, which subsequently leads to savings in cost and time. Taguchi methods combined with analysis of variance can provide accurate results for a fixed number of variables by significantly reducing the number of trials. The use of Taguchi statistical methods for diesel engine combustion optimization is not common, and there are only a few studies that have used this method in the past for engine performance and emission optimization [184, 185, 186, 187].

3.3.1 Taguchi Method of Optimization

Taguchi methods are statistical methods developed by Genichi Taguchi to improve the quality of manufactured goods. Recently, Taguchi methods have been used in engineering but less commonly in the automotive industry. These methods are used to optimize experimental parameters in fewer trials by using an orthogonal array and statistical analysis to evaluate experimental data. Taguchi defined a signal-to-noise (S/N) ratio for evaluating the stability of performance of an output characteristic. The S/N ratio takes both average and variation into account. The S/N ratio is given by Equation 3.7 :

$$S/N\ ratio = -10log\left(\frac{\sum_{i=1}^{n}\frac{1}{y_i^2}}{n}\right) \tag{3.7}$$

Where
- y_i is the value of the quality characteristic measured from the trial
- n is the test number
- S/N is the signal to noise ratio in dB

The Taguchi process starts by defining the goals that need to be identified, e.g. reduction of NO_x and soot or increase of IMEP, and the parameters need to be controlled, e.g. EGR rates, injection timing. The appropriate orthogonal array is defined based on the number of parameters and their levels. Once the matrix experiment is designed, the tests are conducted. Next, the data are subjected to analysis of variance, and the optimum combination of the level of each parameter can be determined. Finally, a confirmation experiment is run to validate the optimum results.

3.3.2 Analysis of Variance

The purpose of Analysis of Variance (ANOVA) is to identify the most significant factors and their contribution (as a percentage) with respect to the response parameters. The F-test, named after R.A. Fischer, evaluates the significance of variance on the output characteristic. Usually, an F value of more than 4 indicates a vital role and that change in the design parameter has a significant effect on the output characteristic.

The F-test can be performed by using the following equation:

$$F = \frac{between - group\ variability}{within - group\ variability} \tag{3.8}$$

The "between-group variability" is given by:

$$\sum_{ij} n_i(\bar{Y}_{i.} - \bar{Y})^2/(K-1) \tag{3.9}$$

Where
- $\bar{Y}_{i.}$ is the sample mean in the i^{th} group
- n_i is the number of observations in the i^{th} group
- $\bar{Y}$ is the overall mean of the data
- K is the number of groups

The "with-in group variability" is given by:

$$\sum_{ij}(Y_{ij} - \bar{Y}_{i.})^2/(N-K) \tag{3.10}$$

Where Y_{ij} is the j^{th} observation in the i^{th} out of K groups

N is the overall sample size

The F value will be large if the between-group variability is large relative to the within-group variability.

3.4 Summary

The HF and PCCI strength factors used in this investigation are defined in this chapter. Furthermore, Taguchi statistical methods for reducing the number of experiments performed and improving emission characteristics are described.

Chapter 4

Model Description and Validation

This chapter includes an overview of the computational sub-models adopted for simulation of the in-cylinder physical and chemical processes governing diesel engine performance and emission characteristics. It also includes a grid independence and model validation analysis using data collected from the Hydra engine described in Chapter 5.

4.1 CFD Sub-Models

Computational Fluid Dynamics (CFD) is defined as the set of methodologies that uses numerical approaches and algorithms to solve and analyse problems that involve fluid flows. The first CFD analysis is dated back to 1910 when Lewis F. Richardson used human computers to perform iterative solutions of Laplace's equation using finite-difference methods [188]. Although this was the very first attempt, the use of modern CFD approaches started by the 1960's and rapidly increased over the following decades. By 1965, CFD tools developed by NASA and Los Alamos were used in research and a high number of scientific articles was published [189]. The computational technology improvement over the years has accelerated the development and use of CFD codes for solving a variety of Fluid Dynamics problems and a lot of useful software packages for the simulation of fluids have been released. The modern CFD tools are based on traditional approaches like finite difference methods, finite element methods, finite volume methods

and boundary element methods.

The numerical simulations in this thesis were conducted by using AVL FIRE CFD code for diesel combustion. The AVL CFD solver is developed to solve the most demanding flow problems in respect to geometric complexity and chemical and physical modelling. The code is based on the Finite Volume approach. The solution algorithm employed enables flexibility in the usage of any unstructured grids including grids consisted of polyhedral calculation volumes. The code solves incompressible and compressible flows including supersonic flows [190]. The state-of-the-art CFD sub-models are implemented for accurate calculations of turbulent flows, combustion and emissions formation. The sub-models employed in the code have been chosen based on previous researchers' work [191, 192, 193, 194, 195, 196, 197, 198]. The original sub-model were used without any modifications as they have been suggested as appropriate for high fuel pressure diesel combustion.

4.1.1 Spray Break-up Model

The atomization of fuel spray can be divided into two separate stages. The primary atomization takes place close to the nozzle and the secondary one occurs further downstream due to aerodynamic interactions. The Wave and Taylor Analogy Break-up (TAB) [199] models do not distinguish between the two processes. However, TAB model has not been used since it is not appropriate for cases with high injection pressures (greater than 40MPa) and predicts too small liquid and vapour penetrations.

Enhanced Taylor Analogy Break-up (ETAB) [200], Fractionnement Induit Par Acceleration (FIPA) [201] or Kelvin Helmholtz-Rayleigh Taylor (KH-RT) [202], are some of the break-up models can be used for predicting the fuel spray atomization. However, these models treat and simulate the primary and secondary regions separately. This fact could cause a difficulty in estimating the correct values for the additional set of tuning parameters. In the code, the primary and secondary atomization of the fuel spray is predicted using the Wave model [203], which has been widely used for highspeed fuel injections. The parameters of the model have been tuned to match the experimental

data.

The Wave model assumes that the droplet size and the breaking up time is related to the fastest growing Kelvin-Helmholtz instability [204]. The details of the newly-formed droplets are predicted using the wavelength and growth rate of this instability. The frequency (Ω) and wavelength (Λ) of the fastest growing surface wave can be determined by the following equations:

$$\Omega = \frac{0.34 + 0.385We^{1.5}}{(1+Z)(1+1.4T^{0.6})}\sqrt{\frac{\sigma}{\rho_1 R_d^3}} \tag{4.1}$$

$$\Lambda = \frac{9.02R_d(1+0.45\sqrt{Z})(1+0.4T^{0.7})}{(1+0.865We^{1.67})^{0.6}} \tag{4.2}$$

	We	is the Weber number for gas
	T	is the Taylor number defined as $T = Z\sqrt{We}$
Where	Z	is the Ohnesorge number defined as $Z = \sqrt{We_1/Re_1}$
	We_1	is the liquid Weber number
	Re_1	is the Liquid Reynolds number

In the Wave model the initial droplets have the diameter of the nozzle orifice. The child droplets formation with radius R_{eq} from a parent droplet with radius R_d can be calculated by the following equation:

$$R_{eq} = \begin{cases} B_o\Lambda, & B_o\Lambda \leq R_d \\ min\left[(3\pi R_d^2 \mid v_d - v_g \mid /2\Omega)^{0.33}\right], & B_o\Lambda > R_d \\ min\left[(3\pi R_d^2\Lambda/4)^{0.33}\right], & B_o\Lambda > R_d \end{cases} \tag{4.3}$$

Where	B_o	is the model constant equal to 0.61

The rate of change of the droplet radius can be expressed by the following equation:

$$\frac{dR}{dt} = -\frac{R_d - R_{eq}}{\tau_{bu}} \tag{4.4}$$

Where	τ_{bu}	is the characteristic breakup time defined as $\tau_{bu} = 3.726 B_1 \frac{R_d}{\Lambda\Omega}$
	B_1	is a model constant dependent on the injector characteristics

4.1.2 Evaporation Model

For heat-up and evaporation prediction of the droplets, the Dukowicz evaporation model [205] is selected for the simulations with diesel fuel. The model tunable constants have been adjusted to match the experimental data. The model is based on the following assumptions:

a) there is a spherically symmetrical flow near the droplets,

b) the quasi-stationary layer of liquid vapour exists near the droplet surface,

c) uniform temperature distribution in the droplets,

d) constant gas properties around the droplets and

e) thermodynamic equilibrium of vapour and liquid on the droplets surface.

The Dukowicz model determines the rate of droplet temperature change by heat balance, which states that the temperature transferred from the gas to the droplet supplies heat for its vapourization. The energy balance equation is defined as:

$$m_p C_p \frac{dT_p}{dt} = Q + L\frac{dm_p}{dt} \tag{4.5}$$

Where

Cp	is the specific capacity of the droplet liquid
L	is the latent heat of the droplet liquid
Q	is the heat flux from the gas to the droplet define as $Q = aS_p(T_\infty - T_p)$
a	is the heat exchange coefficient
S_p	is the area of total droplet surface
Subscript ∞	corresponds to the parameters far from the droplet

The droplet mass balance equation is given by:

$$\frac{dm_p}{dt} = Q\frac{f_{vs}}{q_s} \tag{4.6}$$

Where	q_s	is the specific heat flux to the droplet surface
	f_{vs}	is the specific vapour flux from the droplet surface
	Subscript s	corresponds to the parameters in the droplet surface
	Subscript v	corresponds to the vapour parameters

By knowing the values of Q and f_{vs}/q_s and using Equations 4.5 and 4.6, the mass and temperature of the droplets can be determined at any point.

4.1.3 Wall Interaction Model

The wall interaction model is used for extreme cases where the fuel injected is not instantaneously vapourized but impinges on the wall boundaries of the cylinder. In diesel engine combustion, this is a rare case due to the very high pressure and temperature in the cylinder. However, in cases where the in-cylinder temperature is not high enough, such as when fuel is injected at a very early stage far from the TDC or under cold engine start conditions, wall wetting may occur.

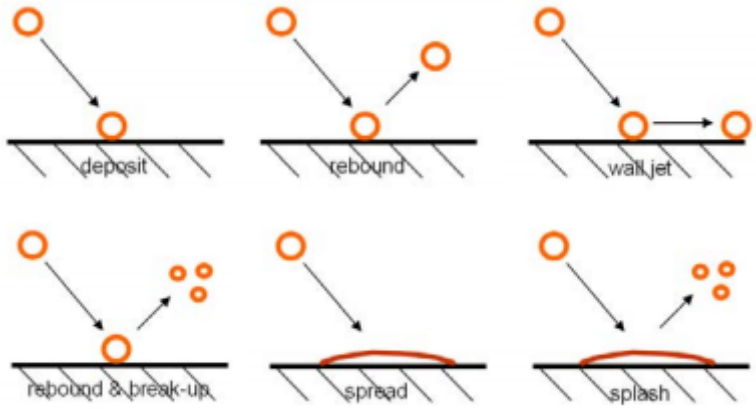

Figure 4.1: Wall interaction behaviour.

For simulating the impingement of the droplets on the walls, the extended Kuhnke spray-wall interaction model [206] was used. The interaction is mainly dependent on the velocity and the diameter of the droplet as well as on the wall surface roughness and temperature. The fuel droplet behaviour is analytically shown in Figure 4.1. At low

inlet velocities, the droplet sticks to the wall, while at higher inlet velocities the droplets tend to rebound and break up. Finally, at very high inlet velocities, the droplets tend to splash or spread across the cylinder wall.

4.1.4 Turbulent Model

Internal combustion engines are characterized by high inlet air flow velocities and turbulent flows within the cylinders. The accurate simulation of turbulence flow within the cylinders is of great importance due to the significant effect of the flow on the physical and chemical processes taking place during air-fuel mixing and combustion. The turbulence flow significantly affects air-fuel mixing within the combustion chamber as well as the evaporation rate, two very important factors that dramatically affect combustion characteristics and emission formation.

In the AVL FIRE Solver, the well-known standard turbulence models, such as standard k-ε [207], realizable k-ε [208], Spalart Allmaras [209] and Reynolds Stress Model (RSM) [210], are available as well as recently developed models such as Hybrid Turbulence Model (HTM) [211] and k-ζ-f model [212] targeting improved simulation accuracy. The k-ζ-f model developed by Hanjalic, Popovac and Hadziabdic (2004) was used for the evaluation of the turbulence effect in the combustion chamber. The k-ζ-f model is widely used in IC flows due to its robustness in computations involving grids with moving boundaries and highly compressed flows. Moreover, for IC flows, the k-ζ-f model leads to more accurate results compared to the standard, much simpler k-ε and RNG k-ε two-equation models.

4.1.5 Combustion Model

The Extended Coherent Flame Model 3 Zones (ECFM-3Z) [213] was applied for modelling combustion behaviour. The ECFM-3Z belongs to the Coherent Flame Models (CFM) family, which is based on the assumption that the turbulent flame brush is composed of an ensemble of laminar flamelets. The length and time scales in the reaction zone are assumed to be smaller than the characteristic turbulent length and time scales.

The advanced ECFM-3Z model separates a computational cell in three zones in order to enable specific treatment for air-fuel mixing, auto-ignition, combustion and pollution formation processes as shown in Figure 4.2.

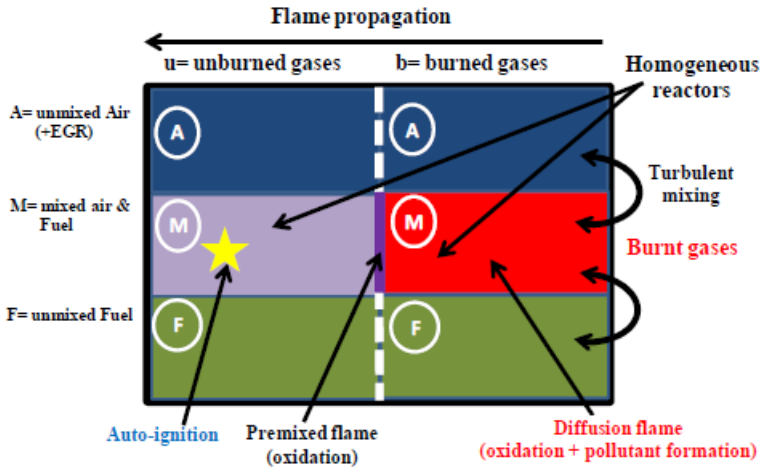

Figure 4.2: Three zones in ECFM-3Z model [214].

Computation using the three different models increases the understanding of turbulence flow and provides data that cannot be obtained by experiment such as fuel mixture fraction distribution and fuel evaporation rate. In addition, the ECFM-3Z model compared to the standard CFM models takes into account three new traces for NO, CO and H_2 and three more species for describing mixing and auto-ignition processes.

The ignition delay of the unburned air-fuel mixture is predicted using tabulated ignition data stored in look-up tables for different fuels. These data, which are available in AVL FIRE, are generated based on chemical kinetic calculations and stored as functions of the parameters pressure, temperature, fuel/air equivalence ratio and residual gas content. The actual determination of the ignition delay time is made by implementing the formation rates derived from the tabulated data into the following equation:

$$\tau_d = 4.804 \times 10^{-8} (N_{o2}^{u,M} \mid_{u,M})^{-0.53} (N_{Fu}^{u,M} \mid_{u,M})^{0.05} (\bar{\varrho}^u)^{0.13} e^{\frac{5914}{T_u}} \tag{4.7}$$

	M	is the molar mass given in mole per cubic meter
Where	T	is the temperature in Kelvin
	Superscript u	corresponds to unburned gases

After auto-ignition, the remaining fuel in the unburned mixed zone is oxidized leading to the formation of CO and CO_2 in the burned gases. The ECFM-3Z provides a new oxidation mechanism with a more accurate description of the formation of CO in the case of lean mixtures.

The post-flame chemistry of the model uses an improved equilibrium package where the CO/CO_2 equilibrium is not considered compared to the standard ECFM model and the N_2/N reaction can be treated separately. The considered equilibrium reactions are as follows:

$$\begin{aligned} N_2 &\leftrightarrow 2N \\ O_2 &\leftrightarrow 2O \\ H_2 &\leftrightarrow 2H \\ 2OH &\leftrightarrow O_2 + H_2 \\ 2H_20 &\leftrightarrow O_2 + 2H_2 \end{aligned} \tag{4.8}$$

Oxidation of C_nH_m constituted fuels and local mean equivalence ratio $\bar{\emptyset}$ is defined by the following equation:

$$\begin{cases} a(1-r_{CO})[C_nH_m + (n+\frac{m}{4})O_2 \rightarrow nCO_2 + \frac{m}{2}H_2O] \\ ar_{CO}[C_nH_m + (\frac{n}{2}+\frac{m}{4})O_2 \rightarrow nCO_2 + \frac{m}{2}H_2O] \\ (1-a)[C_nH_m + \frac{n}{2}O_2 \rightarrow nCO_2 + \frac{m}{2}H_2] \end{cases} \tag{4.9}$$

Where	r_{CO}	is a constant value presuming the CO formation
	a	is a value depended on the local equivalence ratio as shown below:

$$\begin{cases} \bar{\varnothing} < \bar{\phi}_1 \rightarrow a = 1 \\ \bar{\phi}_1 < \bar{\varnothing} < \bar{\phi}_2 \rightarrow a = \frac{1}{2n+m}(\frac{4\times 0.98(n+m/4)}{\bar{\varnothing}} - 2n) \\ \bar{\phi}_2 < \bar{\varnothing} \rightarrow a = 0 \end{cases} \tag{4.10}$$

Where
$\bar{\phi}_1 = 0.99$
$\bar{\phi}_2 = 0.9\bar{\phi}_{crit}$
$\bar{\phi}_{crit}$ is the critical equivalence ratio

The critical equivalence ratio $\bar{\phi}_{crit}$, is the limit point which above this ratio there is not enough oxygen to complete the oxidation of fuel into CO and is defined as follows:

$$\bar{\phi}_{crit} = \frac{2}{n}(n + \frac{m}{4}) \tag{4.11}$$

It can be seen from Equations 4.9 and 4.10 that for lean conditions where $a = 1$, the first two reactions are considered which confirms that CO formation can also take place under lean conditions. The third reaction is performed under rich conditions where there is lack of oxygen for complete combustion and burning the fuel to CO_2.

4.1.6 NO_x Formation Model

The extended Zeldovich model [215] used for the prediction of thermal NO formation is based on the following three reactions.

$$N + O_2 \longleftrightarrow NO + O \tag{4.12}$$

$$O + N_2 \longleftrightarrow NO + N \tag{4.13}$$

$$N + OH \longleftrightarrow NO + H \tag{4.14}$$

The nitrogen oxide reactions are highly dependent on temperature, residence time and oxygen concentration. Due to the high activation energy needed to break the N_2

triple bond, the rate of NO formation is significant only at temperature greater than 1800K. The first reaction, which is significantly fast at high temperatures, represents the rate limit compared to the following two reactions. It can be seen from the reactions above that thermal nitric oxide formation is mainly affected by O, H, OH, N and O_2. The maximum level of NO appears at stoichiometric and fuel-lean flames (at an equivalence ratio of about ~0.9) where the OH concentration is very small. Therefore, the third reaction of the extended Zeldovich model can be neglected.

The calculation of the concentrations of radicals is performed based on the assumption that the reaction rates of the forward and reverse reactions are equal, which has been experimentally proven at high temperatures over 1600K. Using this partial equilibrium, thermal NO formation can be expressed by the reactions shown in Equations 4.15 and 4.16. However, this assumption provides satisfactory results only at high temperatures where partial equilibrium is established.

$$k_1[N][O_2] \longleftrightarrow k_2[NO][O] \tag{4.15}$$

$$k_3[O][N_2] \longleftrightarrow k_4[NO][N] \tag{4.16}$$

Using these expressions, the equation system can be solved and results in a global reaction model for thermal nitric oxide formation that can be expressed as follows:

$$N_2 + O_2 \longleftrightarrow 2NO \tag{4.17}$$

with $k_f = k_1 k_3$ as the forward and $k_b = k_2 k_4$ as the backward reaction rate. The net rate of NO formation can be given by:

$$\frac{d\,[NO]}{dt} = 2k_f[N_2][O_2] \tag{4.18}$$

Equation 4.18 considers only the formation of NO, and the rate of the forward reaction is given by:

$$k_f = \frac{A}{\sqrt{T}} exp\left(-\frac{E_a}{RT}\right) \tag{4.19}$$

Where
- A is the pre-exponential factor
- E_a is the activation energy

The prompt NO formation, formed by the attack of HC fragments on the air-nitrogen mixture has been neglected in this study due to the insignificant effect compared to thermal NO. In addition, fuel-NO formation can be mostly neglected during the combustion process in IC engines.

4.1.7 Soot Formation Model

The Kennedy / Hiroyasu / Magnussen model [216] is used for the prediction of soot formation. This model takes into account the processes of particle formation and surface growth as related functions of local fuel and soot nuclei concentration. The nucleation source is given by the following:

$$S_n = C_n e^{\left(-\frac{(f-f_s)^2}{\sigma_n^2}\right)} \tag{4.20}$$

Where
- C_n is the maximum nucleation rate [1/(m^{3}s)]
- f is the fuel mixture fraction
- f_n is the mixture fraction for maximum nucleation rate
- σ_n is the predefined f$_n$ variance

The surface growth source is defined as:

$$S_g = A \times F(f, \varphi_s) p^{0.5} e^{\left(-\frac{E_a}{RT}\right)} \tag{4.21}$$

Where	A	is the pre-exponential factor
	E_s	is the activation energy
	R	is the universal gas constant (J/mol K)
	p	is the pressure (bar)
	T	is the temperature (K)
	$F(f, \varphi_s)$	is the specific surface growth rate
	f	is the mixture fraction
	φ_s	is the soot mass fraction

The model neglects the reaction of soot with OH due to dominant particle oxidation with O_2. The soot oxidation level is highly affected by factors such as (a) partial pressure of oxygen, (b) local flame temperature and (c) actual soot concentration and integral turbulence time scale. The soot oxidation can be described by the following equation:

$$ {}_2S_{O_2} = -F\left(\varphi_s, p_{O_2,\tau}\right) \tag{4.22} $$

Where	φ_s	is the soot mass fraction
	p_{O_2}	is the partial pressure of oxygen
	τ	is the integral turbulent time scale

4.2 Grid Independence Analysis

A grid independence analysis has been performed for the selected sub-models in order to make sure that the results obtained are not affected by cell size. The piston and the injector geometry parameters have been incorporated into the software using the 2D Sketcher tool. The computational grid was generated and the model tested with six various mesh sizes. The peak in-cylinder pressure, heat release rate and air fuel homogeneity factor were compared for each of the cases as shown in Figure 4.3.

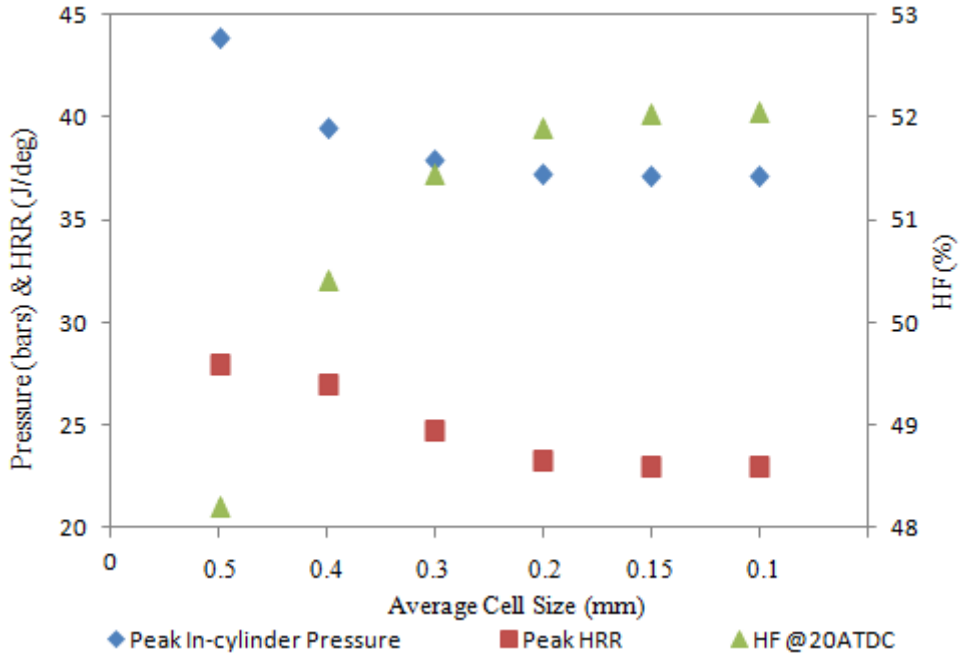

Figure 4.3: Computational grid independence analysis.

It can be clearly seen from Figure 4.3 that the results stabilize for the cases with average cell sizes of 0.15mm and 0.1mm. Therefore, the final grid independent model, shown in Figure 4.4, has an average cell size of 0.15mm with relatively denser meshing closer to the injection tip and the TDC clearance gap. The model consists of 42,052 and 72,052 hexahedral cells at the TDC and BDC, respectively.

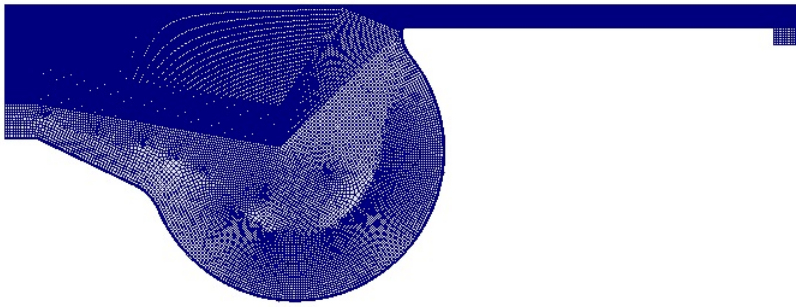

Figure 4.4: Computational grids at the TDC.

4.3 Model Validation

The CFD model was validated using experimental data collected from the single-cylinder research engine with the specifications listed in Table 4.1. The model was validated for both single and multiple injections in order to make sure that fuel strategies would not affect the predicted results. From the results analysed in Sections 4.3.1 and 4.3.2, it can be concluded that simulation results nearly match the experimental results for single injection cases. At the same time, simulation results for multiple injections are also rather similar to actual values. Thus, the model used in this study can confidently simulate, with near-accuracy, the combustion process and emissions.

4.3.1 Single Injection

The model was validated for a single fuel injection at two different engine speeds and loads under the following engine conditions:

Table 4.1: Single injection engine conditions for model validation.

Inlet Valve Closure (IVC)	64°ATDC
Exhaust Valve Opening (EVO)	69°BBDC
Engine speed	1,200rpm and 2,000 rpm
Engine load	18% and 81%
Fuel quantity	6 mg and 14 mg
Fuel injection pressure	1,600 bar
Start of Injection (SOI)	10°BTDC

Figures 4.5 and 4.6 show the comparison between the predicted and measured in-cylinder pressure and heat release rate for low load at 1,200rpm and high load at 2,000rpm, respectively. The result is based on the assumption of uniform wall temperature 470K for the cylinder wall and 570K for the cylinder head and piston top.

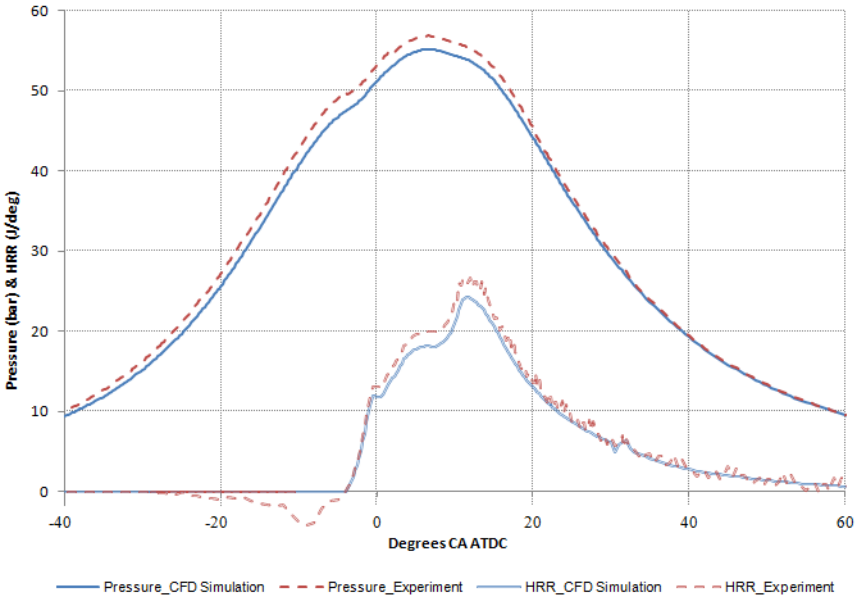

Figure 4.5: Comparison of simulated and measured in-cylinder pressures and heat release rates for single injection at 1,200rpm, low load.

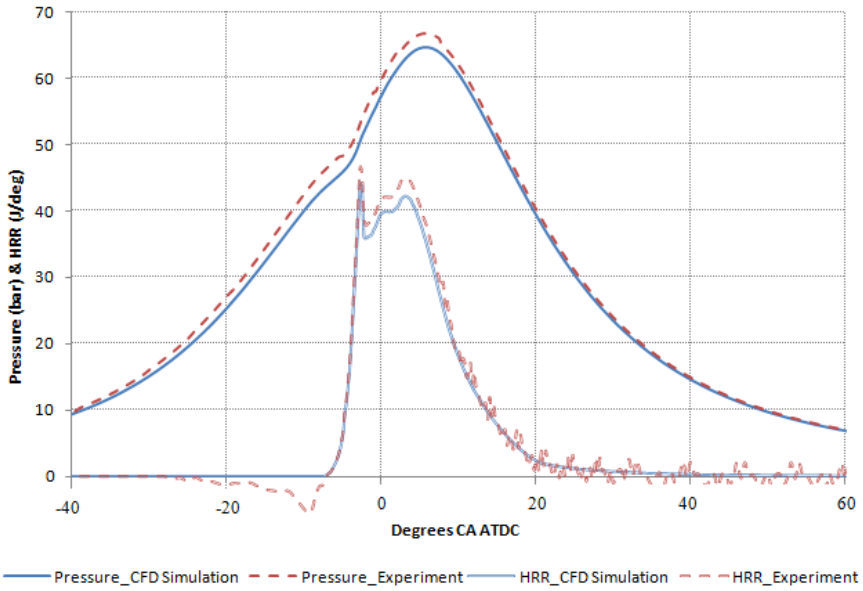

Figure 4.6: Comparison of simulated and measured in-cylinder pressures and heat release rates for single injection at 2,000rpm, high load.

The CFD simulation trend for the in-cylinder pressure seems to be reasonably close to the experimentally measured values for both operating conditions. There is only a slight pressure difference after the start of combustion, which might be related to experimental uncertainties in parameters in the computations such as the precise injection duration, start of injection and gas temperature at the IVC. On the other hand, the calculated heat release rate based on the experimental results seems to follow the same trend as in the simulation. However, the calculated HRR is slightly higher than the simulation experiments, and it seems to have a smoother drop after the end of combustion. Slight pressure and HRR variations between the experimental and simulation results will have a minimum impact on the results of the in-cylinder mixture homogeneity. A contingent small fuel injection variation will not significantly interfere with the air and fuel flow motions within the cylinder.

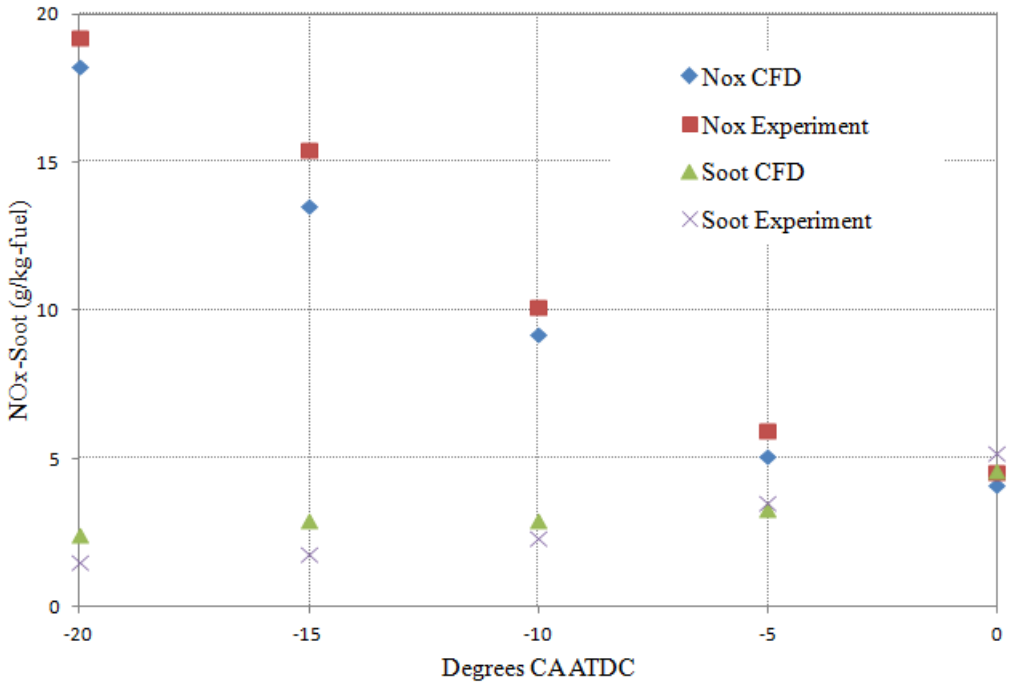

Figure 4.7: Comparison of simulated and measured NO_x and soot emissions for single injection.

Figure 4.7 presents the comparison of NO_x and soot emission formation for single injection cases with different starts of injection timing at 2,000rpm. It can be seen that simulation and experimental emission results are very similar for the cases where the start of injection occurs close to TDC. For cases with an earlier injection start, there is a very slight divergence that has possibly been caused by some air motion instabilities. In addition, the lower NO_x levels predicted by the CFD model are due to the fact that the NO_x formation model neglects the prompt NO formation by the attack of HC fragments on the air-nitrogen mixture, which could comprise up to 5% of total NO_x formation.

4.3.2 Multiple Injections

The model was validated for adopting a pilot and a main injection strategy in order to make sure that multiple injections do not affect the accuracy of the predicted results. The pilot injection was varied from 5% to 20% of the total fuel injected per cycle, while the start of the main injection was kept constant at 10°CA BTDC.

Figure 4.8 shows the NO_x and soot results gathered for three operating conditions featuring a pilot injection at a pressure of 1,600 bar and at a dwell angle of 5°CA. The simulation and experimental results for operating conditions featuring pilot injection are not as similar as the results in the single injection cases. This could possibly be due to variations of the injected fuel mass compared to the simulation model. Injection mass variations can be caused by fuel dribbling after the pilot injection or by failure of the injector's needle to reach its maximum lift due to the very small fuel amount injected during the first pulse. This can also be confirmed by the higher error in the soot and NO_x emissions in the cases with very low pilot fuel amount. Likewise in the single injection cases, the predicted NO_x formation is lower than the actual NO_x levels due to the lack of prompt NO formation in the simulation results.

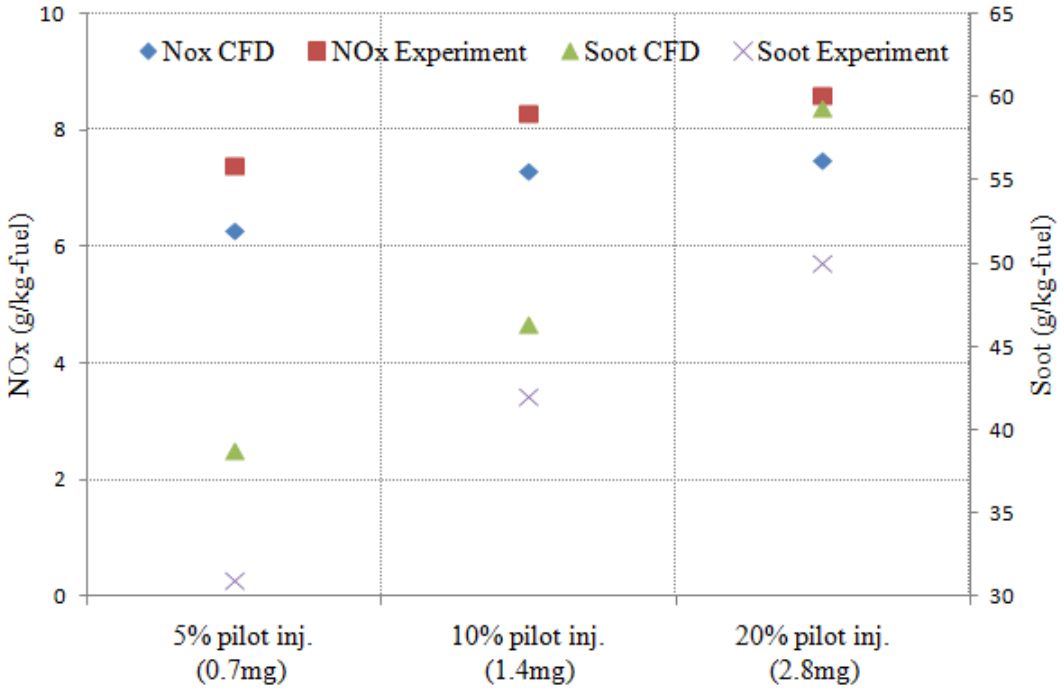

Figure 4.8: Comparison of simulated and measured NO_x and soot emissions for multiple injections.

4.4 Summary

This chapter has presented the CFD software used for simulating diesel engine combustion. A detailed analysis of the sub-models used in this research work has been performed. The chapter also included a grid independence analysis for obtaining mesh independent results and a model validation for single and multiple injection strategies using experimental data obtained from the Hydra engine described in Section 5.

Chapter 5

Experimental Facilities and Data Analysis

This chapter includes a step-by-step description of the research facilities built for this research study. It gives a brief description of the engine block, cylinder head, as well as the cooling, lubrication and fuelling systems of the engine. Moreover, details are given about the dynamometer and the data acquisition systems used. Finally, it also includes a detailed explanation of the data analysis techniques employed in this study.

5.1 Ricardo Single-cylinder Research Engine

5.1.1 General Description

A single-cylinder Ricardo Hydra engine has been used for all experimental testing in this study. The engine block was provided by Ricardo without a cylinder head fitted and no fuel injection or lubrication parts. It was placed on a specially designed steel frame with four rubber dampers for the absorption of vibrations while in operation. The flywheel of the engine was coupled to an ABB dyno using a driveshaft with torsional damper. The dynamometer used for starting and controlling the engine speed is an ABB ACS800-07 with direct torque control and a power range of 45kW.

The Ricardo Hydra engine was designed to be used with the standard production cylinder head of a Ford 2.0 litre ZSD 420 turbocharged engine. The Duratorq four-cylinder head consists of two air induction and two exhaust valves, double overhead camshafts and a centrally located injector. The powertrain for the excessive cylinders has been deactivated by removing the rocker arms, and the corresponding oil feed holes were blocked in order to prevent any oil spillage that could result in an oil pressure drop. The cylinder head also includes a glow plug that was replaced by a pressure transducer for in-cylinder pressure measurement. More details about the in-cylinder pressure sensor as well as the lubrication, cooling and fuelling systems of the engine test-bed can be found in the following sections. Figure 5.1 shows the final engine test-bed facility used for the experimental analysis and Figure 5.2 demonstrates a schematic diagram of the engine test cell.

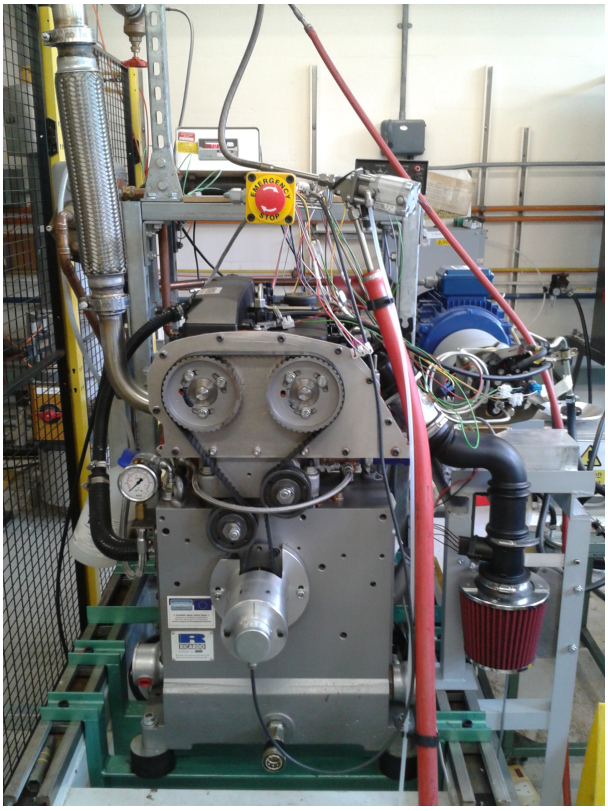

Figure 5.1: Ricardo Hydra engine test-bed.

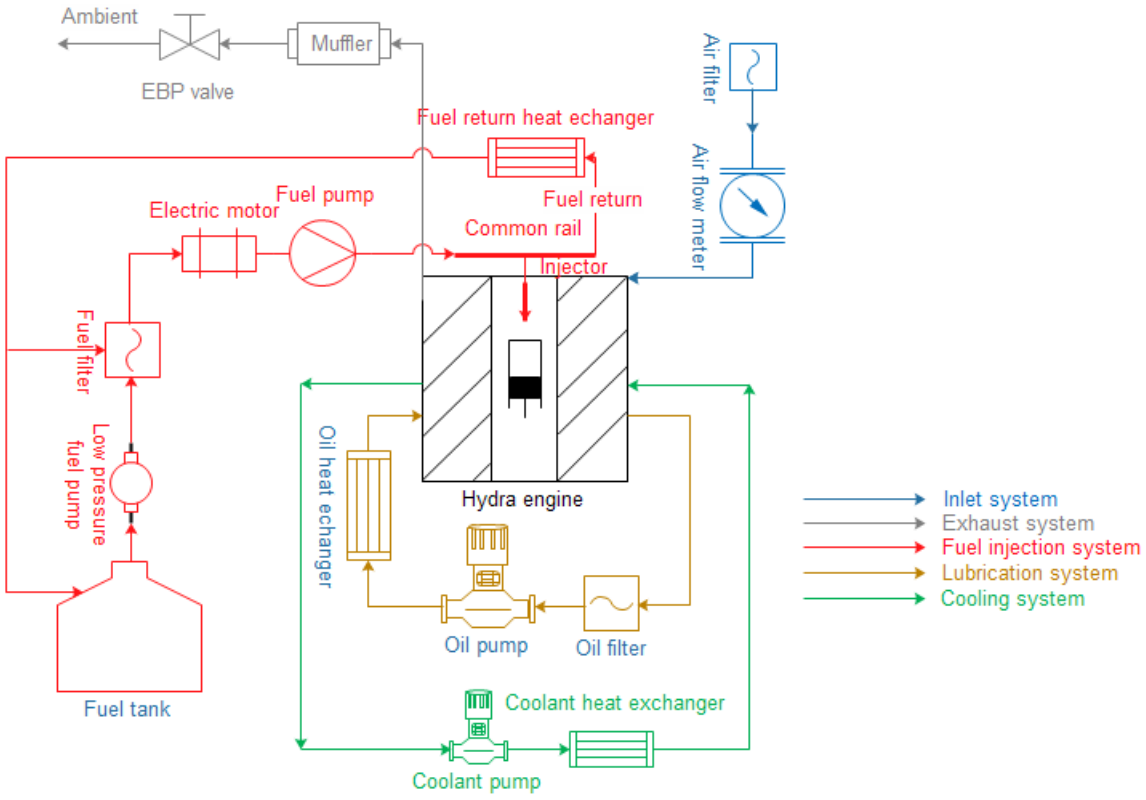

Figure 5.2: Schematic diagram of the engine test cell.

The crankcase assembly of the engine has a heavy cast-iron construction with flat machined outer faces and incorporates two x 1 kW lubricating oil heaters, two removable side plates, front and rear steel main bearing housings with lead bronze plated bush-type main bearings. The flywheel is machined from forged steel and forms four tracks of slots for signal pulsating. The piston and the connecting rod assemblies are from a Ford TDCI 2 litre HSDI diesel multi-cylinder engine. The main characteristics and the valve's timing and lift profiles of the four-cycle liquid-cooled compression ignition engine are shown in Tables 5.1 and 5.2.

Table 5.1: Ricardo Hydra engine specifications.

Ricardo Hydra Single Cylinder Engine	
Bore (mm)	86
Stroke (mm)	86
Swept Volume (l)	0.5
Maximum Rotational Speed (rev/min)	5000
Compression Ratio	18.3:1
Maximum Cylinder Pressure (bar)	165
Piston Shape	Mexican hat style

Table 5.2: Ricardo Hydra valve timing and lift profiles.

Intake Valve Lift	9.45 mm
Exhaust Valve Lift	9.00 mm
Inlet Valve Opening (IVO)	13°CA BTDC
Inlet Valve Closing (IVC)	64°CA ABDC
Exhaust Valve Opening (EVO)	69°CA BBDC
Exhaust Valve Closing (EVC)	33°CA ATDC

5.1.2 Fuel Injection System

A high-pressure fuel injection system has been used to promote a high level of atomization and air-fuel mixing within the combustion chamber. The fuel injection system of the engine test-bed consisted of a low-pressure hand pump that supplies fuel from the fuel storage tank to the motor-driven high-pressure pump. The fuel flows through a filter to remove any dirt and debris. The high-pressure pump can then pressurize the fuel up to 1,600 bar and deliver it to the common rail tube and the solenoid valve injector. The injector is used for precise high-speed multiple injections directly into the cylinder of the Hydra engine. The fuelling system schematic and the equipment used on the engine test-bed are shown in Figures 5.3 and 5.4.

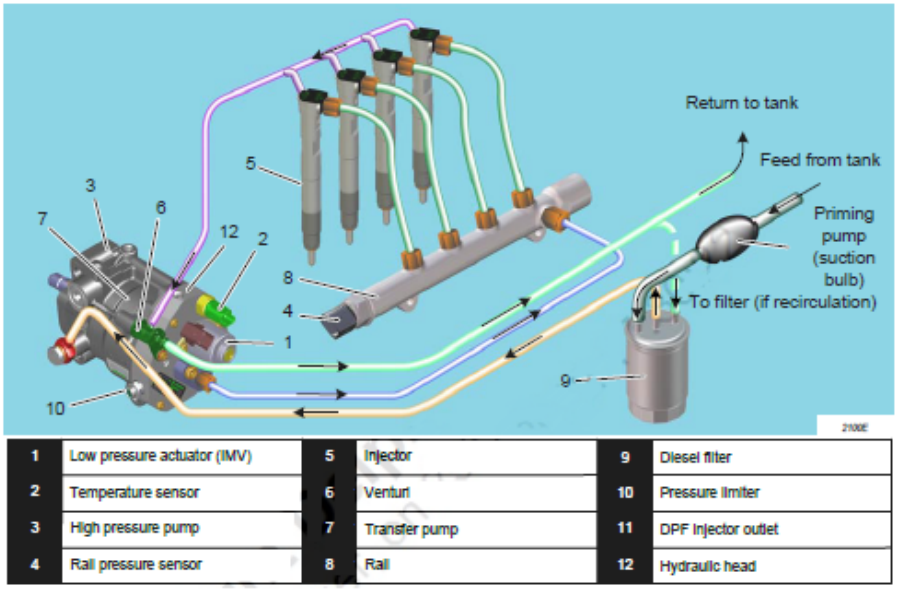

1	Low pressure actuator (IMV)	5	Injector	9	Diesel filter
2	Temperature sensor	6	Venturi	10	Pressure limiter
3	High pressure pump	7	Transfer pump	11	DPF injector outlet
4	Rail pressure sensor	8	Rail	12	Hydraulic head

Figure 5.3: Schematic diagram of fuel injection system [217].

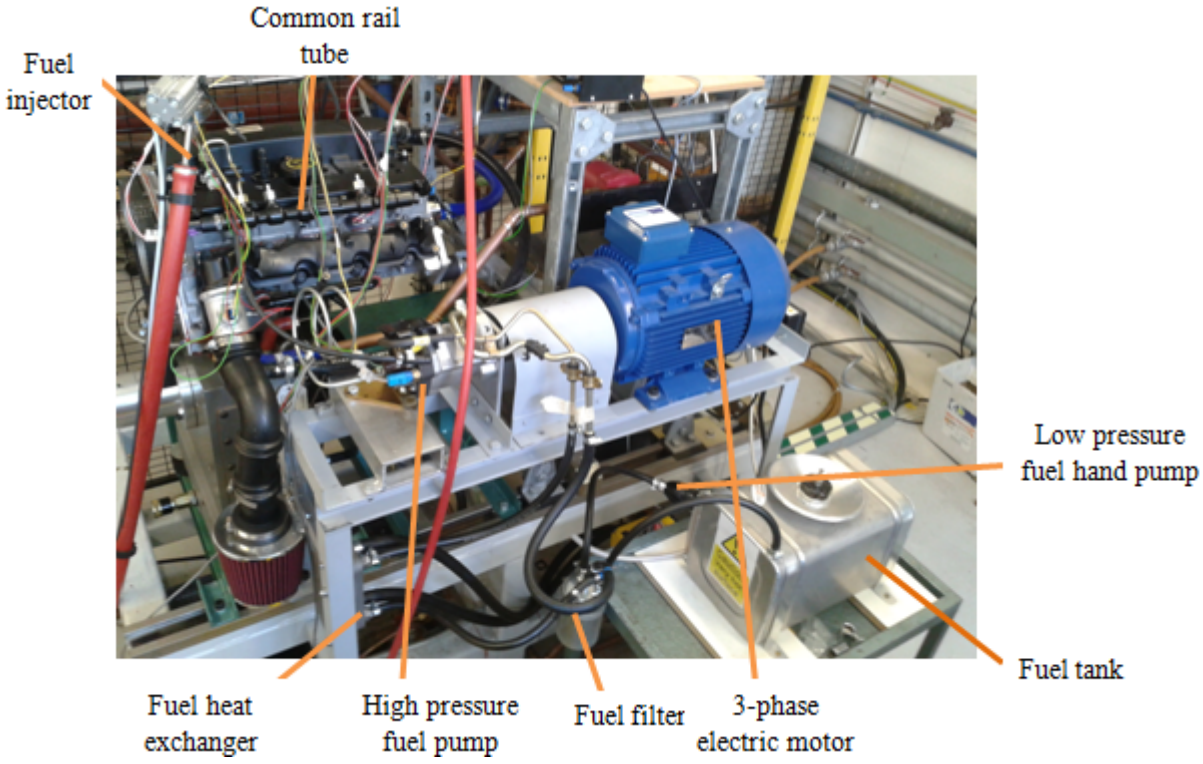

Figure 5.4: Fuel injection system.

5.1.2.1 Fuel Pump

A Delphi high-pressure four-lobe cam fuel pump was used for delivering high injection pressures to the common rail tube. The pump is driven independently by a three-phase electric motor in order to increase the flexibility of fuel pump rotational speed over the engine speed for further research. The electric motor was controlled using a VACON 10 AC drive and a VACON Live 1.1.5 user interface software tool. The rotational speed of the electric motor used for this study was selected based on a drive ratio of 1/2. The main problem faced for driving the pump independently was the vibrations of the CR tube while the engine is running, which may cause a fuel line crack as the pump is fixed on the ground. In order to solve this problem, a specially designed fuel supply line was used. The new fuel line was coiled up, as shown in Figure 5.4, in order to absorb any vibrations from the running engine and avoid any cracks that could lead to fatal accidents as a result of the extremely high fuel pressures.

The pump is equipped with an Inlet Metering Valve (IMV) for controlling the pressure in the rail by regulating the amount of the fuel sent back to the fuel storage tank. The excess fuel is returned back to the tank through a venturi, which creates a depression in the injector return circuit and allows the fuel pressure to decrease. In addition, a fuel temperature sensor is fitted on the pump, which is used in the injection control strategies to make corrections according to the diesel fuel temperature and also protect the system in case of fuel overheating. A cross-sectional view of the pump is shown in Figure 5.5.

One of the main concerns of using a standard production fuel pump to supply fuel to a four-cylinder engine for a single-cylinder research engine is the excessive work done. The Delphi pump used on the test-bed is designed to manage a 2.2l diesel engine and deliver 80-110kW on four injectors. This means that the level of fuel discharging from a single cylinder will be high, which, in turn, results in high amounts of energy and heat. The high heat generation combined with the small fuel tank that can only store a limited amount of fuel can lead to a very high fuel temperature that can be damaging for the pump. For this reason, a heat exchanger has been used (see Figure 5.4) for cooling down

the excessive fuel returned from the high-pressure pump to the fuel tank and to control the fuel temperature.

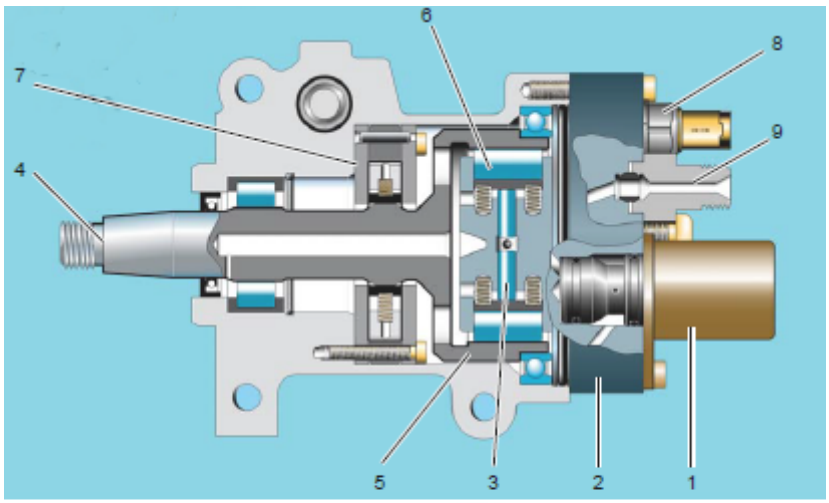

1	Low pressure actuator *(IMV)*	6	Roller / Shoe
2	High pressure pump / Hydraulic head	7	Transfer pump
3	Plunger Piston	8	Fuel temperature sensor
4	Drive transmission shaft	9	High Pressure Exit
5	Rotary cam		

Figure 5.5: High-pressure fuel pump cross-sectional view [217].

5.1.2.2 Common Rail Tube

The common rail system used on the test-bed was provided by Delphi. This is a linear rail providing four injector ports as shown in Figure 5.6 with a maximum pressure up to 1,600 bar and a volume of 18cm3. A high-pressure sensor is fitted on the one side of the tube for pressure measurements. The pressure readings are sent to the ECU of the engine for closed-loop control of the injection pressure and for the calculation of injection flow-rate and timing.

Figure 5.6: Delphi Common Rail tube.

5.1.2.3 Fuel Injector

A Delphi Common Rail six-hole solenoid injector shown in Figure 5.7 was used for the fuel injection system. The injector benefits from operating pressures of up to 1,800 bar and a maximum of five injections per cycle. It is capable of injecting fuel amounts varying from 0.5 to 100mg per injection under pressures from 150 to 1,800 bar. The amount of the fuel injected is proportional to the injection time (pulses) and rail pressure. The injector is also equipped with a back-leak circuit with a special low pressure connector for returning any excessive fuel back to the fuel pump.

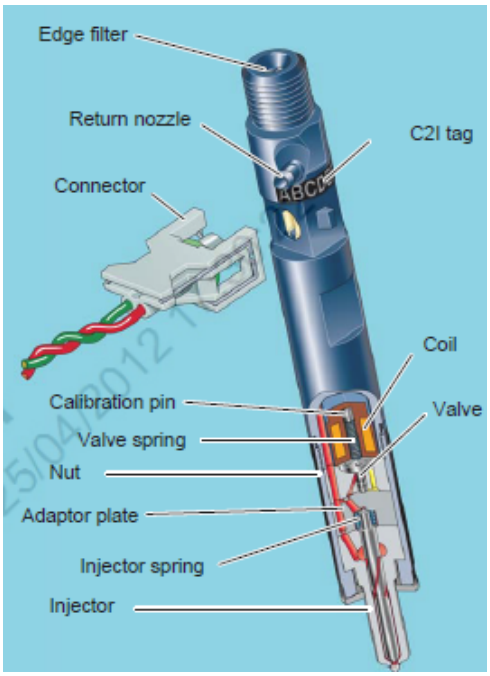

Figure 5.7: Delphi Common Rail solenoid injector [217].

The high operating injection pressure of this injector means that the force needed for the injection needle to be lifted is very large. The force required by the electromagnetic actuator to operate the injector needle can be achieved with a high amount of current. However, the rise time for establishing such currents would be incompatible with the reaction times needed for multiple injections. Also, the high currents would require a lot of power, which can lead to substantial overheating of the ECU system. Therefore, the injection needle is operated indirectly by a valve located above the needle, which manages control pressure rise and discharge. The valve opens in order to discharge the control chamber into the return circuit at the start of injection when the needle has to lift. At the end of injection, the valve closes so that the control chamber pressure resets.

5.1.3 Air Flow System

The air flow system used in this study is quite simple, as this is a naturally aspirated engine. There are no air boosting or EGR devices fitted on the engine. However, the engine is equipped with two adjustable camshaft pulleys that have been designed using Solidworks CAD software and built in the workshop. The adjustable pulleys allow a 30°CA rotation on both sides (positive and negative) of the inlet and exhaust camshaft for varying the opening and closing times of the valves. Figure 5.8 shows the 3D design and prototype of the adjustable camshaft pulleys. More details about the intake and exhaust systems follow in sections 5.1.3.1 and 5.1.3.2.

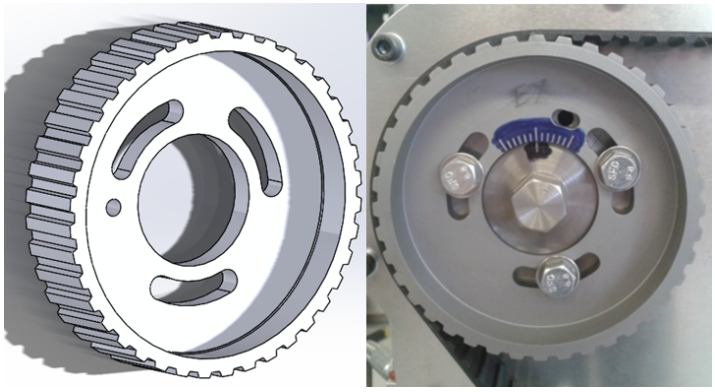

Figure 5.8: Adjustable camshaft pulley 3D design and prototype.

5.1.3.1 Intake System

The intake system of the engine test-bed is analytically shown in Figure 5.9. An air filter is used for removing any solid particles such as dust from the air. The air then flows through a Bosch air flow meter, which is used for measuring the amount of air entering the combustion chamber in order to maintain the air-fuel ratio needed. The air flow meter is also equipped with a temperature sensor for air temperature readings. The air finally flows through a metal tube, before reaching the inlet manifold, where an air temperature sensor is used to provide the exact air temperature entering the cylinder to the ECU of the engine.

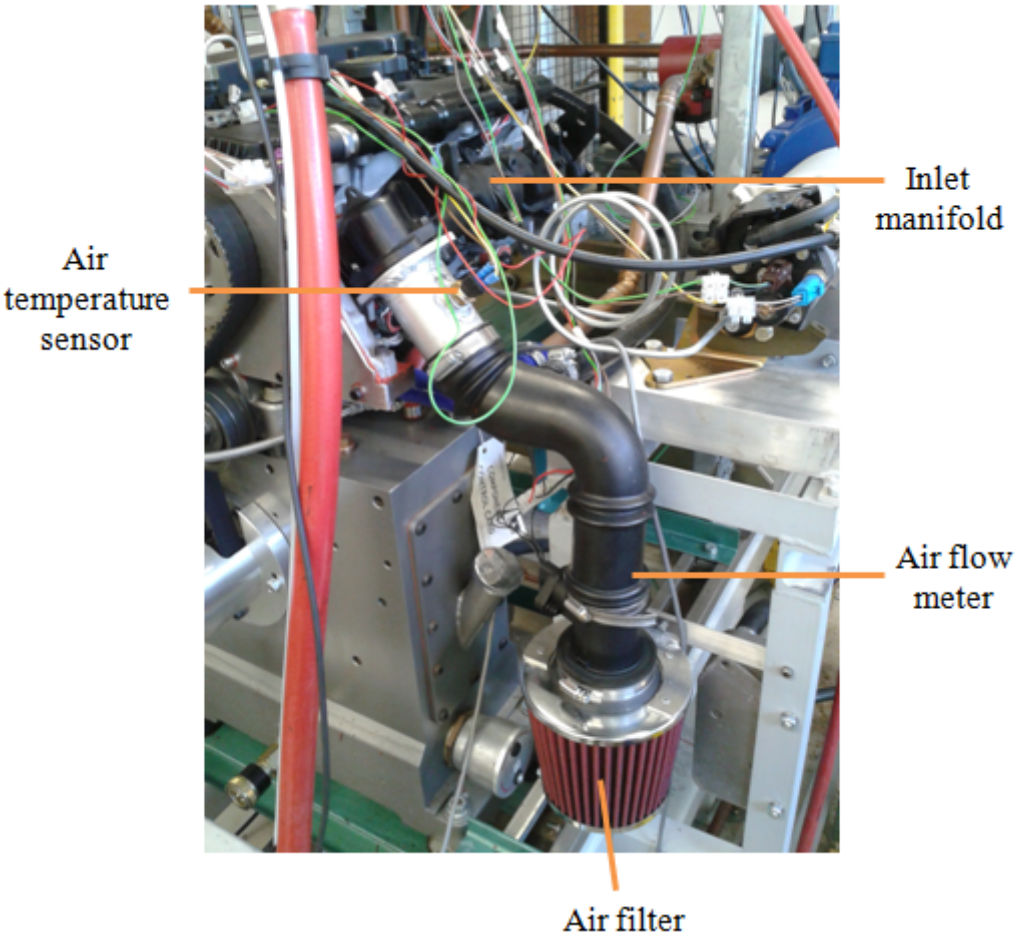

Figure 5.9: Air induction system of Hydra engine test-bed.

5.1.3.2 Exhaust System

A metal flexi pipe is used at the exhaust side of the engine test-bed for the absorption of any vibrations while the engine is running. The exhaust gas flows through the flexi pipe and passes through the emission analyser ports where samples of the exhaust air are taken for measurement of harmful emissions of the engine as well as of oxygen concentration to evaluate the quality of combustion. Moreover, the opacity of the air is also measured using an opacimeter fitted at the exhaust pipe of the engine. A round silencer is also placed on the exhaust side to reduce the amount of noise emitted by the engine. Finally, the engine test-bed is equipped with an exhaust back pressure valve, which can be manually used for restricting the exhaust flow and increasing the back pressure. A pressure sensor is fitted before the valve for exhaust back-pressure readings.

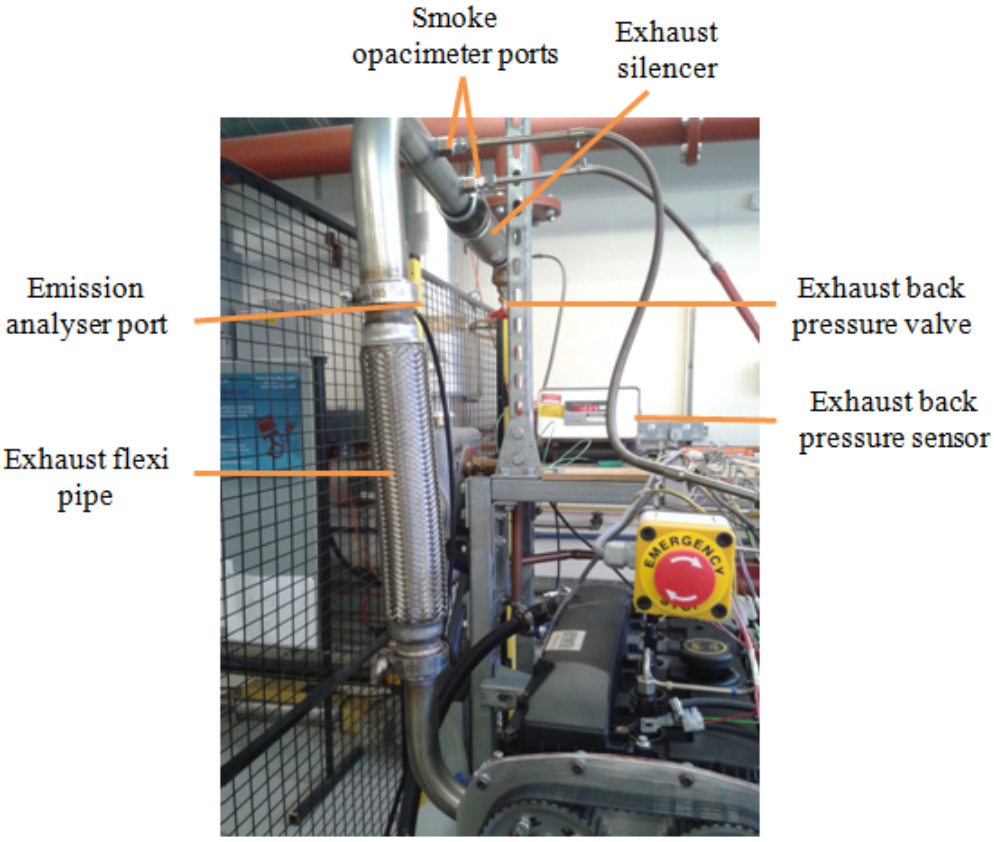

Figure 5.10: Exhaust system of Hydra engine test-bed.

5.1.4 Lubrication System

Engine lubrication is the key to keep things moving and to maintain good performance over a long period of time. The lubricating oil, which is contained in the engine sump, is pumped using an Albany VP3.5 rotary gear pump at a nominal rate of 14L/minute and a 0.75kW motor. The hot oil exiting the engine passes through a Bowman EC 90-1425-1 heat exchanger for heat dissipation and is then pumped back into the engine through an oil filter that removes any dirt or debris. Figure 5.11 shows a schematic diagram of the lubricating and oil cooling system.

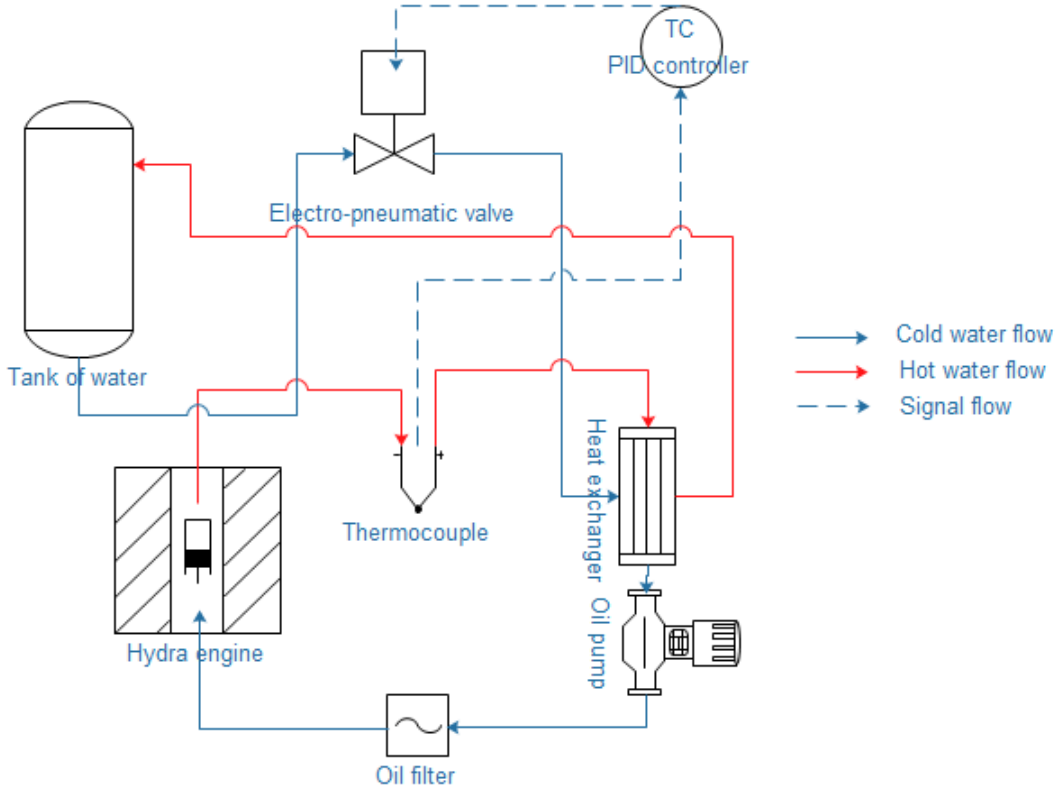

Figure 5.11: Schematic diagram of the lubrication system.

The cooling of the oil is achieved by using a K-type thermocouple, which is fitted at the oil outlet port of the engine for measuring the oil exit temperature. The temperature readings are sent to a ZelioControl REG48 PID controller, which, in turn, controls the

cooling water flows through the heat exchanger by using a Kinetrol electro-pneumatic valve. The oil exit temperature is controlled at 80°C, while the pressure is limited to 4 bar by a relief valve in the engine. A pressure switch on the engine also provides a signal to the safety system in case the oil pressure falls.

5.1.5 Cooling System

The water cooling of the engine works in a similar way as the oil cooling system. The coolant of the engine, which consists of de-mineralised water plus an anti-freeze solution and inhibitor, flows through the engine to dissipate the heat generated from the work done.

At the exit of the coolant from the engine, there are two temperature sensors. The first one provides information about the engine temperature to the ECU, which regulates the appropriate injection strategies based on the engine temperature. The second, a K-type thermocouple, is used for controlling the cooling water rate flow through the Bowman FH100-3182-2 heat exchanger, which is used for reducing the temperature of the coolant of the engine. Similar to the lubrication cooling system, the engine temperature is controlled using a ZelioControl REG48 PID controller and a Kinetrol electro-pneumatic valve. The coolant is circulated using a GRUNDFOS Selectric UPS15-50 water pump with a maximum flow capacity of 15L/sec.

5.1.6 Control Panel

A control panel was built for starting and controlling the engine's driving conditions. The panel consists of two Proportional-Integral-Derivative(PID) controllers used for the engine coolant and oil cooling systems, an accelerator pedal potentiometer, an ECU dashboard monitor and switches for the water, fuel and oil pumps. Figure 5.12 presents the control panel of Hydra engine.

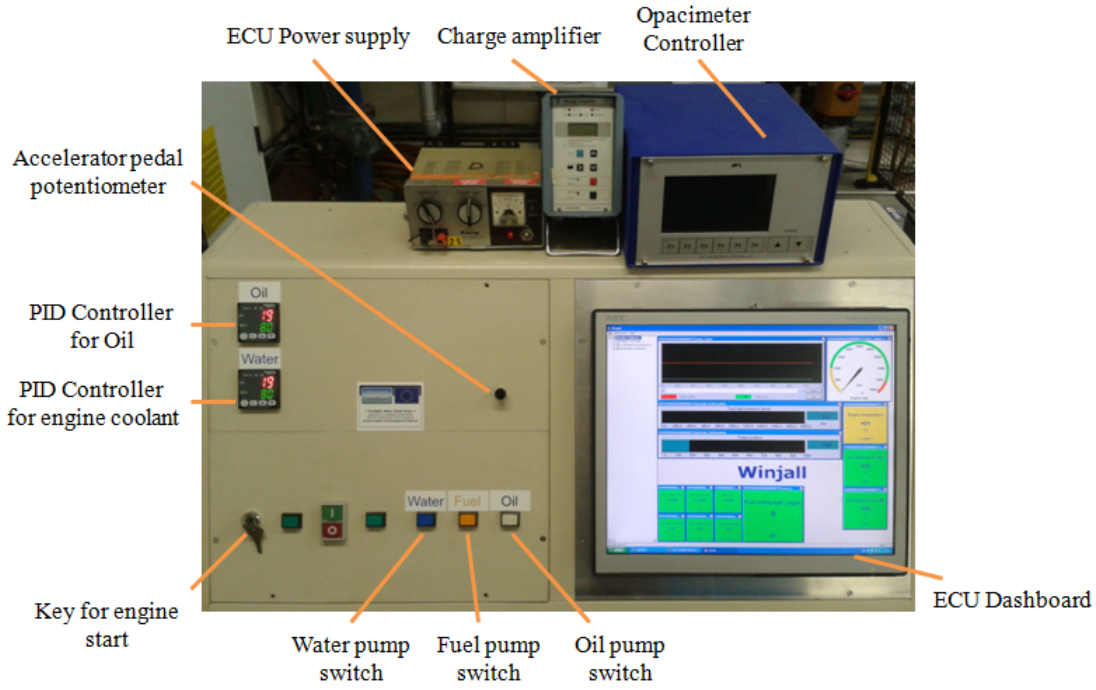

Figure 5.12: Hydra engine control block.

5.1.7 Experimental Procedure

The procedure for the experimental analysis met health and safety standards in order to preclude any serious accidents in the lab. The engine was fully protected with a metal cage, and all high-voltage cables were insulated and properly protected.

The oil and water pumps were activated before the start of the engine. Then, the engine rotation was initiated with the help of the dyno, and the fuel pump was switched on to fuel the engine. The engine warm-up period lasts for approximately half an hour until the water and oil-out temperatures reach 80°C. Once the engine is warmed up, the in-cylinder pressure data were collected using LabVIEW, and the emission levels as well as torque and power were measured. The same procedure was followed for all the tests performed. The in-cylinder pressure for each test was recorded after stabilization of the combustion and for 100 consecutive cycles in order to ensure the data were averaged.

5.2 In-Cylinder Pressure Data Acquisition System

The pressure within the combustion chamber during the engine cycle was measured using an in-cylinder pressure sensor fitted in the glow plug hole of the engine. The pressure measurements were used for calculating the heat release rate during combustion. The heat release rate is a powerful tool for analysing the combustion characteristics of the engine. Moreover, pressure measurements can be used for detecting any air leakage problems from the piston window seals. The next sections describe the equipment and data acquisition system used for the measurement of in-cylinder pressure.

5.2.1 In-cylinder Pressure Measurement

A Kistler 6056A41 un-cooled piezoelectric pressure sensor for combustion engines was used for measuring the in-cylinder pressure of the Hydra engine. The sensor was fitted in the glow plug hole of the engine by using a Kistler 6542Q199 glow plug adapter. The sensor was connected to a Kistler 5011B charge amplifier for converting the electrical charge produced to a proportional signal voltage, which is subsequently fed to the data acquisition system. The measuring range of the transducer is between 0 and 250 bar with a sensitivity of -20pC/bar.

A Baumer incremental push-pull rotary encoder was fitted on the crankshaft of the engine in order to enable in-cylinder pressure recording per engine cycle. The shaft encoder provides 360 pulses per revolution, which is equal to one pulse per crank angle degree.

5.2.2 Data Acquisition System

The data acquisition interface employed for recording the in-cylinder pressure measurement of the engine was built in a LabVIEW software environment. A National Instruments (NI) M-series PCI-6289 data acquisition card was used for this purpose. An NI BNC-2110 shielded connector block was employed for connecting the signal outputs sent from the shaft encoder and the charge amplifier. Then, using software written in Lab-

VIEW, the crank angle position and pressure measurement per cycle were recorded and saved in a Microsoft Excel file. Figure 5.13 shows the computer interface for recording and saving the cycle-to-cycle in-cylinder pressure measurement.

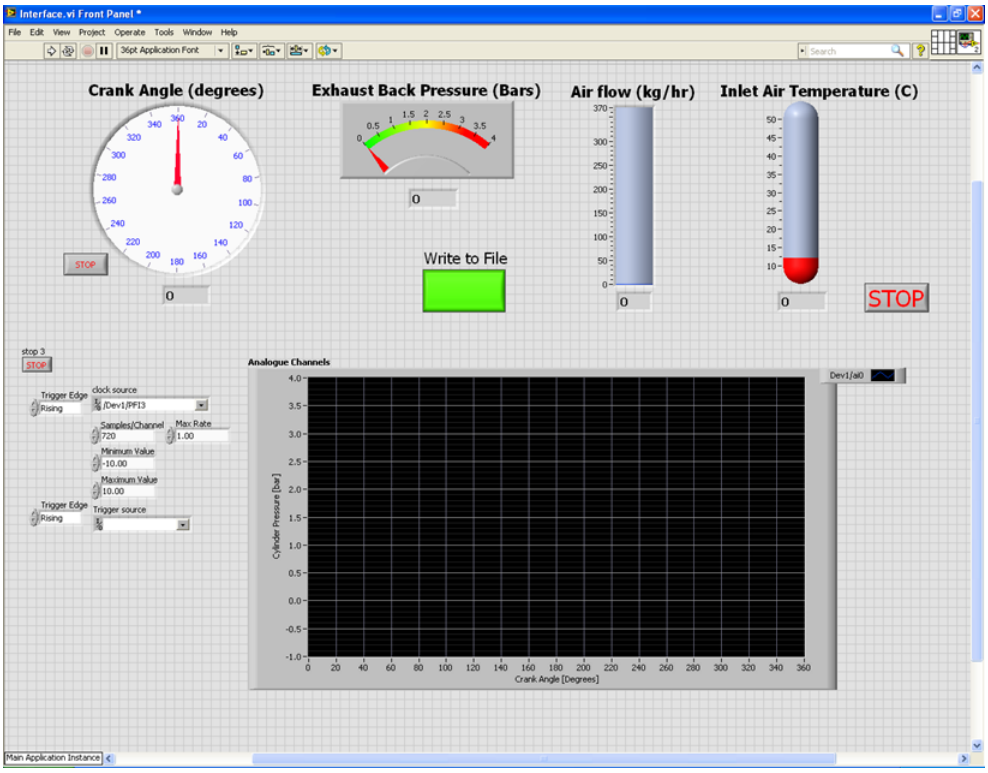

Figure 5.13: LabVIEW data acquisition software.

The two signal outputs obtained from the shaft encoder, one pulse per crank angle and one signal per rotation, were used as reference points for triggering and recording the start of each cycle.

The data acquisition system was used for recording and saving only the pressure data collected from the engine. The saved data were then analysed and used for evaluating the heat release rate and IMEP of the engine in a Microsoft Excel file.

5.3 Electronic Control Unit

A Commander6D Electronic Control Unit (ECU) connected with an injector driver IMg06, both supplied by Skynam, was used for controlling the running conditions of the Hydra engine. The Skynam ECU is a multi-purpose machine that can be re-programmed as many times as necessary according to ad hoc requirements. For this purpose, Skynam have developed a user-friendly computer interface software called Winjall, which allows tuning of engine functions and also works as an ad hoc engine monitor.

5.3.1 ECU Setup

The ECU set-up was established according to the installation manual of the hardware. The ground part of the ECU was connected directly to the engine block at a place where no paint, varnish or oxidation exists for safety reasons. The connection loom supplied also involved two 12-volt after-key power supplies of the ECU wires, two 12-volt after-key power supplies of the driver wires and a 12-volt after-key wire for the power supply of the ECU auxiliary commands. The wires were connected with automotive fuses to guarantee proper operation according to the plan shown in Figure 5.14.

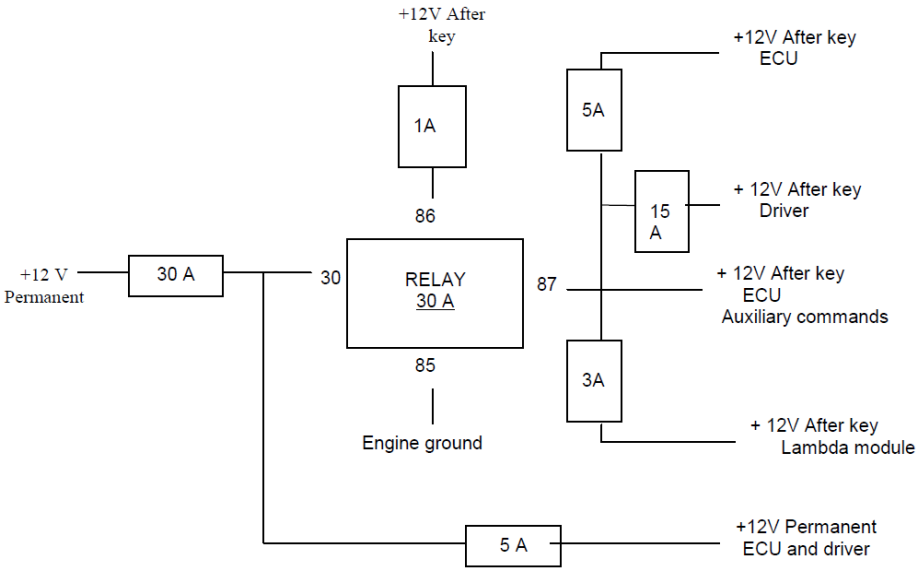

Figure 5.14: Schematic diagram of the ECU connections [218].

5.3.2 Sensors Connection

The standard loom of Commander6D supplies only six connections of sensors: accelerator pedal potentiometer, engine temperature sensor, air intake temperature sensor, air intake pressure sensor, fuel high pressure and temperature sensors. The air intake pressure was not used in the Hydra engine, as this is a naturally aspirated engine, so the air pressure would always be 1 bar.

Extra sensors were added by connecting the additional wires supplied with the loom including the air-flow meter sensor, the fuel low pressure sensor, the Hall Effect rpm and phase sensors. The installation of the Hall Effect rpm and phase sensors is necessary to identify the engine crankshaft position, speed and engine stroke in order to ensure fuel injection takes place only during compression and not at the exhaust stroke. Figure 5.15 shows the final look of the ECU and injector driver connection setup.

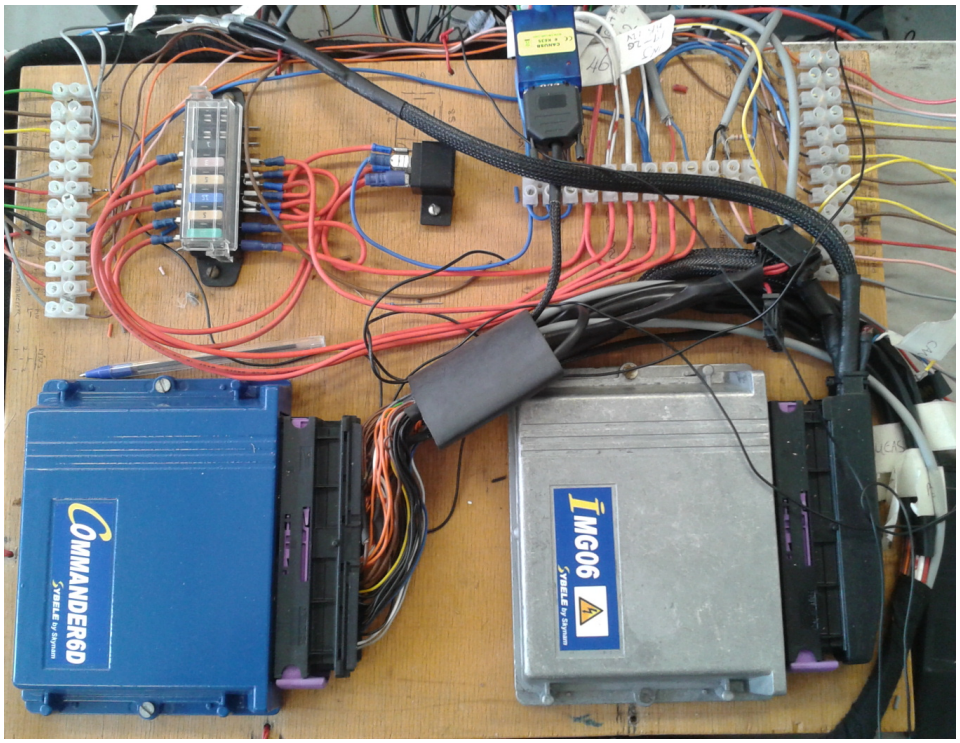

Figure 5.15: ECU and injector driver connection set-up.

5.3.3 Engine Calibration

The engine was calibrated using a stroboscopic lamp and follows the procedure described below. The flywheel configuration of the Hydra engine has 58-2 missing teeth (56 real teeth). The rising edge of the first tooth after the two missing teeth on the flywheel is considered the TDC by the ECU. The engine was set precisely at the real TDC and the TDC positions on the engine block and on the crankshaft flywheel were taken. By using the "Top Dead Centre Reference" calibration function of the ECU software, the injection start angle was set to 0°CA. Then, while the engine was running, the stroboscopic lamp was switched on. The stroboscopic lamp flashes at the time of injection. By setting the right angle in the "Advance of the flywheel TDC mark compared with the engine TDC" tab in the "Top Dead Centre Reference" calibration function as shown in Figure 5.16, the lamp will flash at the point where the mark on the crankshaft faces the mark on the engine block. This means that the TDC point considered by the ECU is the real TDC of the engine.

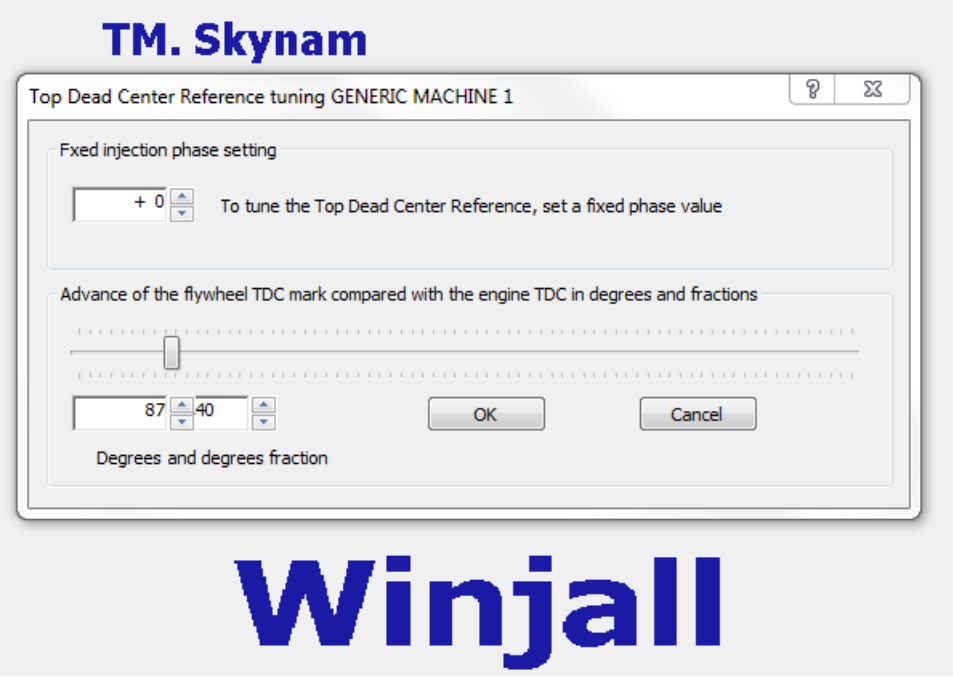

Figure 5.16: Top Dead Centre Reference tuning.

5.3.4 ECU Interface

Winjall software was used for tuning the Skynam ECU and for instantaneous monitoring of engine running conditions. The software allows tuning of air and fuel injection parameters. The dashboard of the software allows the monitoring and saving of engine parameters such as engine speed, pedal position, fuel pressure, fuel consumption and injection timings. Figure 5.17 shows a snapshot of the main injection running as well as the dashboard for monitoring the engine's running conditions.

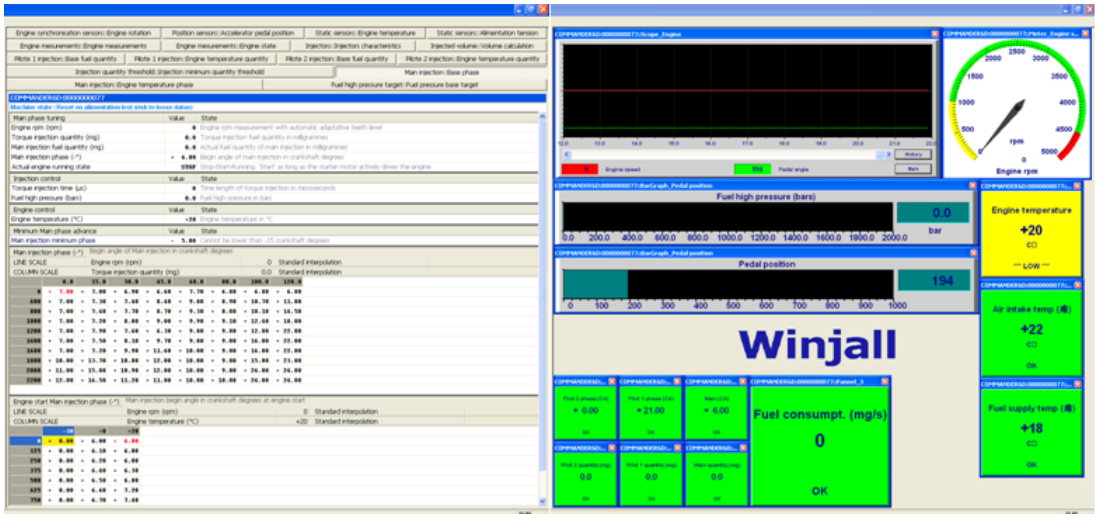

Figure 5.17: ECU main injection tuning and ECU dashboard.

5.4 Data Analysis

The data collected from the shaft encoder fitted on the crankshaft of the engine and the in-cylinder pressure have been used to determine the combustion characteristics of the engine such as HRR, ignition delay, BMEP and BSFC under various operating conditions.

5.4.1 Cylinder Volume

The cylinder volume of the engine for any crank angle degree is calculated based on the piston geometry characteristics using the following equations. The cylinder volume is needed for calculating the HRR of the engine.

$$V = V_c + \frac{\pi B^2}{4}(l + a - s) \tag{5.1}$$

Where

	V	is the cylinder volume
	V_c	is the clearance volume
	B	is the cylinder bore
	l	is the connecting rod length
	a	is the crank radius
	s	is the distance between crankshaft and piston pin axis

Figure 5.18 illustrates the symbols used in Equations 5.1, 5.2, 5.3, 5.4 and 5.5.

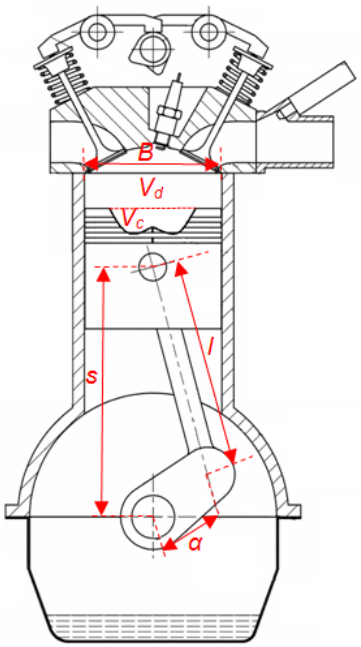

Figure 5.18: Schematic diagram of a typical diesel engine cylinder (symbols definition can be found in Equations 5.1, 5.2, 5.3, 5.4 and 5.5).

The distance between the crankshaft and the piston axis is given by:

$$s = acos\theta + \sqrt{(l^2 - a^2 sin^2\theta)} \tag{5.2}$$

By using Equation 5.3 that describes the compression ratio of the engine:

$$r_c = \frac{V_d + V_c}{V_c} \tag{5.3}$$

Where r_c is the compression ratio
V_d is the displacement volume

and the ratio of the connecting rod length to the crank radius:

$$R = \frac{l}{a} \tag{5.4}$$

Where R is the connecting rod length to crank radius ratio

Then, Equation 5.1 can be rearranged to:

$$V = V_c\{1 + \frac{1}{2}(r_c - 1)[R + 1 - cos\theta - \sqrt{(R^2 - sin^2\theta)}]\} \tag{5.5}$$

5.4.2 Heat Release Rate

The heat release rate of a reciprocating engine is a useful tool for analysing the combustion characteristics and understanding emission formation. The heat release rate is estimated by employing the First Law of Thermodynamics in the system based on the in-cylinder pressure and volume.

$$\frac{dQ}{dt} - p\frac{dV}{dt} + \dot{m_f}h_f = \frac{dU}{dT} \tag{5.6}$$

	$\frac{dQ}{dt}$	is the rate of heat transfer into system across boundary
	$p\frac{dV}{dt}$	is the rate of work transfer by system
Where	$\dot{m}_f$	is the fuel mass flow rate into system
	h_f	is the enthalpy of flux
	U	is the internal energy of cylinder contents

The mass flow rate into the system, at the point where both intake and exhaust valves are closed, includes the mass flow of the fuel injected and the air flow lost from the piston crevice. However, Equation 5.6 neglects any flow losses due to the difficulty in calculating them and the fact that HRR is used as an approximate measure.

The internal energy U is taken as the sensible internal energy, U_s and the enthalpy of flux h_f as the sensible enthalpy of the injected fuel. Then, the rate of heat transfer into the system becomes the net heat release, while dQ_n/dt is the difference between the heat release rate due to combustion and the heat transfer from the system. Since $h_f \approx 0$, then Equation 5.6 can be written as follows:

$$\frac{dQ_n}{dt} + p\frac{dV}{dt} + mc_v\frac{dT}{dt} \tag{5.7}$$

Where	c_v	is the specific heat at constant volume
	T	is the absolute temperature

Based on the ideal gas law, $PV = mRT$ and assuming that R is constant,

$$V\frac{dp}{dt} + p\frac{dV}{dt} = mR\frac{dT}{dt} \tag{5.8}$$

Where	R	is the ideal gas constant

By combining Equations 5.7 and 5.8, the gas temperature can be eliminated and the equation written as follows:

$$\frac{dQ_n}{dt} = (1 + \frac{c_v}{R})p\frac{dV}{dt} + \frac{1}{\gamma - 1}V\frac{dp}{dt} \tag{5.9}$$

By using the ratio of specific heat, $\gamma = \frac{c_p}{c_v}$, Equation 5.9 can be written as follows:

$$\frac{dQ_n}{dt} = \frac{\gamma}{\gamma - 1}p\frac{dV}{dt} + \frac{1}{\gamma - 1}V\frac{dp}{dt} \tag{5.10}$$

The value of γ varies depending on the temperature at different stages of the engine cycle. However, for simplicity, it is common practice to take γ as a constant value equal to 1.3.

5.4.3 Ignition Delay

The ignition delay of each combustion strategy was calculated using the estimated heat release rate. The ignition delay is defined as the timing between the start of the first injection and the start of combustion. The start of combustion can be established as the point where the HRR initially begins to increase.

5.4.4 Brake Mean Effective Pressure

Brake Mean Effective Pressure (BMEP) is used for evaluating engine performance under various fuel and air conditions. The BMEP, which is a measure of the useful power output of the engine, is related to the IMEP by the following equation:

$$BMEP = IMEP - FMEP - PMEP \tag{5.11}$$

Where $FMEP$ is the friction mean effective pressure
$PMEP$ is the pumping mean effective pressure

The IMEP can be calculated from the average in-cylinder pressure over the engine cycle according to the following equation:

$$IMEP = \frac{1}{V_d} \int_{y}^{x} p.dV \tag{5.12}$$

Where p is the in-cylinder pressure

The engine cycle of a four-stroke diesel engine is 720°CA; thus, the limits of integration range from 0 to 720.

The BMEP values of the engine can be simply calculated using the following equation:

$$BMEP = \frac{2\pi \bar{T} n_c}{V_d} \tag{5.13}$$

Where $\bar{T}$ is the average torque

n_c is the number of revolutions per cycle (for a 4-stroke engine n_c= 2)

V_d is the displacement volume

The engine torque values for the calculation of BMEP are obtained from the ABB dynamometer.

5.4.5 Brake Specific Fuel Consumption

Brake Specific Fuel Consumption (BSFC) is used to measure the efficiency of the fuel burnt over the work output of the engine. It is calculated based on the fuel mass flow rate and the IMEP of the engine.

$$BSFC = \frac{r}{P} \tag{5.14}$$

Where r is the fuel consumption rate (g/s)

P is the power produced

The engine power output for the calculation of BSFC is obtained from the ABB dynamometer.

5.5 Exhaust Emissions Measurement

The measurement of harmful emissions of the engine was performed by employing two emission analyser devices at the exhaust port of the Hydra engine. The first, a portable Testo 350XL, is capable of measuring O_2, CO_2, CO, NO, NO_2 and HC emissions. In addition, an AVL Opacimeter 439 model was used for measuring the smoke density in the exhaust gas.

5.5.1 Portable Emission Analyser

The Testo 350XL emission analyser was used for measuring the harmful emission of the Hydra engine. The analyser provides a 0.01ppm resolution and is capable of measuring O_2, CO_2, CO, NO, $NO_2$and HC emissions. The analyser is connected to a computer interface where instantaneous emissions values are displayed and saved in both numerical and graphical formats.

5.5.2 Opacimeter

An AVL Opacimeter 439 is used for measuring the soot emission formed during the operation of the Hydra engine. The opacimeter measures the opacity of the exhaust air by emitting light through a long measurement chamber where exhaust gas is flowing. A light detector on the other side of the measurement chamber receives the light signal sent and measures the opacity of the air. Figure 5.19 shows the operating principle of an AVL opacimeter. The opacimeter readings are sent to an AVL controller connected to a computer interface.

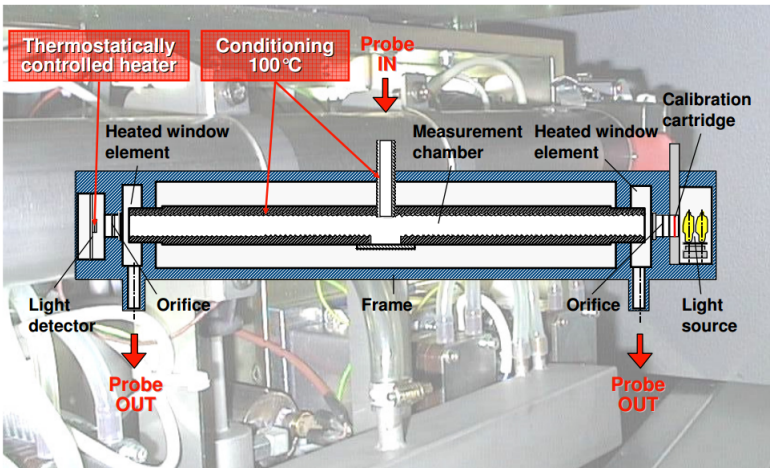

Figure 5.19: AVL opacimeter operating principle [219].

5.6 Summary

This chapter has provided details about the single-cylinder research engine used in this study. A brief description of the mechanical and electrical work for the building of the engine test-bed is given. A full analysis has been provided for the air, fuel, cooling and lubrication systems of the engine test-bed. In addition, details about the data acquisition and ECU systems as well as the data analysis procedures followed have been included. Finally, a description of the exhaust emission measurement devices used is given.

Chapter 6

Air-fuel Mixture Homogeneity Analysis

In this chapter, the effects of advanced injection strategies using multiple injection pulses per cycle are investigated using the HF and compared with single fuel injection approaches. This chapter is divided into three main categories. In the first one, the effect of injection timing of a single injection strategy on the HF is analysed. The second section involves the combustion and air-fuel homogeneity analysis of split injection strategies and split injection with an additional pilot injection early in the combustion chamber. In this section, a large amount of fuel is injected during the first main pulse, and a smaller amount of fuel is sprayed later close to the TDC. In some cases, this works as a post-injection strategy due to the low fuel rates injected during the second pulse. The final section involves the investigation of the effects of pilot fuel injection timing, pressure, amount and dwell angle on air-fuel homogeneity and combustion characteristics.

6.1 Single Injection

A single-injection strategy study was performed in order to understand and validate the newly introduced HF. The purpose of this study was to find the optimum start of the single injection based on the air–fuel homogeneity trend. Five single-injection

simulations were performed in total. The SOI was varied from 20°CA BTDC to 0°CA BTDC while the fuel injection pressure and the quantity were kept constant.

6.1.1 Engine Test Conditions

The single injection tests were performed under the air and fuel conditions shown in Table 6.1.

Table 6.1: Initial air and fuel conditions for single injection study.

Intake air temperature	380K
Intake air pressure	1 bar
Fuel temperature	350K
Fuel injected	14.5 mg/cycle
Injection pressure	1,600 bar
Start of injection	-20°- 0°CA ATDC

The five tests performed with a single injection were named after the start of injection timing following the letter A which stands for one injection. The SOI timing for the five tests is shown in Table 6.2.

Table 6.2: Single injection strategies.

Name	Start of Injection
A340	-20°CA ATDC
A345	-15°CA ATDC
A350	-10°CA ATDC
A355	-5°CA ATDC
A360	TDC

6.1.2 Combustion Analysis

The results obtained from the single injection tests were analysed based on the air-fuel mixing quality at the start of ignition point as well as the ignition delay and not the

engine performance and emission formation.

Figure 6.1 shows that the air–fuel mixture quality into the cylinder is directly influenced by the fuel injection timing. It is shown that, as the SOI advances, a more homogeneous, locally fuel-lean in-cylinder mixture occurs at an earlier stage in the cylinder.

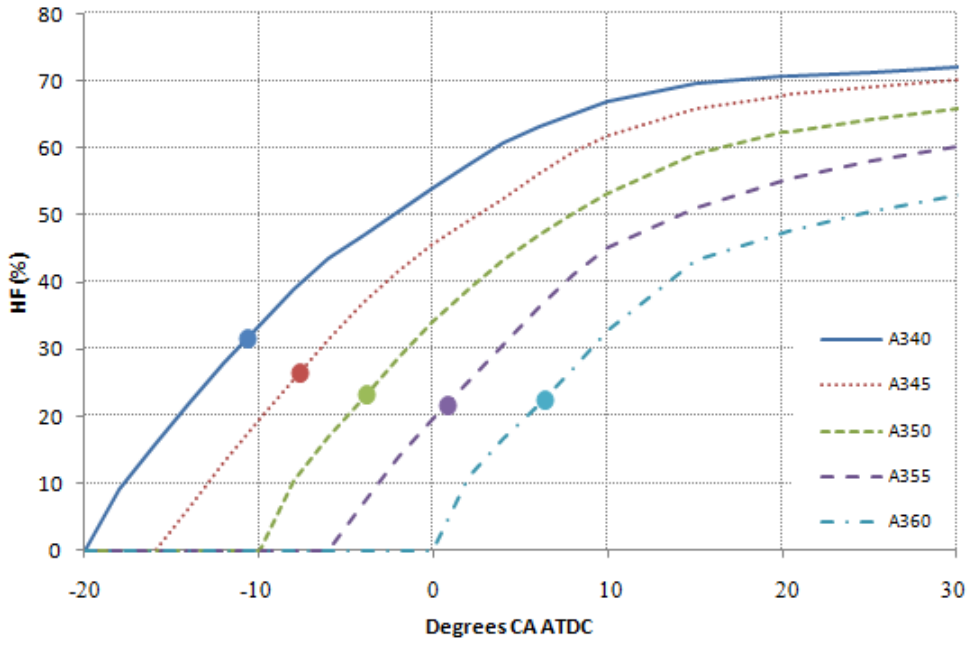

Figure 6.1: Simulation results provide HF for single-injection cases and HF (full circles) at the SOC.

Case A340 with an SOI of 20°CA BTDC was further analysed in Figure 6.2. It is shown that for case A340, where the fuel injection takes place at a very early stage, the in-cylinder pressure increases and a high value of the HF occurs closer to the TDC. The early injection leads to a longer ignition delay; therefore, more time is available to achieve a larger portion of the pre-mixed mixture, which leads to very high temperature and thus to a higher in-cylinder pressure.

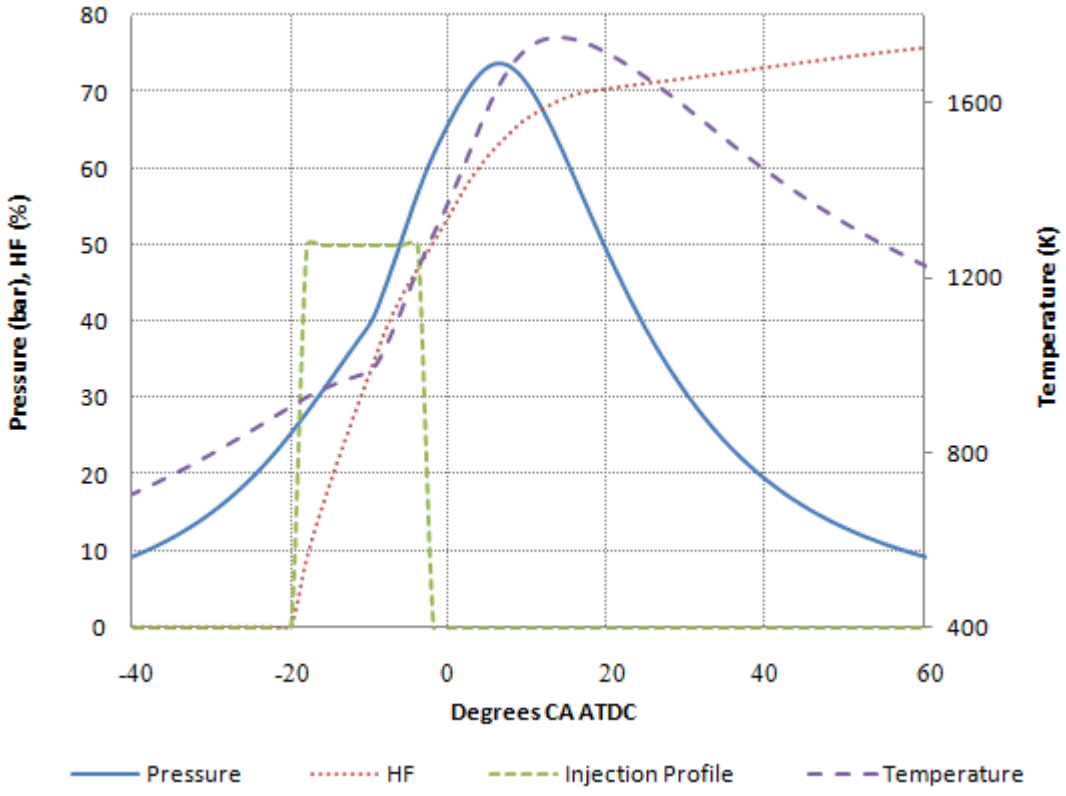

Figure 6.2: HF, injection profile, in-cylinder pressure and temperature for case A340.

As the SOI is retarded, the ignition delay is shorter because of the higher in-cylinder temperature closer to the TDC. Therefore the amount of pre-mixed combustion is reduced. This results in an increased amount of diffusion burning and a lower peak in-cylinder pressure due to late initiation of the combustion process during the expansion stroke where the piston is descending after the TDC.

Late fuel injection leads to fast pre-mixed combustion and less heat release, as shown in Figure 6.3. However, this is compensated by the fast heat release of combustion in a smaller volume near the TDC. As a result, the peak HRR remained almost constant for cases A340, A345 and A350. However, this did not occur for cases A355 and A360 where the heat release is slightly lower as the initiation of combustion took place at a late point where the in-cylinder pressure was relatively lower and the piston was descending after

the TDC.

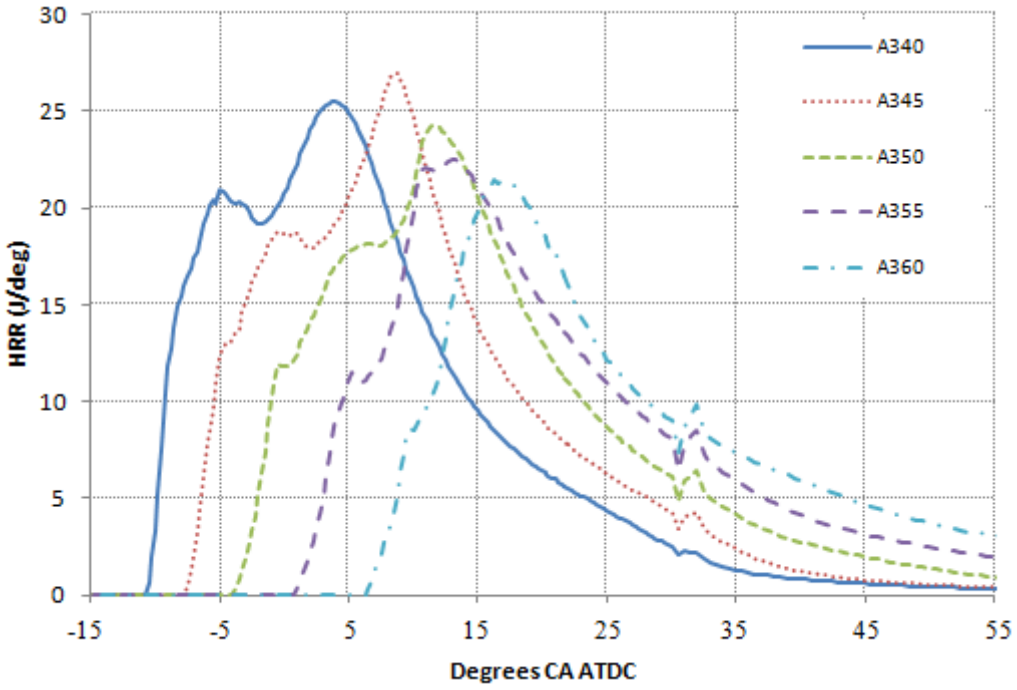

Figure 6.3: HRR graph for all A cases.

From the above study, it can be concluded that the newly introduced HF can be used as a useful measure for analyzing the air–fuel mixture and the combustion process. The simplicity of its format makes the HF an extremely useful indicator for practical applications. It is shown that strategy A350 has the shortest ignition delay and a relatively high HF at the ignition timing, and thus it was decided to use 10 CA BTDC as the SOI for the further experimental work.

6.2 Split Injection

In this section the effect of splitting the main injection into two pulses on the air–fuel homogeneity and the emissions formation is presented. In total, 12 double injection strategies were simulated. In the first pulse, the fuel injected varies from 70% to 80% and 90% at 10°CA BTDC, and the second pulse follows after 5°CA, 10°CA, 20°CA or

30°CA where the rest of the fuel is injected. In addition, two of the above cases were tested for the effects of an early pilot injection combined with splitting the main injection on the engine's performance and emission characteristics.

6.2.1 Engine Test Conditions

The split injection tests were performed under the air and fuel conditions shown in Table 6.3.

Table 6.3: Initial air and fuel conditions for split injection strategies.

Intake air temperature	380K
Intake air pressure	1 bar
Fuel temperature	350K
Fuel injected	14.5 mg/cycle
Injection pressure	1,600 bar
Start of first main injection	-10°CA ATDC
First injection ratio	70%, 80%, 90%
Dwell Angle	5°- 30°CA
Pilot Injection ratio	5%, 10%

The injection rates and dwell angle varies for each test. In order to make it clear, tests have been denoted according to the number of injections: cases B for two injections and cases C for three injections (one pilot injection + two main injections). Cases B and C are followed by the percentage of the fuel injected during the first injection and then by the dwell angle in degrees given in brackets which shows the angle between the end of the first or the second injection and the beginning of the second or the third injection respectively. For example, for case C5(10)70(10)25 the test is defined as follows: there were one pilot injection and two main injections into the cylinder; the pilot injection occurred with 5% of the total fuel injected during the pilot injection; the dwell angle between the pilot and the first main injection was 10°CA, which means that the pilot injection finished at 10°CA before the start of the first main injection; following this,

70% of the total fuel was injected during the first main injection and the last injection of 25% of the fuel occurred after a dwell angle of 10°CA.

6.2.2 Influence of the Split Injection Strategies

Figures 6.4, 6.5 and 6.6 present the air–fuel homogeneities over the cycle for 70%, 80% and 90% respectively of the fuel injected during the first pulse. As shown in these figures, the air–fuel homogeneities for the double-injection cases are improved temporarily at the point where the first injection ends. This is due to the available time for the fuel to be distributed with no more fuel diffusion compared with the single injection. However, when the second injection starts, the HF does not have the same upward trend and is even decreased in some cases. As can be seen in Figures 6.4, 6.5 and 6.6, the longer the dwell angle, the higher is the homogeneity in between the two injections and also the larger is the drop in the homogeneity while the second injection occurs at the end of the cycle. This can be caused by poorer combustion with more residuals left within the cylinder. From the figures below it can also be noted that, the higher the fuel quantity injected during the first pulse, the higher the HF is after the end of the combustion. This trend has different effects on the NO_x emissions, which will be demonstrated later in the document.

Figure 6.7 illustrates the NO_x and soot formation for the double-injection strategies. It is clear, as expected, that double injection with 70% and 80% of the fuel injected during the first pulse causes a significant decrease in the NO_x formation. The NO_x emissions are lower than for the single-injection strategy owing to greater control of the combustion process. The NO_x formation is lower for cases with less fuel injected during the first pulse. This is in agreement with the HF trend as a higher HF (cases with more fuel injected during the first pulse) will increase the rate of air–fuel mixing and therefore more complete combustion will take place, which results in an increase in the NO_x formation.

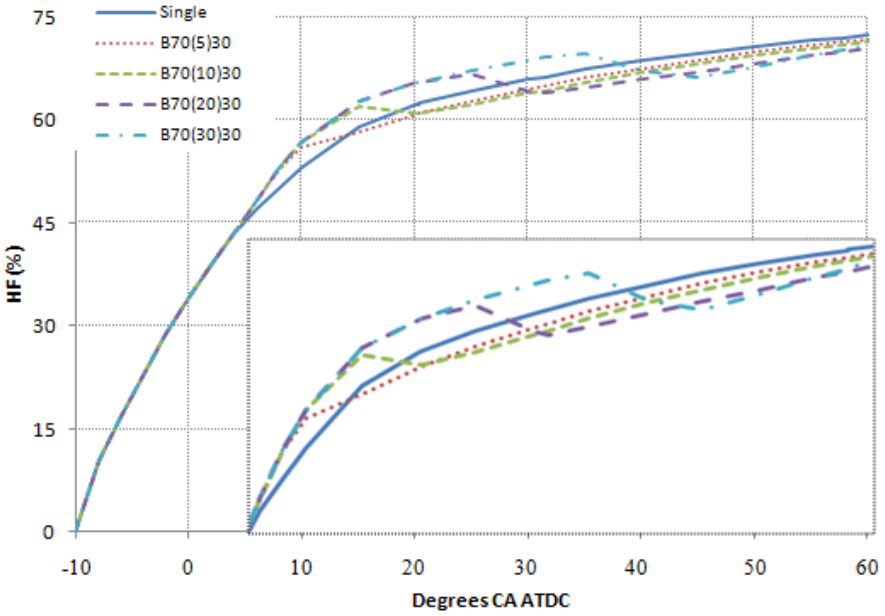

Figure 6.4: HF graph for cases B70.

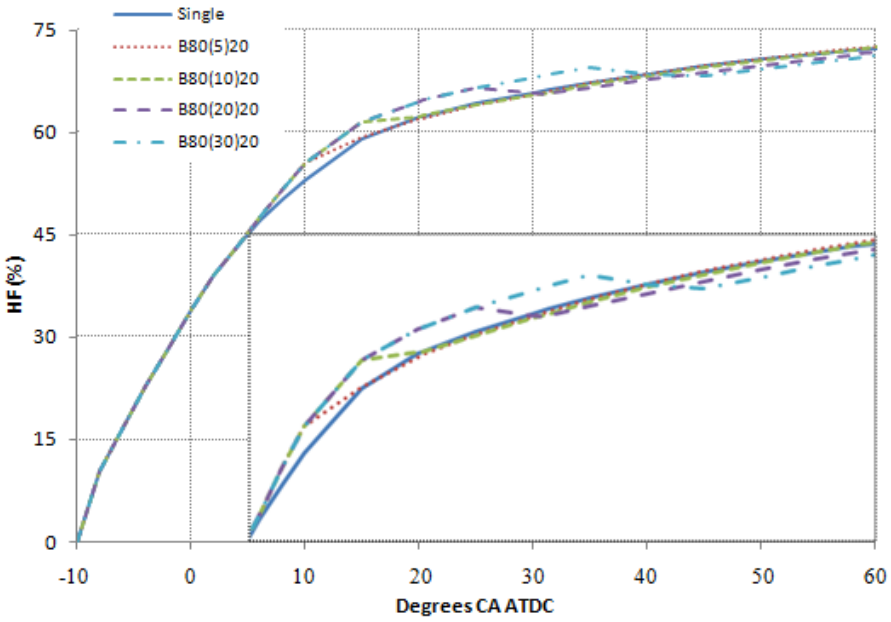

Figure 6.5: HF graph for cases B80.

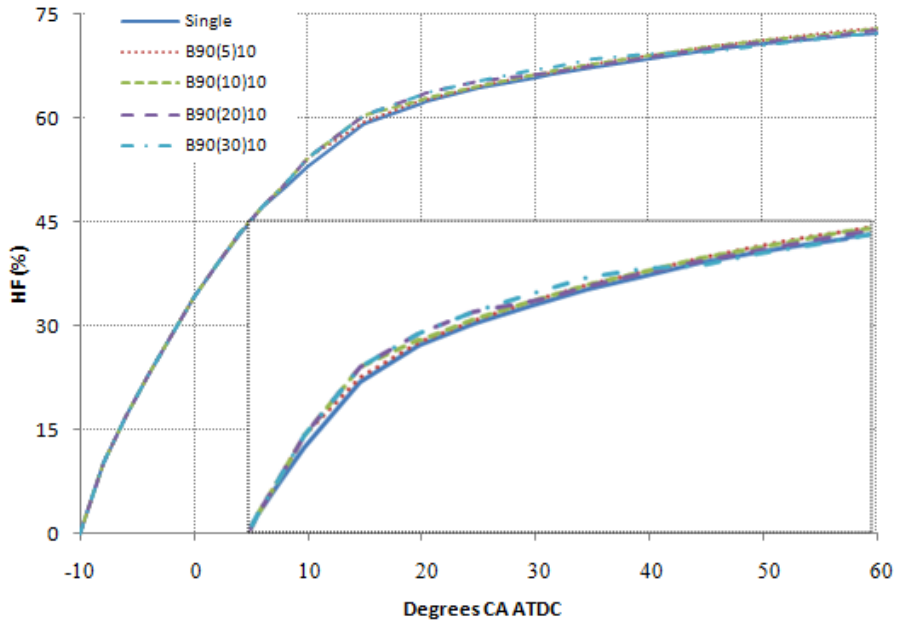

Figure 6.6: HF graph for cases B90.

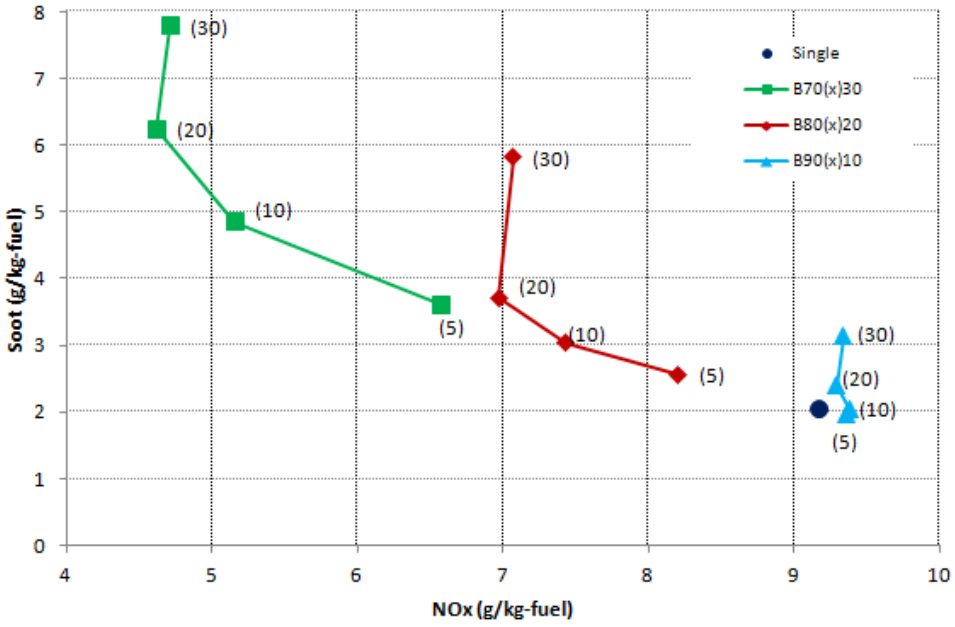

Figure 6.7: Soot–NO_x trade-off for cases A350 and B.

On the other hand, the split of the main injection into two pulses leads to higher soot formation. This is due to the fuel of the second pulse sprayed into burning regions from the first injection, leading to fuel-rich combustion. It is clear that, the higher the fuel quantity during the second injection, the more soot is formed. In addition, the larger the dwell angle, the more soot is formed owing to the poor soot oxidation from the late initiation of fuel combustion in the second pulse.

For the case with 90% of the fuel injected during the first pulse, it seems that this splitting ratio is not able to reduce the NO_x formation. However, for cases B90 with 5°CA and 10°CA dwell, it seems that the soot formation is reduced slightly.

Figure 6.8 illustrates the brake specific fuel consumption (BSFC) over the NO_x formation for the double injection strategies. It is shown that, for cases B90, the variations in both the BSFC and the NO_x emissions are smaller than for the other cases. From this figure, it can be concluded that the split injections show minimal effect on the BSFC when the second injection follows at a small dwell angle, and it has a relatively lower fuel amount compared with that of the main injection. Moreover, it can be noted that a higher HF (strategies with more fuel injected during the first pulse) results in a reduction in the BSFC. This is due to the improved air–fuel mixing quality, which leads to improved combustion and therefore to a lower BSFC.

Figure 6.9 represents the IMEP versus NO_x formation of double-injection strategies. It can be noted that the maximum IMEP levels can be obtained when having a small dwell angle between injections. In this case, a higher fuel quantity injected during the first pulse leads to a higher IMEP.

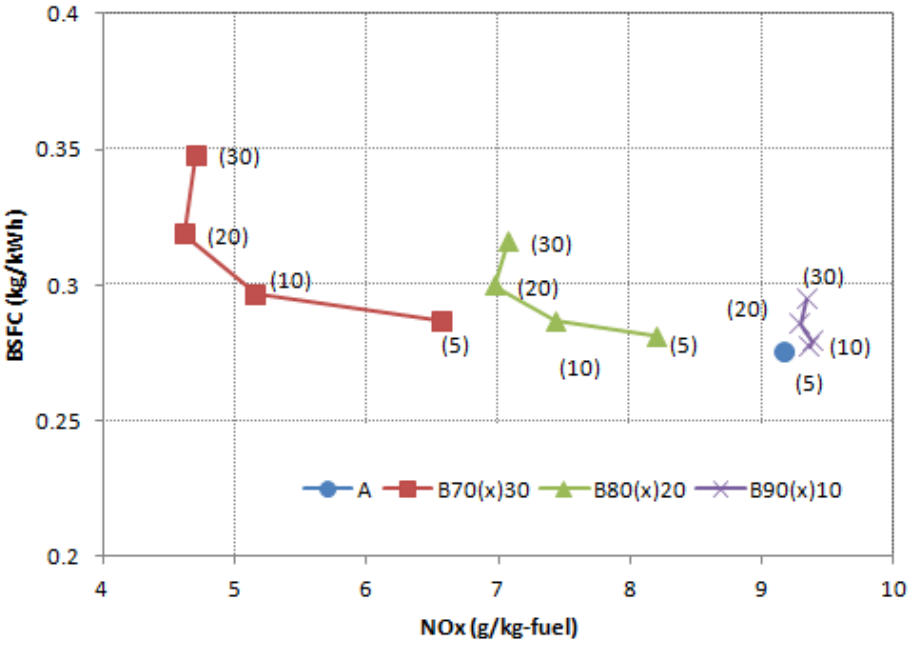

Figure 6.8: BSFC–NO_x trade-off for cases A350 and B.

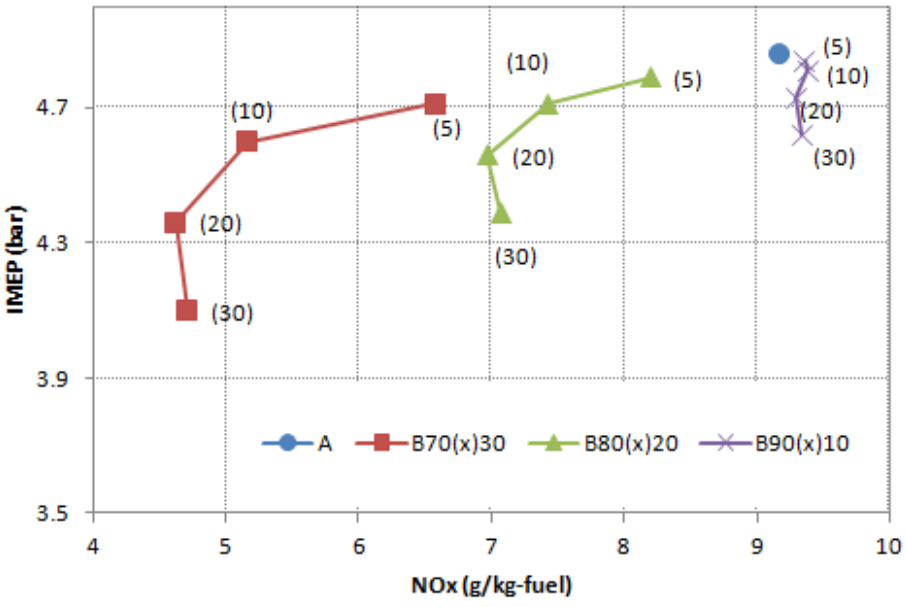

Figure 6.9: IMEP–NO_x trade-off for cases A350 and B.

From all the above figures, cases B70 and B80 with 5°CA and 10°CA dwell were selected owing to the combination of relatively low NO_x and soot formations. These cases are further analysed below on the basis of the air–fuel mixing homogeneity.

Figures 6.10 and 6.11 compare the NO_x and soot formation over the HF at four critical points after the SOI and combustion. In both figures the NO_x and soot trends compared with the HF trend are similar. It can be mentioned that, at 10°CA ATDC, the HF as well as the NO_x level and the soot level have their lowest values. At 20°CA ATDC, the HF increases to over 60% while the soot formation has a rapid increase for cases B70 and a lower increase for cases B80. The NO_x formation is still at low levels for both strategies. The NO_x emissions are increased once the HF rises above 65%. It can easily be seen from the figures below that the variations in the NO_x level and the soot level are based on the HF at different dwell angles. Figure 6.10 shows that the HF is slightly higher for the case with 10°CA dwell than the case with 5°CA at 370°CA. At this point it can also be seen that the NO_x formation is slightly higher in the 10°CA case. Later, at 30°CA ATDC, the HF trend changes and the HF for the 5°CA case is slightly higher than for the 10°CA dwell case. At the same time the NO_x formation trend also changes and the case with 5°CA shows a higher NO_x formation than does the case with 10°CA. Similarly, the soot formation for the 10°CA case is higher than for the 5°CA dwell angle.

From Figures 6.10 and 6.11 it can also be concluded that, the larger the dwell angle between the pulses, the less NO_x formation there is, while there is an increase in the soot formation.

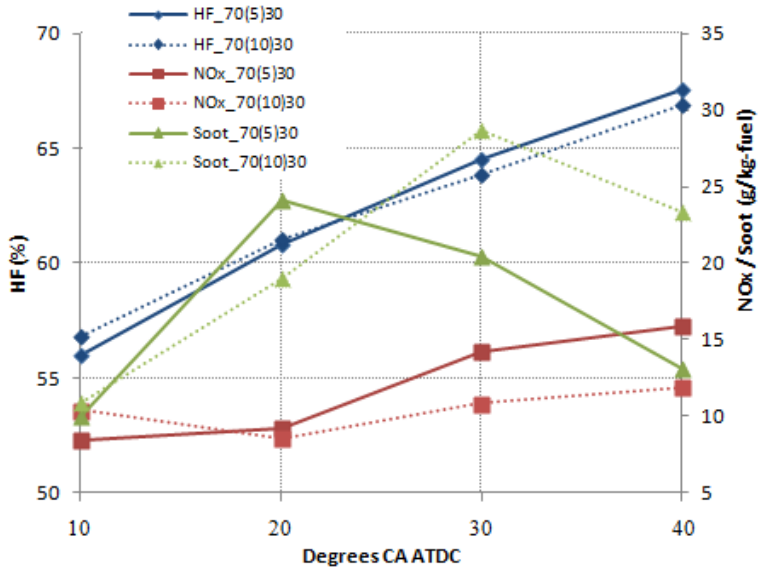

Figure 6.10: HF, NO_x and soot emissions for cases B70 with 5°CA and 10°CA dwell angles.

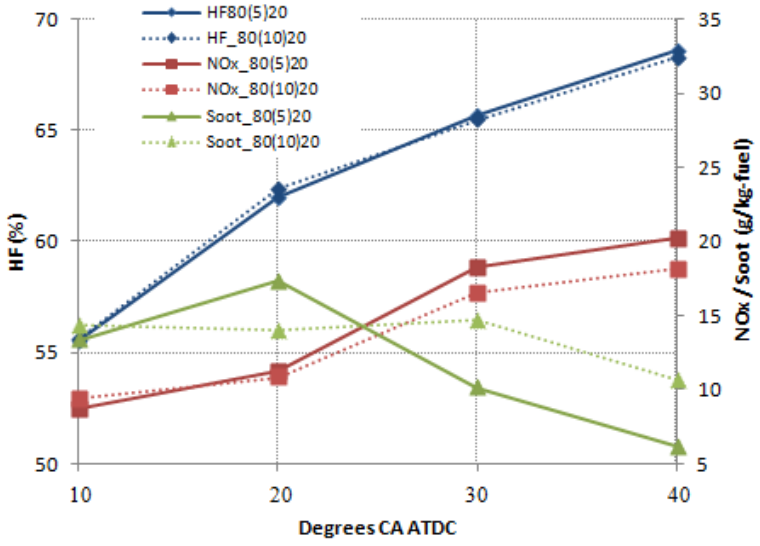

Figure 6.11: HF, NO_x and soot emissions for cases B80 with 5°CA and 10°CA dwell angles.

Finally, Figures 6.12 and 6.13 show the HRRs and the in-cylinder temperatures for the four cases compared with the single-injection strategy. It can be noted that the HRR for the single-injection case varies from the HRR for the split-injection strategies. The HHR graphs for the split injections show two peaks formed by the two injections into the cylinder and an obvious valley in between. It seems that the second peak occurred because of the late combustion stage, which led to high in-cylinder temperatures and pressures. It can also be seen that the second HRR peak is highly affected by both the dwell angle and the injection quantity in the second pulse. The smaller the dwell angle and fuel injection quantity during the second pulse, the higher is the second HRR peak.

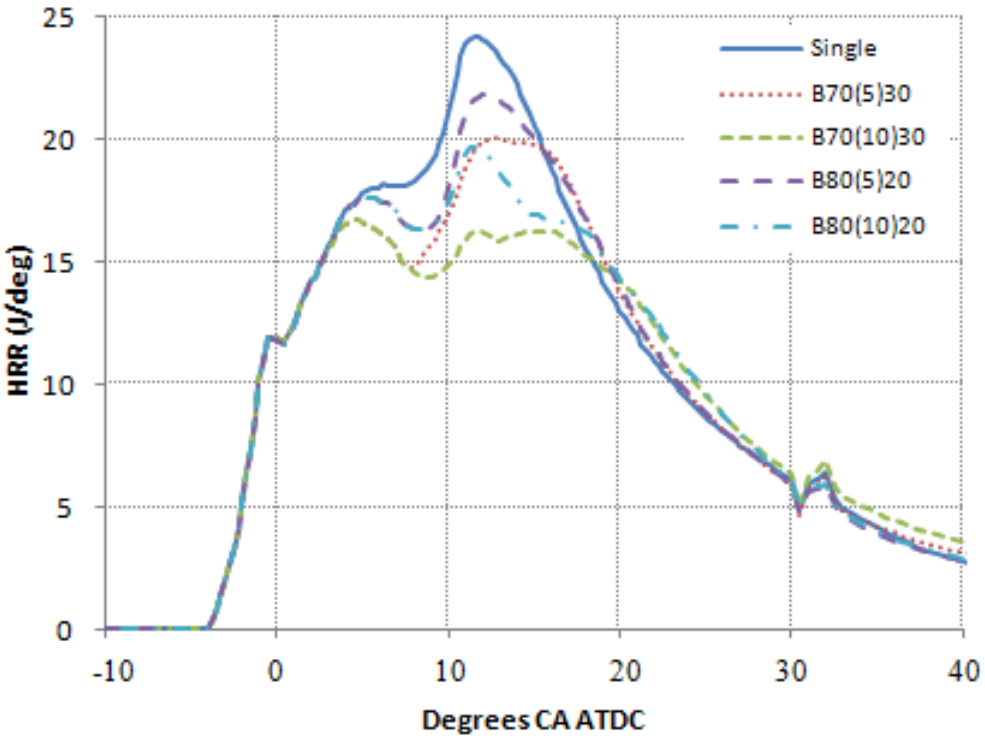

Figure 6.12: HRR graph for cases A350, B70 and B80 with 5°CA and 10°CA dwell angles.

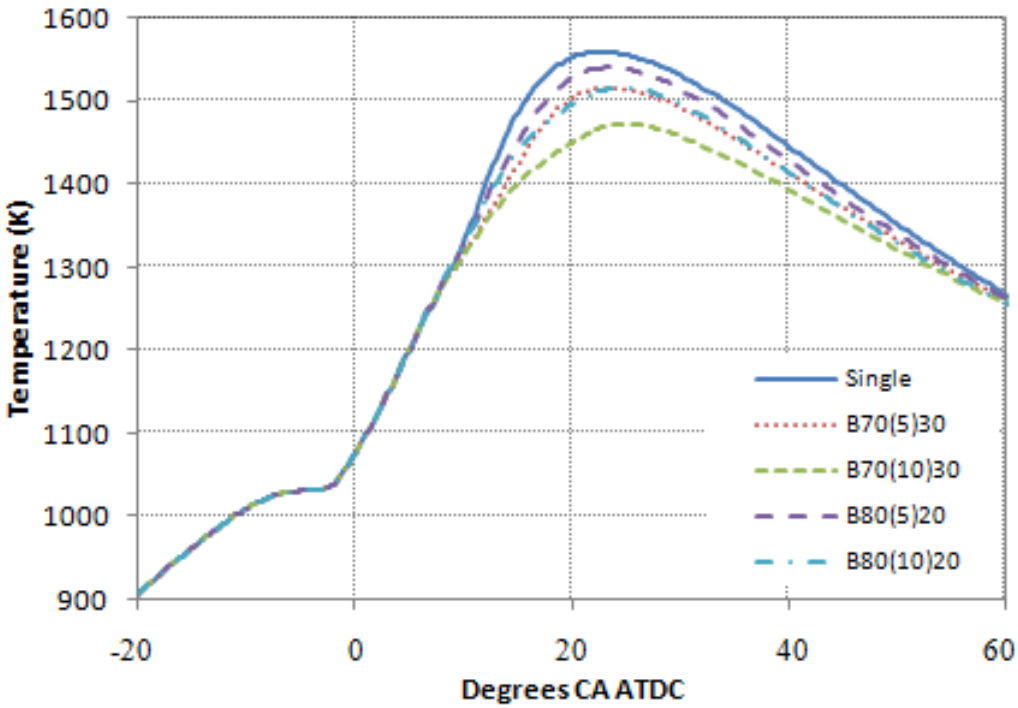

Figure 6.13: In-cylinder temperature graph for cases A350, B70 and B80 with 5 CA and 10 CA dwell angles.

6.2.3 Influence of the Pilot Injection

Cases B70 and B80 with 10°CA dwell angle were chosen owing to the combination of relatively low NO_x and soot emissions with high IMEP and low BSFC values for further research by implementing a pilot injection. The pilot fuel injected varies from 5% to 10% with a dwell angle of 10°CA and the fuel was absorbed from the final injection of each strategy.

Figure 6.14 shows that, owing to the early pilot injection into the cylinder, the HRR increases at an earlier stage. The maximum HRR reached in cases C is higher than those in the split-injection strategies (cases B).

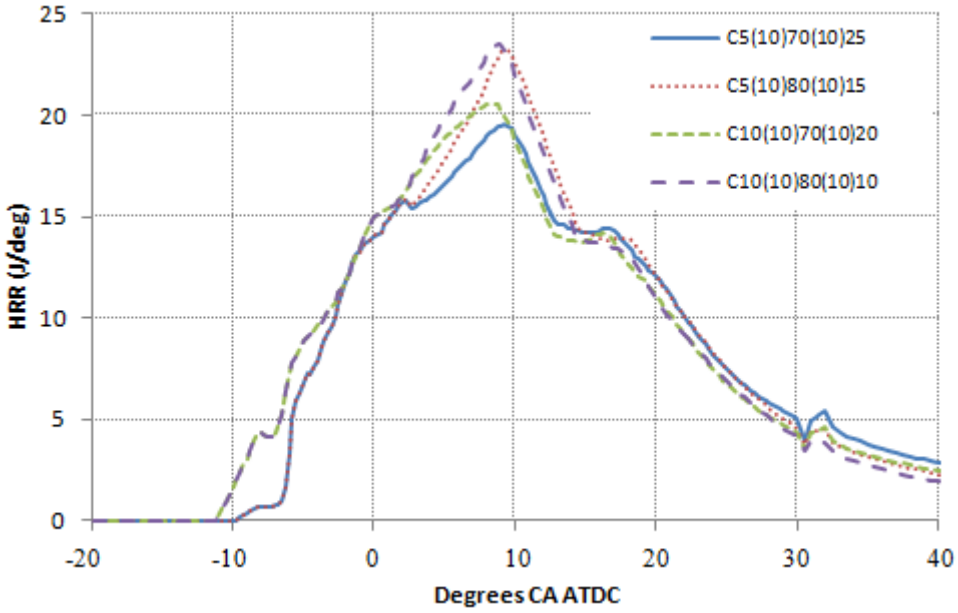

Figure 6.14: HRR graph for cases C.

Comparing Figure 6.12 and Figure 6.14 , we can see that, by implementing a pilot injection into the cylinder at an early stage when the pressure and the temperature are relatively low, it can lead to high sharp increases in the pressure and the HRR. It is also shown in Figure 6.14 that the cases with the same quantity of fuel injected during the pilot pulse have similar and equal heat release trends. It can be concluded that the pilot injection increases the HRR but at the same time the first main injection quantity plays a very important role in the percentage increase. Figure 6.14 clearly shows that cases with 80% of the fuel injected during the first main injection lead to a higher HRR than cases with 70%, irrespective of the pilot injection quantity.

As shown before by splitting the main injection in two pulses, the NO_x emissions can be dramatically reduced. However, there is a soot penalty because of the fuel-rich combustion taking place during the second injection. From Figure 6.15, it can be observed that, by implementing a pilot injection, the NO_x emissions are significantly increased instead of being reduced. The reason for this increase can be given by looking back at the HRR in Figure 6.14 where the high HRR trend indicates that the pilot

injection took place at a very early stage, leading to high temperatures and therefore to the increase in the NO_x emissions.

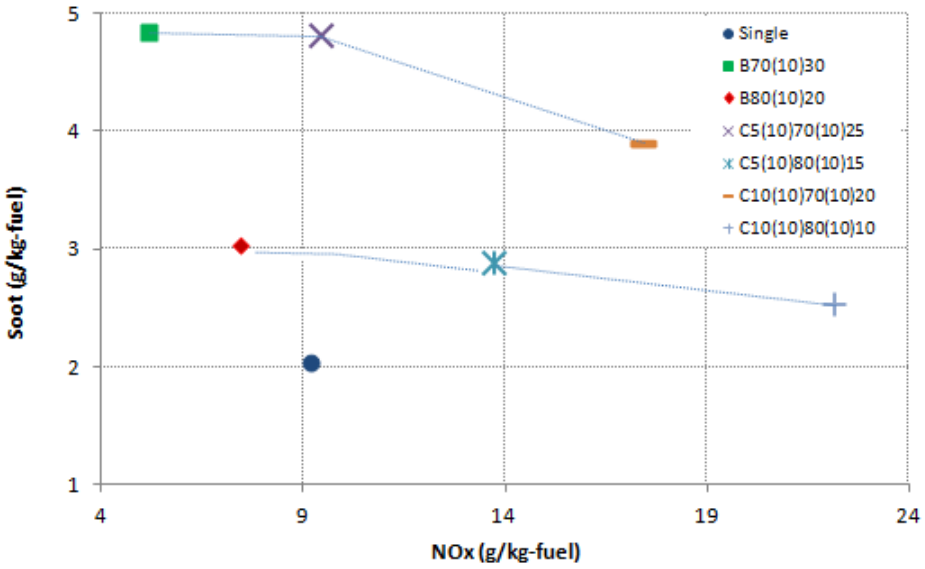

Figure 6.15: Soot–NO_x trade-off for the optimum cases A, B and C.

However, the soot emissions were slightly reduced because less fuel is injected during the second pulse compared with cases B. Therefore, less fuel-rich combustion and more soot oxidation take place in the cylinder. It can also be noted that the cases with 5% of the fuel injected during the pilot injection have lower NO_x emissions and higher soot emissions than the cases with 10% of the fuel injected during the pilot injection (Figure 6.15). This confirms the above justification for the variations in the NO_x emissions and the soot emissions.

The HF diagram in Figure 6.17 shows the air–fuel mixing quality into the cylinder for cases C relative to cases B70 and B80 with 10°CA dwell angle. The lines for the same SOI strategies overlap each other until the moment where some variation in the injection pulse occurs. It is shown that the HF at 5°CA BTDC, at the point where roughly the start of combustion for cases B occurs, is already at high rates because the pilot injection took place earlier in the cylinder. The HF for 10% of the fuel pilot injected is almost ten units higher than those for 5% of the fuel pilot injected. This is due to the earlier SOI,

as the pilot injection in cases with 10% fuel started almost 1°CA in advance. Looking at this high air–fuel homogeneity at the initiation of combustion after the first main pulse, we can definitely justify the expected NO_x increase compared with cases B, as shown previously. Moreover, it can also be noted from the following figures that the HF for cases C remain at higher levels than for cases B until a very late state of combustion. We can conclude that there is optimal and more complete fuel combustion in the cylinder with fewer residuals and therefore higher homogeneity. The results shown in Figure 6.17 once again prove the importance of the first main injection to the air–fuel homogeneity levels and as a result to the emissions formation. It can be seen that the cases with 70% of the fuel injected during the first main pulse have higher HFs at the end of the main injection as it still occurs in the cases with 80% injection. However, after a while when the first main injections in both the 70% case and the 80% case are over, the HF for 70% decreases and drops below that for the 80% case, which perfectly justifies the higher NO_x emissions.

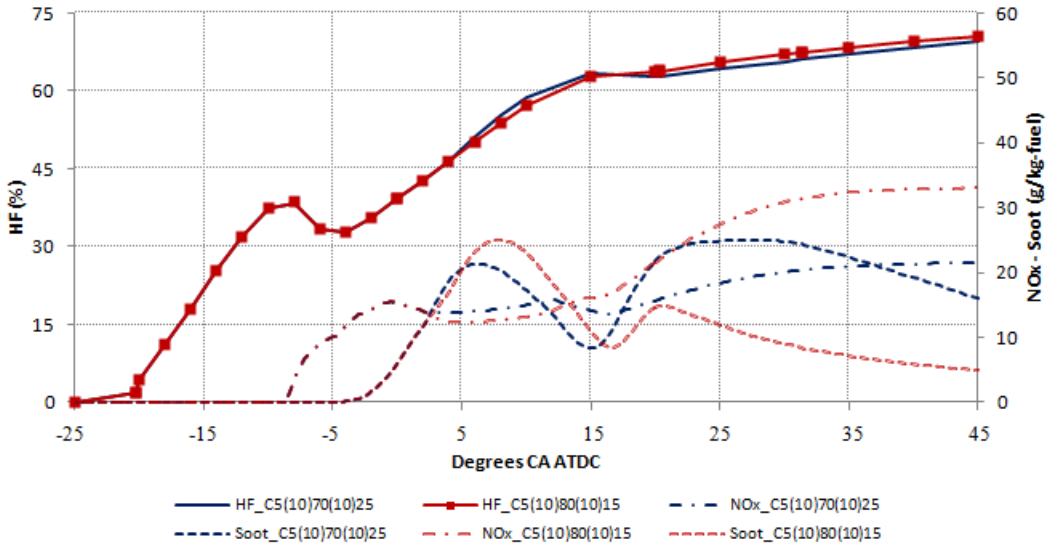

Figure 6.16: HF, NO_x and soot emissions for cases C with 5% pilot injection.

Finally, Figure 6.16 represents the HF trends for the NO_x formation and the soot formation for cases C with 5% pilot injection. It can be seen that the homogeneity for the

case with 70% of the fuel injected during the first main injection is temporarily improved after the end of the first main injection compared with the other case where there is still fuel injection taking place for a few more degrees. However, at almost 15°CA ATDC, the HF for case C5(10)80(10)15 becomes higher than for case C5(10)70(10)25. This occurs because a smaller amount of fuel is injected during the second main injection, which does not cause the in-cylinder mixing to deteriorate too much. Another point worth mentioning is the identical behaviours of the HF trend and the NO_x emission trend. At the point where the HF for case C with 70% fuel for the first main injection becomes higher than for the other case, the emissions formation is also higher. When the trend of this case decreases below the trend of case C with 80% of fuel during the first main injection, the NO_x trend also decreases and moves to a lower level than for case C5(10)70(10)25. The opposite occurs for the soot emissions where it is lower for the cases with a higher HF at any point in the cycle.

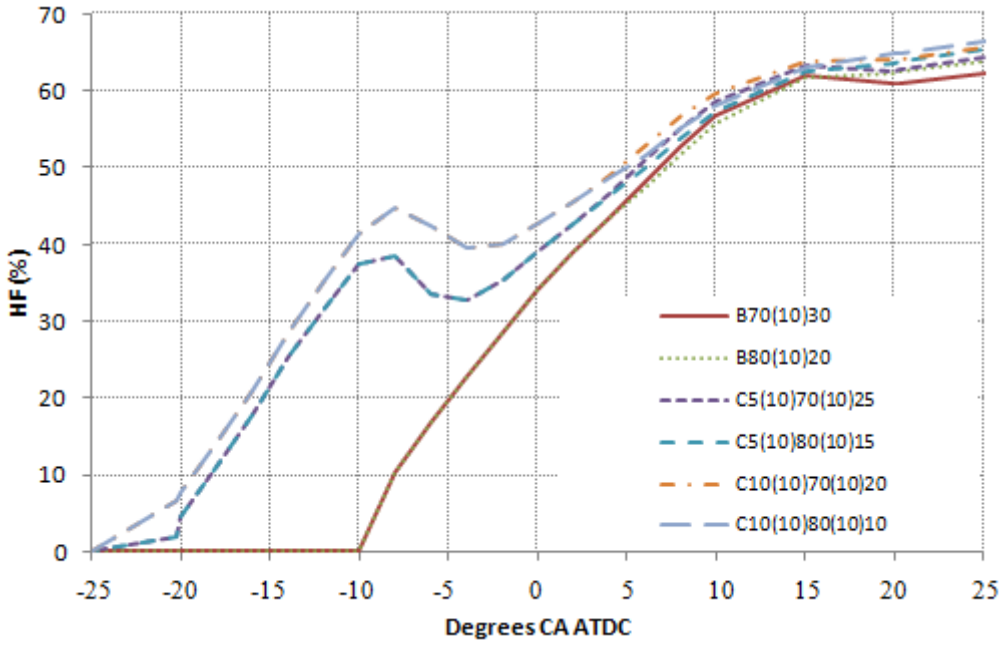

Figure 6.17: HF graph for cases C compared with the HF graphs for cases B70 and B80 with 10°CA dwell angle.

6.3 Pilot Injection Strategies

In this section the Homogeneity Factor is used for exploring the effects of pilot injection, fuel pressure, dwell angle and air swirl on the air-fuel mixing quality, engine performance and emissions formation. Firstly simulations for six modes with different injection pressure and dwell time between pilot and main injection are performed for various pilot injection ratios. Finally, additional simulations are carried to examine the effect of different swirl ratios to the air-fuel mixing homogeneity.

6.3.1 Engine Test Conditions

The tests were performed under the air and fuel conditions shown in Table 6.4.

Table 6.4: Initial air and fuel conditions for pilot injection strategies.

Intake air temperature	380K
Intake air pressure	1 bar
Fuel temperature	350K
Fuel injected	14 mg/cycle
Injection pressure	800 - 1,600 bar
Pilot injection ratio	5% - 20%
Start of pilot injection	19.12°- 5.73°CA BTDC
Dwell angle	5°- 15°CA
Start of first main injection	TDC

Tests were divided into two main categories. The first category involves the study of six different modes as shown in Table 6.5 with variation of the injection pressure and dwell angle between the injections. The six modes defined below in table 5 were simulated for three different pilot injection quantities of 0.7, 1.4 and 2.8 mg/cycle.

Table 6.5: Engine test conditions for pilot injection strategies.

Mode	Injection Pressure (bars)	Dwell Angle (°CA)
1	800	5
2	1,200	5
3	1,600	5
4	800	15
5	1,200	15
6	1,600	15

The second set of tests performed analyses the swirl effect on the air-fuel mixing quality and emissions of the engine. Mode 1 is compared for three different swirl ratios of 1.5, 2 and 2.5.

6.3.2 Combustion Analysis

The six modes were tested for variable injection pressures and dwell angles between the pilot and main injection at three different pilot injection strategies (0.7, 1.4 and 2.8mg/cycle). Figure 6.18 represents the in-cylinder pressure for all the modes at each injection strategy. It can be clearly seen by looking at the pressure graphs of all six modes that the highest pilot injection quantity produces the highest in-cylinder peak pressure. The in-cylinder pressure also seems to rise slightly as the injection pressure is increased as shown by comparing pressure graphs of Modes 1, 2, 3 and 4, 5 and 6. This is happening due to two main reasons. Firstly, the better fuel atomization corresponding to the smaller fuel droplets size and also the higher momentum of the jet caused by the injection pressure increase which has improved the air-fuel mixing quality [78, 134]. The in-cylinder pressure increase caused by those two main factors is leading to a more complete combustion and a more intense heat release rate as shown by comparing the HRR graphs of Modes 1, 2, 3 and 4, 5, 6 in Figure 6.18. It is also demonstrated that the higher injection pressure and longer dwell angle result in higher average in-cylinder combustion temperatures due to the enhanced air-fuel mixing. Improved mixing has

been achieved due to the longer available time between pilot and main injection which resulted to a more complete combustion. From Figure 6.18, it can also be noticed by comparing the pressure graphs 1, 2, 3 with 4, 5 and 6 that the peak in-cylinder pressure is depended upon the pilot fuel injection timing and is highly affected by the pilot injection fuel quantity.

Figure 6.18 also shows the rate of the heat release as a function of crank angle degrees at three different injection quantities. It can be clearly seen from the HRR graphs that in Modes 1, 2 and 3 where the dwell angle between the two injections is 5°CA, combustion has not taken place until the point where main injection starts. On the other hand, as shown in the HRR graphs for Modes 4, 5 and 6, the cases with increased fuel quantity benefit from adequate combustion conditions before the injection of the remaining fuel and therefore extend the combustion duration by advancing the premixed combustion phase and extending the mixing-controlled combustion phase. This has a negative impact on the NO_x and soot formation as analysed below.

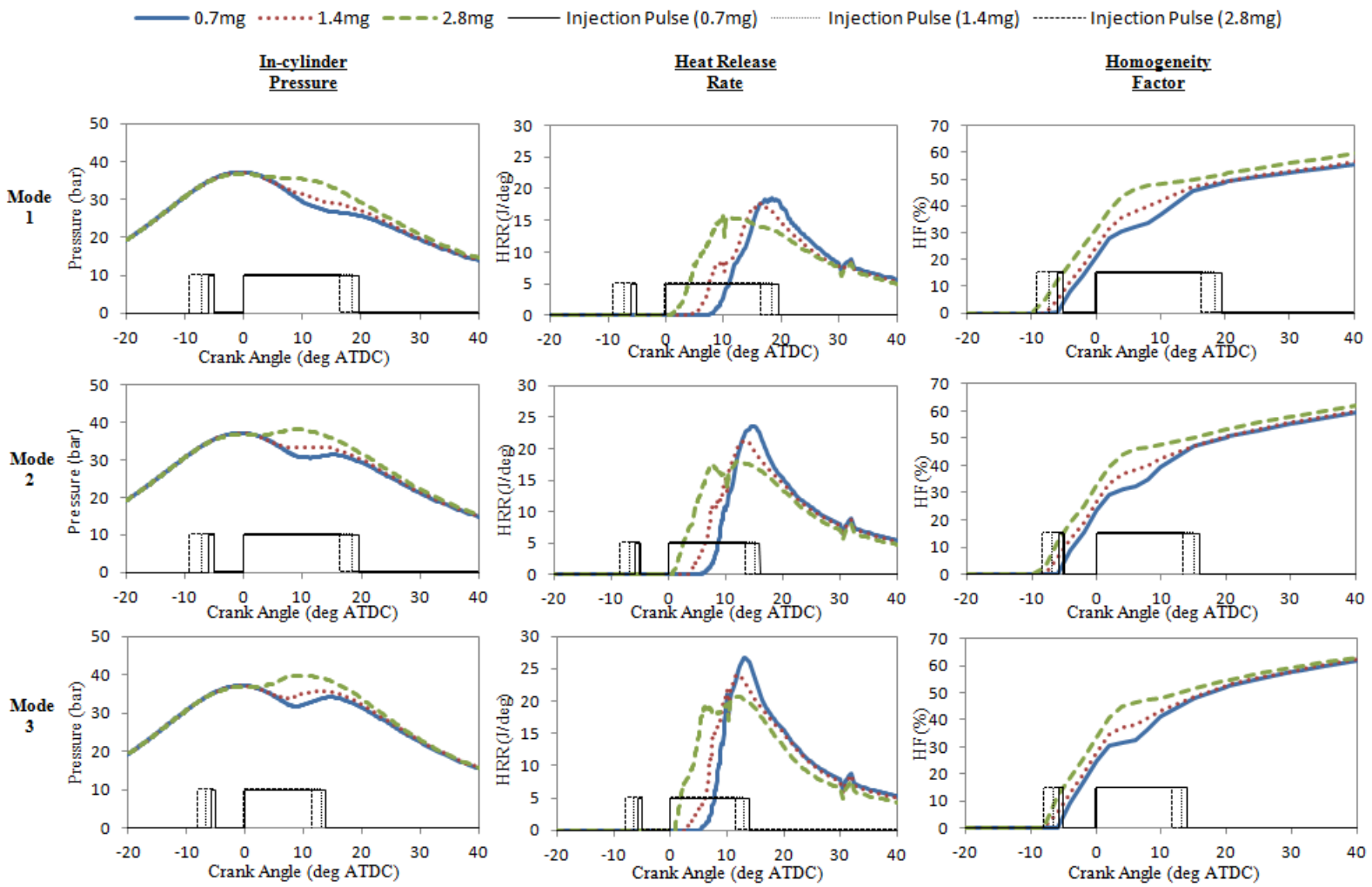

(Figure continues in the following page)

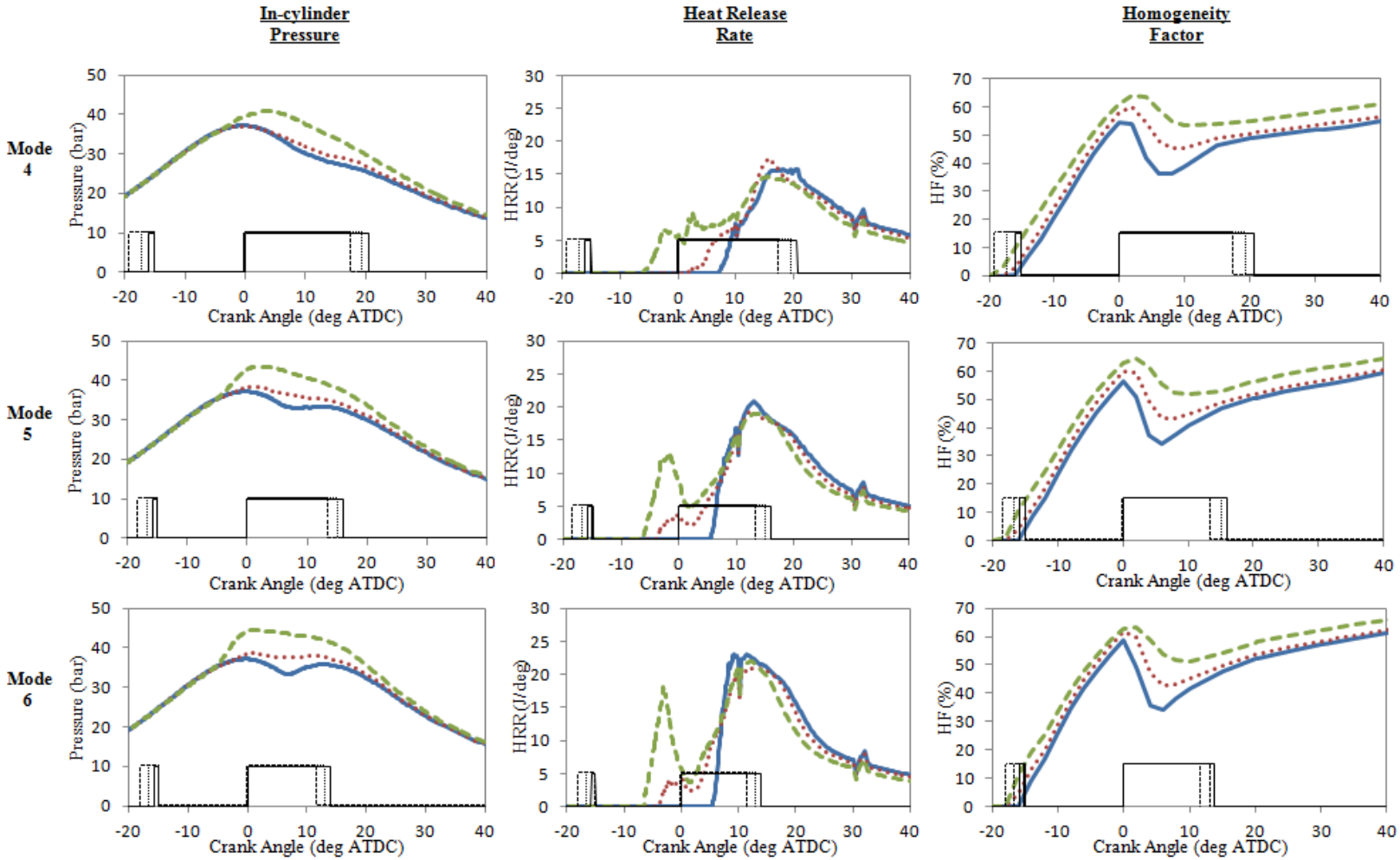

Figure 6.18: In-cylinder pressure, HRR and HF profiles for different injection modes (see Table 6.5).

6.3.3 Homogeneity Factor

It is obvious that the in-cylinder air-fuel mixing quality is the main factor contributing to the performance and emissions characteristics of diesel engine. It is crucial to understand how air-fuel mixture quality can be improved by altering various injection specifications and how this improvement will affect in a positive or negative way the performance and emissions characteristics. The HF parameter used in this work can demonstrate the in-cylinder air-fuel mixing quality of each test at any crank-angle position. Figure 6.18 compares the air-fuel homogeneity percentage of all six modes for three different pilot injections (0.7, 1.4 and 2.8mg).

It suggests that the more the pilot injection quantity is, within the above ranges, the higher the air-fuel mixing quality. Improved air-fuel mixing in cases with higher pilot injections occurs for two reasons. Firstly, more fuel is injected during the pilot pulse which means that injection needs to start at an earlier point as the dwell angle is kept constant at 5° or 15°CA. Secondly, higher amount of fuel injected during the first pulse leads to a more balanced injection strategy with less fuel injected over the second pulse which reduces the injection time and enables a better fuel particles spread within the combustion chamber. It can be noted from the HF graphs in Figure 6.18 that the HF rises faster in cases with higher pilot injection quantities as the injection starts at an earlier stage. From the HF graphs in Figure 6.18, it can also be seen that there is a significant reduction in homogeneity at the point where second injection takes place for Modes 4, 5 and 6. This is happening due to the long dwell angle of 15° CA between the two injections leading to an optimum air-fuel mixture quality before the second injection and a sharp fall during the second pulse. On the other hand, for Modes 1, 2 and 3 with 5° CA dwell, HF keeps raising at a lower ratio than prior the second pulse due to the very short gap between the end of the first and start of the second injection.

Figure 6.19 illustrates contours of the equivalence ratio for three different Modes (1, 2 and 3) at the point where maximum heat release takes place (15° CA ATDC). It can be clearly noticed the effect of injection pressure to the mixing quality. The equivalence ratio shown in the contour for Mode 1 is still at a very high level close to the injector

nozzle. As the injection pressure increases, the fuel seems to be spread faster and finer within the cylinder as shown in Modes 2 and 3. The high injection pressure leads to a better fuel atomization and a higher momentum of the jet which as a result lead to a better mixture quality. The better mixing quality for the cases with higher injection pressure can be confirmed by the HF levels. The HF for case with 1,600 bar injection pressure (47.77%) is almost 5% higher than the combustion case with 800 bar injection pressure (45.68%).

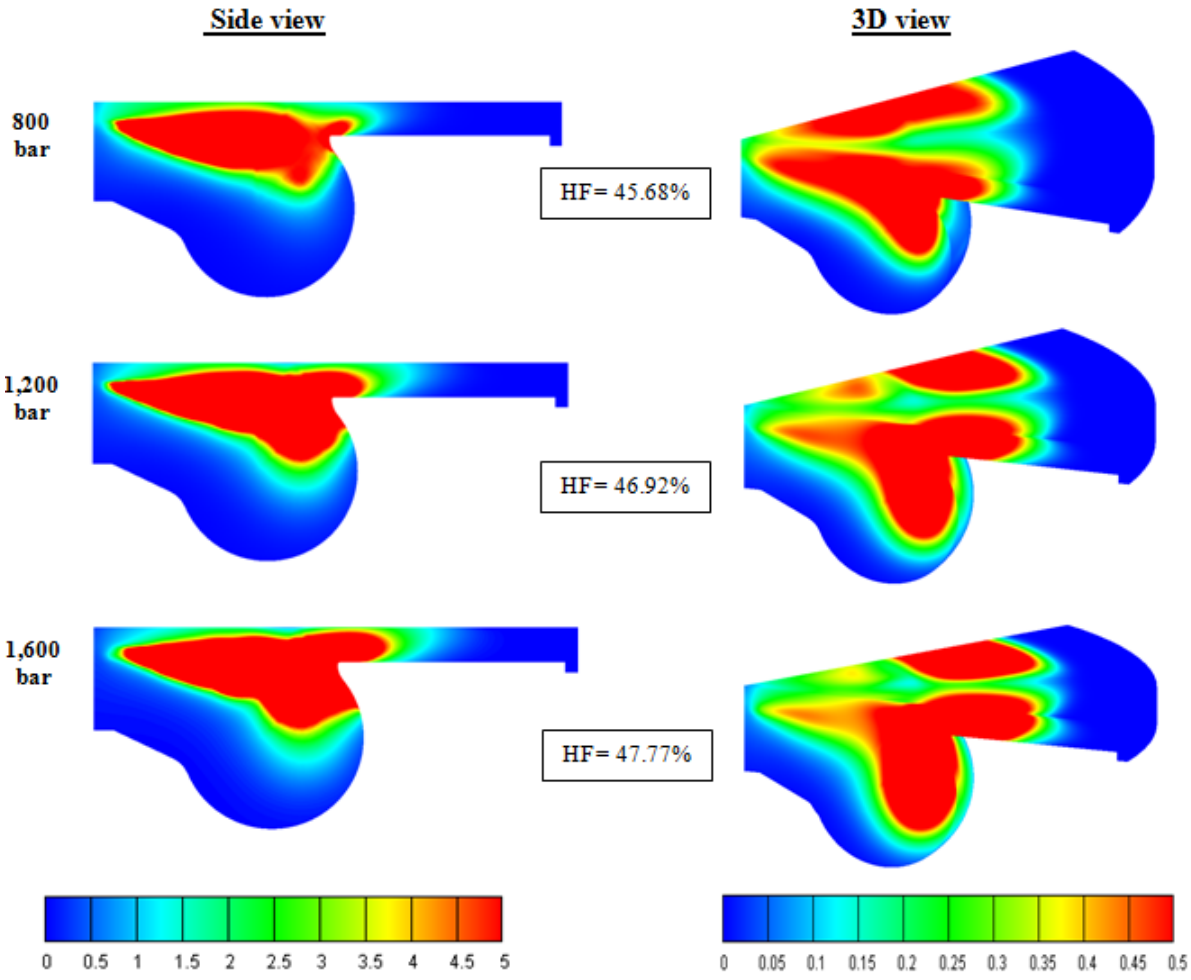

Figure 6.19: Equivalence ratio contours [side (0-5 range) and 3D (0-0.5 range) views] at 15° CA ATDC for different injection pressures with 5° CA dwell period and 0.7mg of pilot fuel.

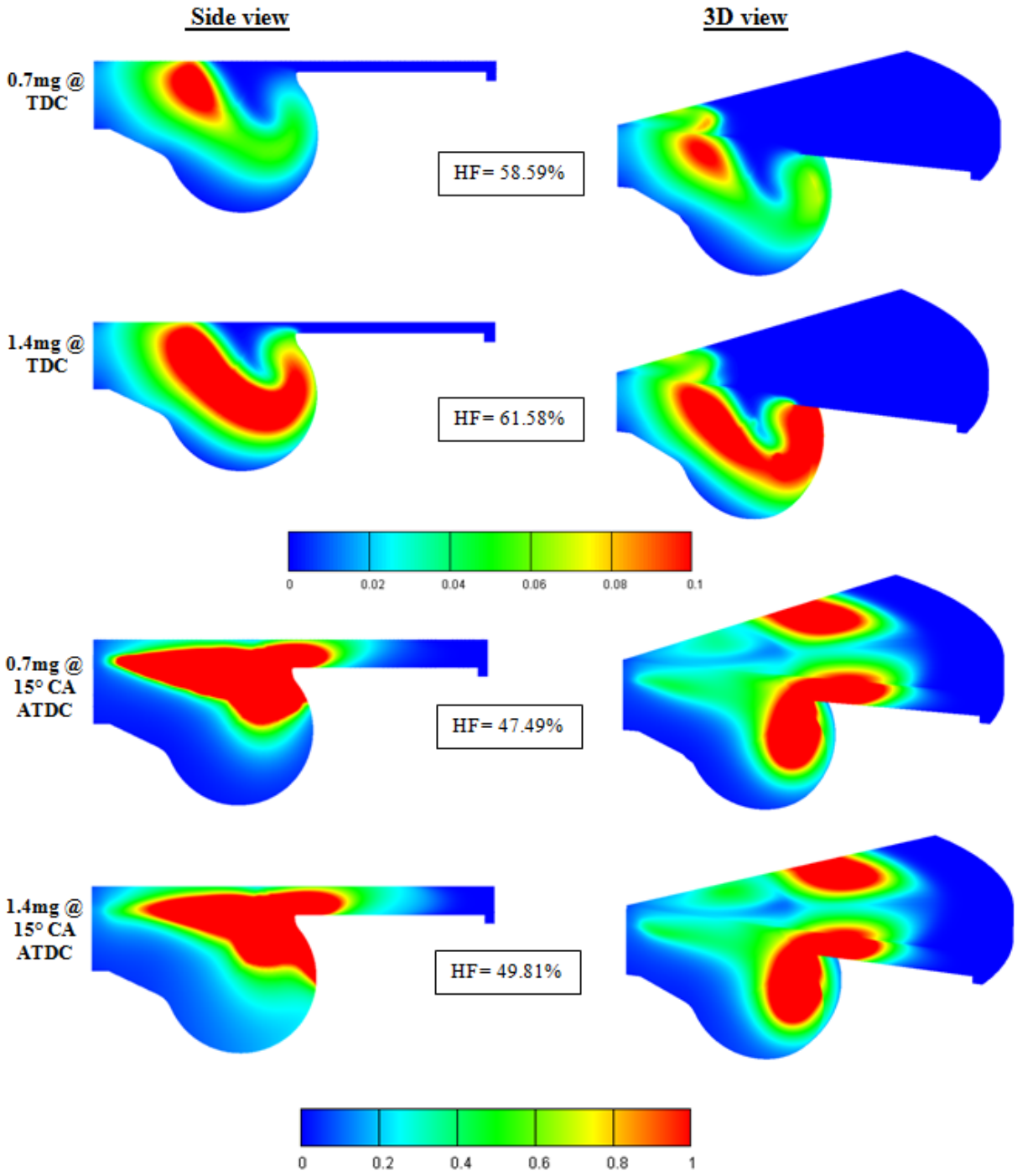

Figure 6.20: Equivalence ratio contours (side and 3D views) at TDC and 15° CA ATDC for different pilot quantities with 1,600bar fuel pressure and 15° CA dwell period.

Figure 6.20 shows the difference in the mixing quality caused by altering the pilot injection quantity. It seems that high pilot fuel quantities can lead to enhanced fuel stratification. This is due to the fact that higher amount of fuel has been injected during the first pulse which can be translated to the higher equivalence ratio at the bottom and the sides of the cylinder. The HF rises at 61.58% for the 1.4mg pilot injection case at the TDC compared to 58.59% for the case with 0.7mg pilot quantity. It's clear that the more fuel injected has been spread faster at the bottom and the sides of the cylinder where the equivalence ratios seem to be higher than 0.7mg case. Also, at 15° CA ATDC the HF is 49.81% for the case with 1.4mg of pilot fuel injection compared to 47.49% for the case with 0.7mg of pilot fuel. Comparing the 15°dwell angle contours of Figure 6.20, it can be noticed that the higher pilot injection quantity has improved the fuel stratification at the bottom and sides of the cylinder. Pilot injection can be used for improving the air-fuel mixture quality and it can be concluded that, within the ranges investigated above, high amounts of fuel injected during the first pulse lead to enhanced air-fuel homogeneity. However, the limit on the maximum amount of pilot fuel can be used for improving fuel stratification needs to be found by sweeping the pilot fuel fraction.

Figure 6.21 represents the contour plots of Modes 3 and 6 with 2.8mg of fuel injected during the first pulse. They show the effect of dwell to the equivalence ratio at the TDC. It can be noted that the fuel spread over the cylinder for Mode 6 is more advanced due to the fact that injection occurred much earlier compared to Mode 3. The fuel has been spread efficiently over the chamber and the combustion has started in comparison with Mode 3 where pilot injection process has almost been completed and combustion process is still expected. This can be confirmed by the very high number of HF for the case with the longer dwell angle (63.48%) relative to short dwell angle case (33.73%).

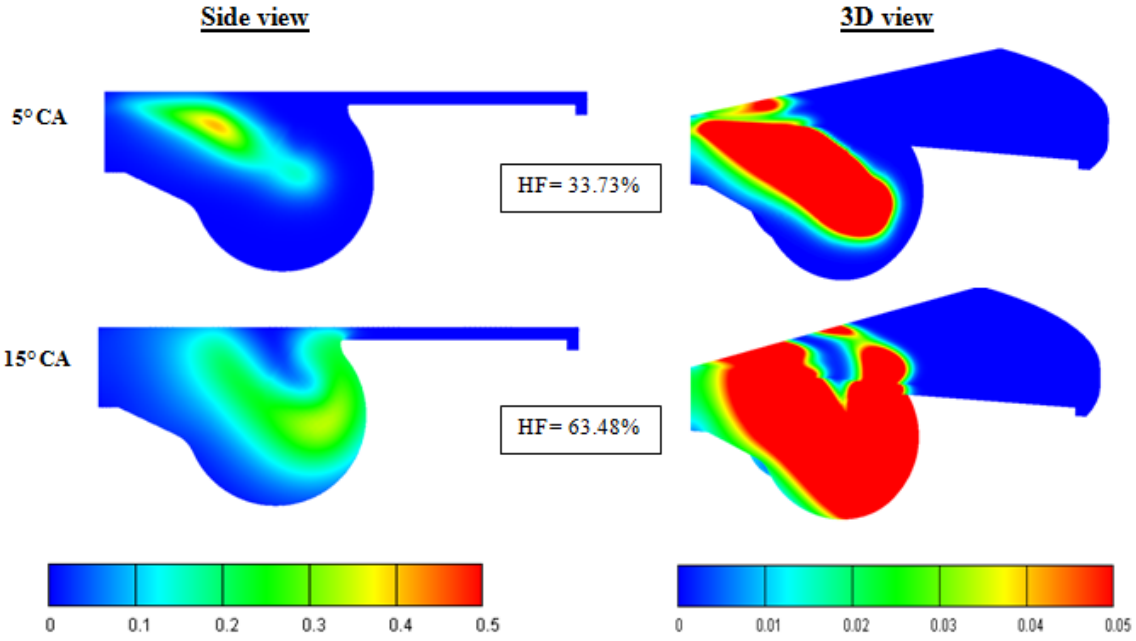

Figure 6.21: Equivalence ratio contours [side (0-0.5 range) and 3D (0-0.05 range) views] at the TDC for different dwell angles with 2.8mg pilot fuel injection and 1,600bar injection pressure.

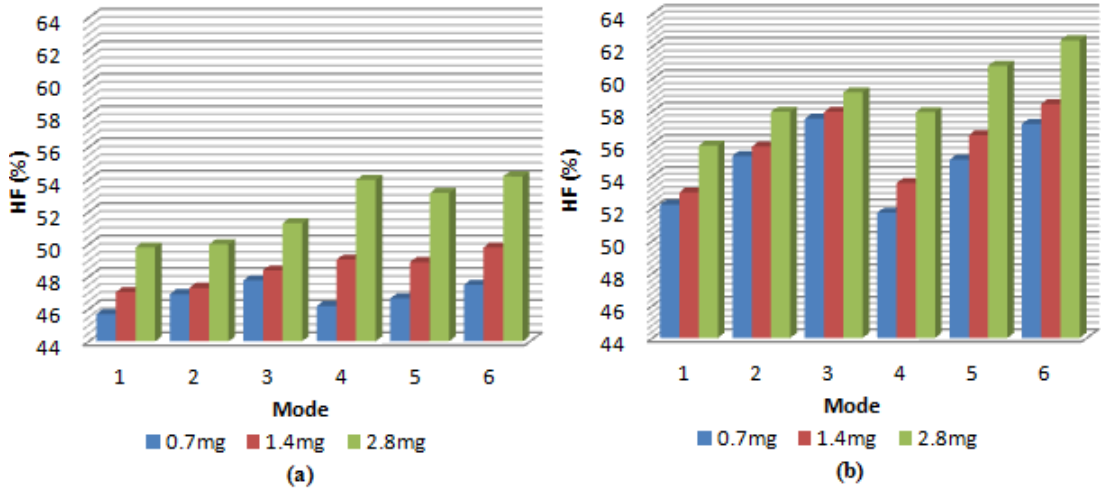

Figure 6.22: HF profiles for all cases at two different angles (a) angle where maximum heat release takes place (15° CA ATDC) and (b) 50% burnt location (30° CA ATDC).

All the above results can be collected and fully explained in Figure 6.22 which shows the in-cylinder HF at the points where maximum heat release takes place (15° CA ATDC) and at a later stage (30° CA) which is roughly the 50% burnt location.

It is clear to see that the HF is almost up to 8 units higher for the cases with 2.8mg of pilot injection compared to 0.7mg per cycle. Moreover, it is clear that the homogeneity rises as the pressure and dwell angle is increased. Cases with 15° CA dwell and 1600 bars fuel pressure have the highest in-cylinder homogeneity at 15° CA ATDC.

6.3.4 Engine Performance & Emissions

NO_x emissions are directly influenced by the air-fuel mixing quality within the cylinder and the homogeneity percentage. Under similar testing conditions, a more complete combustion usually leads to higher in-cylinder temperatures and as a result to higher NO_x formation. Figure 6.23 shows the NO_x emissions for all the modes in terms of different pilot injection quantities. It can be clearly seen that emissions were increased dramatically as the pilot quantity was increased in all cases. This is happening due to the increase in fuel burnt in the premixed combustion at an early stage leading to a sharp temperature increase and therefore more NO_x formation.

Also, in Figure 6.23 it can be seen that the higher dwell period (Modes 4,5 and 6) increases the NO_x formation as a result of early combustion and high in-cylinder temperature rise. On the other hand, for short dwell angle cases, the pilot fuel spray works as a premixing injection and the fuel is ignited only at the point where second fuel injection starts resulting to lower in-cylinder temperatures. Moreover, it can be mentioned that NO_x emissions are highly influenced by the fuel injection pressure. From the Figure 6.23 it can be seen that within the ranges tested, the higher the injection pressure is (Modes 3 and 6 at 1,600 bar compared to 2 and 5 at 1,200 bar and 1 and 4 at 800 bar), the more NO_x formation. This is due to the smaller fuel droplets, leading to a faster combustion process. In addition, the NO_x formation is increased for cases with larger pilot injection fuel amount. This occurs as the richer fuel combustion conditions during the pre-mixed combustion phase which is mainly responsible for the NO_x generation due

to the high in-cylinder temperatures experienced. However as shown in Figure 6.23, this is not the case for Mode 4 with 1.4mg of fuel injected in the pilot pulse. This can be justified by looking back to the HRR graph of Mode 4 in Figure 6.18 showing that this combustion case benefits from a slow HRR increment at the beginning of the pre-mixed phase compared to the 0.7mg and 2.8mg cases. Finally, it should be mentioned that comparing Figure 6.23 with the HF figures (Figure 6.18 and Figure 6.22), it is obvious for the cases tested in this research work that when the HF of a combustion analysis is increased then it leads to higher NO_x formation.

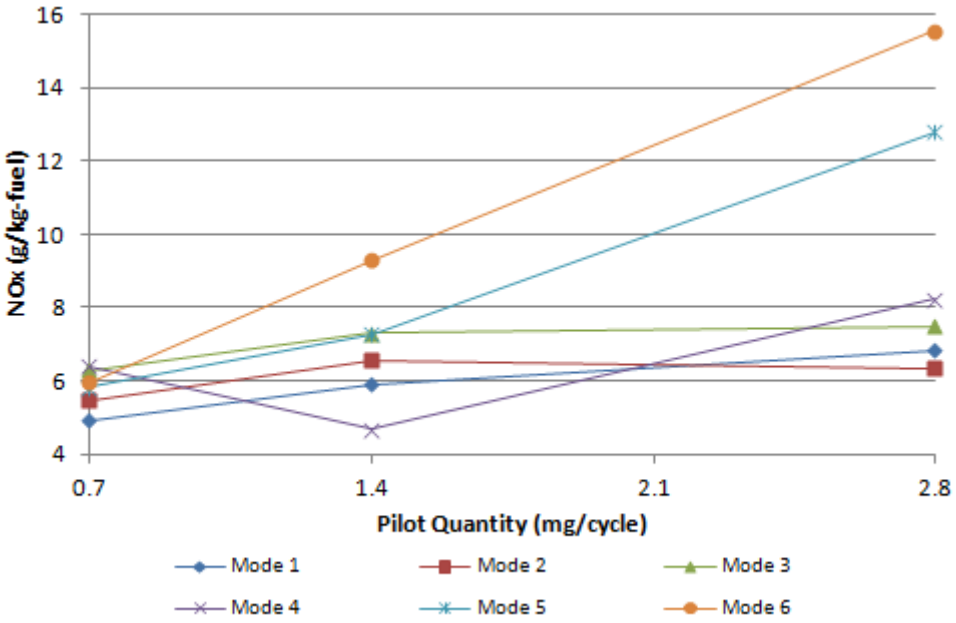

Figure 6.23: NO_x emissions for all pilot injection cases.

Figure 6.24 presents the soot formation over the pilot fuel quantities. It is obvious that soot formation and NO_x emissions as well as soot formation and the HF follow a vice versa bend. It is clear that the cases with lower NO_x and air-fuel homogeneity form higher soot than those cases with higher NO_x emissions. This is happening as a result of the injection pressure which is the main factor affecting the NO_x formation and the in-cylinder homogeneity. High injection pressures lead to a mixture with less

significant fuel rich regions and therefore produce less soot. At the same time, the higher combustion temperature helps to improve the soot oxidation.

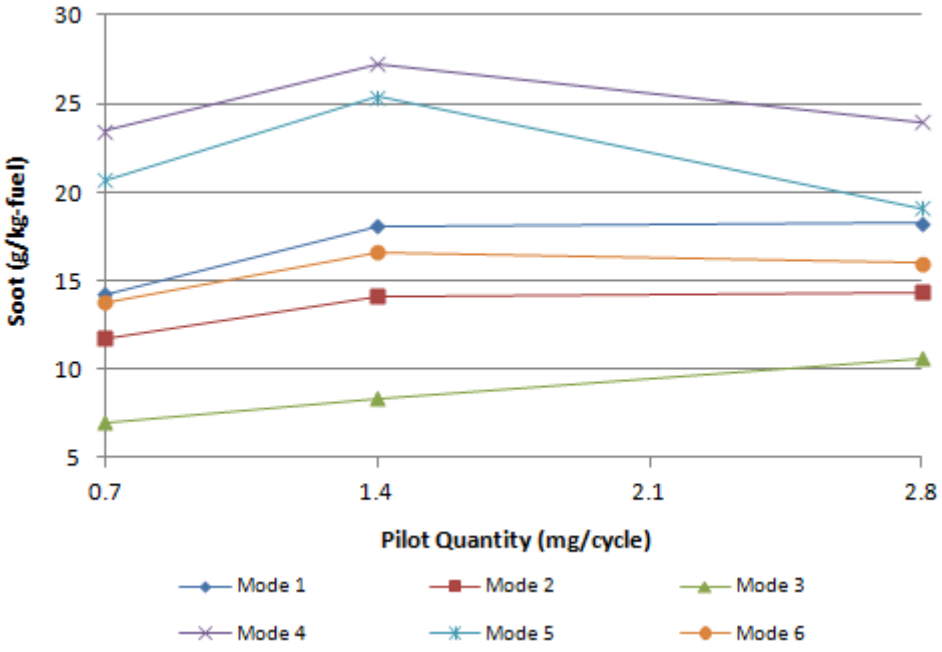

Figure 6.24: Soot emissions for all pilot injection cases.

The pilot injection quantity increase seems to have a negative effect on the soot formation for cases with short dwell angle. This is due to the shorter reaction time for the fuel to mix with the air which leads to a less complete combustion. However, this is not happening for cases with long dwell angle due to the improved mixing process and less fuel-rich regions.c

Figure 6.25 illustrates the BSFC and IMEP trends for all the cases tested. It shows that the higher the pressure is, the higher the IMEP levels and the lower the BSFC. A more homogenous and therefore complete combustion caused by the fuel pressure increase led to better performance and lower fuel consumption. It can also be noted from Figure 6.25 that the cases with increased pilot quantity and longer dwell angle tend to have lower BSFC and higher IMEP values. This is strongly related to the mixing process and air-fuel homogeneity. As shown in Figure 6.23, the cases with increased pilot fuel

and longer dwell angle can reach higher levels of homogeneity which results to reduced BSFC and increased IMEP values due to the fact that a more complete combustion taking place within the cylinder chamber.

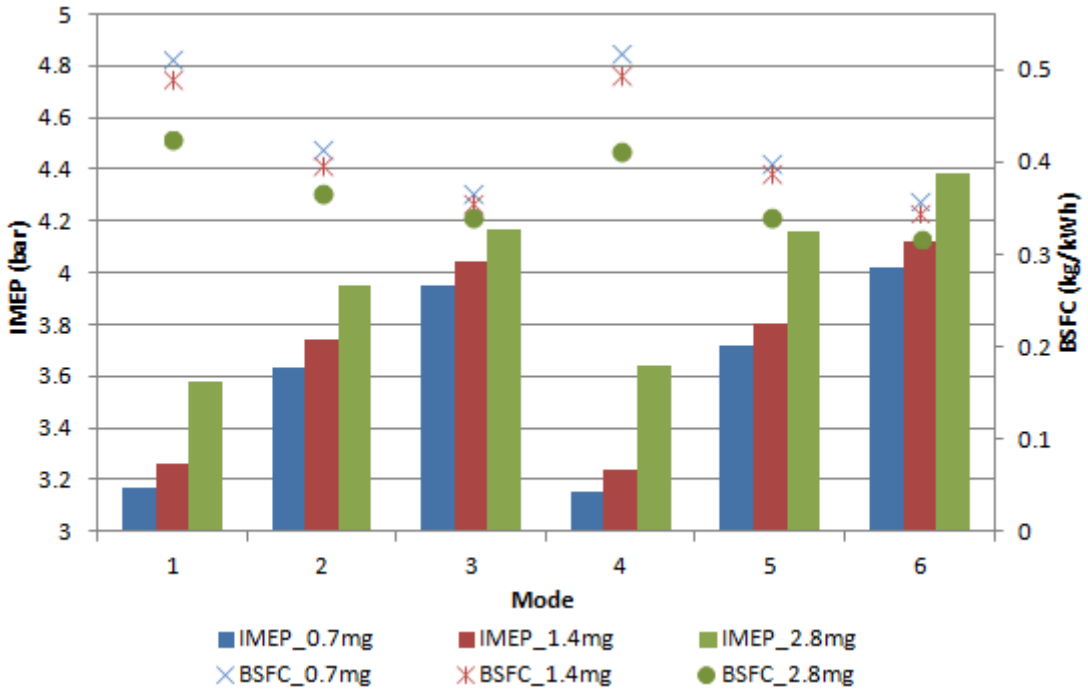

Figure 6.25: BSFC and IMEP results for all pilot injection cases.

6.3.5 Effects of Swirl Ratio on HF

Air swirl in the combustion chamber plays an important role in the mixing process between the fuel and the air but also between the partially oxidized products (soot, CO, etc.) and air. Within the ranges tested in this work, by increasing the swirl ratio, it enhances the combustion efficiency as a result of increased in-cylinder pressure and temperature caused by the optimized air-fuel mixing.

Figure 6.26 illustrates the effects of air swirl effect on Mode 1 case. It proves that the mixing quality for the simulations with increased swirl motion is better than the case with swirl ratio of 1.5. As shown, the HF is slightly improved during the first pulse. Second fuel pulse seems to have a higher impact to the cases with high swirl

ratio leading to a reduced ascending ratio of the HF. This is happening due to the fact that swirling motion drags fuel droplets and vapour away from the spray centreline to the downstream volume between two adjacent sprays. This causes fuel to be distributed temporarily less homogenous within the cylinder. After the end of second injection, the HF for the cases with high swirl ratios climbs up again which means better air-fuel mixing and thus more complete combustion. The optimized combustion can be also confirmed by the NO_x emissions. It is clear that NO_x are increased for cases with high swirl ratios as a result of the optimized air-fuel homogeneity. Also, this can be concluded by the high HF variance among the cases at the end of the cycle which declares that less residual fuel is left within the cylinder. On the other hand, soot formation is reduced for cases with high swirl motion. As it can be seen from Figure 6.26, the case with swirl ratio of 2.5 show the best combination of NO_x and soot formation. The NO_x emissions have been slightly increased, while the soot formation is dramatically decreased. The high soot reduction mainly occurs due to the avoidance of local fuel rich regions within the cylinder and the improved soot oxidation.

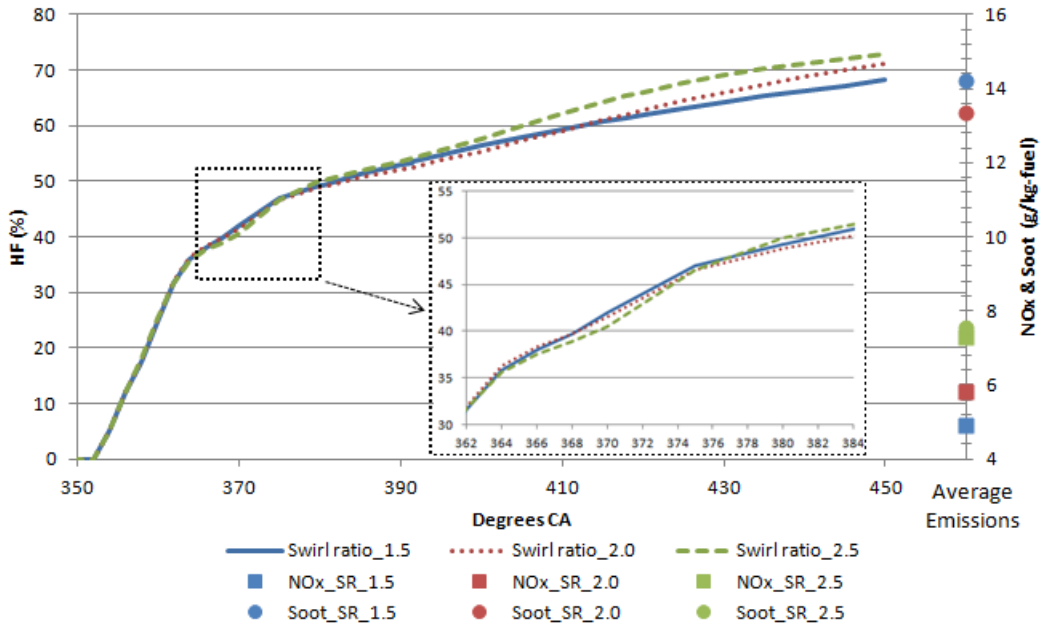

Figure 6.26: HF of Mode 1 for different swirl ratios.

6.4 Summary

In this section, a recently developed parameter, namely HF, was incorporated in order to study the effect of air-fuel mixing quality on the combustion characteristics and the emissions formation of a single-cylinder DI diesel engine. The section analyses the effects of pilot and split fuel injection strategies on air-fuel mixing quality. The effects of air-fuel mixing quality at the SOC and during combustion on emission formation are detailed.

It was shown that air-fuel mixing quality within the combustion chamber is directly influenced by the fuel injection strategy followed. Pilot injection and splitting the main injection into two pulses can significantly increase air-fuel homogeneity and the IMEP and optimize soot formation. In addition, higher fuel injection pressure and air swirl motions can contribute to improved air-fuel mixing before the SOC.

Chapter 7

Premixed Charge Compression Ignition Analysis

In this chapter, experimental analysis is performed to investigate the effects of injection strategy, exhaust valve timing and exhaust back pressure on the combustion characteristics and emission mechanisms of diesel engines. The chapter is divided into two main sections; the first section analyses the effects of injection timing, ratio and dwell angles on the pre-mixed combustion phase and its impact on emissions and performance of the engine. In the second section, an experimental analysis is performed with the aid of statistical methods for investigating the effects of early pilot injection with variable exhaust valve timing and exhaust back pressure on diesel engine emissions characteristics.

7.1 PCCI strength

Experimental analysis was performed under two different loads, 10mg and 15mg, of fuel injection, for investigating the effects of injection timing, ratio and dwell angle on the pre-mixed combustion phase of diesel engines using the PCCI strength factor defined in Section 3.2.

7.1.1 Engine Test Conditions

The investigation was performed using two injections per cycle and by varying the injection ratio and timing. The first injection early in the cycle provides fuel for optimizing air-fuel mixing quality within the combustion chamber, while the second injection closer to the TDC works as a triggering point for the SOC. The engine operates in PCCI combustion mode without exhaust gas recirculating back to the inlet manifold and, therefore, early SOC timings are experienced. The engine air and fuel conditions for this analysis are presented in Table 7.1.

Table 7.1: Engine test conditions for PCCI Strength study.

Intake air temperature	300K
Intake air pressure	1 bar
Fuel temperature	350K
Fuel injected	10mg and 15mg per cycle
Injection pressure	around 1,200 bar
Start of first injection	-50°, -40°, -30°CA ATDC
Start of second injection	-10°, -5°CA ATDC
First injection ratio	50%, 70%, 80%

Three different injection ratios were tested. The first injection ratio is a 50:50 strategy denoted by "A" for 10mg of fuel load and "AA" for 15mg of fuel load. Half of the fuel amount is injected during the first injection, which takes place between -50°and -30°CA ATDC, and the other half is injected closer to the TDC at -10°or -5°CA ATDC. The second strategy applies a 70:30 injection ratio denoted by "B" and "BB" for medium and higher loads, respectively. Finally, the third category is denoted by "C" and "CC" and is an 80:20 injection ratio strategy. Table 7.2 details the testing performed for each strategy.

Table 7.2: Injection strategies for PCCI strength study.

Strategy		**SOI 1st** (°CA ATDC)	**SOI 2nd** (°CA ATDC)	**Injection Ratio**	**1st Inj.** (mg)		**2nd Inj.** (mg)	
10mg	***15mg***				**10mg**	***15mg***	**10mg**	***15mg***
A1	***AA1***	-50	-10	50:50	5	*7.5*	5	*7.5*
A2	***AA2***	-40	-10	50:50	5	*7.5*	5	*7.5*
A3	***AA3***	-30	-10	50:50	5	*7.5*	5	*7.5*
A4	***AA4***	-50	-5	50:50	5	*7.5*	5	*7.5*
A5	***AA5***	-40	-5	50:50	5	*7.5*	5	*7.5*
A6	***AA6***	-30	-5	50:50	5	*7.5*	5	*7.5*
B1	***BB1***	-50	-10	70:30	7	*10.5*	3	*4.5*
B2	***BB2***	-40	-10	70:30	7	*10.5*	3	*4.5*
B3	***BB3***	-30	-10	70:30	7	*10.5*	3	*4.5*
B4	***BB4***	-50	-5	70:30	7	*10.5*	3	*4.5*
B5	***BB5***	-40	-5	70:30	7	*10.5*	3	*4.5*
B6	***BB6***	-30	-5	70:30	7	*10.5*	3	*4.5*
C1	***CC1***	-50	-10	80:20	8	*12*	2	*3*
C2	***CC2***	-40	-10	80:20	8	*12*	2	*3*
C3	***CC3***	-30	-10	80:20	8	*12*	2	*3*
C4	***CC4***	-50	-5	80:20	8	*12*	2	*3*
C5	***CC5***	-40	-5	80:20	8	*12*	2	*3*
C6	***CC6***	-30	-5	80:20	8	*12*	2	*3*

7.1.2 Effects of Injection Strategy on PCCI Strength and SOC Timing

7.1.2.1 50:50 Injection Ratio

The effect of injection timing on the strength of the PCCI combustion for the 50:50 injection ratio is shown in Figure 7.1.

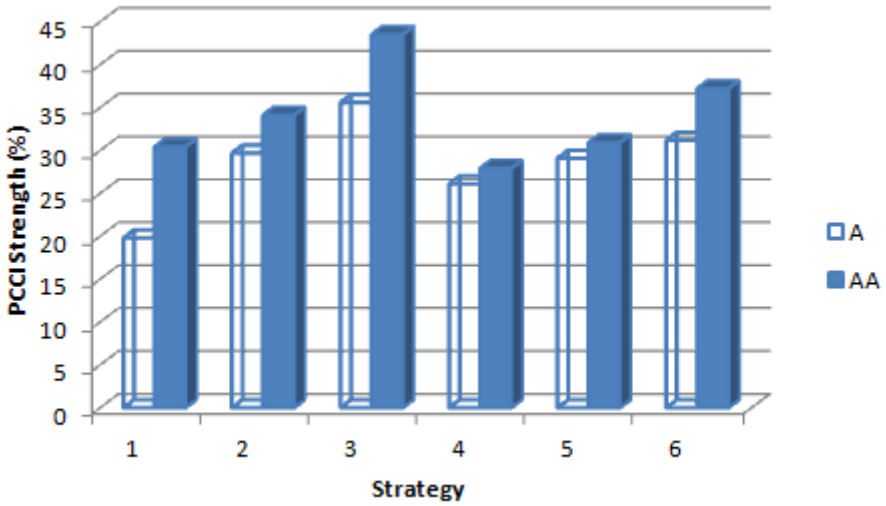

Figure 7.1: Effects of injection strategy on PCCI strength for 50:50 injection ratio.

It can be seen that the PCCI Strength level increases for higher load cases, as more fuel leads to an earlier SOC, which can be translated to more time available for the premixed combustion to take place. Comparing strategies 1 with 2 and 3 as well as 4 with 5 and 6, it can be seen that the later the first fuel is sprayed into the cylinder, the higher the strength of the premixed combustion. The same can be concluded for the start of the second injection by comparing strategies 1, 2 and 3 with 4, 5 and 6. An early first injection leads to improved air-fuel mixing and reduces the combustion temperatures, which results in lower burning rate during the premixed combustion phase. A late first injection closer to the TDC leads to a more rapid and robust combustion, which, as a result, increases the ratio of the premixed combustion compared to the diffusion combustion.

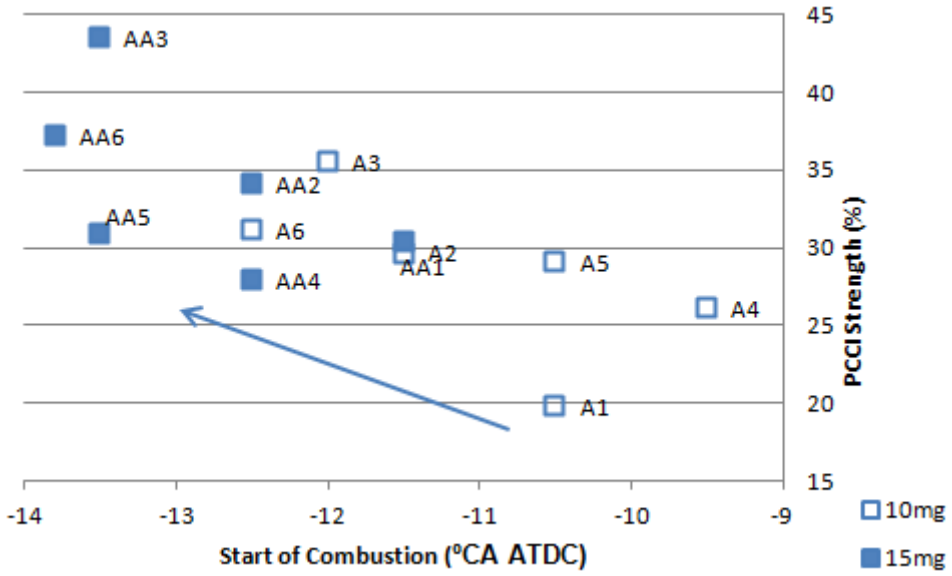

Figure 7.2: SOC timing for 50:50 injection ratio strategies.

Figure 7.2 presents the SOC timing for all 50:50 injection ratio cases. Clearly, the cases with higher load tend to have an earlier SOC due to the higher amount of fuel injected, leading to increased premixed combustion as shown in Figure 7.1. In addition, the SOC timing for cases with the second injection taking place at -5°CA ATDC is delayed for approximately 1°CA compared to the cases with the second injection taking place at -10°CA ATDC. However, this delay seems to be shorter for the cases where the first injection occurs closer to the TDC. It can be concluded from Figure 7.2 that early SOC timing increases the available time for the premixed combustion phase to take place before the injection of the remaining fuel and the start of diffusion combustion.

7.1.2.2 70:30 Injection Ratio

The strength of the PCCI combustion for the 70:30 injection ratio does not follow the same trend as for the 50:50 ratio. As can be seen from Figure 7.3, the strength of the PCCI combustion is higher for the 70:30 cases compared to 50:50 strategies due to the decrease of the fuel amount injected during the second pulse, which as a result reduces

the level of diffusion combustion. In this case, it can still be seen that a second injection far from the TDC leads to higher strength due to the earlier SOC. However, the strength does not exhibit the same trend based on the first injection timing as for the 50:50 ratio case.

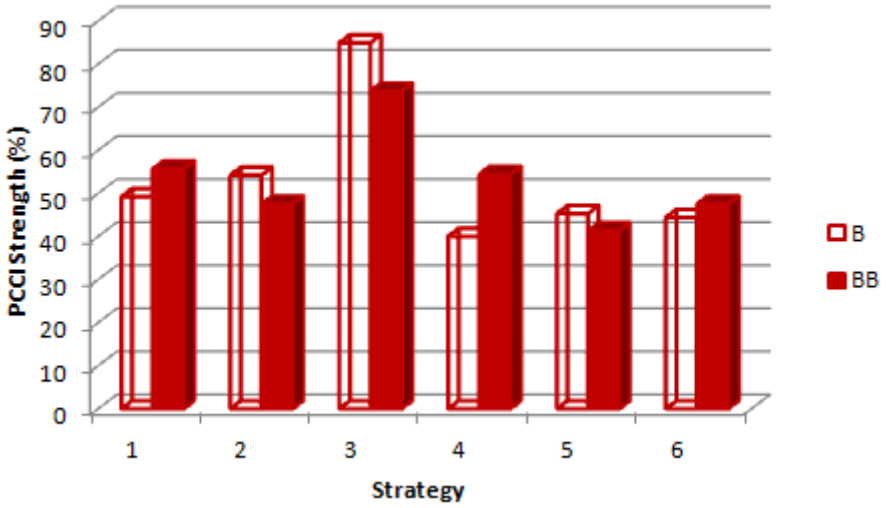

Figure 7.3: Effects of injection strategy on PCCI strength for 70:30 injection ratio.

It can be noted from Figure 7.3 that the strength level for BB1 is higher than BB2, although the first injection takes place 10°CA earlier. This can be explained by looking at Figure 7.4 where the SOC timing for case BB1 is approximately 2°CA earlier than in case BB2. The early SOC was achieved due to the earlier first injection and the higher fuel amount compared to cases with the 50:50 ratio. The same occurs for case BB4 compared to BB5 and BB6. In addition, in many cases the strength of PCCI combustion is higher for the cases with low load conditions compared to high load. This mainly happens in cases with the second injection taking place at -10°CA ATDC where the SOC timing of the low load cases occurs very close to the start of the second injection. Therefore, the newly introduced fuel contributes to the strengthening of the premixed combustion, and this can be clearly seen in case B3 (in circle), where the premixed combustion ratio is higher than the ratio of the fuel injected during the first injection pulse.

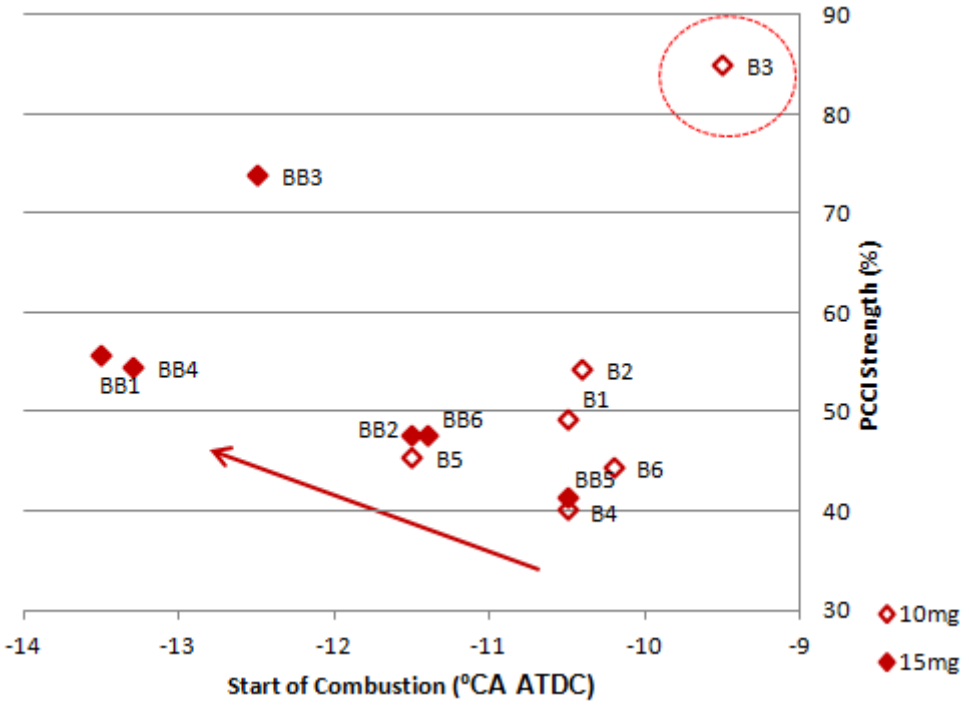

Figure 7.4: SOC timing for 70:30 injection ratio strategies.

By looking at Figures 7.3 and 7.4, it can be concluded that SOC timing plays a key role in the strength of premixed combustion. An early SOC increases the available time for the premixed combustion phase to take place and, therefore, the PCCI strength level. On the other hand, a late SOC close to or after the start of the second fuel injection can also increase the PCCI strength with the contribution of freshly introduced fuel.

7.1.2.3 80:20 Injection Ratio

Figure 7.5 illustrates the PCCI strength levels for cases with an 80:20 injection ratio.

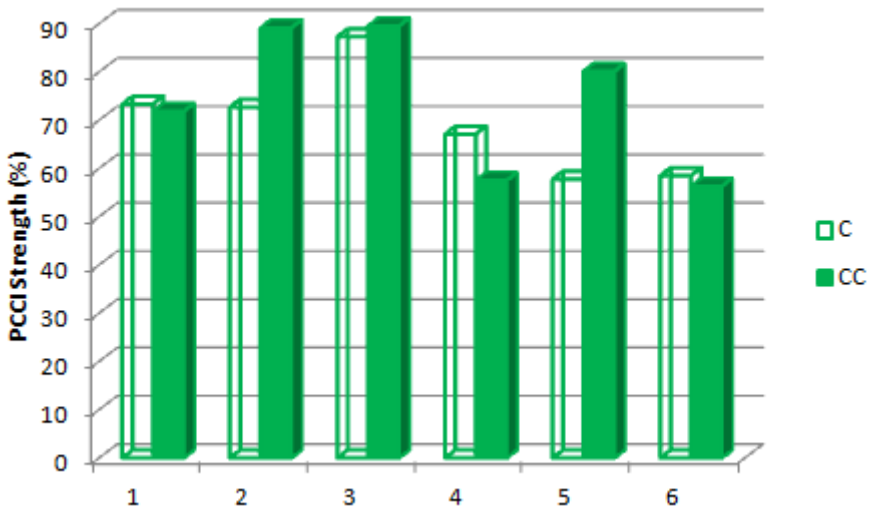

Figure 7.5: Effects of injection strategy on PCCI strength for 80:20 injection ratio.

It can be seen that the PCCI strength for case C1 is higher than for C2. This can be explained by the very early SOC, almost 16°CA BTDC as shown in Figure 7.6. The high amount of fuel injected during the first pulse and the high in-cylinder temperature led to an advanced SOC, which resulted in high levels of premixed combustion. However, the SOC for the CC1 case is a few degrees later, which could be attributed to lower in-cylinder temperature caused by the higher amount of cold fuel entering the combustion chamber and the air-fuel homogeneity level.

From Figure 7.6, it can be also seen that that cases CC2, C3 and CC3 (in circle) exhibit a PCCI strength level higher than 80%, which is the amount of the first fuel injection. It is obvious that all three cases have a SOC timing after or near the start of the second injection, and the premixed combustion is enhanced by the freshly introduced fuel. This is not the case for strategies 4, 5 and 6, where the second injection takes place at -5°CA ATDC.

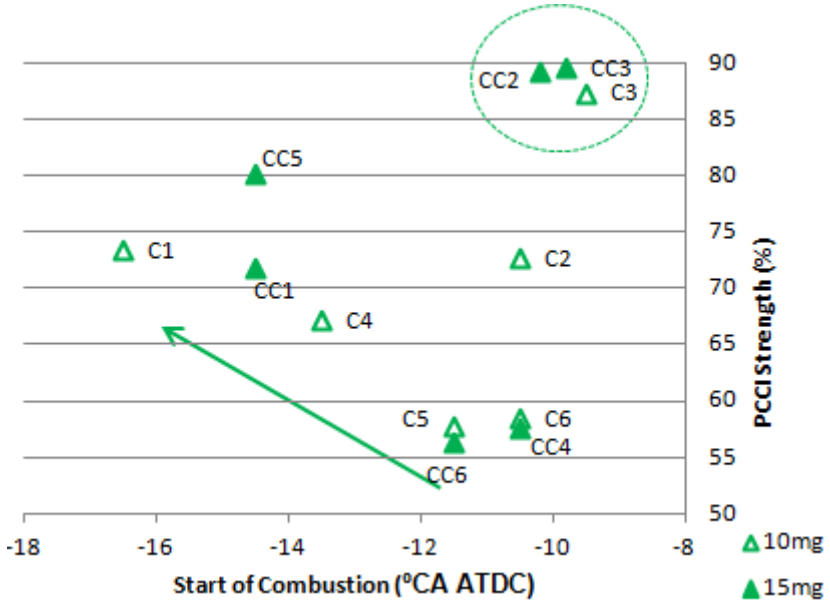

Figure 7.6: SOC timing for 80:20 injection ratio strategies.

From the figures above, the level of PCCI strength varies with injection ratio, injection timing and fuel load. It can be concluded that the strength of the premixed combustion is highly affected by the fuel amount of the first injection, the start of the second fuel injection and SOC timing.

7.1.3 Effects of PCCI Strength on Performance

7.1.3.1 50:50 Injection Ratio

The effects of PCCI strength level on the performance of the diesel engine for the 50:50 fuel injection ratio are shown in Figure 7.7.

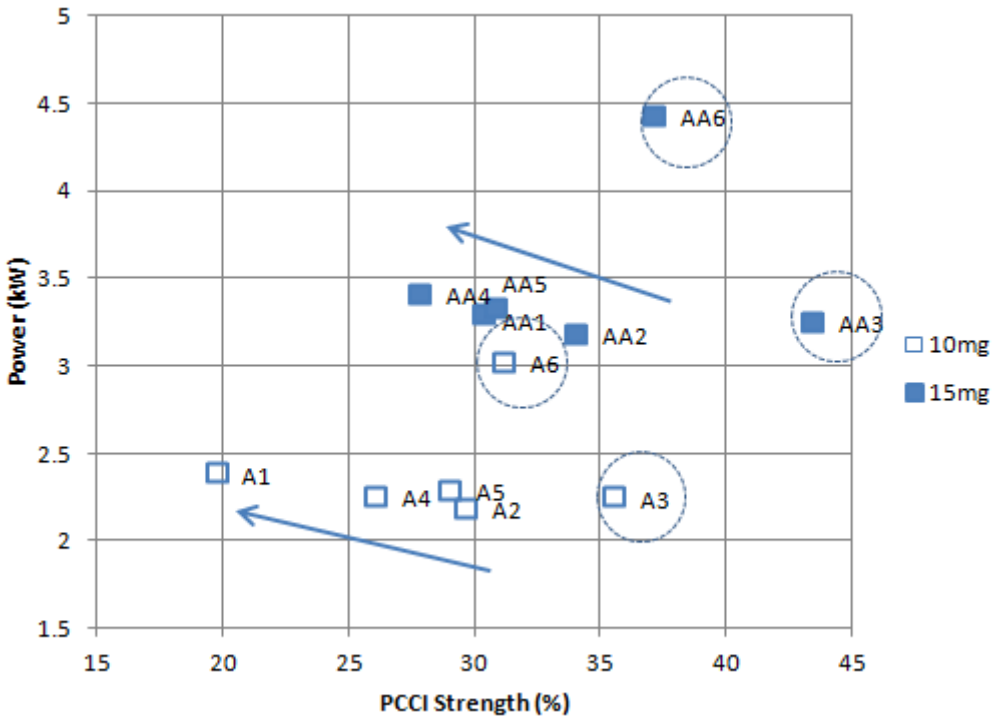

Figure 7.7: Effects of PCCI strength level on engine performance for 50:50 injection ratio.

It can be noted from Figure 7.7 that a lower level of premixed combustion leads to higher power output in most of the fuel injection strategies. A low premixed combustion at an early stage before the TDC will reduce the opposing forces applied on the cylinder while it is moving upwards towards the TDC and will reduce the pumping losses. At the same time, the increased diffusion burning rate at a later stage will improve the performance and power output of the engine.

Strategies with the first injection taking place at -30°CA ATDC (A3, AA3, A6 and AA6) exhibit higher power outputs compared to the other strategies, although their PCCI strength level is higher. The power output of the engine is directly influenced by the injection strategy followed. A late first injection overcomes one of the main disadvantages of PCCI combustion, which is small power limits due to lean flammability.

However, as can be seen in the following sections, a very late first injection reduced the premixed charge level and this is reflected in engine emissions.

7.1.3.2 70:30 Injection Ratio

Figure 7.8 presents the power rating over the PCCI strength level for the 70:30 injection ratio strategies. It can be immediately seen by comparing Figures 7.7 and 7.8 that the power rating for the strategies with 30% of the fuel injected during the second pulse is significantly reduced compared to the cases where a higher amount of fuel is injected close to the TDC.

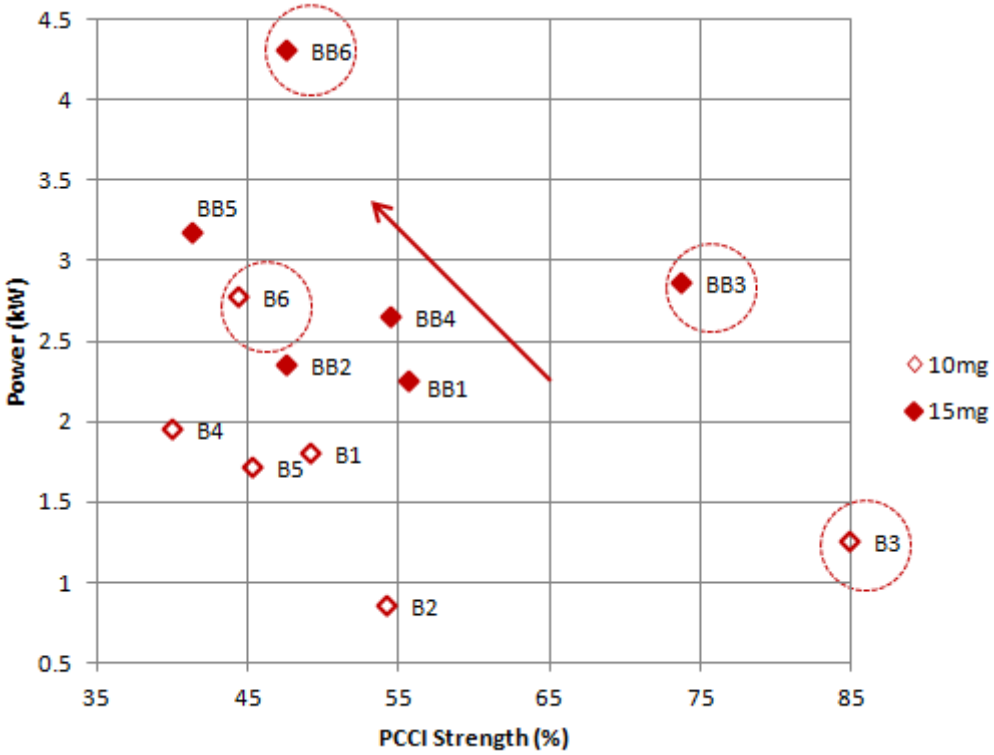

Figure 7.8: Effects of PCCI strength level on engine performance for 70:30 injection ratio.

It can also be noticed that strategies with the same SOI for the second pulse and engine load show increased power output for lower premixed combustion phases. However,

strategies 3 and 6 for both fuel loads do not follow the same trend. In the same way as in the 50:50 injection ratio cases, strategies BB3, B6 and BB6 have a high power output, although their PCCI strength level is high. Strategy B3, which exhibits the highest PCCI strength level, has a lower power output than strategy B1 due to the extremely high level of premixed combustion.

7.1.3.3 80:20 Injection Ratio

Injection strategies with an 80:20 fuel ratio follow a similar trend compared to the other two injection ratio strategies as shown in Figure 7.9.

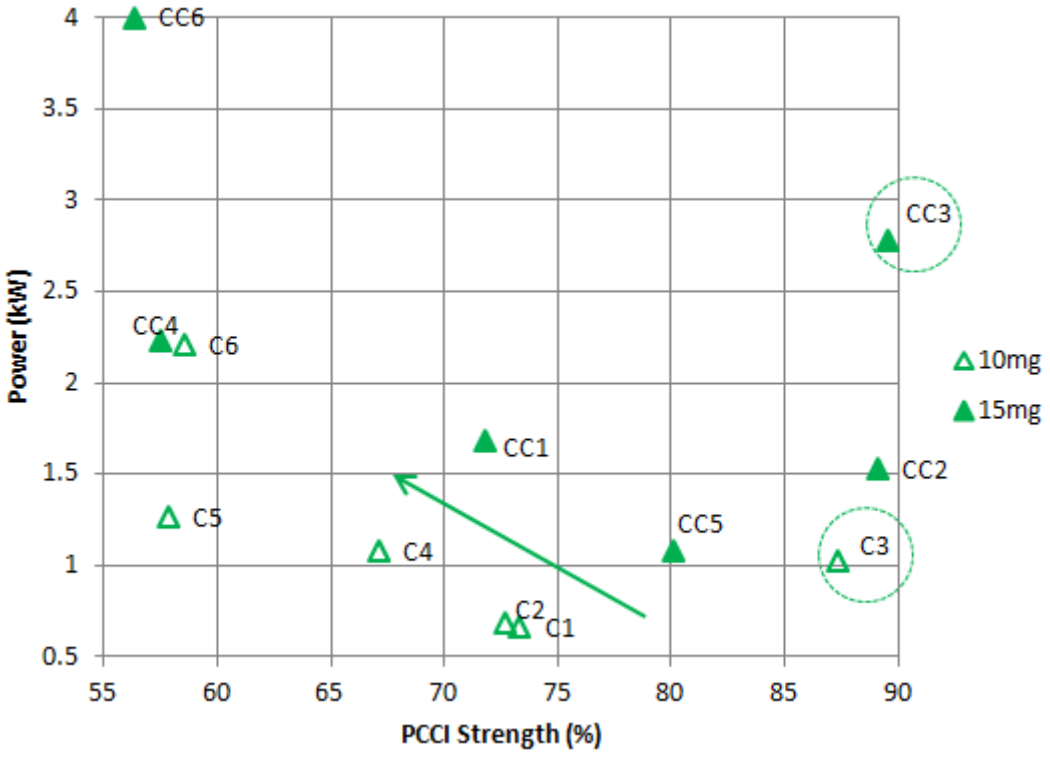

Figure 7.9: Effects of PCCI strength level on engine performance for 80:20 injection ratio.

The power output for cases C1 and C2 is very similar, with C2 being slightly higher due to the slim difference in the PCCI strength level. This difference is similar to

the power output for case C5, which is higher than C4, which has an increased PCCI strength level. However, for cases C3 and CC3, an increased PCCI strength does not lead to reduced power output. The power rating for case C3 is higher than C2 and C1 and for case CC3 is much higher than CC1 and CC2. The injection timing plays a significant role in the power output characteristics. Cases C3 and CC3 supply an increased amount of fuel at -30°CA ATDC. The increased fuel amount over the first injection pulse extends the first injection duration and reduces the dwell angle between the end of the first and start of the second injections. The short dwell angle leads to extremely high premixed phase and combustion characteristics similar to single injection strategies. This can be concluded by the power output of these two cases and the emission characteristics shown in the following sections.

7.1.4 Effects of PCCI Strength on Emissions

The effects of the combustion ratio between the premixed and diffusion combustion stages and the SOC timing on NO_x and exhaust smoke are analysed in the following sections.

7.1.4.1 NO_x Emissions

Figure 7.10 presents the effects of PCCI strength level on NO_x formation of all injection ratio cases. It is clear for strategies with a fuel injection ratio of 50:50 that NO_x formation is increased as the PCCI strength level is enhanced. The premixed combustion phase often leads to rapid and intense in-cylinder pressure and temperature increase, which are mainly responsible for NO_x formation due to high in-cylinder temperatures. The higher premixed rates lead to very high temperatures and NO_x levels.

It can also be seen from the 50:50 injection ratio results that strategies A3, AA3, A6 and AA6, with the shortest dwell angle between the two injections, exhibit the highest NO_x emissions. As described in Section 7.1.3.1 where these strategies were found to have the higher power ratings, the very short dwell angle overcomes the lean flammability combustion drawback of PCCI combustion, but at the same time limits its ability to

reduce NO_x formation.

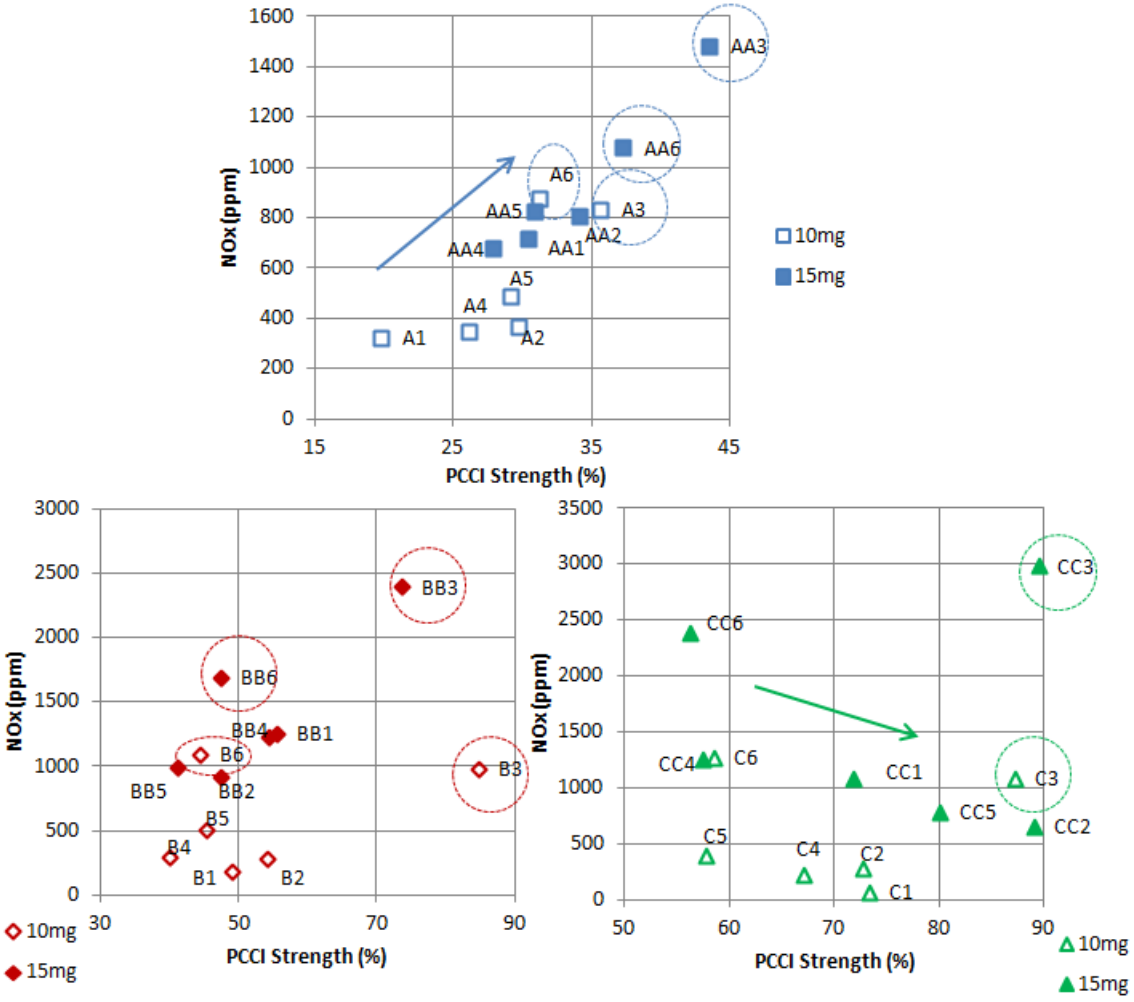

Figure 7.10: Effects of PCCI strength level on NO_x emissions for all strategies.

The NO_x versus PCCI strength trend for 70:30 injection ratio cases does not follow the same trend as in the 50:50 ratio cases. It seems that the PCCI strength does not play a key role in NO_x formation. It can be seen from the chart that for the low load cases, NO_x emissions are lower when the first and second injections take place earlier in the cylinder (B1<B2<B3 and B4<B5<B6). However, the same falling trend for NO_x emissions do not occur for the higher load strategies where the cases with the first

injection occurring at -40°CA (BB2 and BB5) show the lowest NO_x formation. In the same way as the 50:50 injection ratio cases, strategies with short dwell angle show the higher NO_x formation rates.

On the other hand, the 80:20 injection ratio strategies follow an opposite pattern to the 50:50 injection ratio cases where NO_x emissions are reduced when the PCCI strength level is increased. A very high first injection ratio leads to combustion that exhibits the benefits of HCCI combustion without a triggering injection close to TDC, which is the high homogeneous mixing of fuel and air that leads to cleaner combustion. For the 80:20 injection ratio cases, the lowest NO_x formation is shown in cases with the first injection taking place at -50°CA (C1 and C4) for the medium engine load and at -40°CA (CC2 and CC5) for the higher engine load. Similar to the previous injection ratio strategies and for both engine loads, strategies with the shortest dwell angle have the highest NO_x level.

Figure 7.11 shows the effect of SOC timing on NO_x formation. It can be observed that for cases with injection ratios of 50:50 and 70:30 with low and medium PCCI strength levels, respectively, that NO_x formation is reduced as SOC timing is retarded. This happens due to the shorter time available for the premixed combustion to take place, which directly reduces the period of high temperatures in the combustion chamber and, therefore, NO_x emission.

On the other hand, the 80:20 injection ratio strategy with very high PCCI strength levels shows a different trend where early SOC timing exhibits lower NO_x emission. In this case, early SOC timing advances the premixed combustion, which is nearly identical to full combustion, to an earlier stage where the in-cylinder pressure and temperatures are lower and, therefore, NO_x formation is reduced. As the SOC timing is retarded, the in-cylinder temperature is increased and the formation of NO_x is further enhanced by the injection of the second amount of fuel as shown in Figures 7.10 and 7.11.

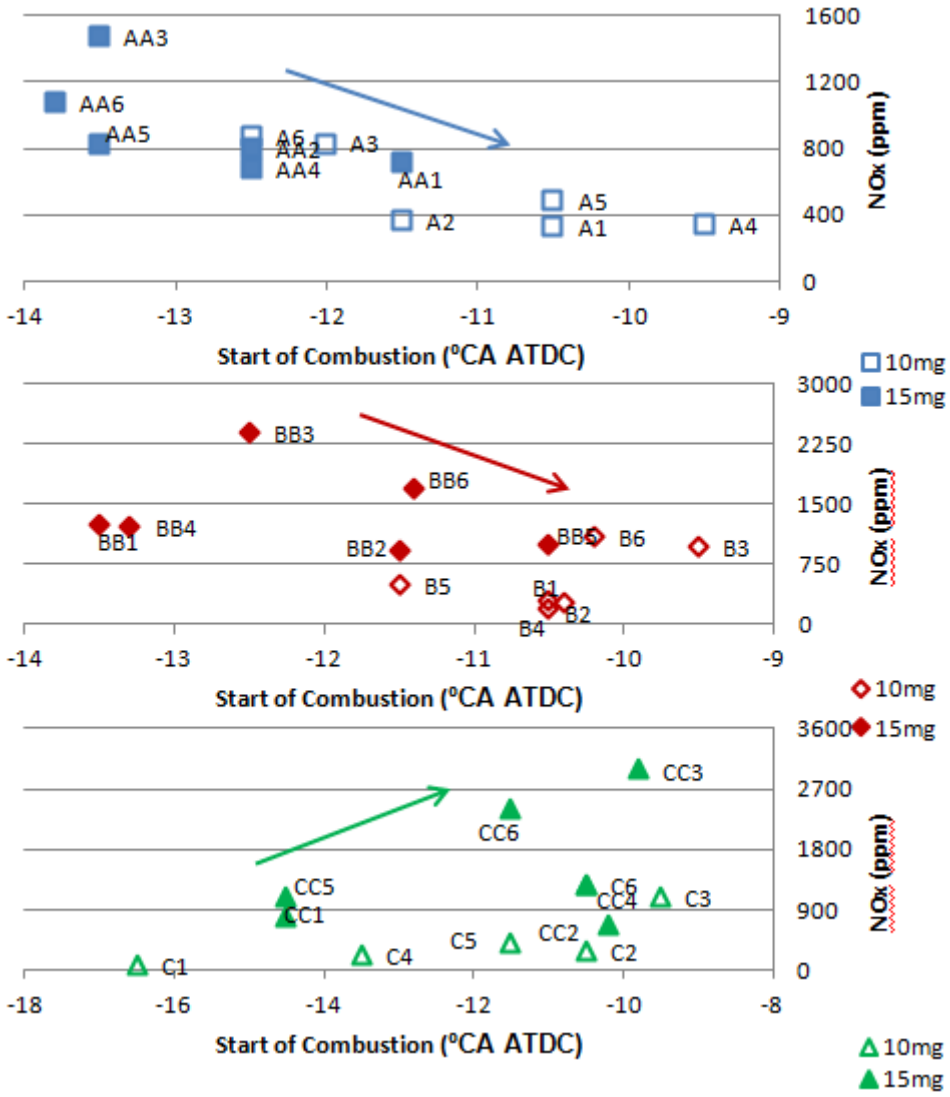

Figure 7.11: Effects of SOC timing on NO_x emissions for all strategies.

7.1.4.2 Opacity

Figure 7.12 presents the exhaust gas opacity over the PCCI strength for all injection strategies. It can be noticed that smoke follows a descending trend when the PCCI strength is increased. This can be explained due to the reduction of the diffusion combustion, which is a low temperature combustion that lacks oxygen and leads to a slow burn rate rich in soot production. Soot formation mainly takes place during the diffusion

combustion where the soot particles are largely and densely formed due to fuel oxidation and/or pyrolysis at high temperatures. The smoke emission follows the same trend for all injection ratio strategies.

It can be also seen that smoke levels are lower for low load combustion due to the lower amount of fuel injected during the second pulse, and also smoke is reduced as the second injection ratio decreases. The strategy with the 80:20 ratio exhibits the lowest levels of smoke for the majority of the cases. However, strategies AA6 and BB6 show lower smoke levels compared to BB6 and CC6, respectively. This can be explained by the very low premixed combustion rates in both strategies, which lead to a high ratio of diffusion combustion and increased smoke.

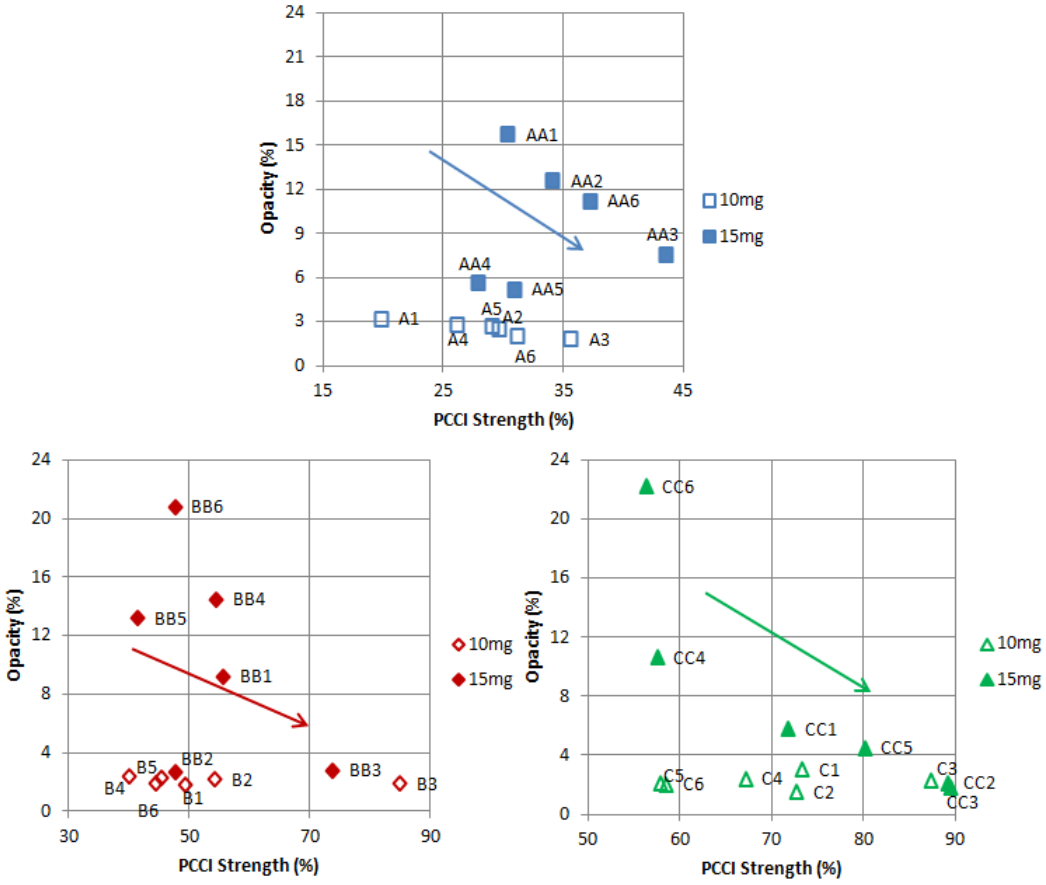

Figure 7.12: Effects of PCCI strength level on smoke for all strategies.

7.2 Emission Optimization using Statistical Methods

The effects of splitting the first injection of the PCCI strategy into two injection pulses followed by a final triggering injection closer to TDC have been investigated in this section under two engine loads: 10mg and 15mg of fuel. An experimental analysis has been carried out to simultaneously optimize diesel engine fuel and air operating parameters for low exhaust emissions using the Taguchi method. The three parameters investigated are the first and second fuel injection ratios while keeping constant the final fuel injection amount, the valve opening time for the exhaust ports and the exhaust back pressure.

Three parameters were modified and tested under various operating conditions. The first parameter investigated is the first and second fuel injection ratio while keeping the final fuel injection amount constant. It was shown earlier that the injection ratio and timing can have a significant effect on emission formation and engine performance. The second tested parameter is the valve opening time for the exhaust ports. Exhaust valve timing can have a significant effect on the exhaust gas extrusion process and, therefore, change the amount of exhaust gases trapped in the cylinder working as internal EGR. The final parameter is the exhaust back pressure. The EBP is commonly met in the state-of-the-art diesel engines where modern after-treatment and advanced EGR systems are used. The EBP can have negative effects on engine performance and fuel consumption due to high pumping losses, but at the same time can contribute to the optimization of some harmful emissions due to the restricted exhaust gas extrusion from the cylinders.

7.2.1 Engine Test Conditions

The investigation was performed by varying the first injection ratio from 0 to 50%, while the final triggering injection was kept constant at a 50% ratio of the total fuel amount injected. This high amount of fuel at the final stage of the strategy was selected for high power output as seen previously in Chapter 7.1, while the further splitting of the first injection contributes to the improvement of air-fuel homogeneity and reduction of

emissions.

The EVO time was varied between 94°and 64°CA BBDC to investigate the effects of valve timing on the exhaust gas trapping and emissions formation of the engine. Finally, the EBP was varied between 1 and 1.3 bars by adjusting the closure of the exhaust valve fitted on the Hydra's exhaust system from 0 to 95% in order to analyse the effects of EBP on engine performance and emissions. The maximum EBP that can be reached for a single-cylinder engine is relatively small compared to modern multi-cylinder engines with advanced EGR and after-treatment systems. Table 7.3 analytically presents the engine test conditions for this study.

Table 7.3: Engine test conditions for Taguchi study.

Intake air temperature	300K
Intake air pressure	1 bar
Fuel temperature	350K
Fuel injected	10mg and 15mg per cycle
Injection pressure	around 1,200 bar
Start of first injection	-50°CA ATDC
Start of second injection	-30°CA ATDC
Start of third injection	-5°CA ATDC
First injection ratio	0-50%
Second injection ratio	0-50%
First injection ratio	50%
EVO timing	94°- 69°CA BBDC
Exhaust back pressure	1 - 1.3 bar

7.2.2 Taguchi Method of Optimization

The Taguchi process starts by defining the goals that need to be identified and the parameters that need to be controlled. In this case, the parameters under investigation are the first/second fuel injection ratio, the EVO time and the EBP. Each parameter

will be tested under five different levels. Based on the number of parameters and their levels, the appropriate experimental layout of L_{25} orthogonal array is used. Table 7.4 presents the process parameters and their levels used in this study. The level of each factor used in the 25 experiments performed based on the L_{25} orthogonal array is shown in the Appendix B section.

Table 7.4: Process parameters.

Symbol	Parameter	Unit	Level 1	Level 2	Level 3	Level 4	Level 5
A	1^{st}/ 2^{nd} injections ratio	%	0/50	10/40	20/30	30/20	40/10
B	EVO time	°CA BBDC	69	57	44	63	50
C	Exhaust valve position	% of closure	0	63	75	88	95
		(≈ bars)	(1)	(1.03)	(1.06)	(1.12)	(1.3)

The 25 different air and fuel injection strategies for both engine loads were performed, and the results are fully listed in the Appendix C. Three trials for each experiment were conducted, and the results obtained were used to calculate the S/N ratios shown in Table 7.6.

7.2.3 Optimal Factors

The optimum set of parameters is determined by choosing the levels with lowest S/N ratio as our target to reduce emissions and BSFC. Before selecting the parameters, an analysis of variance (ANOVA) was performed for understanding the significance of each of the tested parameters on the output characteristics. The ANOVA experiment was carried out using Minitab 17 software and its results are listed in Table 7.5.

Table 7.5: ANOVA experiment results.

	10mg								
	NO_x			Opacity			BSFC		
Parameter	F value	ρ *(%)*		F value	ρ *(%)*		F value	ρ *(%)*	
A	48.6	*84*	✓	24.0	*63.2*	✓	21.3	*71.3*	✓
B	1.6	*3.6*		3.8	*10.2*	✓	4.2	*14.6*	✓
C	1	*2.3*		6.2	*16.3*	✓	3.4	*12.2*	✓
	15mg								
	NO_x			Opacity			BSFC		
Parameter	F value	ρ *(%)*		F value	ρ *(%)*		F value	ρ *(%)*	
A	5.2	*40.6*	✓	21.3	*58.2*	✓	53.5	*84.2*	✓
B	2.7	*18.3*	✓	6	*17.7*	✓	1	*3.5*	
C	3.8	*27.8*	✓	6.6	*19.4*	✓	1.6	*5.1*	

The contribution of the parameters on the emissions and BSFC changes for different fuel loads is clear. For low load conditions, NO_x emissions are highly influenced by the EBP levels, while in the higher load conditions all parameters have a significant effect on the emission output. The opacity levels are highly influenced at all testing levels under both fuel load conditions. Finally, the EBP level highly affects the BSFC at high load conditions while at lower fuel loads BSFC is influenced by all tested conditions.

The optimum parameters for low NO_x, opacity and BSFC were selected using Table 7.6 .

Table 7.6: S/N ratios for NO_x, opacity and BSFC (in blue font are the parameters counted for choosing the optimum levels for low NO_x, opacity and BSFC).

		10 mg				15mg			
Parameter	Level	NO_X	Opacity	BSFC	Optimum	NO_X	Opacity	BSFC	Optimum
A	1	58.85	4.62	-16.05		62.31	18.02	-15.95	
	2	53.75	3.09	-13.73		61.50	12.76	-15.57	
	3	52.84	5.16	-12.92		57.99	16.48	-16.04	
	4	46.11	5.73	-9.10	**A4**	56.57	11.52	-14.72	**A4**
	5	48.89	6.75	-11.10		56.14	11.64	-14.11	
B	1	52.89	4.80	-12.66		59.58	14.68	-15.33	
	2	53.30	5.44	-13.78	**B2**	59.36	14.42	-15.09	
	3	51.69	5.58	-12.24		56.50	15.07	-15.17	**B3**
	4	52.25	5.39	-12.38		59.31	14.41	-15.01	
	5	51.71	5.10	-12.54		58.94	13.40	-15.25	
C	1	51.51	5.55	-12.68		59.65	13.93	-15.29	
	2	52.68	5.57	-13.08		59.19	12.85	-15.26	
	3	51.83	4.81	-12.39		59.53	14.27	-15.11	
	4	52.75	5.76	-13.26		59.18	15.12	-15.13	
	5	53.79	4.32	-12.87	**C5**	56.31	15.03	-15.24	**C5**

7.2.4 Confirmation Experiments

The final step of the Taguchi analysis for emission optimization is to perform the confirmation experiments for both fuel loads in order to make sure that the optimal factors contribute to the reduction in harmful emissions and BSFC. The results of optimized engine performance for both fuel loads were compared with the baseline engine, which are cases P1 and PP1 with no EBP, no early pilot injection and EVO at 69°CA BBDC.

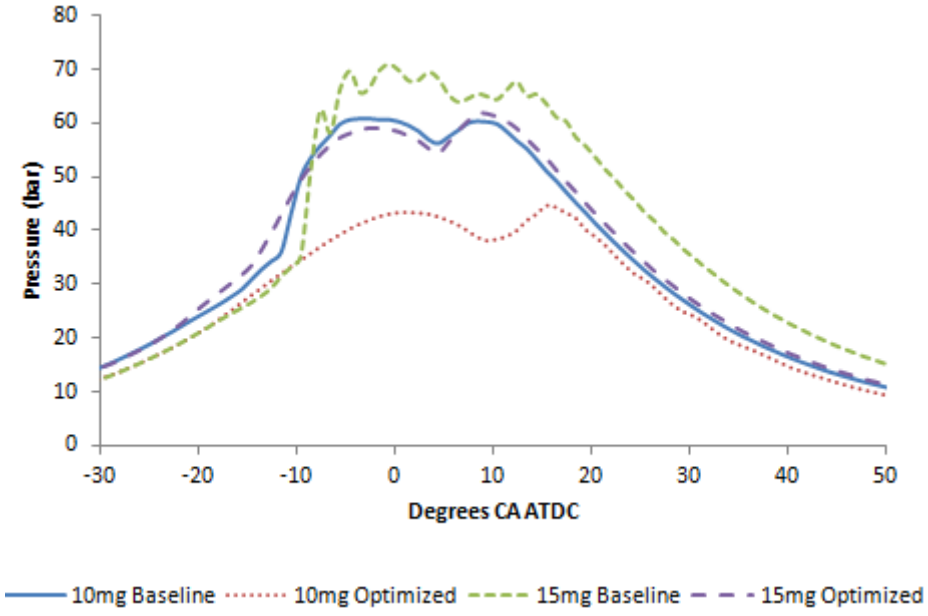

Figure 7.13: Comparison of in-cylinder pressure of baseline and optimized engines.

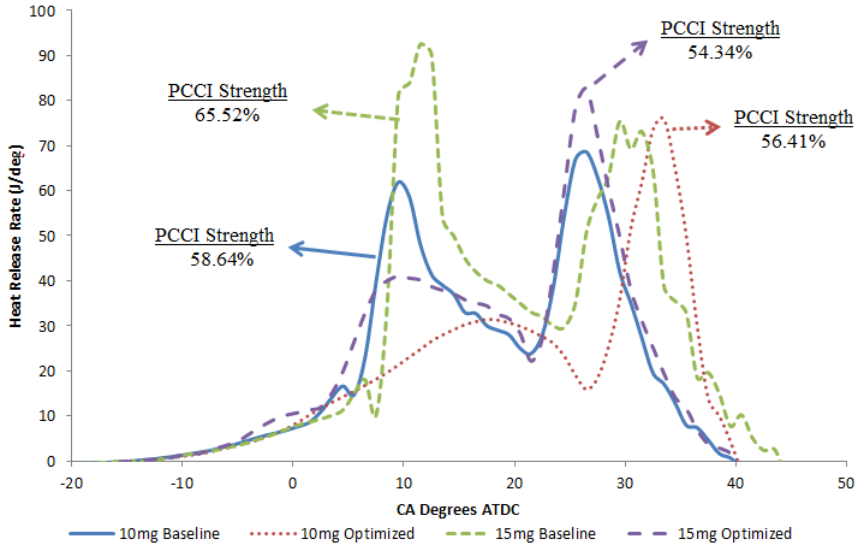

Figure 7.14: Comparison of heat release rate of baseline and optimized engines.

Figure 7.13 shows the in-cylinder pressure variation for the optimized engine compared to the baseline for both fuel loads. It seems that for both fuel loads, the baseline

engines exhibit a sharp in-cylinder pressure, which is usually a triggering point for high flame temperatures and NO_x formation. The optimized engines show a smoother in-cylinder pressure increase due to the pilot fuel injected early in the cylinder, which can significantly contribute to air-fuel mixing improvement and reduction of NO_x emission. This can also be confirmed by Figure 7.14 where the heat release rate for the baseline and optimized cases is shown.

It can be seen from Figure 7.14 that the baseline engines have a more intense and rapid HRR increase at the beginning of combustion, leading to high HRR peak values and PCCI strength levels. On the other hand, the optimized engines show a smoother inclination with lower pre-mixed combustion phases and HRR peak values. This happens due to better air-fuel mixing quality at SOC timing as a result of the early pilot fuel injection, which eliminates any fuel-rich points in the cylinder and prevents high flame temperatures.

Figure 7.15 presents the NO_x over the opacity readings for all engine tests at both fuel loads. As can be seen, the optimized engine performance for both fuel loads exhibits a combination of the lowest NO_x and soot emissions. It is obvious that emission formation mainly depends on the pilot fuel injection ratio where a 30% fuel injection gives the lowest NO_x and soot emissions for both fuel loads. On the other hand, strategies without pilot injection exhibit high NO_x emission due to the rapid HRR increase at the SOC as shown before. The small EBP and exhaust valve timing testing regions seem to have little effect on emission formation, which can be confirmed by the ANOVA experiment results in Table 7.5.

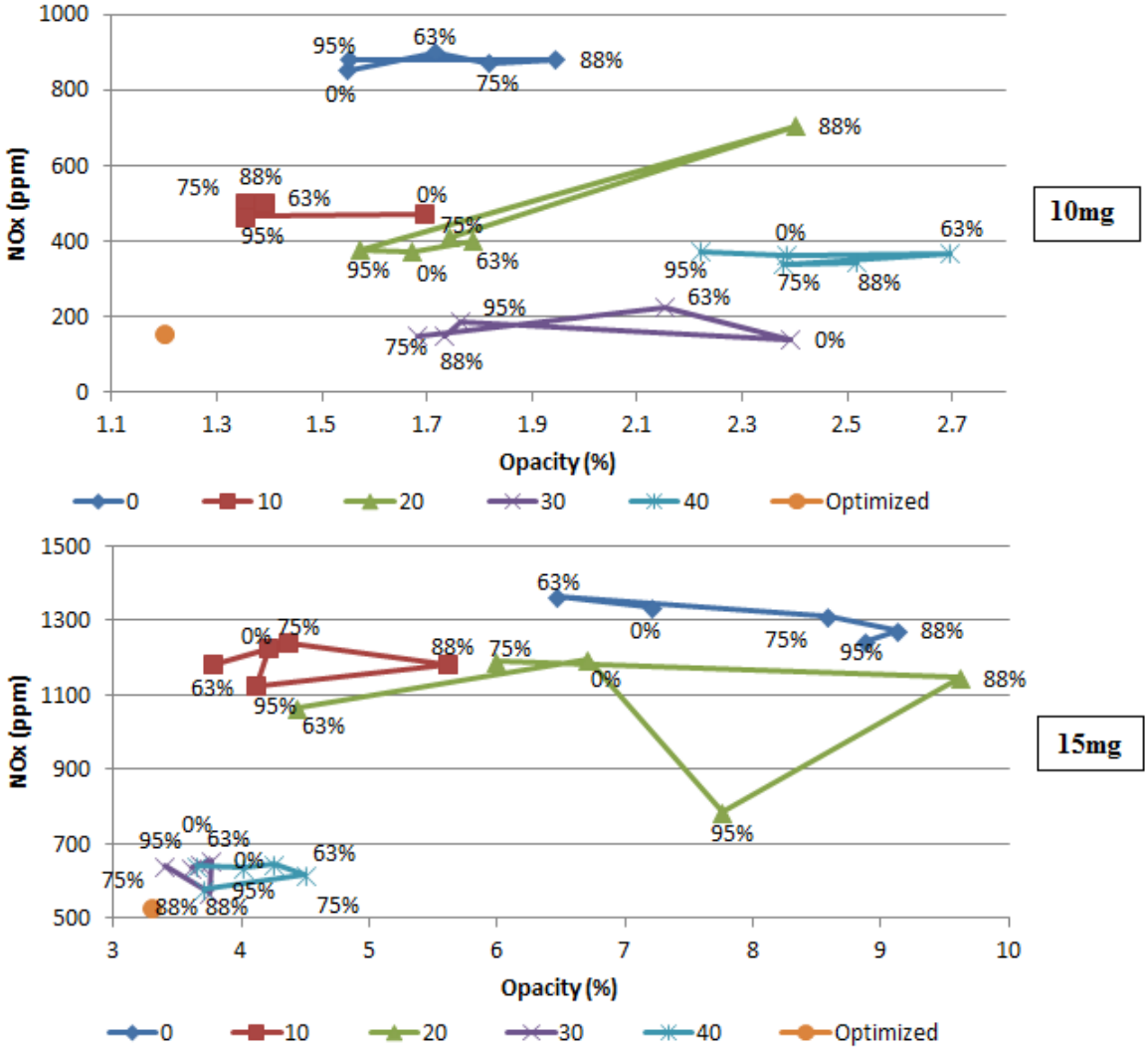

Figure 7.15: NO_x over opacity for all cases at both fuel loads; values in the legend are the percentage of pilot injection while data labels are the percentage of EBP valve closure.

However, the simultaneous reduction in NO_x and soot is expected to negatively impact the BSFC and power output of the engine. Figure 7.16 presents the BMEP over the BSFC for all the engine tests. It can be seen that although the fuel consumption and BMEP values for the optimized engine are relative low, the values achieved are the highest possible for the pilot injection strategy followed. The high contribution value of the pilot injection ratio as shown in Table 7.5 limits the effects of the other parameters

on the reduction of BSFC. However, the ANOVA and Taguchi experimental analysis provided the highest possible BSFC reduction within the allowed limits set by the pilot fuel injection ratio.

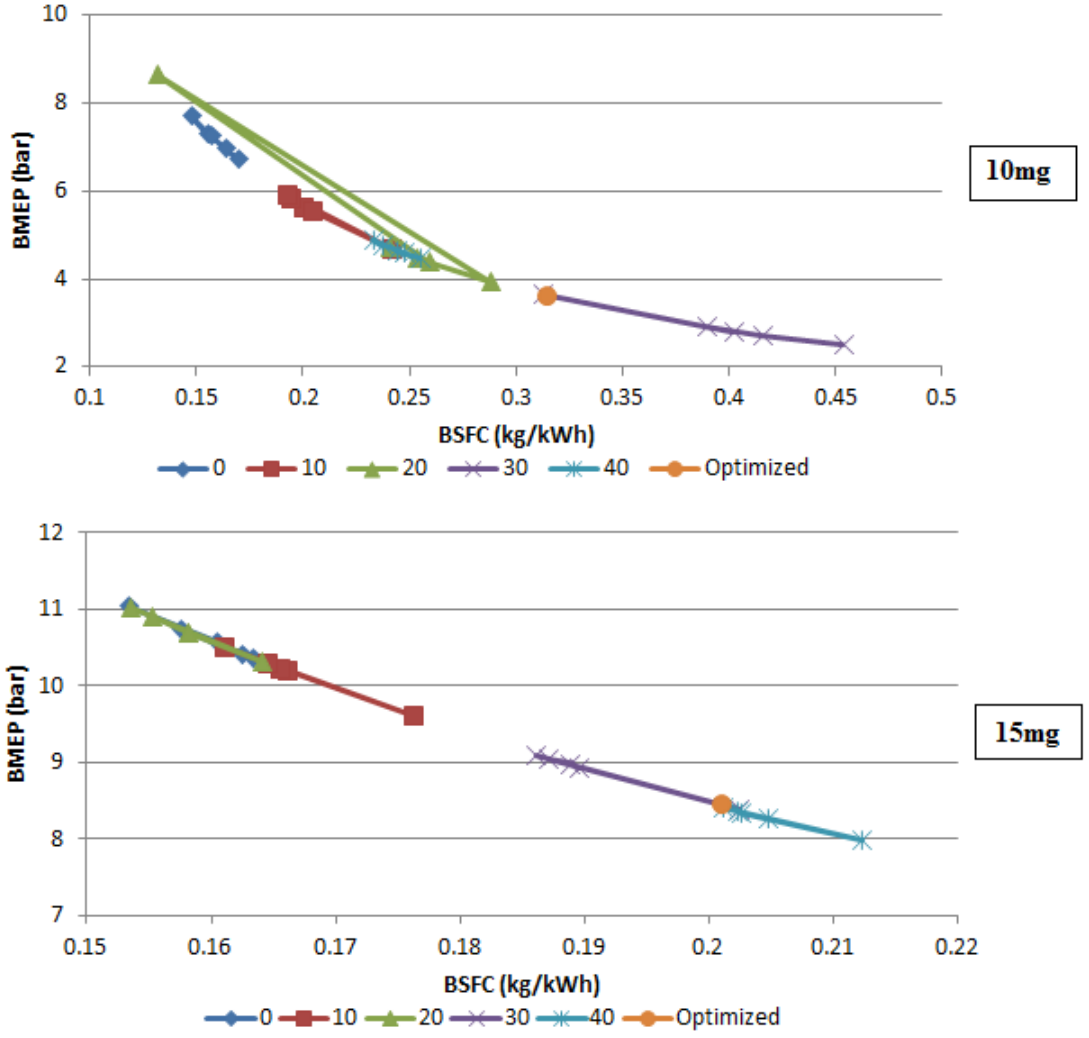

Figure 7.16: BMEP over BSFC for all cases at both fuel loads; values in the legend are the percentage of pilot injection.

Unfortunately, due to the implementation of three variables in our analysis, it is not feasible to present results on the effects of each parameter on the NO_x, smoke and BSFC. However, as forecasted by the ANOVA, it is clear that pilot fuel injection has the highest

contribution to emission formation and fuel consumption.

7.3 Summary

In this chapter, experimental analysis was performed to investigate the effects of fuel injection ratio and timing with variable exhaust flow strategies on the combustion characteristics of a diesel engine. In order to fully understand combustion performance, the heat release rate of each strategy was calculated based on the in-cylinder pressure, and the ratio of the pre-mixed combustion over the whole combustion process was measured.

From the results, it is clear that the amount of the pre-mixed combustion phase plays a key role in soot formation. An increased pre-mixed combustion phase leads to lower soot formation as a result of the short diffusion combustion phase. On the other hand, NO_x formation is increased when the pre-mixed phase is long. However, at very high pre-mixed combustion phases, NO_x formation is reduced due to the high homogeneity of the air-fuel mixture providing the benefits of HCCI low NO_x combustion without triggering a fuel injection.

Chapter 8

Piston Geometry and Nozzle Spray Angle

In this chapter the effects of piston geometry and spray angle on the air-fuel mixing quality, emissions formation, and engine performance are investigated using CFD simulations. The results are analysed with the aid of the Homogeneity Factor in order to indicate the importance of the parameters of the air-fuel mixing quality and combustion process. The purpose of the research is to indicate how the air-fuel mixing phenomena within the cylinder can influence the combustion characteristics and the emission formation. The investigation is performed under various engine loads and speeds with variable injection timings. The study is divided into the following two categories. First, simulations for nine different piston geometries under various engine conditions are performed. Finally, the piston geometry with relatively low emissions and high performance is further tested to investigate the effects of the injection spray angle with respect to the injection timing on the air-fuel mixing quality within the combustion chamber.

8.1 Piston Geometry Configuration

The baseline piston geometry of Hydra engine was modified in the direction of finding the optimum piston geometry aiding to an improved air-fuel mixing. The compression

ratio of the engine was locked at 18.3:1 for all piston models in order to make sure that results are only affected by the geometry and not the engine conditions.

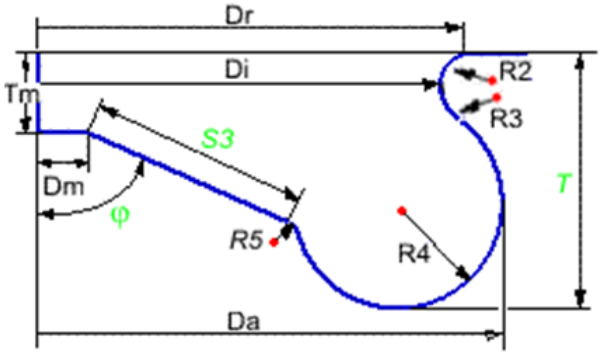

Figure 8.1: Ricardo Hydra piston template.

Table 8.1: Piston geometry parameters and their ranges.

		Piston Geometry								
	Range (mm)	Baseline (mm)	1 (mm)	2 (mm)	3 (mm)	4 (mm)	5 (mm)	6 (mm)	7 (mm)	8 (mm)
Outer bowl diameter (Da)	**45.68 – 68.00**	48.00	51.86	49.16	46.41	45.68	53.00	58.00	63.00	68.00
Inner bowl diameter (Di)	**40.00 – 66.40**	43.40	40.00	41.29	42.60	42.98	46.40	51.40	58.40	66.40
Bowl radius (R4)	**3.60 – 10.10**	8.10	6.10	7.10	9.10	10.10	6.10	4.60	3.60	4.10
Bowl depth (T)	**7.35 – 15.89**	14.75	14.33	14.91	15.57	15.89	12.87	10.57	8.37	7.35
Clearance gap (TDC)	**1.05 – 1.26**	1.20	1.10	1.18	1.16	1.15	1.22	1.26	1.05	1.24
Bowl centre depth (Tm)	**4.00 – 7.29**	6.00	7.29	6.68	6.06	5.91	6.00	6.00	6.00	4.00

The outer and inner bowl diameter (Da, Di) along with the re-entrant bowl radius (R4) and the bowl depth (T) were the four main parameters modified and tested for their contribution to the air-fuel mixing behaviour within the cylinder. However, it is very difficult to change one variable without affecting other dependent variables. Therefore, some of the changes have occurred in the rest of the piston variables are as shown in Table 8.1.

The nine piston geometry configurations tested are shown in the Figure 8.2.

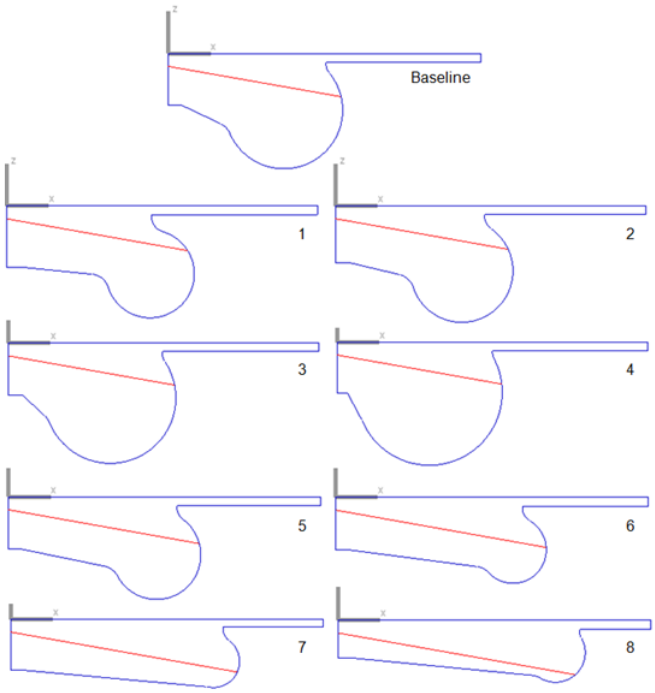

Figure 8.2: Piston geometry configuration.

8.2 Engine Test Conditions

The engine test conditions were kept the same for all piston configurations and nozzle spray angles. According to the results in literature, piston geometry has little influence on the in-cylinder flow during the intake stroke and the first part of the compression stroke. Therefore, the calculation starts at the inlet valve closure (IVC) and ends just

before the exhaust valve opening (EVO) for time reduction reasons. The simulation is carried out on a 60°sector for reduced calculation time due to the symmetric location of the six-hole injector at the centre of the combustion chamber. The air and fuel conditions were applied on the tests are shown in Table 8.2.

Table 8.2: Initial air and fuel test conditions.

Intake air temperature	380K
Intake air pressure	1 bar
Fuel temperature	350K
Fuel injected	5.82 – 19.05 mg/cycle
Injection duration	6.04°to 11.85°CA
Start of injection	15°– 5°CA BTDC
Inlet Valve Close	64°ABDC
Exhaust Valve Open	69°BBDC
Engine Speed and (load)	1,200rpm (80%), 1,600rpm (60%), 2,000rpm (40%)

8.3 Effects of Piston Geometry

The re-entrant piston geometry is crucial in DI diesel engines for enhancing fuel distribution within the combustion chamber. As previous research has shown, there is no optimum piston geometry for the entire engine operating conditions. On the contrary, the air flow within the chamber is highly affected by the engine speed and load.

Figure 8.3 presents air-fuel mixing quality within the combustion chamber at TDC, a point just before the start of combustion. In this figure, HF is plotted against the piston internal diameter (Di), bowl radius (R4) and bowl depth (T). The tests were performed in three different operating conditions. The engine speed varied from 1,200 rpm for 80% load to 1,600 rpm for 60% load and 2,000 rpm for 40% load.

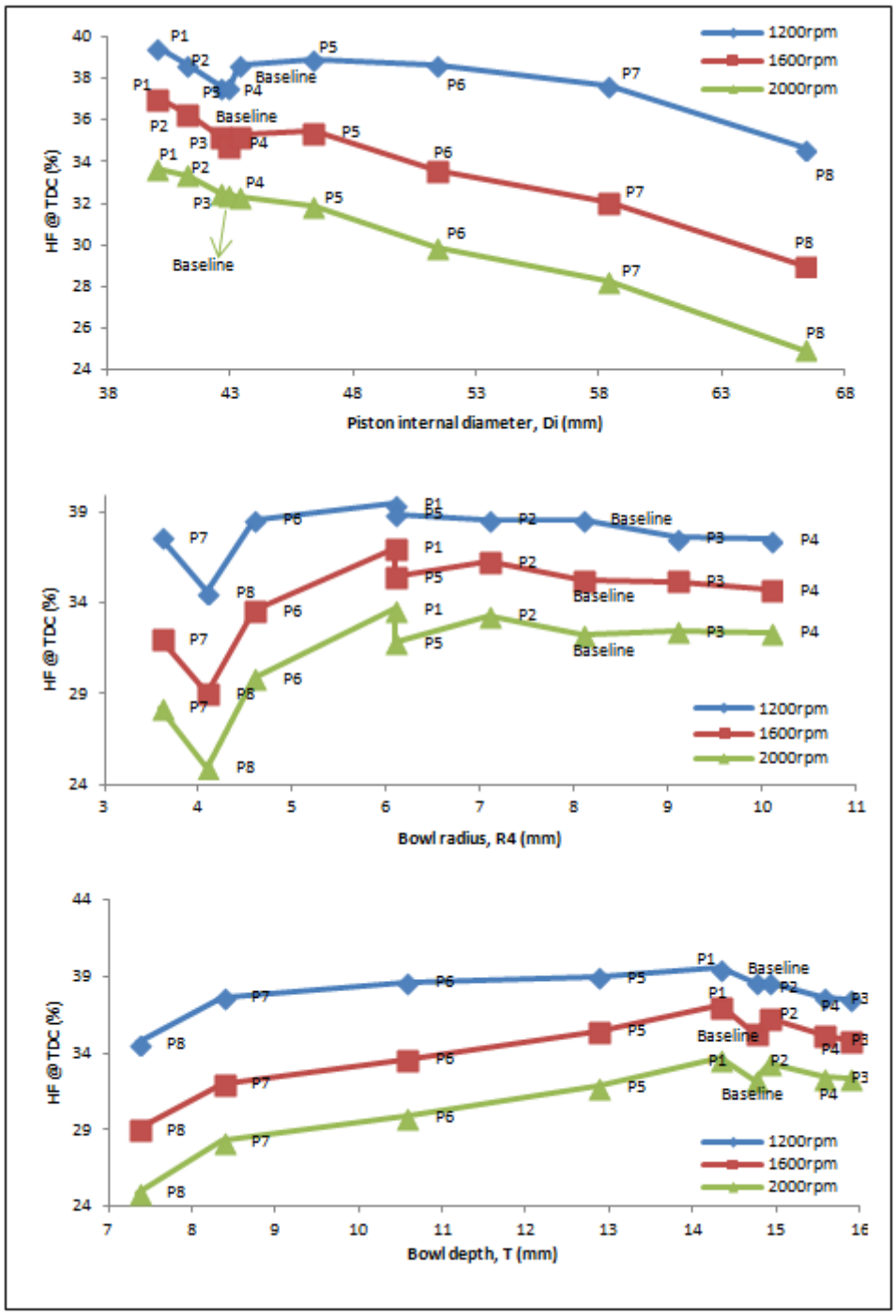

Figure 8.3: HF against the piston the internal diameter (Di), bowl radius (R4) and bowl depth (T) at TDC.

The HF is reduced while the piston internal diameter is increased. This agrees with results in literature that show a smaller diameter piston bowl will generate higher swirl around the TDC and consequently will increase the air-fuel mixing quality. It is clear that HF is relatively high for pistons with the lowest piston internal diameter. However, the results demonstrate that pistons 3 and 4 have relatively lower HF due to the small difference between the outer (Da) and inner (Di) piston diameters. On the other hand, pistons with progressive diameter increments lead to higher swirl ratios and enhanced air-fuel mixing.

It can be concluded by reviewing Figure 8.3 that a narrow entrance with deep combustion re-entrant chambers would significantly increase the air-fuel mixing quality within the chamber. This happens due to the increased air speed that enters the piston bowl, forming a strong squish. On the other side, larger piston bowl diameters with a shallow depth have significantly less swirl within the cylinder leading to a poorer air-fuel mixing.

In Figure 8.3, HF is shown to be higher for simulations performed at 1,200 rpm compared to 1,600 rpm and 2,000 rpm. This is due to the following two reasons. First, the engine load and speed difference mean that the injection quantity and timing varies for each case. The injection strategy variation leads to a difference in the availability of time for the air and fuel to mix. Moreover, for full load test conditions (1,200 rpm case), the start of combustion has already taken place a couple degrees before the TDC leading to a more homogenous mixture at the TDC. The start of combustion for medium load cases (1,600 rpm) starts roughly a couple degrees after the TDC and for the low load conditions strategy (2,000 rpm), the start of combustion occurs five to six degrees after the TDC. In addition, the HF is higher in low speed cases as there is more available time (slower engine rotation) for the air-fuel mixing process to take place. This can also be confirmed by the subsequently lower influence of the piston geometry on the HF.

In Figure 8.4 the NO_x and soot formation for all the piston geometries at 1,600 rpm over the homogeneity levels, at a point just before the combustion starts, at the TDC, and during the combustion process, 20°ATDC are presented.

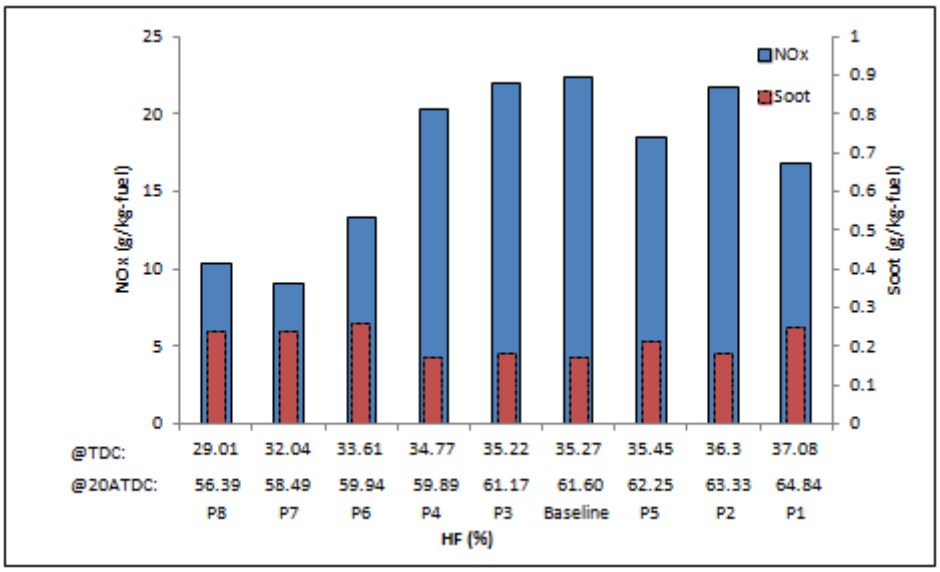

Figure 8.4: Average NO_x and soot formation over the HF levels at TDC and 20°ATDC for 1,600rpm case.

It can be seen that for the pistons with lower HF, NO_x formation is reduced while the soot formation is increased. Pistons with higher HF have an increased NO_x formation and reduced soot levels. However, piston geometries with the highest HF levels show a lower NO_x formation than geometries with medium levels of homogeneity. Although air-fuel mixing quality is important for the performance and emissions formation characteristics of a DI diesel engine, generalizations about air-fuel mixing homogeneity and emissions formation cannot be made.

In Figure 8.5 (a), the NO_x over the soot formation for all the piston geometries under the three operating conditions is presented. It is obvious for the first two operating conditions that none of the pistons can simultaneously combine low levels of soot and NO_x formation. For the 2000 rpm case, piston geometry 8 has very low levels of soot and NO_x at the same time. However as shown in Figure 8.5 (b), the low IMEP and high BSFC indicate that this is due to an incomplete combustion taking place within the piston at 2000 rpm engine speed.

Piston geometries 3 and 4 have the highest IMEP and lowest BSFC values for all

of the operating conditions as shown in Figure 8.5(b). However, as it is expected, the higher IMEP levels caused by a more complete combustion within the cylinder, lead to very high NO_x formation and low soot levels as shown in Figure 8.5 (a).

Piston geometry 5 benefits from relatively low levels of NO_x and soot at low load conditions with high IMEP and low BSFC levels. In the medium and high load conditions, the soot levels are relatively low while the NO_x formation is slightly increased compared to the other geometries for the 1,600 rpm case.

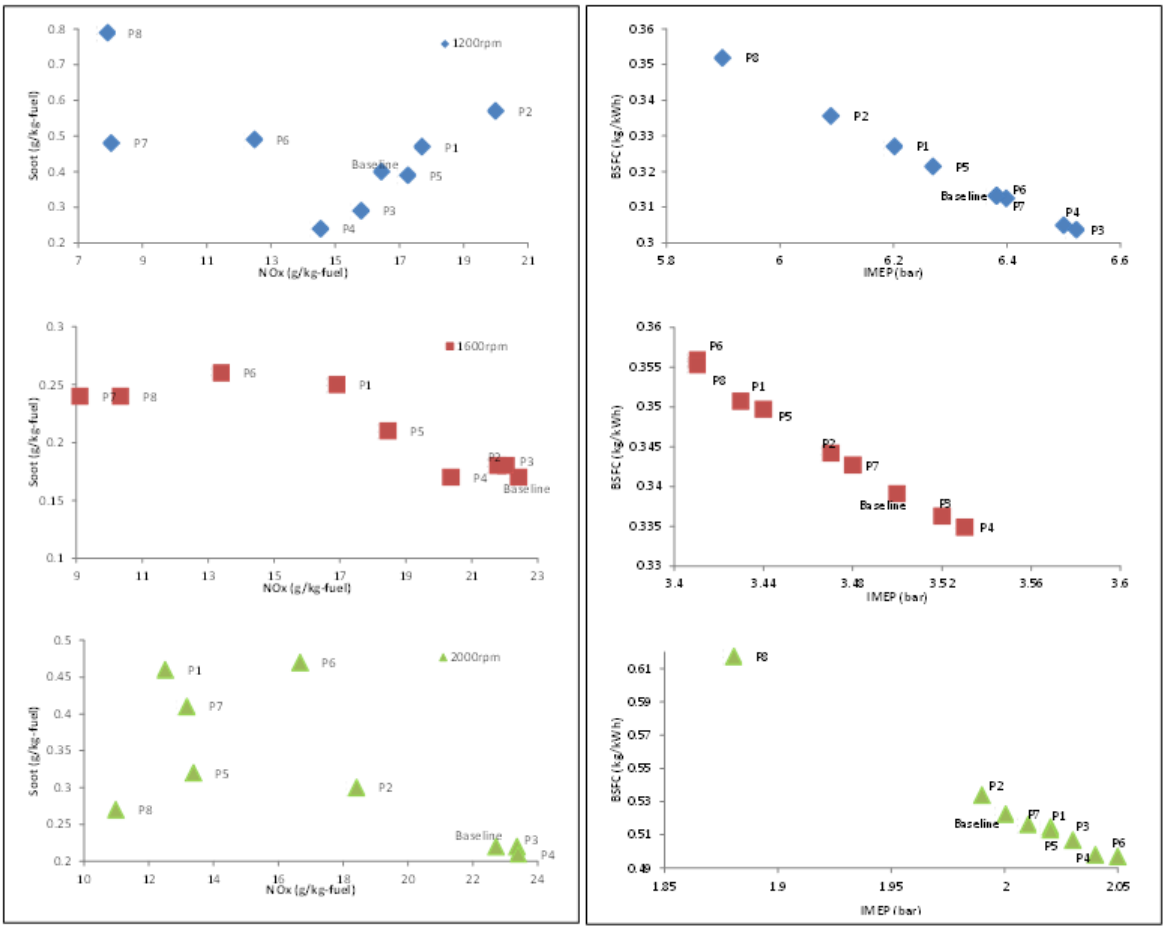

Figure 8.5: (a) NO_x over soot formation and (b) IMEP over BSFC for all piston geometries.

Figures 8.5(a) and (b) demonstrate that the performance of each of the piston geometries varies with the difference of the engine conditions. For instance, piston geometry 1 has relatively low NO_x and increased soot levels at 2,000 rpm while it has very high NO_x and medium soot levels at 1,200 rpm. However, the conclusion can be drawn that pistons with reduced bowl diameter and increased bowl depth result in lower BSFC levels, higher NO_x formation, and IMEP.

In Figure 8.6, the air flow velocity and direction for three piston geometries are presented. The three pistons were selected in order to represent the difference of the air flow between shallow, wide geometries and deep, narrow pistons. Piston geometry 1 represents combustion chambers with a narrow entrance and wide protuberance. Piston geometry 3 is a narrow entrance combustion chamber with a deep re-entrant protuberance. Finally, geometry 8 is a wide and shallow piston.

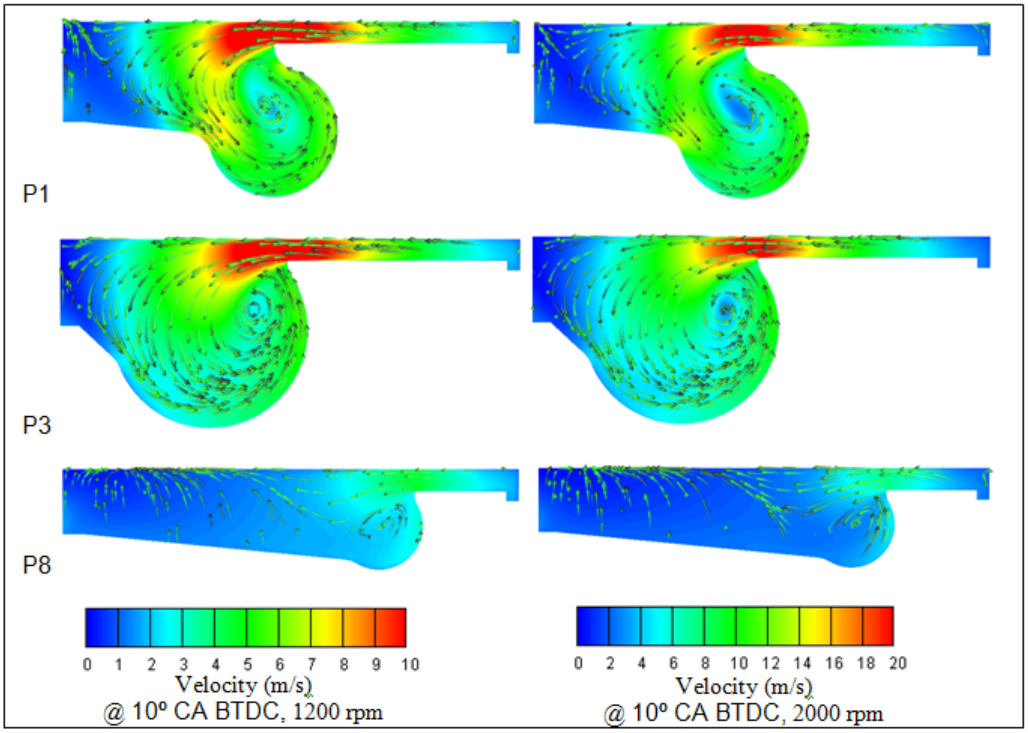

Figure 8.6: Air velocity contours and flow streamlines at 10°CA BTDC for piston geometries 1, 3 and 8 at 1,200rpm and 2,000rpm.

The overall velocity within the narrow entrance pistons is greater than the velocity in the wider piston geometry at 10°BTDC in both engine speed conditions. The magnitude of the air speed is higher in high rpm conditions compared to the low rpm conditions due to the increased piston speed. The squish velocity in pistons 1 and 3 are almost twice that in piston 8. The narrow entrance into a deep combustion chamber significantly increases the speed of the air entering the piston bowl, developing strong squish flow. The squish flow in the narrow pistons geometries is roughly similar due to the very close internal diameter widths of the two pistons. However, the flow velocity changes at the centre and bottom of the combustion chambers. The swirl flow in piston geometry 1 is higher than geometry 3 due to the smaller bowl area, which increases the angular velocity. Although the higher swirl velocity occurs within chamber 1, the magnitude of the flow is higher at the centre of piston 3. This is caused by better interaction between the squish and swirl flow within cylinder 3.

As expected, piston geometry significantly impacts the air flow within the combustion chamber. The stronger squish-swirl interaction can develop toroidal vortices within the chamber, improving the fuel distribution and enhancing the evaporation process. The equivalence ratio and HF of the three pistons examined at 20°ATDC is shown in Figure 8.7. It is obvious that equivalence ratio contours cannot be easily compared for pistons with different geometries. Although piston 1 has an improved air-fuel mixing within the bowl of the combustion chamber at 1,200 rpm, the fuel is not finely distributed at the squish area for the 1,200 rpm engine speed. This is due to the low squish flow formed during the expansion stroke of the piston as a result of the bowl shape. The HF trend shows that the air-fuel mixing quality is slightly better for piston 3 compared to geometry 1. For piston geometry 8, the lack of swirl flow within the cylinder caused a low quality air-fuel mixture, which can be clearly observed by both the contour and the HF value.

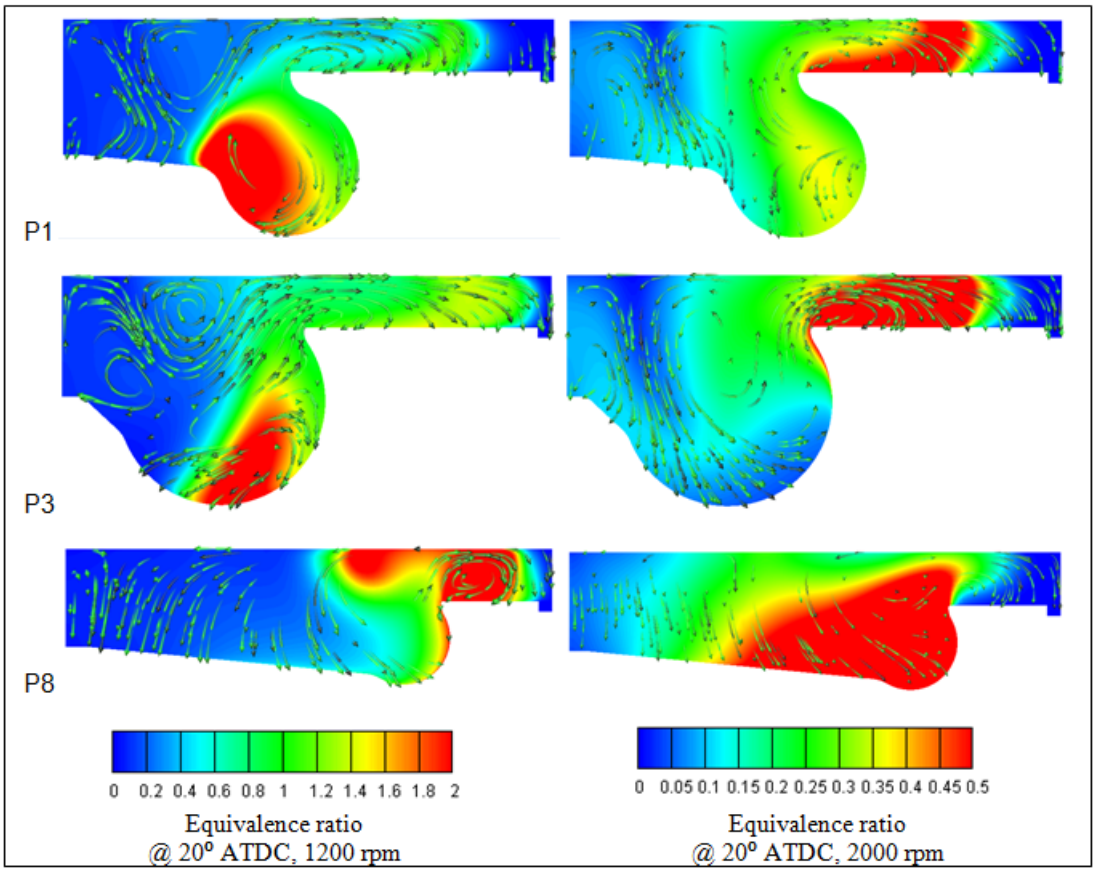

Figure 8.7: Equivalence ratio contours and flow streamlines at 20°CA ATDC for piston geometries 1, 3 and 8 at 1,200rpm and 2,000rpm.

The equivalence ratio (ER) contour of piston geometry 1 at 2,000 rpm shows a more balanced fuel distribution at the bowl and squish area of the piston compared to geometry 3. The HF for piston 1 rises at 67.38% at 20°CA ATDC, while for geometry 1 is 63.16%. The large HF difference between the two geometries has a high impact on the emissions and performance of the engine as shown in Figure 8.5 (a) and (b). The low air-fuel mixing quality within piston geometry 3 resulted in highly increased NO_x formation due to fuel-rich bulky regions at the squish area as shown in Figure 8.8. The increased temperature resulted in higher IMEP values, lower BSFC, and lower soot formation but rapidly increased NO_x formation. On the other hand, piston geometry 1 benefits from

lower temperature combustion, with very low NO_x and increased particulate matter.

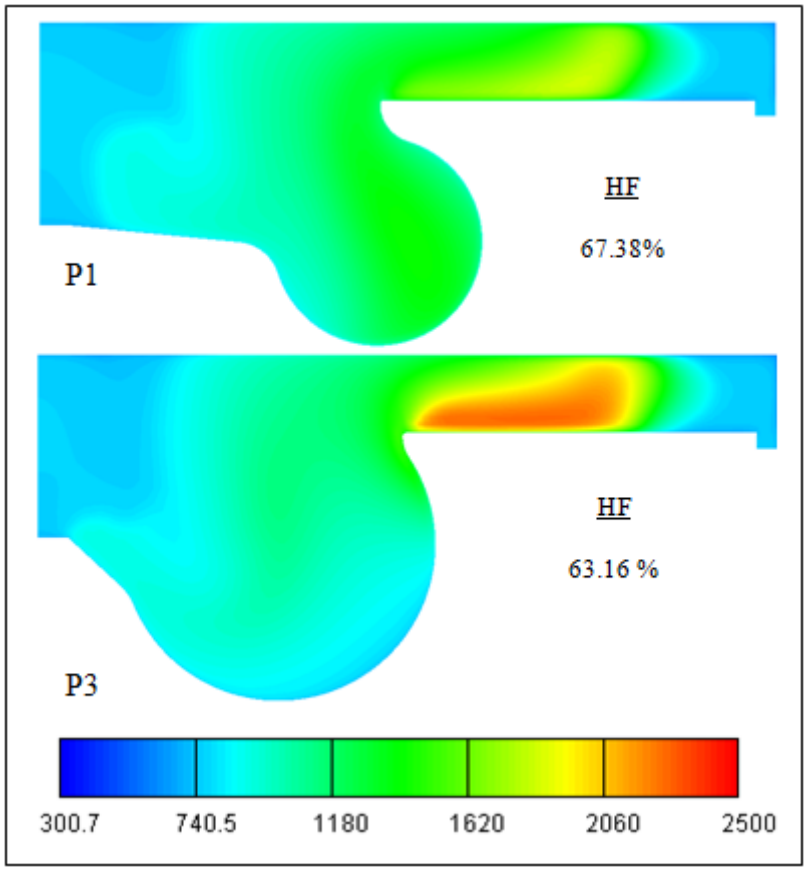

Figure 8.8: Temperature contours of pistons 1 and 3 at 2000rpm, 20°ATDC.

As shown in the figures above, the air-fuel mixing quality improvement can have either negative or positive effects on the emissions formation of the engine. It seems that an improved air-fuel mixing can lead to a more complete combustion, which subsequently means higher NO_x and less soot formation. However, an improved air-fuel mixing can also aid less fuel-rich regions within the combustion chamber and therefore reduce high temperature points and NO_x formation in the combustion chamber.

8.4 Effects of Included Spray Angle

Piston geometry 5, which benefits from medium levels of air-fuel homogeneity and relatively low NO_x and soot formation at all operating conditions, was selected to analyse the effects of the injection spray angle on the air-fuel mixing within the combustion chamber. Three spray angles were tested under different start of injection (SOI) timings. The three spray angles were targeting the main fuel injection quantity at three different locations of the piston bowl. The 130°injection spray angle points at the lower bottom of the bowl, the 145°injection spray angle points at the centre of the bowl, while the 145°spray angle injects the fuel toward the upper area of the piston bowl. Figure 8.9 illustrates the spray cloud and HF readings at 10°CA ATDC for piston geometry 5 at 1,600 rpm engine speed under three different starts of injection timings.

The piston geometry is a key factor for picking the optimum injection angle. Figure 8.9 shows that an injection angle of 135°will result in some of the fuel to wet the surface of the piston as it moves upwards. This results in a poorer fuel distribution within the cylinder as shown by the HF comparison in Figure 8.9. The injection timing variation influences the air-fuel mixing quality. An early injection results in a high degree of homogeneity within the cylinder at an early point. On the other hand, a late start of injection reduces the time available for the air-fuel mixing to occur and therefore reduces the homogeneity. However, the HF variation among the different injection angles is not highly influenced by the start of injection timings.

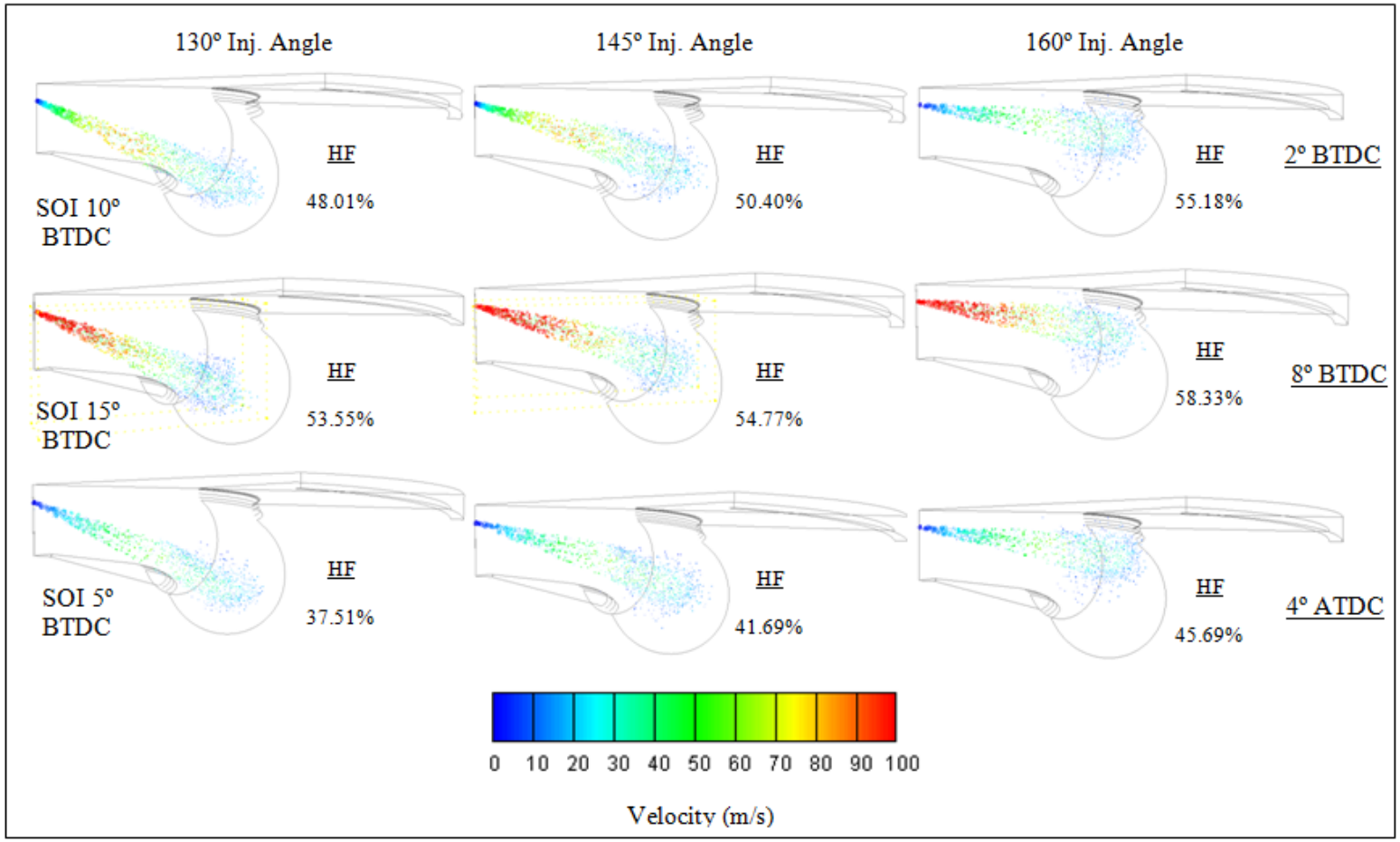

Figure 8.9: Spray clouds and HF of piston 5 for 3 different injection angles at 1,600rpm.

Figure 8.9 demonstrates that although the 145°spray angle points at the centre of the re-entrant bowl, the air-fuel mixing quality levels are lower than in the cases with 160°spray angles. This can be justified by looking at Figure 8.10, which presents the equivalence ratio contours and the HF levels for piston geometry 5 at three different pistons positions. As shown in the figure, the fuel flow for the 130°spray angle follows the air flow vectors at the air swirl region of the piston bowl. This results in a high amount of fuel vapour concentrated at the bowl edges and the squish area. The 145°spray angle hits at the centre of the swirl region while the fuel flow for the 160°spray angle case has an opposite direction than the air flow within the piston bowl. The opposite air and fuel flow directions create small vortices within the bowl aiding in an enhanced mixing quality. The equivalence ratio contour for the 160°spray angle shows that the fuel concentration in the squish region has been reduced while the fuel vapour distribution has been enhanced at the centre of the piston bowl.

The effects of the air-fuel mixing quality on the in-cylinder temperatures are presented in Figure 8.11. The fuel rich squish regions due to the poor air-fuel mixing in the 130°and 145°spray angle cases have resulted in in-cylinder high local temperatures, which increased the NO_x formation. On the other hand, the 160°spray angle case exhibits relatively low in-cylinder temperatures at the squish region and the sides of the piston bowl. The NO_x emissions levels are 8.6% reduced for the 160°spray angle case compared to the 145°case. On the other hand, the soot formation is increased by 28% for the 160°case compared to the 130°spray angle case. Increased air fuel homogeneity aids in avoiding fuel rich bulky points and reducing NO_x formation. However, the increased homogeneity leads to an increase in particulate matter within the cylinder.

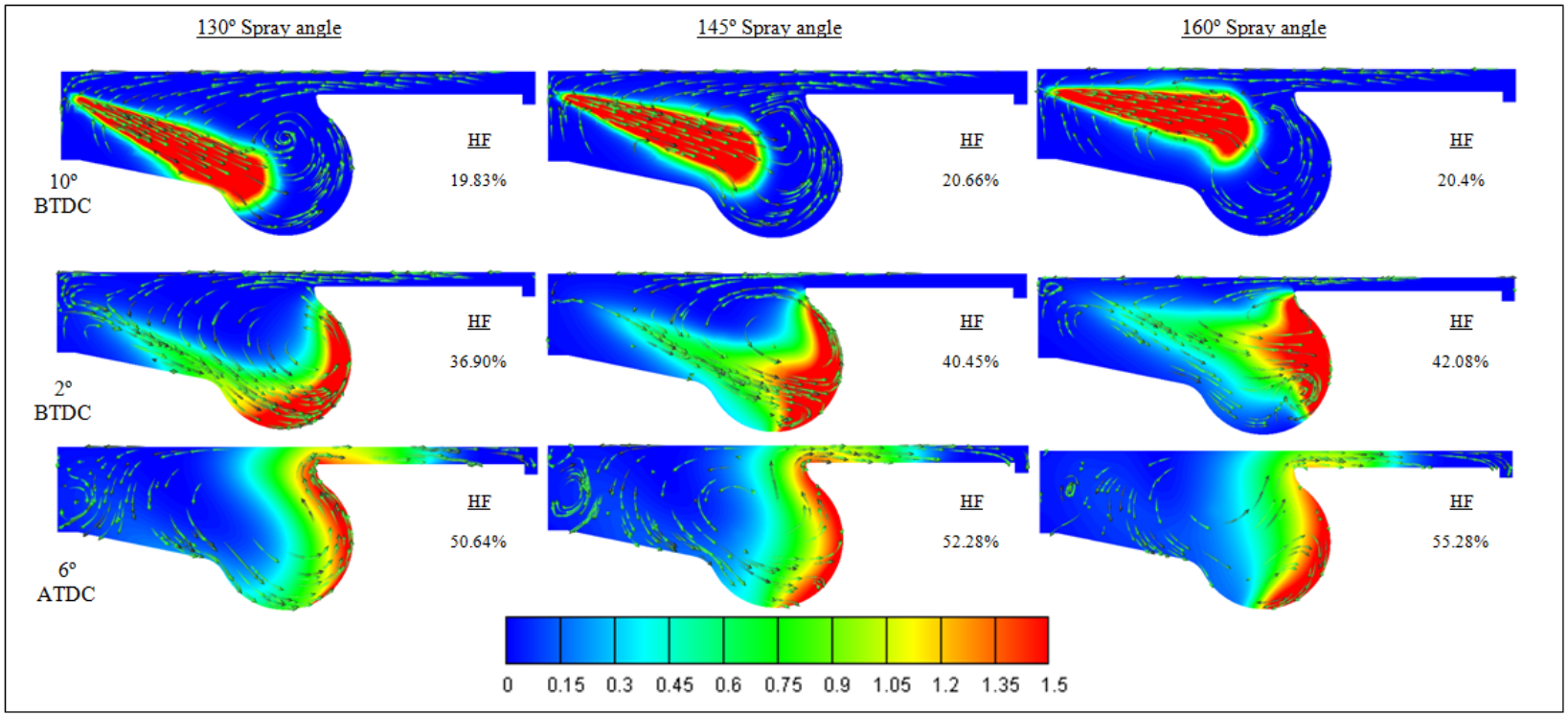

Figure 8.10: ER contours and flow streamlines of piston 5 with SOI at 15°CA BTDC for three different injection angles at 1,600rpm.

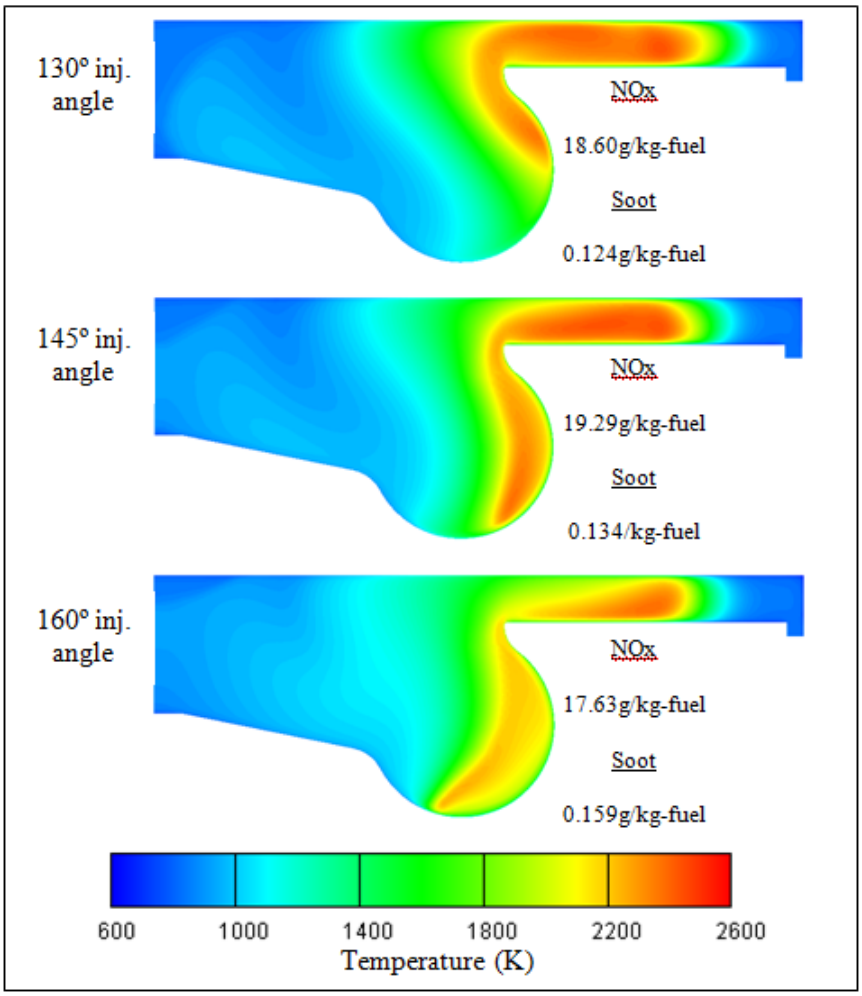

Figure 8.11: Temperature contours at 15°CA ATDC for three different injection angles, NO_x and soot emissions levels at 1,600rpm.

8.5 Summary

In this section, the HF has been used for investigating the effects of piston geometry and fuel injection angles on air-fuel mixing, emissions, and performance of a DI single-cylinder diesel engine. Investigations were carried out for nine different piston geometries and three different injection angles.

It was found that piston geometry and nozzle spray angle play a key role in air-fuel

mixing phenomena occurring in the combustion chamber. A narrow entrance with a deep combustion re-entry chamber can significantly increase the air-fuel mixing quality within the chamber due to the increased speed of air entering the piston bowl, forming a strong squish. It was also found that the opposite air and fuel flow directions create small vortices within the bowl, enhancing mixing quality.

Chapter 9

Conclusions and Recommendations for Future Work

9.1 Conclusions

9.1.1 Air-fuel Homogeneity Analysis

In Chapter 6, a recently developed parameter, namely the HF, was applied in order to study the effect of the air–fuel mixing quality on the combustion characteristics and the emissions formation of a single-cylinder DI diesel engine. The study of the air–fuel mixing behaviour is of great importance for understanding the engine's performance and emissions behaviour. The HF parameter can be an extremely helpful tool for finding the correlation between the in-cylinder mixing quality and the emissions formation. Simulations were performed for various single-injection timings as well as split-injection and multiple-injection strategies. The main findings of this work can be summarized as follows.

- The air–fuel mixing quality in the cylinder is directly influenced by the fuel injection timing. As the SOI advances, a more homogeneous fuel-lean mixture occurs

at an earlier stage in the cylinder.

- A split injection can be used to improve the air– fuel mixture temporarily at the point where the first injection ends. This is due to the available time when the fuel has to be distributed into the cylinder with no more fuel diffusion compared with the single injection.

- Although a split injection can be used to improve the air–fuel mixture locally, the homogeneity level decreases when the second injection takes place. This leads to a reduction in the NO_x emissions but to a rapid increase in the soot formation.

- The decrease in the HF at the start of the second main pulse in the split-injection strategy is mainly affected by the dwell angle between the two injections. It seems that, the smaller the dwell angle, the less the HF falls, which leads to more NO_x and less soot formation.

- The addition of a pilot fuel injection in the split injection strategy leads to an improved air–fuel mixing quality at the point where the first main injection occurs. However, the early in-cylinder fuel injection and the high HF lead to a high HRR and more NO_x formation.

- High fuel injection pressure leads to higher in-cylinder pressure, temperature and heat release rate as a result of better fuel atomization corresponding to the smaller fuel droplets size resulting to a more complete combustion. However, high in-cylinder temperature results to an increased NO_x formation. As the injection pressure increases, fuel is spread faster and finer into the cylinder therefore Homogeneity Factor is increased resulting to better IMEP values, less fuel consumption and soot formation.

- Increased pilot fuel quantity results to better air-fuel homogeneity and therefore higher pressure, HRR and NO_x formation. The larger pilot fuel injections contribute to richer pre-mixed combustion phase which is mainly responsible for the NO_x formation due to very high in-cylinder temperatures.

- The results show that in most of the cases an increased HF leads to improved IMEP and reduced soot formation as a result of better air-fuel mixing. However, a close connection between the HF and NO_x formation cannot be established.
- The longer the dwell angle is, the more time is available for the pilot fuel to be spread uniformly within the cylinder. This results to a more complete high in-cylinder pressure combustion and faster heat release which increases the NO_x formation.
- Increasing the air swirl ratio enhances the air-fuel mixing quality which has been reflected in the variation of HF. As a result, increased in-cylinder pressure and temperature caused by the optimized air-fuel mixing improved the combustion efficiency.
- All the simulations performed in this thesis clearly show that a high HF leads to more complete combustion, which, as a result, increases the NO_x emissions and reduces the soot emissions.

The findings of this research work partially agree with the expected results. It has been shown that soot formation is highly depended on the air-fuel mixing quality, however, a strong connection between HF and NO_x formation cannot be established. HF is an important parameter that can be employed for analyzing results such as air-fuel mixing quality, engine power output and soot formation. The research work carried out in this chapter focuses on the effects of the injection pressure, ratio, dwell angles and swirl ratios to the air-fuel mixing quality and emissions formation and engine performance. However, there are many factors such as advancing or retarding injection timings, varying the compression ratio, EGR, turbo-charging which could all affect the HF readings, hence the engine performance and emissions.

9.1.2 Premixed Charge Compression Ignition Analysis

In Chapter 7, the PCCI strength of combustion for different fuel injection ratios, injection timings and engine loads has been calculated by experimentally measuring the

ratio of the pre-mixed combustion phase over the whole combustion cycle of the engine. Firstly, a detailed analysis was provided for the effect of different parameters of a split injection strategy on PCCI strength, performance and emission characteristics. Subsequently, statistical analysis was performed in order to determine the lowest set of engine parameters for reduced emissions through the application of a pilot injection, exhaust back pressure and variable exhaust valve timing. The main findings of this work can be summarized as follows.

• Increased fuel loads lead to higher PCCI strength levels due to an earlier SOC and more available time for the pre-mixed combustion phase to take place. In addition, the PCCI strength is increased when the second fuel injection is retarded.

• An advanced first fuel injection improves air-fuel homogeneity within the cylinder and reduces the combustion temperatures, which results in lower burning rate during the pre-mixed combustion phase and lower PCCI strength. In contrast, a late first injection leads to rapid and robust combustion with increased burning rates.

• A second fuel injection taking place close to SOC timing caused from the first fuel injection can enhance the pre-mixed combustion ratio and increase the flame temperatures and NO_x emission.

• A high pre-mixed combustion phase at an early stage before the cylinder reaches the TDC increases the opposing forces applied on the cylinder as it moves upwards and reduces the work efficiency of the engine.

• Increased PCCI strength often leads to rapid and intense in-cylinder pressure rise, which is mainly responsible for the increased NO_x formation. The NO_x formation is also highly dependent on the dwell angle between the injections, as this highly affects the air-fuel homogeneity conditions and burning rates.

• The start of combustion timing plays a significant role in PCCI strength and NO_x formation of the engine. A late SOC reduces the available time for the pre-mixed combustion phase to take place and, therefore, NO_x formation is reduced. However, for cases where the PCCI strength is very high and the engine exhibits HCCI combustion characteristics, an early SOC, where the in-cylinder pressure and temperature is low,

results in lower NO_x formation.

• The higher the PCCI strength level, the lower the soot of the engine, as soot formation mainly takes place during the diffusion combustion phase.

• Statistical methods can be employed to reduce the number of experimental trials and saves cost and time. The results show that a pilot injection can improve air-fuel homogeneity and reduce the pre-mixed combustion phase and NO_x emission. Exhaust back pressure can also contribute to the reduction of NO_x and soot formation by restricting the flow of the exhaust gases expelled from the cylinder and work as an internal EGR method. However, increased EBP enhances the pumping losses of the engine and increases the BSFC.

9.1.3 Piston Geometry and Nozzle Spray Angle

The HF has been used for investigating the effects of piston geometry and fuel injection angles on the air-fuel mixing, emissions, and performance of a DI single cylinder diesel engine. The research work carried out investigates the importance of the HF to be used as a parameter for analyzing results. The main findings of this work, within the ranges tested, can be summarized as follows:

- A large piston bowl diameter with a shallow depth has significantly less swirl flow within the cylinder leading to a poorer air-fuel mixing. On the other hand, a narrow entrance with a deep combustion re-entrant chamber would significantly increase the air-fuel mixing quality within the chamber. This happens due to increased air speed that enters the piston bowl, forming strong squish. Moreover, pistons with progressive diameter increments benefit from high swirl and enhanced air-fuel mixing.

- The piston geometry effects on the air-fuel mixing is minimized for the low engine speed cases as there is more available time (slower engine rotation) for the air-fuel mixing process to take place.

- The air-fuel mixing quality is important for the performance and emissions forma-

tion characteristics of a DI diesel engine, however, generalizations about air-fuel homogeneity and emissions formation cannot be made. Results show that an improved air-fuel mixing can lead to a more complete combustion, which subsequently means higher NO_x and less soot formation. However, an improved air-fuel mixing can also aid in less fuel-rich regions within the combustion chamber and therefore reduce high temperature points and NO_x formation in the combustion chamber.

- Piston geometries with increased swirl – squish interaction flows benefit from better air-fuel mixing at the centre of the cylinder.

- The opposite air and fuel flow directions create small vortices within the bowl aiding in an enhanced mixing quality. The equivalence ratio contour for the 160°spray angle shows that the fuel concentration in the squish region has been reduced while the fuel vapour distribution has been enhanced at the centre of the piston bowl.

- It was confirmed that there is no piston geometry that can benefit from low emissions and high engine performance for all engine operating conditions.

The findings of this research work demonstrated that HF is a very useful indicator for studying and understanding in-cylinder air-fuel mixing and emissions formation behaviour. The HF is an important parameter that can be employed for analyzing results. The research work carried out in this section focuses on the effects of the piston geometry and spray angle on the air-fuel mixing quality, emissions formation, and engine performance. However, there are many other factors, which can highly affect the air-fuel mixing quality of a DI diesel engine.

9.2 Recommendations for Future Work

The recommendations for future work in this section cover some of the main weaknesses and limitations of this research.

Initially, the CFD model used in this study was validated using experimental results obtained in a single-cylinder engine. However, for the purpose of validating the HF, an

optical engine with the use of modern imaging and laser technologies is required.

In addition, modern diesel engines are equipped with advanced air boosting and EGR systems that were not included in this study. Exhaust gas recirculation is widely used in PCCI combustion for delaying SOC timing and avoiding any knocking caused by a very early combustion start, which can be damaging to engine components. On the other hand, turbochargers are widely used in modern diesel engines in order to increase the mass of the oxygen within the cylinder and, therefore, the fuel quantity injected for increased power output. Both of these technologies have a significant effect on the air-fuel mixture, and further research is required to investigate their effects on air-fuel homogeneity and combustion characteristics.

Further research is also required in the fields of the operating range of both simulation and experimental results. CFD model and experimental analysis need to be performed on a more comprehensive range of engine speeds and fuel load operating conditions in order to analyse their effects on the air-fuel mixing and combustion processes.

Finally, the two factors (HF and PCCI strength) implemented in this study showed a close trend in NO_x and particulate matter emissions. An increased HF leads to reduced PM, while very low and very high PCCI strength levels lead to reduced NO_x formation. It is recommended that these two factors are implemented as virtual sensors under transient engine operating conditions. The two virtual sensors with the help of advanced methods of process control such as Model Predictive Control (MPC) and Adaptive Neuro Fuzzy Inference System (ANFIS) can contribute to more active control of air and fuel injection parameters for the reduction of harmful engine-out emissions. Additional research is needed for adequate inputs for the dynamic prediction of these two factors.

References

[1] Heywood, J., *Internal Combustion Engine Fundamentals.* McGraw-Hill Science Engineering, 1988.

[2] Thomas, D., *Diesel: Technology And Society In Industrial Germany.* University of Alabama Press, 2004.

[3] Fontenoy, P., *Submarines: An Illustrated History of Their Impact.* ABC-CLIO, 2007.

[4] Eckermann, E., *World History of the Automobile.* Society of Automotive Engineers, 2001.

[5] Robson, G., *Turbo: An A-Z of Turbo Charged Cars.* Book Sales, 1988.

[6] Pirotte, M., "Citroën BX 19 TRD. Le Moniteur de l'Automobile (in French) (Brussels, Belgium: Editions Auto-Magazine)", vol. 35, p. 20, 1984.

[7] ICCT,, "European vehicle market statistics - pocketbook 2013", tech. rep., The International Council of Clean Transportation, 2013.

[8] EEA,, "European environment agency". Available from: http://www.eea.europa.eu/data-and-maps/, Cited on 28/05/2014.

[9] Wray, R., "The guardian". Available from: http://www.theguardian.com/business, Cited on 28/05/2014.

[10] Swift, D. and Foster, W., *Air Pollutants and the Respiratory Tract.* Marcel Dekker, 1999.

[11] EU,, "Official websit of the european union". Available from: http://europa.eu/, Cited on 28/05/2014.

[12] DENSO,, "Annual report 2011", tech. rep., DENSO Corporation Japan, 2011.

[13] US Environment Protection Agency, *Proceedings of the 1999 Source Testing in the New Regulatory World Workshop II*, January January 2000.

[14] E.H. Pechan & Associates, I., "Analysis of national low emission vehicle program benefits", tech. rep., Vehicle Programs and Compliance Division U.S. Environmental Protection Agency, July 1997.

[15] EPA,, "Control of air pollution from motor vehicles: Tier 3 motor vehicle emission and fuel standards", tech. rep., United States Environmental Protection Agency, March 2014.

[16] Posada, F., Bandivaderak, A., and German, J., "Estimated cost of emission reduction technologies for ldvs", tech. rep., Washington DC: International Council on Clean Transportation (ICCT), 2012.

[17] Sanchez, F., Bandivadekar, A., and German, J., "Estimated cost of emission reduction technologies for light-duty vehicles", tech. rep., The International Council on Clean Transportation, March 2012.

[18] Group, A. Q. E., "Particulate matter inthe united kingdom - summary", tech. rep., Prepared for: Department for Environment, Food and Rural Affairs; Scottish Executive; Welsh Assembly Government; and Department of the Environment in Northern Ireland, 2005.

[19] Xi, J. and Zhong, B., "Soot in diesel combustion systems", *Chemical Engineering & Technology*, vol. 29, no. 6, 2006.

[20] Atkins, R., *An Introduction to Engine Testing and Development.* SAE International, 2009.

[21] EPA,, "United States Environment Protection Agency". Available from: http://www.epa.gov, Cited on 28/05/2014.

[22] Jimoda, L., "Effects of particulate matter on human health, the ecosystem, climate and materials: A review", *Working and Living Environmental Protection*, vol. 9, no. 1, pp. 27–44, 2012.

[23] Liu, L., "Human health effects of fine particulate matter: Update in support of the canada-wide standards for particulate matter and ozone", tech. rep., Canadian council of ministers of the environment, 2004.

[24] EPA,, "Smog - who does it hurt? what you need to know about ozone and your health", tech. rep., United States Environmental Protection Agency, July 2009.

[25] Heisler, H., *Advanced Engine Technology.* Butterworth-Heinemann Ltd, 1995.

[26] Morawska, L., Moore, M., and Ristovski, Z., "Health impacts of ultrafine particles - desktop literature review and analysis", tech. rep., Australian Government - Department of the Environment and Heritage, 2004.

[27] Carslaw, D., Beevers, S., Westmoreland, E., and Williams, M., "Trends in nox and no2 emissions and ambient measurements in the uk", tech. rep., Department for Environment, Food & Rural Affairs, July 2011.

[28] Zeldovich, Y., "The oxidation of nitrogen in combustion and explosions", *Acta Physiochim. U.R.S.S.*, vol. 21, pp. 577–628, 1946.

[29] Lavoie, G., Heywood, J., and Keck, J., "Experimental and theoretical study of nitric oxide formation in internal combustion engines", *Comb. Sci. Technology*, vol. 1, pp. 313–326, 1970.

[30] Stone, R., *Introduction to Internal Combustion Engines 4th Edition.* Palgrave Macmillan, 2012.

[31] Badran, O., Emeish, S., Abu-Zaid, M., Abu-Rahma, T., Al-Hasan, M., and Al-Ragheb, M., "Impact of emulsified water/diesel mixture on engine performance and environment", *Int. J. of Thermal & Environmental Engineering*, vol. 3, no. 1, pp. 1–7, 2011.

[32] Hountalas, D., Mavropoulos, G., Zannis, T., and Mamalis, S., "Use of water emulsion and intake water injection as NOx reduction techniques for heavy duty diesel engines", *SAE Paper 2006-01-1414*, 2006.

[33] Bedford, F. and Rutland, C., "Effects of direct water injection on DI diesel engine combustion", *SAE Paper 2000-01-2938*, 2000.

[34] Murotani, T., Hattori, K., Sato, E., Chryssakis, C., Babajimopoulos, A., and Assanis, D., "Simultaneous reduction of NOx and soot in a heavy-duty diesel engine by instantaneous mixing of fuel and water", *SAE Paper 2007-01-0125*, 2007.

[35] Vu, P., Nishida, O., Fujita, H., Harano, W., Toyoshima, N., and Iteya, M., "Reduction of NOx and PM from diesel engines by WPD emulsified fuel", *SAE Paper 2001-03-05*, 2001.

[36] Nazha, M., Rajakaruna, H., and Wagstaff, S., "The use of emulsion, water induction and EGR for controlling diesel engine emissions", *SAE Paper 2001-05-07*, 2001.

[37] Kegl, B., Kegl, M., and Pehan, S., *Green Diesel Engines: Biodiesel Usage in Diesel Engines.* Springer, 2013.

[38] Clean Air Technology Center (MD-12),, "Nitrogen oxides (nox), why and how they are controlled", tech. rep., United States Environmental Protection Agency, November 1999.

[39] Ferguson, C. R., *Internal combustion engines - Applied thermodynamics.* John Wiley & Sons, 1986.

[40] Greeves, G., Khan, L., and Onion, G., "Effect of water introduction on diesel engine combustion and emissions", *16th Symp. (Int.) on Combustion*, 1977.

[41] Yu, R. and Shahed, S., "Sources of hydrocarbon emissions from direct injection diesel engines", *SAE Paper 800048*, 1980.

[42] Dent, J. and Lakshminarayanan, P., "A model for absorption and desorption of fuel vapour by cylinder lubricating oil films and its contribution to hydrocarbon emissions", *SAE Paper 830652*, 1983.

[43] Ikegami, M., Xin-he, L., Nakayama, Y., and Keimiwa,, "Trend and origins of particulate and hydrocarbon emission from direct injection diesel engines", *SAE Paper 831290*, 1983.

[44] Xiao, Z., Ladommatos, N., and Zhao, H., "The effect of aromatic hydrocarbons and oxygenates on diesel engine emissions", *Proceedings of the Institution of Mechanical Engineers, Part D: Journal of Automobile Engineering*, vol. 214, pp. 307–322, 2000.

[45] Nakayama, Y., Maruya, T., Oikawa, T., Fujiwara, M., and Kawamata, M., "Reduction of HC emission from VTEC engine during cold start combustion", *SAE Paper 940481*, 1994.

[46] Tsunemoto, H., Ishitani, H., and Honno, A., "The increase of HC emissions from a direct injection diesel engine during long idling operation", *SAE Paper 922227*, 1992.

[47] Kaiser, E., Yang, J., Culp, T., Xu, N., and Maricq, M., "Homogeneous charge compression ignition engine-out emissions- does flame propagation occur in homogeneous charge compression ignition?", *Int. J. Engine Research*, vol. 3, no. 4, 2002.

[48] Zhao, H., *Overview of CAI/HCCI Gasoline Engines / HCCI and CAI Engines for the Automotive Industry*. Woodhead Publishing Limited, 2007.

[49] Rani, B., Singh, U., Chuhan, A., Sharma, D., and Maheshwari, R., "Photochemical smog pollution and its mitigation measures", *Journal of Advanced Scientific Research*, vol. 2, no. 4, pp. 28–33, 2011.

[50] Herfatmanesh, M., *Investigation of single and split injection strategies in an optical diesel engine*. PhD thesis, School of Engineering and Design - Brunel University, 2010.

[51] Tandonn, P., Heibel, A., Whitmore, J., Kekre, N., and Chithapragada, K., "Measurement and prediction of filtration efficiency evolution of soot loaded diesel particulate filters", *Chemical Engineering Science*, vol. 65, pp. 4751–4760, 2010.

[52] Dwyer, H., Ayala, A., Zhang, S., Collins, J., Huai, T., and Chau, W., "Emissions from a diesel car during regeneration of an active diesel particulate filter", *Journal of Aerosol Science*, vol. 41, no. 6, pp. 541–552, 2010.

[53] Schejbal, M., Stepanek, J., Marek, M., Koci, P., and Kubicek, M., "Modelling of soot oxidation by NO2 in various types of diesel particulate filters", *Fuel*, vol. 89, no. 9, pp. 2365–2375, 2010.

[54] Manufacturers of Emission Controls Association,, "Catalyst-based diesel particulate filters and nox adsorbers: A summary of the technologies and the effects of fuel sulfur", tech. rep., Manufacturers of Emission Controls Association, 2000.

[55] Diesel Vehicle Emission Control,, "Sulfur effects (DVECSE) project, Phase I final Report", tech. rep., Oak Ridge National Laboratory, 2000.

[56] Azzara, A., Rutherford, D., and Wang, H., "Feasibility of imo annex vi tier iii implementation using selective catalytic reduction", tech. rep., The International Council on Clean Transportation, 2014.

[57] Manufacturers of Emission Controls Association ,, "Emission control technologies for diesel-powered vehicles", tech. rep., Manufacturers of Emission Controls Association, 2007.

[58] Dou, D., "Application of diesel oxidation catalyst and diesel particulate filter for diesel engine powered non-road machines", *Platinum Metals Rev.*, vol. 56, no. 3, pp. 144–154, 2012.

[59] Brain, M., "How diesel two-stroke engines work". Available from: http://auto.howstuffworks.com/diesel-two-stroke1.htm, Cited on 10/06/2014.

[60] Brain, M., "How diesel engines work". Available from: http://auto.howstuffworks.com/diesel1.htm, Cited on 10/06/2014.

[61] Onishi, S., Jo, S., Shoda, K., Jo, P., and Kato, S., "Active Thermo-Atmosphere Combustion (ATAC) - A new combustion process for internal combustion engines", *SAE Paper 790501*, 1979.

[62] Noguchi, M., Tanaka, Y., Tanaka, T., and Takeuchi, Y., "A study on gasoline engine combustion by observation of intermediate reactive products during combustion", *SAE Paper 790840*, 1979.

[63] Najt, P. and Foster, D., "Compression-ignited homogeneous charge combustion", *SAE Paper 830264*, 1983.

[64] Thring, R., "Homogeneous-Charge Compression-Ignition (HCCI)", *SAE Paper 1989-09-01*, 1989.

[65] Song, H., *Low-load extension of residual-effected homogeneous charge compression ignition using recompression reaction.* PhD thesis, Stanford University, 2009.

[66] Peng, Z. and Jia, M., "An investigation and evaluation of variable-valve-timing and variable-valve-actuation strategies in a diesel homogeneous charge compression ignition engine using three-dimensional computational fluid dynamics", *Proceedings*

of the Institution of Mechanical Engineers, Part D: Journal of Automobile Engineering, vol. 222, no. 6, pp. 1047–1064, 2008.

[67] Ebrahimi, K., "HCCI combustion timing control with variable valve timing", *American Control Conference (ACC)*, 2013.

[68] Yeom, K., Jang, J., and Bae, C., "Homogeneous charge compression ignition of LPG and gasoline using variable valve timing in an engine", *Fuel*, vol. 86, no. 4, pp. 494–503, 2007.

[69] Milovanovic, N., Chen, R., and Turner, J., "Influence of the variable valve timing strategy on the control of a homogeneous charge compression (HCCI) engine", *SAE Paper 2004-01-1899*, 2004.

[70] Ryan, T. and Callahan, T., "Charge compression ignition of diesel fuel", *SAE Paper 961160*, 1996.

[71] Olsson, J.-O., Tunestål, P., Ulfvik, J., and Johansson, B., "The effect of cooled EGR on emissions and performance of a turbocharged HCCI engine", *SAE Paper 2003-01-0743*, 2003.

[72] Law, D., Allen, J., Kemp, D., and Williams, P., "Stroke Active Combustion (Controlled Auto-Ignition) investigations using a single cylinder engine with Lotus Active Valve Train (AVT)", *Proceedings of the 21st Century Emissions Technology Conference, I. Mech. E.*, 2000.

[73] Law, D., Kemp, D., Allen, J., Kirkpatrick, G., and Copland, T., "Controlled combustion in an IC-engine with a fully variable valve train", *SAE Paper 2000-01-0251*, 2000.

[74] Shi, L., Cui, Y., Peng, H., and Chen, Y., "Study of low emission homogeneous charge compression ignition (HCCI) engine using combined internal and external exhaust gas recirculation (EGR)", *Energy*, vol. 31, no. 14, pp. 2665–2676, 2006.

[75] Peng, Z., Zhao, H., and Ladommatos, N., "Effects of air/fuel ratios and EGR rates on HCCI combustion of n-heptane, a diesel type fuel", *SAE Paper 2003-01-0747*, 2003.

[76] U.S. Department of Energy,, "Homogeneous charge compression ignition (hcci) technology - a report to the u.s. congress", tech. rep., U.S. Department of Energy - Energy Efficiency and Renewable Energy - Office of Transportation Technologies, 2001.

[77] Neely, G., Sasaki, S., Huang, Y., Leet, J., and Stewart, D., "New diesel emission control strategy to meet US Tier 2 emissions regulations", *SAE Paper 2005-01-1091*, 2005.

[78] Siebers, D., "Liquid-phase fuel penetration in diesel sprays", *SAE Paper 980809*, 1998.

[79] Aoyama, T., Hattori, Y., Mizuta, J., and Sato, Y., "An experimental study on premixed-charge compression ignition gasoline engine", *SAE Paper 960081*, 1996.

[80] Keeler, B. and Shayler, P., "Constraints on fuel injection and EGR strategies for diesel PCCI-type combustion", *SAE Paper 2008-01-1327*, 2008.

[81] Takeda, Y., Keiichi, N., and Keiichi, N., "Emission characteristics of premixed lean diesel combustion with extremely early staged fuel injection", *SAE Paper 961163*, 1996.

[82] Kong, S., Ra, Y., and Reitz, R., "Performance of multi-dimensional mmodel for simulating diesel premixed charge compression ignition engine combustion using low- and high-pressure injectors", *International Journal of Engine Research*, vol. 6, no. 5, pp. 475–486, 2005.

[83] Liu, B., *Numerical Investigation and Evaluation of Applying PCCI Combustion in HSDI Diesel Engine.* PhD thesis, University of Sussex, 2014.

[84] Kanimoto, T. and Bae, M., "High combustion temperature for the reduction of particulate in diesel engines", *SAE Paper 880423*, 1988.

[85] Kiplimo, R., Tomita, E., Kawahara, N., and Yokobe, S., "Effects of spray impingmnent, injection parameters and EGR on the combustion and emission characteristics of a PCCI diesel engine", *Applied Thermal Engineering*, vol. 37, pp. 165–175, 2012.

[86] Hardy, W. and Reitz, R., "A study of the effects of high EGR, high equivalence ratio and mixing time on emissions level in a heavy-duty diesel engine for PCCI combustion", *SAE Paper 2006-01-0026*, 2006.

[87] Zala, M., "Optimization of EGR rate on multi cylinders 4-stroke diesel engine", *International Journal of Engineering Research & Technology*, vol. 1, no. 4, 2012.

[88] Zhao, H., ed., *Advanced Direct Injection Combustion Engine Technologies and Development - Volume 2: Diesel engines*. Woodhead Publishing L, 2010.

[89] Kimura, S., Aoki, O., Ogawa, S., Muranaka, S., and Enomoto, Y., "New combustion concept for ultra-clean and high-efficiency small DI diesel engines", *SAE Paper 1999-01-3681*, 1999.

[90] Park, Y. and Bae, C., "Influence of EGR and pilot injection on PCCI combustion in a single-cylinder diesel engine", *SAE Paper 2011-01-1823*, 2011.

[91] Horibe, N., Harada, S., Ishiyama, T., and Shioji, M., "Improvement of premixed charge compression ignition-based combustion by two-stage injection", *International Journal of Engine Research*, vol. 10, no. 2, pp. 71–80, 2009.

[92] Kokjohn, S. and Reitz, R., "A computational investigation of two-stage combustion in a light-duty engine", *SAE Paper 2008-01-2412*, 2008.

[93] Mosbach, S., Su, H., Bhave, A., Mauss, F., Wang, Z., and Wang, J.-X., "Dual injection homogeneous charge compression ignition engine simulation using a stochastic

reactor model", *International Journal of Engine Research*, vol. 8, no. 1, pp. 41–50, 2007.

[94] Su, H., Mosbach, S., Kraft, M., Bhave, A., Kook, S., and Bae, C., "Two-stage fuel direct injection in a diesel fuelled hcci engine", tech. rep., University of Cambridge, 2007.

[95] Murata, Y., Kusaka, J., Daisho, Y., Kawano, D., Suzuki, H., Ishii, H., and Goto, Y., "Miller-PCCI combustion in an HSDI diesel engine with VVT", *SAE Paper 2008-01-0644*, 2008.

[96] Kook, S., Bae, C., Miles, P., Choi, D., Bergin, M., and Reitz, D., "The effect of swirl ratio and fuel injection parameters on CO emission and fuel conversion efficiency for high-dilution, low temperature combustion in an automotive diesel engine", *SAE Paper 2006-01-0197*, 2006.

[97] Mobasheri, R., *Investigations of advanced injection and combustion strategies on DI diesel engine performance and emissions.* PhD thesis, University of Sussex, 2012.

[98] Rakowski, S., Eckert, P., and Witt, A., *Combustion Engines Development.* Springer Berlin Heidelberg, 2012.

[99] Karuppa, R. and Manimaran, R., "Effect of swirl in a constant speed DI diesel engine using Computational Fluid Dynamics", *CFD Letters*, vol. 4, pp. 214–224, 2012.

[100] Shundoh, S., Kakegawa, T., Tsujimura, K., and Kobayashi, S., "The effect of injection parameters and swirl on diesel combustion with high pressure fuel injection", *SAE 910489*, 1991.

[101] Ogawa, H., Matsui, Y., Kimura, S., and Kawashima, J., "Three-dimensional computation of the effects of the swirl ratio in direct-injection diesel engines on NOx and soot emissions", *SAE Paper 961125*, 1996.

[102] Gunasekaran, J. and Ganesan, V., "Effect of swirl and tumble on the stratified combustion of a DISI engine - a CFD study", *SAE Paper 2011-01-1214*, 2011.

[103] Jie, M., Kim, M., and Kim, W., "The effect of tumble flow on engine performance and flame propagation", *SAE Paper 931946*, 1993.

[104] Robert Bosch GmbH,, "Diesel systems - downsizing of diesel engines", tech. rep., BOSCH, 2011.

[105] Zage,, "Zage turbosystem inc.". Available from: http://www.zageturbo.com/, Cited on 16/06/2014.

[106] Uchida, N., Daisho, Y., Saito, T., and Sugano, H., "Combined effects of EGR and supercharging on diesel combustion and emissions", *SAE 930601*, 1993.

[107] Tanin, K., Wickman, D. D., Montgomery, D. T., Das, S., and Reitz, R. D., "The influence of boost pressure on emission and fuel consumption of a heavy-duty single-cylinder D.I. diesel engine", *SAE Paper 1999-01-0840*, 1999.

[108] Zhang, L., Takatsuki, T., and Yokota, K., "An observation and analysis of the combustion under supercharging on a DI diesel engine", *SAE Paper 940844*, 1994.

[109] Ladommatos, N., Abdelhalim, S., Zhao, H., and Hu, Z., "The dilution, chemical, and thermal effects of exhaust gas recirculation on diesel engine emissions - Part 4: effects of carbon dioxide and water vapour", *SAE Paper 971660*, 1997.

[110] Ladommatos, N., Abdelhalim, S., Zhao, H., and Hu., Z., "Effects of EGR on heat release in diesel combustion", *SAE Paper 980184*, 1998.

[111] Mattarelli, E., Bianchi, G., and Ivaldi, D., "Experimental and numerical investigation on the EGR system of a new automotive diesel engine", *SAE Paper 2000-01-0224*, 2000.

[112] Hountalas, D., Mavropoulos, G., and Binder, K., "Effect of exhaust gas recirculation (EGR) temperature for various egr rates on heavy duty DI diesel engine performance and emissions", *Energy*, vol. 33, no. 2, pp. 272–283, 2008.

[113] Ladommatos, N., Balian, R., Horrocks, R., and Cooper, L., "The effect of exhaust gas recirculation on combustion and NOx emissions in a high-speed direct-injection diesel engine", *SAE Paper 960840*, 1996.

[114] Arcoumanis, C., Nagwaney, A., Hentschel, W., and Ropke, S., "Effect of EGR on spray development, combustion and emissions in a 1.9L direct-injection diesel engine", *SAE Paper 952356*, 1995.

[115] Peng, H., Cui, Y., Shi, L., and Deng, K., "Effects of exhaust gas recirculation (EGR) on combustion and emissions during cold start of direct injection (DI) diesel engine", *Energy*, vol. 33, no. 3, pp. 471–479, 2008.

[116] Dürnholz, M., Eifler, G., and Endres, H., "Exhaust-gas recirculation - a measure to reduce exhaust emissions of DI diesel engines", *SAE Paper 920725*, 1992.

[117] Baumgarten, C., *Mixture Formation in Internal Combustion Engine.* Springer, 2006.

[118] Millo, F., Mallamo, F., Arnone, L., Bonanni, M., and Franceschini, D., "Analysis of different internal EGR solutions for small diesel engines", *SAE Paper 2007-01-0128*, 2007.

[119] Li, W., Ge, Y., and Liu, J.Y. amd Hu, F., "Research on application of internal EGR to turbo-diesel engines", *Neiranji Gongcheng / Chinese Internal Combustion Engine Engineering*, vol. 27, no. 6, pp. 43–46, 2006.

[120] Nakamura, H., Nakashima, T., Aihara, H., and Ookubo, M., "Development of gear parts for VVT unit", *SAE Paper 970337*, 1997.

[121] Akima, K., Seko, K., Taga, W., Torii, K., and Nakamura, S., "Development of new low fuel consumption 1.8L i-VTEC gasoline engine with delayed intake valve closing", *SAE Paper 2006-01-0192*, 2006.

[122] Matsuda, T., Wada, H., Kono, T., Nakamura, T., and Urushihara, T., "A study of a gasoline-fueled HCCI engine mode changes from SI combustion to HCCI combustion", *SAE Paper 2008-01-0050*, 2008.

[123] Bermúdez, V., Lujan, J., Pla, B., and Linares, G., "Effects of low pressure exhaust gas recirculation on regulated and unregulated gaseous emissions during NEDC in a light-duty diesel engine", *Energy*, vol. 36, pp. 5655–5665, 2011.

[124] Reinfarth, S. and Ångström, H.-E., "Transient EGR in a high-speed DI diesel engine for a set of different EGR-routings", *SAE Paper 2010-01-1271*, 2010.

[125] Zamboni, G. and Capobianco, M., "Experimental study on the effects of HP and LP EGR in an automotive turbocharged diesel engine", *Applied Energy*, vol. 94, pp. 117–128, 2012.

[126] Zamboni, G. and Capobianco, M., "Influence of high and low pressure EGR and VGT control on in-cylinder pressure diagrams and rate of heat release in an automotive turbocharged diesel engine", *Applied Thermal Engineering*, vol. 51, pp. 586–596, 2013.

[127] Bolt, J., Bergin, S., and Vesper, F., "The influence of the exhaust back pressure of a piston engine on air consumption, performance, and emissions", *SAE Paper 730195*, 1973.

[128] Cong, S., Garner, C., and McTaggart-Cowan, G., "The effects of exhaust back pressure on conventional and low-temperature diesel combustion", *Proceedings of the Institution of Mechanical Engineers, Part D: Journal of Automobile Engineering*, vol. 225, no. 2, pp. 222–235, 2011.

[129] Tokuda, H., "Denso news conference remarks", *2003 SAE World Congress*, 2003.

[130] Dronniou, N., Lejeune, M., I., B., and Higelin, P., "Combination of hight EGR rates and multiple injection strategies to reduce pollutant emissions", *SAE Paper 2005-01-3726*, 2005.

[131] Shayler, P., Brooks, T. D., Pugh, G., and Gambrill, R., "The influence of pilot and split-main injection parameters on diesel emissions and fuel consumption", *SAE Paper 2005-01-0375*, 2005.

[132] Eastwood, P., Morris, T., Tufail, K., Winstanley, T., Hardalupas, Y., and Taylor, A., "The effects of fuel-injection schedules on emissions of NOx and smoke in a diesel engine", *SAE Paper 2007-24-0011*, 2007.

[133] Lee, J., Jeon, J., Park, J., and Bae, C., "Effect of multiple injection strategies on emissions and combustion characteristics in a single cylinder direct-injection optical engine", *SAE Paper 2009-01-1354*, 2009.

[134] Siebers, D., "Scaling liquid-phase fuel penetration in diesel sprays based on mixing-limited vaporization", *SAE Paper 1999-01-0528*, 1999.

[135] Badami, M., Nuccio, P., and Trucco, G., "Influence of injection pressure on the performance of a DI diesel engine with a common rail fuel injection system", *SAE Paper 1999-01-0193*, 1999.

[136] Agarwal, A., Dhar, A., Shrivastava, D., Maurya, R., and Singh, A., "Effect of fuel injection pressure on diesel particulate size and number distribution in a CRDI single cylinder research engine", *Fuel*, vol. 107, pp. 84–89, 2013.

[137] Gumus, M., Sayin, C., and Canakci, M., "The impact of fuel injection pressure on the exhaust emissions of a direct injection diesel engine fueled with biodiesel-diesel fuel blends", *Fuel*, vol. 95, pp. 486–494, 2012.

[138] Icingur, Y. and Altiparmak, D., "Effect of fuel cetane number and injection pressure on a DI diesel engine performance and emissions", *Energy Conversion and Management*, vol. 44, no. 3, pp. 389–397, 2003.

[139] Hountalas, D., Kouremenos, D., Binder, K., Schwarz, V., and Mavropoulos, G., "Effect of injection pressure on the performance and exhaust emissions of a heavy duty DI diesel engine", *SAE Paper 2003-01-0340*, 2003.

[140] Jindala, S., Nandwanaa, B., Rathoreb, N., and Vashisthaa, V., "Experimental investigation of the effect of compression ratio and injection pressure in a direct injection diesel engine running on jatropha methyl ester", *Applied Thermal Engineering*, vol. 30, no. 5, pp. 442–448, 2010.

[141] Green Car Congress,, "Denso develops new 2500-bar diesel common rail system; reductions in fuel consumption and emissions". Available from: http://www.greencarcongress.com/2013/06/denso-20130627.html, Cited on: 20/06/2014.

[142] Pierpont, D., Montgomery, D. T., and Reitz, R., "Reducing particulate and NOx using multiple injection and EGR in a D.I. diesel.", *SAE Paper 950217*, 1995.

[143] Minami, T., Takeuchi, K., and Shimazaki, N., "Reduction of diesel engine NOx using pilot injection", *SAE Paper 950611*, 1995.

[144] Montgomery, D. T. and Reitz, R., "Effects of multiple injections and flexible control of boost and EGR on emissions and fuel consumption of a heavy-duty diesel engine", *SAE Paper 2001-01-0195*, 2001.

[145] Yamaki, Y., Mori, K., Kamikubo, H., Kohketsu, S., Mori, K., and Kato, T., "Application of common rail fuel injection system to a heavy duty diesel engine", *SAE Paper 942294*, 1994.

[146] Uchida, N., Shimokawa, K., Kudo, Y., and Shimoda, M., "Combustion optimization by means of common rail injection system for heavy-duty diesel engines", *SAE Paper 982679*, 1998.

[147] Mikulic, L., Kühn, M., Schommers, J., and Willig, E., "Exhaust-emission optimization of DI-diesel passenger car engine with high-pressure fuel injection and EGR", *SAE Paper 931035*, 1993.

[148] Park, C., Kook, S., , and Bae, C., "Effects of multiple injections in a HSDI diesel

engine equipped with common rail injection system", *SAE Paper 2004-01-0127*, 2004.

[149] Han, Z., Uludogan, A., Hampson, G., and Reitz, R., "Mechanism of soot and NOx emission reduction using multiple-injection in a diesel engine", *SAE Paper 960633*, 1996.

[150] Farrell, P., Chang, C., and Su, T., "High pressure multiple injection spray characteristics", *SAE Paper 960860*, 1996.

[151] Mendez, S. and Thirouard, B., "Using multiple injection strategies in diesel combustion: Potential to improve emissions, noise and fuel economy trade-off in low CR engines", *SAE Int. J. Fuels Lubr.*, vol. 1, no. 1, pp. 662–674, 2009.

[152] Tow, T., Pierpont, D., and R., R., "Reducing particulate and NOx emissions by using multiple injections in a heavy duty D.I. diesel engine", *SAE Paper 940897*, 1994.

[153] Mobasheri, R., Peng, Z., and Mirsalim, S., "Analysis the effect of advanced injection strategies on engine performance and pollutant emissions in a heavy duty DI-diesel engine by CFD modeling", *Int J Heat Fluid Flow*, vol. 33, no. 1, pp. 59–69, 2012.

[154] Ricaud, J. and Lavoisier, F., "Optimizing the multiple injection settings on an HSDI diesel engine", *THIESEL 2002 conference*, 2002.

[155] Diez Rodriguez, A., *Investigation of Split Injection in a Single Cylinder Optical Diesel Engine*. PhD thesis, Brunel University, 2009.

[156] Jaichandar, S. and Annamalai, K., "Effects of open combustion chamber geometries on the performance of pongamia biodiesel in a DI diesel engine", *Fuel*, vol. 98, pp. 272–279, 2012.

[157] Li, J., Yang, W., An, H., Maghbouli, A., and Chou, S., "Effects of piston bowl geometry on combustion and emission characteristics of biodiesel fueled diesel engines", *Fuel*, vol. 120, pp. 66–73, 2014.

[158] Harshavardhan, B. and Mallikarjuna, J., "CFD analysis of in-cylinder flow and air-fuel interaction on different combustion chamber geometry in DISI engine", *International Journal on Theoretical and Applied Research in Mechanical Engineering (IJTARME)*, vol. 2, no. 3, pp. 104–108, 2013.

[159] Payri, F., Benajes, J., Margot, X., and Gil, A., "CFDmodeling of the in-cylinder flow in direct-injection diesel engines", *Computer & Fluid*, vol. 33, pp. 995–1021, 2004.

[160] Tsao, K., Y. Dong, Y., and Xu, Y., "Investigation of flow field and fuel spray in a direct-injection diesel engine via Kiva-II program", *SAE Paper 901616*, 1990.

[161] Zhang, L., Ueda, T., Takatsuki, T., and Yokota, K., "A study of the effect of chamber geometries on flame behavior in a DI diesel engine", *SAE Paper 952515*, 1995.

[162] De Risi, A., Donateo, T., and Laforgia, D., "Optimization of the combustion chamber of direct injection diesel engines", *SAE Paper 2003-01-1064*, 2003.

[163] Genzale, C., Wickman, D., and Reitz, R., "An advanced optimization methodology for understanding the effects of piston bowl design in late injection low temperature diesel combustion", *In Proceedings of THIESEL 2006 conference on thermo and fluid dynamic processes in diesel engines, Valencia- Spain*, 2006.

[164] Liu, Y. and Reitz, R., "Optimizing HSDI diesel combustion and emissions using multiple injection strategies", *SAE Paper 2005-01-0212*, 2005.

[165] Hiroyasu, T., Miki, M., Kim, M., Watanabe, S., Hiroyasu, H., and Miao, H., "Reduction of heavy duty diesel engine emission and fuel economy with multi-

objective genetic algorithm and phenomenological model", *SAE Paper 2004-01-0531*, 2004.

[166] Senecal, P., Pomraning, E., and Richards, K., "Multi-mode genetic algorithm optimization of combustion chamber geometry for low emissions", *SAE Paper 2002-01-0958*, 2002.

[167] Song, J., Chunde, Y., Liu, Y., and Jiang, Z., "Investigation on flow field in simplified piston bowls for DI diesel engine", *Engineering Applications of Computational Fluid Mechanics*, vol. 2, no. 3, pp. 354–365, 2008.

[168] Siewert, R., "Spray angle and rail pressure study for low NOx diesel combustion", *SAE Paper 2007-01-0122*, 2007.

[169] Hult, J., Matlok, S., and Mayer, S., "Particle image velocimetry measurements of swirl and scavenging in a large marine two-stroke diesel engine", *SAE Paper 2014-01-1173*, 2014.

[170] Krishna, M. and Mallikarjuna, J., "Comparative study of in-cylinder tumble flows in an internal combustion engine using different piston shapes-an insight using particle image velocimetry", *Experiments in Fluids*, vol. 48, no. 5, pp. 863–874, 2010.

[171] Wu, Z., Zhu, Z., and Huang, Z., "An experimental study on the spray structure of oxygenated fuel using laser-based visualization and particle image velocimetry", *Fuel*, vol. 85, no. 10-11, pp. 1458–1464, 2006.

[172] Aleiferis, P., Hardalupas, Y., Kolokotronis, D., Taylor, A., and Kimura, T., "Investigation of the internal flow field of a diesel model injector using particle image velocimetry and CFD", *SAE Paper 2007-01-1897*, 2007.

[173] Li, Y., Leach, B., Zhao, H., Ma, T., and Ladommatos, N., "In-cylinder flow visualisation by particle image velocimetry (PIV)". Avail-

able from: http://www.brunel.ac.uk/cedps/mechanical-aerospace-civil-engineering/mecheng/research/capf/piv, Cited on 16/08/2014.

[174] Castanet, G., Lavieille, P., Lebouché, M., and Lemoine, F., "Measurement of the temperature distribution within monodisperse combusting droplets in linear streams using two-color laser-induced fluorescence", *Experiments in Fluids*, vol. 35, no. 6, pp. 563–571, 2003.

[175] Payri, F., Pastor, J., Pastor, J., and Juliá, J., "Diesel spray analysis by means of planar laser-induced exciplex fluorescence", *International Journal of Engine Research*, vol. 7, no. 1, pp. 77–89, 2006.

[176] Wolff, M., Delconte, A., Schmidt, F., Gucher, P., and Lemoine, F., "High-pressure diesel spray temperature measurements using two-colour laser-induced fluorescence", *Measurement Science and Technology*, vol. 18, no. 3, pp. 697–706, 2007.

[177] Verbiezen, K., Klein-Douwel, R., Van Vliet, A., Donkerbroek, A., Meerts, W., Dam, N., and Ter Meulen, J., "Quantitative laser-induced fluorescence measurements of nitric oxide in a heavy-duty diesel engine", *Proceedings of the Combustion Institute*, vol. 31, no. 1, pp. 765–773, 2007.

[178] Kollár, L. and Farzaneh, M., "Modeling the evolution of droplet size distribution in two-phase flows", *International Journal of Multiphase Flow*, vol. 33, no. 11, pp. 1255–1270, 2007.

[179] Sick, V., "High speed imaging in fundamental and applied combustion research", *Proceedings of the Combustion Institute*, vol. 34, no. 2, pp. 3509–3530, 2013.

[180] Pickett, L., Kook, S., and Williams, T., "Visualization of diesel spray penetration, cool-flame, ignition, high-temperature combustion, and soot formation using high-speed imaging", *SAE International Journal of Engines*, vol. 2, no. 1, pp. 439–459, 2009.

[181] Nandha, K. and Abraham, K., "Dependence of fuel-air mixing characteristics on injection timing in an early-injection diesel engine", *SAE Paper 2002-01-0944*, 2002.

[182] Peng, Z., Liu, B., Tian, L., and Lu, L., "Analysis of homogeneity factor for diesel PCCI combustion control", *SAE Paper 2011-01-1832*, 2011.

[183] Maiboom, A., Tauzia, X., and Hetet, J., "Experimental study of various effects of exhaust gas recirculation (EGR) on combustion and emissions of an automotive direct injection diesel engine", *Energy*, vol. 33, pp. 22–34, 2008.

[184] Nataraj, M., Arunachalam, V., and Dhandapani, N., "Optimizing diesel engine parameters for low emissions using Taguchi method: variation risk analysis approach - part 1", *Indian Journal of Engineering & Materials Sciences*, vol. 12, pp. 169–181, 2005.

[185] Wu, H. and Wu, Z., "Combustion characteristics and optimal factor determination with Taguchi method for diesel engines port-injecting hydrogen", *Energy*, vol. 47, pp. 411–420, 2012.

[186] Tamilvendhan, D., Ilangova, V., and Karthikeyan, R., "Optimization of engine operating parameters for eucalyptus oil mixed diesel fuel DI diesel engine using Taguchi method", *ARPN Journal of Engineering and Applied Sciences*, vol. 6, no. 6, pp. 14–22, 2011.

[187] Dimitriou, P., Peng, Z., Lemon, D., Gao, B., and Soumelidis, M., "Diesel engine combustion optimization for bio-diesel blends using Taguchi and ANOVA statistical methods", *SAE Paper 2013-24-0011*, 2013.

[188] Pletcher, R. H., Tannehill, J., and Anderson, D., *Computational Fluid Mechanics and Heat Transfer*. CRC Press, third ed., 2012.

[189] Niyogi, P., Chakrabartty, S. K., and Laha, M., *Introduction to Computational Fluid Dynamics*. Pearson Education, 2006.

[190] AVL,, "AVL FIRE Release notes", tech. rep., AVL, 2011.

[191] Kim, H. and Sung, N., "Combustion and emission modeling for a direct injection diesel engine", *SAE Paper 2004-01-0104*, 2004.

[192] Yuan, W., Hansen, A., Tat, M., Gerpen, J., and Tan, Z., "Spray, ignition, and combustion modeling of biodiesel fuels for investigating NOx emissions", *Transactions of the American Society of Agricultural Engineers*, vol. 48, no. 3, pp. 933–939, 2005.

[193] Shi, X., Li, G., and Zhou, L., "DI diesel engine combustion modeling based on ECFM-3Z model", *SAE Paper 2007-01-4138*, 2007.

[194] Sazhin, S., Martynov, S., Kristyadi, T., Crua, C., and Heikal, M., "Diesel fuel spray penetration, heating, evaporation and ignition: modelling vs. experimentation", *Int. J. of Engineering Systems Modelling and Simulation*, vol. 1, no. 1, pp. 1–19, 2008.

[195] Gorji-Bandpy, M., Soleimani, S., and Ganji, D., "The effect of different injection strategies and intake conditions on the emissions characteristics in a diesel engine", *International Journal of Vehicular Technology*, 2009.

[196] Mühlbauer, M., *Modelling wall interactions of a high-pressure, hollow cone spray.* PhD thesis, Technischen Universität Darmstadt, 2010.

[197] Abdelghaffar, W., Elwardany, A., and Sazhin, S., "Effects of fuel droplet break-up, heating and evaporation in diesel engines", *Proceedings of the World Congress on Engineering*, vol. 1, p. 1667, 2011.

[198] Dembinski, H., *In-cylinder Flow Characterisation of Heavy Duty Diesel Engines Using Combustion Image Velocimetry.* PhD thesis, KTH Royal Institute of Technology, 2013.

[199] O'Rourke, P. and Amsden, A., "The TAB method for numerical calculation of spray droplet breakup", *SAE Paper 872089*, 1987.

[200] Tanner, F., "Liquid jet atomization and droplet breakup modeling of non-evaporating diesel fuel sprays", *SAE Paper 970050*, 1997.

[201] Habchi, C., Verhoeven, D., Huynh, C., Lambert, L., Vanhemelryck, J., and Baritaud, T., "Modeling atomization and breakup in high-pressure diesel sprays", *SAE Paper 970881*, 1997.

[202] Patterson, M. and R. D. Reitz, R., "Modeling spray atomization with the Kelvin-Helmholtz/Rayleigh-Taylor hybrid model", *Atomization and Sprays*, vol. 9, pp. 623–650, 1999.

[203] R.D., R., "Modeling atomization processes in high-pressure vaporizing sprays", *Atomization and Sprays*, vol. 3, pp. 309–337, 1987.

[204] Kelvin, L. and Thomson, W., "Hydrokinetic solutions and observations", *Philosophical Magazine Series 4*, vol. 42, no. 281, pp. 362–377, 1871.

[205] Dukowicz, J., "Quasi-steady droplet phase-change in the presence of convection - technical report la-7997-ms", tech. rep., Los Alamos Scientific Laboratory, 1979.

[206] D., K., *Spray/wall-interaction modelling by dimensionless data analysis.* Shaker Verlag GmbH, 2004.

[207] Jones, W. and Launder, B., "The prediction of laminarization with a two-equation model of turbulence", *Int. J. Heat Mass Transfer*, 1972.

[208] Yakhot, V. and Smith, L., "The renormalization group, the epsilon-expansion and derivation of turbulence models", *Journal of Scientific Computing*, vol. 7, pp. 35–61, 1992.

[209] Spalart, P. and Allmaras, S., "A one-equation turbulence model for aerodynamic flows", *AIAA-92-0439*, 1992.

[210] Launder, B. E., Reece, G. J., and Rodi, W., "Progress in the development of a Reynolds-stress turbulent closure", *Journal of Fluid Mechanics*, vol. 68, no. 3, pp. 537–566, 1975.

[211] Basara, B. and Jakirlic, S., "A new hybrid turbulence modelling strategy for industrial CFD", *International Journal for Numerical Methods in Fluids*, vol. 42, no. 1, pp. 89–116, 2003.

[212] Hanjalic, K., Popovac, M., and Hadziabdic, M., "A robust near-wall elliptic-relaxation eddy-viscosity turbulence model for CFD", *Int J Heat Fluid Flow*, 2004.

[213] Colin, O. and Benkenida, A., "The 3-zones extended coherent flame model (ECFM3Z) for computing premixed/diffusion combustion", *Oil & Gas Science and Technology*, vol. IFP., 159, no. 6, pp. 593–609, 2004.

[214] AVL,, "Combustion / emission module", tech. rep., AVL, 2011.

[215] De Soete, G., "Overall kinetics of nitric oxide formation in flames", *La Revista dei Combustibili*, p. 35, 1975.

[216] Magnussen, B. and Hjertager, B., "On mathematical modeling of turbulent combustion with special emphasis on soot formation and combustion", *Proceedings of the 16th International Symposium on Combustion*, 1977.

[217] Delphi,, "Principles of operation - common rail", tech. rep., Delphi France SAS, 2011.

[218] Skynam,, *Commander6D - Motorsport installation of the direct injection diesel system*. Skynam sprl, 1.11 ed., October 2010.

[219] AVL,, *AVL Opacimeter 439*. AVL, April 2010.

Appendix A

C Programming Code For HF

Appendix A provides the programming code for the HF implemented on AVL Fire software.

Global Formula Variables

```
// --- HomogeneityFactor_EquivalenceRatio.h ---
// computes homogeneity factor [-]/[%] based on two definitions:;
//   mode = 0: SAE 2002-02-0944, Nandha's  approach;
//   mode = 1: Modified approach;
// prints results into *.fla file and also into an additional *.txt file;
// computes local dispersion of chemical equivalence ratio as 3D result;
#define outputFileName "homogeneityFactor.txt"
#define outputMode 1
double ValInCell(int ind) {
// equivalence ratio formula...;
        double egr_mf = YEGRMF[ind];
        double fmixc = YFMIXC[ind];
        double fo2e = (1.0-egr_mf)*FO2 + egr_mf*EGRCMP[1];
        double eqr = STO2 / (fo2e+1.0e-10) * fmixc / (1.0-fmixc+1.0e-10);
        return eqr;
}
int mode;
char outputText[64];
double eps;
double valEqr;
double avgEqr;
double sumEqrMass;
double sumEqr2Mass;
double sumCellMass;
double hetEqr;
double hfEqr;
```

Formula Initialization

```
FILE *fp;
int i;
mode = outputMode;
eps = 1.0e-10;
sumEqrMass = 0.0;
sumEqr2Mass = 0.0;
sumCellMass = 0.0;
valEqr = 0.0;
avgEqr = 0.0;
hfEqr = 0.0;
hetEqr = 0.0;
if(mode == 0) outputText = "(SAE 2002-02-0944)";
if(mode == 1) outputText = "(Modified)";
for(i = 0; i < NCELL-NUMBUF ; i++) {
        // sum up to global sums;
        sumEqrMass += ValInCell(i) * VOL[i] * DEN[i];
        sumEqr2Mass += ValInCell(i) * ValInCell(i) * VOL[i] * DEN[i];
        // sum up mass to variable sumCellMass;
        sumCellMass += VOL[i] * DEN[i];
}
// account for MPI;
MPI_SUM_D(sumEqrMass);
MPI_SUM_D(sumEqr2Mass);
MPI_SUM_D(sumCellMass);
if(sumCellMass < 1.0e-30) sumCellMass = 1.0e-30;
if(sumEqrMass == 0.0) {
        hfEqr = 0.0;
}else{
        avgEqr = sumEqrMass/sumCellMass;
        if( mode == 0){
                hfEqr = sumEqrMass / sqrt(sumEqr2Mass / sumCellMass - pow(sumEqrMass /
sumCellMass, 2) ) / sumCellMass;
        }
        if( mode == 1){
        // loop over all visited cells and compute homogeneity factor;
        for(i = 0; i < NCELL-NUMBUF ; i++) {
                hetEqr = hetEqr +=  fabs( ValInCell(i) - avgEqr ) * VOL[i] * DEN [i] / ( 2 * avgEqr *
sumCellMass * ( 1 + ( ValInCell(i) / STAFR )));
        }
        MPI_SUM_D(hetEqr);
        hfEqr = 100.0 * ( 1.0 - hetEqr );
        }
}
if(IAMPRO < 2 ){
    print " ========== Homogeneity Factor Formula ==============================";
        print " >>> angle, average mass weighted equivalence ratio:", t, avgEqr;
        print " >>> angle, homogeneity factor ",outputText,":", t, hfEqr;
    print " ================================================================";
        fp = fopen(outputFileName, "a");
        if(!fp){
```

```
                print "Formula: cannot open output file ", outputFileName;
                return;
        }else{
                if(ITST <= 1){
                        // write header if first timestep is encountered;
                        fprintf(fp, "%s\n", "# CrankAngle AverageEquivalenceRatio
HomogeneityFactor");
                        fprintf(fp, "\t%g" "\t%g" "\t%g\n" , t , avgEqr, hfEqr );
                        fclose(fp);
                }else{
                        fprintf(fp, "\t%g" "\t%g" "\t%g\n" , t , avgEqr, hfEqr );
                        fclose(fp);
                }
        }
}
```

Formula Body

```
if (index < NCELL-NUMBUF) {
valEqr = ValInCell(index);
return 100. * ( valEqr / (avgEqr + eps ) - 1.0 );
}else{
return 0.0;
}
```

Appendix B

Layout of L_{25} orthogonal experiments

Appendix B presents the level of each factor used in the 25 experiments performed based on the L_{25} orthogonal array in Chapter 7.2.

10mg of fuel	15mg of fuel	A (ratio)	B (°CA BBDC)	C (% of closure)
P1	PP1	0/50	69	0
P2	PP2	0/50	57	63
P3	PP3	0/50	94	75
P4	PP4	0/50	63	88
P5	PP5	0/50	50	95
P6	PP6	10/40	69	63
P7	PP7	10/40	57	75
P8	PP8	10/40	94	88
P9	PP9	10/40	63	95
P10	PP10	10/40	50	0
P11	PP11	20/30	69	75
P12	PP12	20/30	57	88
P13	PP13	20/30	94	95
P14	PP14	20/30	63	0
P15	PP15	20/30	50	63
P16	PP16	30/20	69	88
P17	PP17	30/20	57	95
P18	PP18	30/20	94	0
P19	PP19	30/20	63	63
P20	PP20	30/20	50	75
P21	PP21	40/10	69	95
P22	PP22	40/10	57	0
P23	PP23	40/10	94	63
P24	PP24	40/10	63	75
P25	PP25	40/10	50	88

Appendix C

Experimental Results - Chapter 7.2

Appendix C lists the results obtained from the experimental analysis carried out for the Taguchi method of optimization in Chapter 7.2.

10mg of fuel load

	NOx (ppm)			Opacity (%)			Power (kW)			BSFC (kg/kWh)		
	1st	2nd	3rd	1st	2nd	3rd	1st	2nd	3rd	1st	2nd	3rd
P1	867	848	845	1.55	1.47	1.63	2.882	2.83	2.998	0.1561	0.159	0.15
P2	891	897	905	1.8	1.71	1.64	3.08	2.92	3.19	0.1461	0.154	0.141
P3	876	872	867	1.82	1.68	1.96	2.86	2.93	2.844	0.1573	0.154	0.158
P4	864	886	890	1.9	1.77	2.17	2.453	2.89	2.695	0.1834	0.156	0.167
P5	875	878	883	1.61	1.47	1.58	2.761	2.65	2.888	0.163	0.17	0.156
P6	496	500	508	1.36	1.44	1.38	2.211	2.21	2.31	0.2035	0.204	0.195
P7	507	500	490	1.55	1.25	1.26	2.327	2.28	2.343	0.1934	0.198	0.192
P8	502	496	499	1.39	1.33	1.45	2.228	2.11	2.266	0.202	0.214	0.199
P9	463	467	463	1.33	1.32	1.41	1.854	1.96	1.766	0.2428	0.229	0.255
P10	472	472	474	1.68	1.71	1.7	2.25	2.45	2.321	0.2	0.183	0.194
P11	402	408	418	1.74	1.81	1.68	1.793	1.68	1.749	0.251	0.267	0.257
P12	710	698	704	2.55	2.4	2.26	3.366	3.52	3.41	0.1337	0.128	0.132
P13	379	376	379	1.63	1.57	1.52	1.634	1.49	1.579	0.2755	0.302	0.285
P14	380	360	376	1.59	1.78	1.65	1.716	1.73	1.903	0.2622	0.26	0.236
P15	404	397	398	1.8	1.83	1.73	1.87	1.86	1.887	0.2406	0.241	0.239
P16	149	156	137	1.55	1.92	1.73	0.924	0.91	1.183	0.487	0.493	0.381
P17	186	180	188	1.64	1.88	1.77	1.155	1.1	1.007	0.3896	0.409	0.447
P18	127	150	142	2.05	2.33	2.8	1.111	1.16	1.21	0.405	0.39	0.372
P19	218	225	230	2.12	2.16	2.18	1.386	1.38	1.579	0.3247	0.327	0.285
P20	150	148	152	1.48	1.39	2.18	1.128	1.16	1.078	0.3991	0.39	0.417
P21	364	373	378	2.24	2.32	2.1	1.865	1.89	1.947	0.2414	0.239	0.231
P22	360	365	363	2.4	2.34	2.42	1.837	2.01	1.958	0.245	0.224	0.23
P23	371	372	360	2.7	2.65	2.74	1.705	1.76	2.035	0.2639	0.256	0.221
P24	344	339	337	2.41	2.39	2.34	1.689	1.68	1.958	0.2665	0.268	0.23
P25	361	330	333	2.49	2.52	2.54	1.782	1.82	1.958	0.2525	0.248	0.23

15mg of fuel load

	NOx (ppm)			Opacity (%)			Power (kW)			BSFC (kg/kWh)		
	1st	2nd	3rd	1st	2nd	3rd	1st	2nd	3rd	1st	2nd	3rd
PP1	1330	1344	1337	6.9	7.23	7.5	4.307	4.33	3.971	0.1563	0.156	0.17
PP2	1362	1354	1370	7.16	5.9	6.36	4.433	4.38	4.356	0.1519	0.154	0.155
PP3	1310	1310	1313	8.24	8.57	8.94	4.07	4.19	4.098	0.1654	0.161	0.164
PP4	1270	1275	1276	8.69	9.81	8.9	4.18	4.2	4.054	0.1611	0.16	0.166
PP5	1237	1242	1251	8.85	8.8	9	4.268	4.24	4.318	0.1577	0.159	0.156
PP6	1209	1223	1118	3.53	3.95	3.86	4.098	4.03	4.037	0.1643	0.167	0.167
PP7	1233	1244	1237	4.37	4.19	4.54	3.927	4.15	4.125	0.1714	0.162	0.163
PP8	1177	1183	1184	5.41	5.17	6.27	4.021	4.16	4.098	0.1674	0.162	0.164
PP9	1125	1120	1122	3.57	4.6	4.2	3.883	3.83	3.74	0.1734	0.176	0.18
PP10	1216	1245	1213	4.65	4.06	3.94	4.125	4.24	4.18	0.1632	0.159	0.161
PP11	1260	1068	1249	5.66	5.94	6.4	4.334	4.5	4.318	0.1553	0.149	0.156
PP12	1165	1118	1160	9.74	9.07	10.06	4.147	4.12	4.043	0.1623	0.163	0.167
PP13	1110	119	1124	7.86	8.03	7.4	4.252	4.27	4.246	0.1583	0.158	0.159
PP14	1181	1232	1180	6.46	7.13	6.54	4.373	4.29	4.345	0.154	0.157	0.155
PP15	1255	700	1246	4.34	4.57	4.43	4.197	4.26	4.312	0.1604	0.158	0.156
PP16	695	520	708	3.1	3.77	3.34	3.498	3.77	3.592	0.1925	0.178	0.187
PP17	525	664	526	3.5	3.8	3.97	3.13	3.33	3.548	0.2151	0.202	0.19
PP18	668	633	670	3.74	3.57	4.01	3.603	3.6	3.592	0.1869	0.187	0.187
PP19	625	645	640	3.55	3.47	3.83	3.498	3.83	3.394	0.1925	0.176	0.198
PP20	639	650	650	3.91	3.57	3.59	3.493	3.55	3.614	0.1928	0.19	0.186
PP21	645	645	635	3.36	3.6	4.02	3.102	3.4	3.372	0.217	0.198	0.2
PP22	630	645	633	4.22	3.85	3.97	3.284	3.4	3.361	0.205	0.198	0.2
PP23	644	645	646	4.05	4.76	3.97	3.399	3.34	3.245	0.1981	0.201	0.207
PP24	615	620	614	4.36	4.46	4.69	3.108	3.32	3.097	0.2166	0.203	0.217
PP25	587	580	575	3.35	4.07	3.7	3.322	3.33	3.311	0.2026	0.202	0.203